PYRIDAZINE AND ITS RELATED COMPOUNDS. 15[1] PHOTOLYSIS OF 3-AZIDO-4,5-DIPHENYL-1*H*-PYRAZOLO[3,4-*c*]-PYRIDAZINE IN DIFFERENT SOLVENTS

Ali Deeb[a]*, Mohamed Zayed[b], Atef Amer[a] and Ahmed Ali[b]

Keywords: 3-Azido-4,5-diphenyl-1*H*-pyrazolo[3,4-*c*]pyridazine, photolysis in solvents; nitrene formation

The photochemistry of 3-azido-1*H*-pyrazolo[3,4-*c*]pyridazine ring-system has been investigated. The irradiation of 3-azido-4,5-diphenyl-1*H*-pyrazolo[3,4-*c*]pyridazine **1** in various solvents brings to a photolytic nitrene intermediate, which involves into a ring-opening to give 3-substituted pyridazine derivatives. During the photolysis of **1** in toluene and/or anisole the photoattack reaction of nitrene with the solvents is faster than the ring opening thus the corresponding 3-(arylanilino)pyrazolo[3,4-*c*]pyridazine derivatives are formed. The photolysis in the presence of diethyl malonate led to a mixture of three pyridazine derivatives.
.

* Corresponding Authors
E-Mail: dralideeb@hotmail.com
[a] Department of Chemistry, Faculty of Science,Zagazig University, Zagazig, Egypt.
[b] Laboratory of Photochemistry, National Research Center, Dokki, Giza, Egypt.

Introduction

Photolysis of aryl and heteroaryl azides is a well documented reaction[2] to give rise to a varied group of products, whose identity is influenced by many factors such as reaction medium, substituents, etc. The generally accepted pathway includes primary formation of an open-shell singlet nitrene[3] by lose of N_2 followed by intersystem crossing (ISC) to the ground state triplet nitrene and/or cycloaddition to a neighboring C=C double bond in arene system. On the other hand, pyridazine derivatives and heterocyclic annelated pyridazines continue to attract considerable attention for their application in agriculture and in practical for their biological activity for use as potential drugs.[4]

In a previous paper directed towards the synthesis of new pyridazine derivatives,[1] we presented the photolysis of 3-diazo-4,5-diphenylpyrazolo[3,4-*c*]pyridazine in different solvents. The present paper reports the photolysis (300 W, λ 320 nm) of the azido derivative in different solvents at room temperature.

Results and Discussion

3-Azido-4,5-diphenyl-1*H*-pyrazolo[3,4-*c*]pyridazine **1** was prepared in 85% yield as a yellow crystals (mp 167°C) by addition of sodium azide in portion wise to 3-diazo-4,5-diphenylpyrazolo[3,4-*c*]pyridazine[5] in concd. HCl at room temperature. The processes are quick and are readily carried out in a beaker or open flask. The reaction progress was completed until no diazo compound could be detected by thin-layer chromatography as well as no coupling colour with β-naphthol.

Irradiation of the azido derivative **1** in methanol and/or ethanol resulted in the formation of 5,5',6,6'-tetraphenyl-[3,3'-bipyridazine]-4,4'-dicarbonnitrile **2** in moderate yield. A mechanism for the transformation of **1** into **2** could involve the formation of a singlet nitrene followed by ring opening concerted with nitrogen molecule and hydrogen radical elimination producing the radical species which dimerized to form **2** (Scheme1).

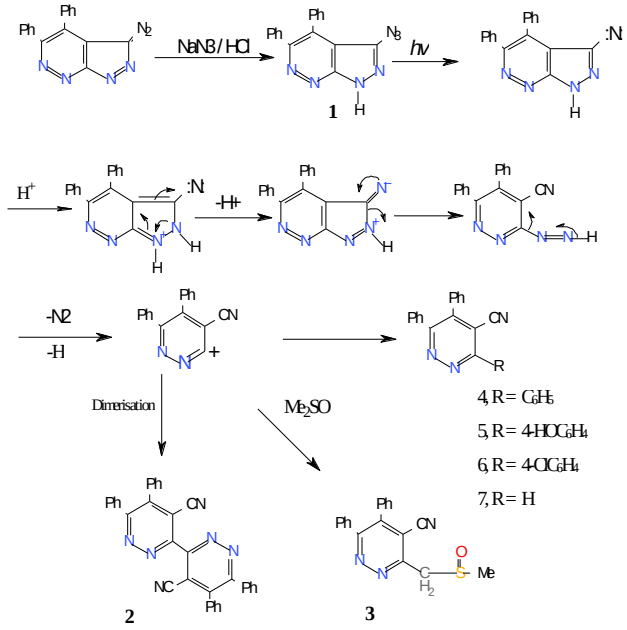

Scheme 1. Caption should be given.

The structure of compound **2** was inferred from the analytical data and spectral feature. The IR spectrum had strong absorption band at 2239 cm^{-1} due to CN stretching vibration. The mass spectrum exhibited a characteristic strong molecular ion peak at *m/z* 512 and the fragmentations are outlined as follows:

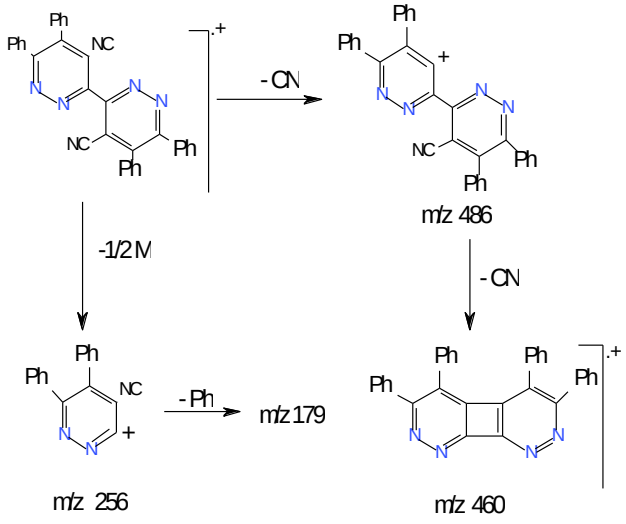

Scheme 2. Caption should be given

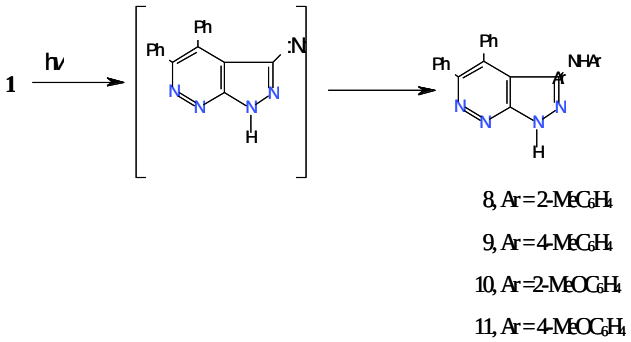

Scheme 3. Caption should be given

The ^{1}H-NMR spectrum showed a multiplet at δ 7.60-7.90 attributed to the aromatic phenyl protons (4 Ph).

When compound **1** was irradiated in dimethyl sulfoxide, a ring opening reaction was occurred with nitrogen and hydrogen molecules (there were detected these molecules or counted only form the formula? Other N-H compds can also be elimininated !) elimination to give 3-((methylsulfinyl) methyl)-5,6-diphenylpyridazine-4-carbonitrile **3** as was evidenced by the analytical and spectral data.

Irradiation of **1** in benzene (or derivatives) showed the same patterns. Irradiation of **1** in benzene led to the isolation of 3,5,6-triphenylpyridazine-4-carbonitrile **4** in 50% yield, and irradiation of **1** in phenol or chlorobenzene gave pyridazines **5** and **6** in 89% and 51% yields, respectively.

Irradiation of a solution of **1** in nitrobenzene led to the isolation of the product **7**. This result could be interpreted in terms of nitrobenzene is not reactive enough to attack the intermediate. The proof for the structures of compounds **4-7** results on their elemental analyses and spectral data and is summarized in experimental section.

On the other hand, the irradiation of 3-azido derivative **1** in toluene did not give the corresponding nitrile instead gave a mixture of *ortho* and *para* substituted anilino derivatives **8** and **9** of anilino compounds could be explained assuming that the photo attack reaction of the nitrene compound with toluene is faster than the ring opening to give the corresponding anilino derivatives.

In the photolysis of compound **1** with anisole, the behavior is analogous to that observed in toluene, leading to the corresponding products **10** and **11** (Scheme 2).

Lastly, compound **1** was irradiated in presence of diethyl malonate. The thin-layer chromatographic results of the crude product shows the presence of three products.

Separation by column chromatography on silica gel (20 – 600 mesh) led to the isolation of 3,4-diphenylpyridazine-5-carbonitrile **7** in 10.8% yield. The carboxamides **12**, **13** were also obtained in 34.3% and 37.8% yields, respectively.

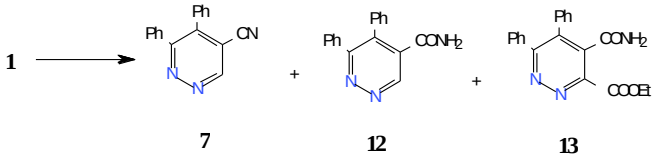

Scheme 4. Caption should be given.

The structure of compounds **12** and **13** were established on the basis of their elemental and spectral data.

The photoreaction of 3-azido derivative **1** with a variety of reagents proceeds smoothly to yield substituted 4-cyanopyridazine, substitutd aminopyrazolopyridazine and/or pyridazine-carboxamide derivatives, depending on the nature of the reagents, the photoreaction described here would be an efficient and novel method for their synthesis.

Experimental

Melting points were determined on a Büchi 510 apparatus and are reported uncorrected. IR spectra were recorded as potassium bromide disks on a Perkin-Elmer 383 spectrophotometer. ^{1}H-NMR spectra were obtained on a Bruker Ac 200 F instrument. Mass spectra were obtained at 70 eV by using a AEI MS 30 mass spectrometer. Elemental analysis (C, H, N) were carried out using a Perkin-Elmer 240C Microanalyzer the Microanalytical Laboratory-Cairo University. All reactions were monitored by thin layer chromatography, carried out on 0.2 mm silica gel 60 F-254 (Merck) plates using UV. light (254 and 366 nm). The photoreactions were carried out in a Pyrex immersion apparatus equipped with 300 W high-pressure mercury lamps at room temperature. Commercially available reagents and solvents were usually reagent grade and distilled or recrystallized prior to use.

3-Azido-4,5-diphenyl-1*H*-pyrazolo[3,4-*c*]pyridazine 1.

M.p. 167° (dec.). It was prepared from 3-diazo-4,5-diphenylpyrazolo[3,4-*c*]pyridazine as follow: To a solution of 3-diazo derivative (0.6 g, 2 mmol) in conc. hydrochloric acid (5 mL), sodium azide (0.4 g, 6 mmol) was added in portion-wise at room temperature with stirring. A yellow deposit product was separated, filtered and recrystallized from benzene (0.54 g, 85%), m.p. 167 °C. IR: 3150-3090 (NH), 2150 (N_3), 1650 (C=N) and 1520 cm^{-1} (C=C); ^{1}H-NMR (DMSO-d_6): δ 14.5 (s, 1H, NH) and 7.10-7.60 (m, 10H, 2Ph). Anal.: Calcd for $C_{17}H_{11}N_7$: C, 65.16; H, 3.54; N, 31.29. Found: C, 65.00; H, 3.40; N, 31.20.

General Procedure for the Photochemical Reactions:

A sample of compound **1** in the appropriate anhydrous solvent/reagent was irradiated until disappearance of the starting material. After removing the solvent under reduced pressure, the residue was recrystallized.

Irradiation in methanol

Irradiation of compound **1** (0.5 g, 1.6 mmol) in methanol (250 mL) for 40 h gave 5,5',6,6'-tetraphenyl-[3,3'-bipyridazine]-4,4'-dicarbonnitrile **2**, (0.2 g, 24.4 %), m.p. 298-299 °C (from methanol). IR: 3085 (C-H, aromatic), 2239 (C≡N), 1630 (C=N), and 1442, 1338, 1258, 1120 cm^{-1}; ^{1}H-NMR (DMSO-d_6): δ 6.91 – 7.46 (m, 20H, 4Ph); MS *m/z* : 512 (M^+, 100%), 435 (M^+ - Ph, 9.5% ion A), 409 (ion A – CN, 10.1%), 256 (½ M^+, 10.1%), and 178 (½ M^+-Ph, 97.6%). Anal.: Calcd for $C_{34}H_{20}N_6$: C, 79.67; H, 3.93; N, 16.39. Found: C, 79.50; H, 3.80; N, 16.20.

Irradiation in ethanol

Using the same procedure, irradiation of compound **1** (0.5 g, 1.6 mmol) in absolute ethanol (250 mL) for 3 h gave the dimer product **2** (0.24 g, 30.5%), identical m.p., mixed m.p. and IR spectrum with the aforementioned sample.

Irradiation in dimethylsulfoxide

Irradiation of compound **1** (0.5 g, 1.6 mmol) in dimethylsulfoxide (250 mL) for 14 h. The reaction mixture was poured into ice water (100 mL), the solid filtered off and recrystallized from ethanol to give 3-((methylsulfinyl) methyl)-5,6-diphenylpyridazine-4-carbonitrile **3** (0.3 g, 56.3%), m.p. > 300 °C (from dimethyl formamide). IR: 3090 (CH, aromatic), 2920, 2850 (CH, aliphatic), 2218 (CN), 1633 (C=N), 1445, 1338 and 1065 cm^{-1} (S=O); ^{1}H-NMR (DMSO-d_6): δ 2.56 (s, 3H, CH_3), 3.38 (s, 2H, CH_2), 7.36 – 7.56 (m, 10H, 2Ph); MS *m/z* : 332 (M^+-1, 6.2%), 331 (M^+-2, 9.9%, ion A), 313 (ion A – NH_4, 6.7%, ion B), 285 (ion B - N_2, 38.0% ion C), 271 (ion C - 15, 77.1%), 256 (M^+ - $CH_2S(=O)Me$, 100%). Anal. Calcd for $C_{19}H_{15}N_3OS$: C, 68.44, 4.54; N, 12.60. Found: C, 68.50; H, 4.40; N, 12.40.

Irradiation in benzene

Irradiation of compound **1** (0.5 g, 1.6 mmol) in benzene (250 mL) for 2 h, gave 3,5,6-triphenylpyridazine-4-carbonitrile **4** (0.3 g, 51.7 %), m.p. 157-158 °C (from benzene). IR: 3057 (CH, aromatic), 2228 (CN), 1607 (C=N), and 1445, 1358, 1225, 1129 cm^{-1}; ^{1}H-NMR (DMSO-d_6): δ 6.58 – 7.54 (m, 15H, 3Ph); MS *m/z* : 333 (M^+, 34.3%), 256 (M^+ - Ph, 100%), 178 (M^+ - 2Ph, 70.9%). Anal. Calcd for $C_{23}H_{15}N_3$: C, 82.86; H, 4.54; N, 12.60. Found: C, 82.70, H, 4.40; N, 12.50.

Irradiation in phenol

Irradiation of compound **1** (0.5 g, 1.6 mmol) in phenol (50 mL) for 60 h. The reaction mixture was evaporated on a steam-bath and the residue was washed with diethyl ether, the solid product was filtered off and recrystallized from benzene to give (0.5 g, 89.6 %) of 3-(4-hydroxyphenyl)-5,6-diphenylpyridazine-4-carbonitrile **5**, m.p. 165-166 °C. IR: 3454, 3360 (OH), 3146, 3054 (CH, aromatic), 2229 (CN), 1624 (C=N), 1444, 1382, 1231 cm^{-1}; ^{1}H-NMR (DMSO-d_6): δ 6.80 (d, , *J*=7.0, 2H, aromatic), 7.50 (d, *J*=7.0, 2H, aromatic), 7.66 – 7.90 (m, 10H, 2Ph), 12.99 (s, 1H, OH); MS *m/z* : 349 (M^+, 6.2%), 256 (M^+ - C_6H_4OH, 75%). Anal. Calcd for $C_{23}H_{15}N_3O$: C, 79.06; H, 4.33; N, 12.04. Found: C, 78.90; H, 4.20; N, 11.90.

Irradiation in chlorobenzene

Irradiation of compound **1** (0.5 g, 1.6 mmol) in chlorobenzene (150 mL) for 16 h. The reaction mixture was evaporated and the residue was washed with diethyl ether, the solid product was filtered off and recrystallized from benzene to give (0.3 g, 51.2 %) of 3-(4-chlorophenyl)-5,6-diphenylpyridazine-4-carbonitrile **6**, m.p. 191-192 °C. IR: 3010 (CH, aromatic), 2234 (CN), 1639 (C=N), 1453, 1206, 1160 and 696 cm^{-1} (C-Cl); ^{1}H-NMR (DMSO-d_6): δ 7.70 (d, , *J* = 6.5, 2H, aromatic), 7.50 (d, , *J* = 6.5, 2H, aromatic), 7.20 – 7.42 (m, 10H, 2Ph); MS *m/z* : 368 (M^+, 11.4%), 256 (M^+-C_6H_4Cl, 13.9%). Anal. Calcd for $C_{23}H_{14}ClN_3$: C, 74.89; H, 3.83; N, 11.39. Found: C, 75.00, H, 3.90; N, 11.20.

Irradiation in nitrobenzene

Irradiation of compound **1** (0.5 g, 1.6 mmol) in nitrobenzene (150 mL) for 6 h, gave 3,4-diphenylpyridazine-5-carbonitrile **7** (0.3 g, 68.6%), m.p. 143-144 °C. IR: 3021 (CH, aromatic), 2129 (CN), 1605 (C=N), 1443, 1380, 1177 cm^{-1}; ^{1}H-NMR (DMSO-d_6): δ 7.40 – 7.56 (m, 10H, 2Ph), 9.7 (s, 1H, 6-H); MS *m/z* : 257 (M^+, 58%), 256 (M^+-1, 100%, ion A), 230 (ion A – CN, 25%). Anal. Calcd for $C_{17}H_{11}N_3$: C, 79.36; H, 4.31; N, 16.33. Found: C, 79.40; H, 4.20; N, 16.40.

Irradiation in toluene

Irradiation of compound **1** (0.5 g, .1.6 mmol) in toluene (250 mL) for 3 h. The resulting reaction mixture was concentrated to its third volume, the solid obtained was collected by filtration to give (0.3 g, 49.9 %) of 4,5-diphenyl-N-(*o*-tolyl)-1*H*-pyrazolo[3,4-c]pyridazin-3-amine **8**, m.p. 141 – 142 °C (from toluene). IR: 3420 (NH), 3040 (CH, aromatic) 2922, 2855 (CH, aliphatic), 1609 (C=N), 1580, 1428, 1382 and 753, 701 cm^{-1} attributed to the *ortho* substituted; ^{1}H-NMR (DMSO-d_6): δ 1.24 (s, 3H, CH_3), 6.88 – 7.23 (m, 4H, toluene aromatic protons), 7.39 – 7.64 (m,

10H, 2Ph), 9.8 (s, 1H, NH), 12.01 (s, 1H, pyrazole NH). Anal. Calcd for $C_{24}H_{19}N_5$: C, 76.36; H, 5.08; N, 18.56. Found: C, 76.20; H, 4.90; N, 18.90.

The filtrate was evaporated under reduced pressure and the residue was triturated with diethyl ether to give (0.15 g, 25 %) of **9** 4,5-diphenyl-N-(*p*-tolyl)-1*H*-pyrazolo[3,4-c]pyridazin-3-amine, m.p. 228 – 229 °C (from ethanol). IR: 3405, 3150 (NH), 3090 (CH, aromatic), 2927 (CH, aliphatic, 1633 (C=N); ^{1}H-NMR (DMSO-d_6: δ 1.23 (s, 3H, CH_3), 6.07 – 7.05 (m, 4H, toluene protons), 7.55 – 7.70 (m, 10H, 2Ph), 9.76 (s, 1H, NH), 12.55 (s, 1H, pyrazole NH); MS *m/z* : 377 (M^+, 9.5%), 376 (M^+ - 1, 10.5%), 286 (M^+ - $C_6H_4CH_3$, 10.1%), 271 (M^+ - $NHC_6H_4CH_3$, 77%, ion A), 256 (ion A-NH, 100%). Anal. Calcd for $C_{24}H_{19}N_5$: C, 76.36; H, 5.08; N, 18.56. Found: C, 76.40; H, 4.90; N, 18.60.

Irradiation in anisole

Irradiation of compound **1** (0.5 g, 1.6 mmol) in anisole (150 mL) for 14 h. The resulting reaction mixture was concentrated to its third volume, the solid obtained was filtered off to give (0.2 g, 30.3 %) of *N*-(2-methoxyphenyl)-4,5-diphenyl-1*H*-pyrazolo[3,4-*c*]pyridazine-3-amine **10**, m.p. 134-135 °C (from anisole). IR: 3421 (NH), 3059 (CH, aromatic), 2924, 2854 (CH, aliphatic), 1601 (C=N); ^{1}H-NMR (DMSO-d_6): δ 3.32 (*s*, 3H, OMe), 6.90-7.29 (*m*, 4H, anisole protons), 7.33-7.59 (*m*, 10H, 2Ph), 9.68 (*s*, 1H, NH), 12.01 (*s*, 1H, pyrazole NH). Anal. Calcd for $C_{24}H_{19}N_5O$: C, 73.26; H, 4.86; N, 17.81. Found: C, 73.10; H, 4.70; N, 18.70.

The filtrate was evaporated under reduced pressure and the residue was triturated with diethyl ether to give (0.25 g, 38.01 %) of *N*-(4-methoxyphenyl)-4,5-diphenyl-1*H*-pyrazolo[3,4-*c*]pyridazine-3-amine **11**, m.p. 271-272 °C (from benzene). IR: 3320 (NH), 3054 (CH, aromatic), 2932, 2850 (CH, aliphatic), 1620 (C=N); ^{1}H-NMR (DMSO-d_6): δ 3.75 (s, 3H, OCH_3), 6.35 – 7.15 (m, 4H, anisole protons), 7.25 – 7.40 (m, 10H, 2Ph), 9.37 (s, 1H, NH), 12.15 (s, 1H, pyrazole NH); MS *m/z*: 393 (M^+, 30.1 %), 362 (M^+ - OMe, 4.0 %), 271 (M^+ - NHC_6H_4OMe, 3.0 %), 256 (M^+-NH, NHC_6H_4OMe, 100 %). Anal. Calcd for $C_{24}H_{19}N_5O$: C, 73.29; H, 4.83; N, 17.81. Found: C, 73.10; H, 4.90; N, 17.70.

Irradiation in diethyl malonate

Irradiation of compound **1** (1.0 g, .3.2 mmol) in diethyl malonate (150 mL). After 5 h the reaction mixture was evaporated under reduced pressure. TLC analysis of the crude product showed the presence of three compounds, which was separated through column chromatography (2.0 × 60 cm) on silica gel and was eluted with pet-ether 40/60 °C. The material was collected and recrystallized from chloroform to give (0.15 g, 34.3 %) of 3,4-diphenylpyridazine-5-carboxamide **12**, m.p. 267 – 268 °C.

IR: 3429, 3310 (NH), 3125, 3061 (CH, aromatic), 1663 (C=O amide), 1567 (C=N); ^{1}H-NMR (DMSO-d_6): δ 7.35 – 7.55 (m, 10H, 2Ph), 9.74 (s, 1H, H-6), 14.13 (s, 2H, NH_2); MS *m/z* : 274 (M^+, 26.4 %), 273 (M^+-1, 100 %), 258 (M^+ - NH_2, 10.1%), 230 (M^+ - $CONH_2$, 18.5 %). Anal. Calcd for $C_{17}H_{13}N_3O$: C, 74.16; H, 4.76; N, 15.27. Found: C, 74.00; H, 4.60; N, 15.10.

The second fraction was collected when eluted with petroleum ether (40/60 °C) - methylene chloride (8:2) gave (0.09 g, 10.85 %) of 3,4-diphenylpyridazine-5-nitrile **7**, m.p. 143-144 °C.

The third fraction was collected when eluted with methylene chloride-methanol (8: 2) gave (0.21 g, 37.1 %) of ethyl 4-carbamoyl-5,6-diphenylpyridazine-3-carboxylate **13**, m.p. 259–260 °C. IR: 3427, 3313 (NH_2), 3062, 3006 (CH, aromatic), 2931, 2885 (CH, aliphatic), 1739 (C=O ester), 1660 (C=O amide), 1600 (C=N), and 1444, 1269, 1076 cm^{-1} for the aromatic system; ^{1}H-NMR (DMSO-d_6): δ 1.2 (t, 3H, CH_3), 4.05 (q, 2H, CH_2), 7.28 – 7.54 (m, 10H, 2Ph), 14.13 (s, 2H, NH_2); MS */z m* : 347 (M^+, 1.6 %), 274 (M^+ - COOEt, 22.6 %, ion A), 273 (ion A – 74, 100 %, ion B), 157 (ion B –NH_2, 29.5%), 229 (M^+ - $COONH_2$, - COOEt, 11.2%). Anal. Calcd for $C_{20}H_{17N3}O_3$: C, 69.15; H, 4.93; N, 12.10. Found: C, 69.00; H, 4.80; N, 12.00.

REFERENCES

[1]Part 14: Amer, A. M., Zayed, M. F., Deeb, A., Ali, A., *J. Chem. Res*., **2005,** 643.

[2]Smith, P. A. S., *Azides and Nitrenes*, Ed. By Scriven, E.F.V., Academic Press, Inc., 1984, pp. 95-204.

[3]Bucher, G., Siegler, F., Wolff, J. J., *Chem. Commum*., **1999,** 2113 and references therein.

[4]a) Heinisch, G., Kopelent-Frank, H., *Progr. Med. Chem*., **1992**, *29*, 141-183., Ed., Ellis G.P. b) Tisler, M., Stanovnik, B., Adv. Heterocyclic Chem., **1990**, *49*, 385-474; Ed. Katritzy, A. R., Academic Press, San Diego

[5]Deeb, A., Kotb, M., *Heterocycles*, **2004,** *63*, 1143.

Received: 10.10.2013.
Accepted: 12.12.2013.

CATIONIC MICELLAR EFFECT ON THE REACTION BETWEEN DIPEPTIDE GLYCYL-ALANINE (GLY-ALA) AND NINHYDRIN WITH AND WITHOUT SALT ADDITIVES

Mohd. Akram,[a]* Adel A. M. Saeed[a] and Kabir-ud-Din[a]

Keywords: surfactant, dipeptide (Gly-Ala), ninhydrin, catalysis, micelles, TTAB, CTAB, CPC, salts

The effect of cationic conventional surfactants myristyltrimethylammonium bromide (TTAB), cetyltrimethylammonium bromide (CTAB), and cetylpyridinium chloride (CPC) on the interaction of dipeptide glycyl-alanine (Gly-Ala) with ninhydrin has been studied spectrophotometrically under different conditions. The reaction rates are higher in the presence of surfactants but the reaction order remains the same in both the media (first- and fractional-order with respect to [Gly-Ala] and [ninhydrin]). Quantitative kinetic analyses of k_ψ–[surfactant] data were performed on the basis of pseudo-phase model of the micelles (proposed by Menger and Portnoy and developed by Bunton and Romsted) and Piszkiewicz model wherein the micellar binding constants K_S for Gly-Ala and K_N for ninhydrin with surfactant micelles were evaluated. The catalytic efficiency in TTAB increased by added electrolytes which had been discussed in detail.

* Corresponding Authors
Tel: +91 09411040048
E-Mail: drmohdakram@rediffmail.com
[a] Department of Chemistry, Aligarh Muslim University, Aligarh–202002, India

Introduction

Surfactants are amphiphiles that contain polar or ionic head groups and apolar tails. They form association colloids, known as micelles, when they self-associate at concentrations above the critical micelle concentrations. In ionic head micelles, for example, the aqueous solution-micelle interfacial region contains the ionic head groups, the Stern layer of the electrical double layer with the bound counterions, and water. The remaining counterions are contained in the Gouy-Chapman portion of the double layer that extends further into the aqueous phase.[1]A micelle or a micellar aggregate constitutes an inhomogeneous microreaction environment, which is highly dynamic, in the sense that it is in rapid equilibrium with the constituent monomers in aqueous phase. So that, a micelle is not a separate phase, like aqueous phase, although it does provide microreaction medium, which is called pseudophase, in which micellar mediated reactions occur. Micellar catalysis of numerous reactions is an area of current research because of the parallel behaviour of macromolecules and enzymes.[2]

The ninhydrin (triketohydrindene hydrate)–mediated colour formation is the most widely used method for detection and quantitative estimation of amino acids/peptides.[3] The so-called *'ninhydrin reaction'* forms a product known as *'Ruhemann's purple'* which is attributed to be anion of diketohydrindylidenediketohydrindamine (DYDA), and this product can be quantitatively measured at 570 nm. To improve the sensitivity, however, modifications in the method are continuously being made.[3,4] In this regard studies by our group had shown success toward increased sensitivity of ninhydrin-amino acid reaction by involving surfactant micelles, solvents and complexation with metal cations.[5-10] As studies on ninhydrin-peptide reaction are limited,[11-13] systematic kinetic and mechanistic studies of the Gly-Ala-ninhydrin reaction in absence and presence of cationic micelles of myristyltrimethylammonium bromide (TTAB), cetylpyridinium chloride (CPC), and cetyltrimethyl-ammonium bromide (CTAB) at different temperatures have been performed. Also, it is found that various added salts can affect the overall course of the reaction. Therefore, the investigation concerns the reaction in aqueous and micellar media with and without salts.

Experimental Section

Materials and Methods

The surfactants (TTAB, ≥99%, Sigma, India; CPC, 99%, Merck, Germany; CTAB, 99%, Merck, Germany), glycyl-L-alanine (≥99% (NT), Aldrich, Switzerland), ninhydrin (99%, Merck, India), sodium acetate anhydrous (≥ 99%, Merck, India), acetic acid glacial (99-100%, Merck, India), sodium nitrate purified (99 %, Merck, India), sodium sulphate (≥ 98%, Merck, India), sodium phosphate (96%, Aldrich, USA) , sodium salicylate (99.5%, CDH, India), sodium benzoate (99.5%, Merck, India), sodium tosylate (70-80%, (HPLC), Fluka, Switzerland), and sodium oxalate (≥ 99.5%, S.D. Fine-chem Ltd., India) were used as received. Demineralized double-distilled water was used throughout the work (specific conductivity (Λ): $(0.8 – 2.1)\times10^{-6}$ $S^{-1}cm^{-1}$). Stock solutions of the reactants and the surfactants were prepared in acetic acid – sodium acetate buffer which was prepared by mixing acetic acid (0.2 mol dm^{-3}) and sodium acetate (0.2 mol dm^{-3}) up to desired volume.[14] The pH measurements were made using a digital Systronics pH meter model MK-VI (Ahmedabad-India) in conjugation with a combined electrode (glass-saturated calomel electrode) and standardized using WTW buffer solutions

(Germany). A Systronics conductivity meter model 306 (Ahmedabad-India) with platinized electrodes was used for the conductivity measurements.

Kinetic measurements

For each set of kinetic experiments, the requisite volumes of Gly-Ala, buffer and surfactant solutions (when required) were taken in a three-necked reaction vessel (also fitted with a double-surface water condenser), which was then kept in an oil bath at the experimental temperature. The reaction was started by adding a requisite volume of thermally equilibrated ninhydrin solution; zero-time was taken when half of the ninhydrin solution had been added. Pure N_2-gas (free from O_2 and CO_2) was bubbled through the reaction mixture for stirring as well as to maintain an inert atmosphere. Pseudo-first-order conditions were maintained in all the kinetic runs by using excess of ninhydrin over Gly-Ala concentration (≥10 times). The absorbance of the product DYDA was measured at 570 nm (λ_{max}-vide infra) at definite time intervals with a Shimadzu UVmini-1240 Spectrophotometer. Other details regarding kinetic methodology were the same as described elsewhere.[5-13]

Determination of CMC

The critical micellar concentration (CMC) values of the TTAB, CPC, and CTAB solutions under the experimental conditions were determined conductometrically. The values in the presence and absence of reactants have been obtained from the break points of nearly two straight line portions of the specific conductivity *vs.* concentration plots.[15] Experiments were carried out under different conditions, i.e., solvent being water, water + Gly-Ala, water + ninhydrin or water + Gly-Ala + ninhydrin and the respective CMC values are recorded in Table 1.

Viscosity measurements

Using Ubbelohde viscometer the viscosity measurements were made at 70 ± 0.1 °C. The method of viscosity measurements was the same as reported elsewhere.[16]

Results and Discussion

Spectra of the product

The UV-visible spectra of the product formed by the reaction between Gly-Ala and ninhydrin in the buffer solution were recorded in the absence and presence of surfactant micelles (Figure 1). We see that the absorbance is higher in presence of micelles than in aqueous medium with no shift in λ_{max}(570 nm), i.e., the wave length of maximum absorbance remains the same in both aqueous and micellar media. It is, therefore, concluded that the purple-coloured product of Gly-Ala reaction with ninhydrin to be the same in aqueous and micellar systems.

Table 1. The CMC values for CPC, CTAB, and TTAB at 30 ºC and 70 ºC using electrical conductivity technique.

System	CMC·10^3 mol dm^{-3} 30 ºC	CMC·10^3 mol dm^{-3} at 70 ºC
Pure CPC	1.06	1.40
CPC + Ninhydrin	1.26	1.35
CPC + Gly-Ala	1.05	1.29
CPC + Gly-Ala+ Ninhydrin	1.19	1.31
Pure CTAB	0.98	1.27
CTAB + Ninhydrin	1.29	1.41
CTAB + Gly-Ala	0.93	1.09
CTAB + Gly-Ala+ Ninhydrin	1.07	1.38
Pure TTAB	3.90	5.11
TTAB + Ninhydrin	4.32	5.40
TTAB + Gly-Ala	3.80	4.30
TTAB + Gly-Ala+ Ninhydrin	4.25	5.53

The kinetics of the reaction of glycyl-alanine and ninhydrin was, therefore studied under varying experimental conditions spectrophotometrically by following the appearance of purple colour at 570 nm. The results are described below.

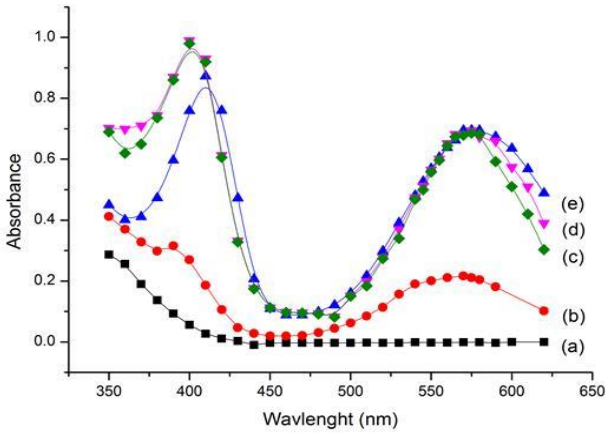

Figure 1. Spectra of reaction product of ninhydrin (6.0 x 10^{-3} mol dm^{-3}) with Gly-Ala (2.0 x 10^{-4} mol dm^{-3}), surfactant (20 x 10^{-3} mol dm^{-3}), pH = 5.0 and temperature = 70 °C in the absence of surfactant immediately after mixing the reactants (a) in the absence of surfactant (b), in the presence of TTAB (c), CTAB (d), and CPC (e), spectra (b) to (e) were recorded after the completion of the reaction

Dependence of Reaction Rate on pH

To find out the sensitivity of the reaction on the pH, the kinetic experiments were performed at pH varying from 4.0 to 6.5 while all other parameters were kept fixed in aqueous as well as in micellar media (Figure 2.).

Table 2. Dependence of pseudo-first order rate constants (k_{obs} or k_Ψ) on [Gly-Ala], [ninhydrin] and temperature at pH = 5.0.

10^4[Gly-Ala], mol dm^{-3}	10^3[Ninhydrin], mol dm^{-3}	Temperature, °C	10^5 k_{obs}[a], s^{-1}	$10^5 k_\Psi$[b], s^{-1}		
				TTAB	CTAB	CPC
1.0	6.0	70	13.0	60.9	61.7	30.2
1.5			13.5	63.2	64.4	30.8
2.0			14.1	63.9	65.1	30.2
2.5			14.3	61.0	62.6	29.6
3.0			14.6	64.8	60.6	27.9
2.0	6.0	70	14.1	63.9	65.1	30.3
	10		16.5	96.8	69.1	55.2
	15		31.5	110	95.9	55.5
	20		47.8	124	96.9	81.5
	25		45.5	122	106	81.7
	30		52.7	126	123	89.0
	35		53.5	123	120	85.8
	40		51.2	115	129	88.7
2.0	6.0	60	3.15	18.9	14.4	7.80
		65	8.23	33.2	49.9	17.6
		70	14.1	63.9	65.1	30.3
		75	20.8	101	96.9	36.7
		80	47.9	127	98.8	51.5

[a] in the absence of surfactant.[b] in the presence of [surfactant] = 20 x 10^{-3} mol dm^{-3}

It is observed that the optimum pH value is 5.0 and then the reaction rate becomes almost constant. Every elementary reaction of α-amino acids/dipeptides and ninhydrin depends upon the [H^+] because the reaction proceeds through the formation of an intermediate which has Schiff base linkage (>C=N-). The product of this reaction also has this type of linkage. Since the Schiff base formation is acid catalysed and pH 5.0 is the optimum pH, all subsequence kinetic runs were made at pH =5.0 (vide infra).

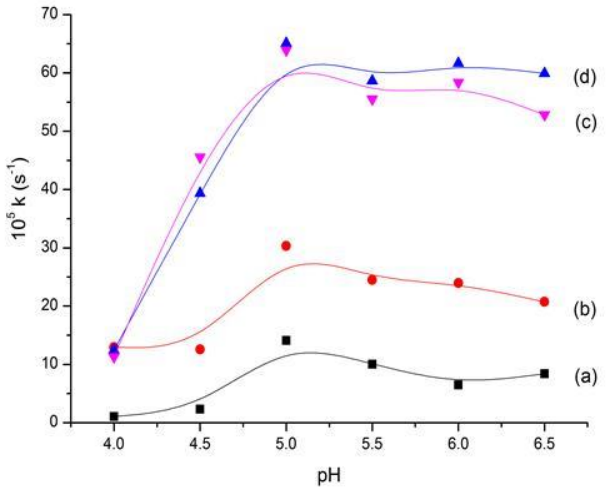

Figure 2. Plots of reaction rate constant vs. pH for the reaction of ninhydrin with Gly-Ala in the absence (a) and presence of [CPC] = 20 x 10^{-3} mol dm^{-3} (b), [TTAB] = 20 x 10^{-3} mol dm^{-3} (c), and [CTAB] = 20 x 10^{-3} mol dm^{-3} (d). Reaction conditions: [Gly-Ala] = 2.0 x 10^{-4} mol dm^{-3}, [ninhydrin] = 6.0 x 10^{-3} mol dm^{-3}, temperature = 70 °C.

Dependence of Reaction Rate on Gly-Ala Concentration

To find the dependence on [Gly-Ala], the reaction was carried out under pseudo-first-order conditions of [ninhydrin] >> [Gly-Ala] in the range of (1.0 x 10^{-4} to 3 x 10^{-4} mol dm^{-3} of [Gly-Ala] at constant [ninhydrin] of 6.0 x 10^{-3} mol dm^{-3}, temperature (70 °C) and pH (5.0). The k_{obs} values are recorded in Table 2. As the values of rate constants (k_{obs} and k_Ψ) were found to be independent of the initial concentration of Gly-Ala, the order of reaction with respect to [Gly-Ala] is unity in both the media.

Dependence of Reaction Rate on Ninhydrin Concentration

The effect of ninhydrin concentration was determined by carrying out a series of kinetic experiments at different concentrations of ninhydrin with fixed [Gly-Ala] (2.0 x 10^{-4} mol dm^{-3}), temperature (70 °C) and pH (5.0) constant (Table 2). The plots of rate constants *versus* [ninhydrin] (Figure 3) give non-linear profile and curved passing through the origin that indicates the order to be fractional with respect to [ninhydrin] in both the media.

Dependence of Reaction Rate on Temperature

A series of kinetic runs were carried out at different temperatures (60 to 80 °C), with fixed reactant concentrations both in the absence and presence of micelles (Table 2). The calculated rate constant values were found to satisfy the Arrhenius and Eyring equations. The activation energy (E_a) resulted from the slope of the lines of Figure 4. The activation enthalpy ($\Delta H^{\neq}$) and activation entropy ($\Delta S^{\neq}$) were calculated using linear least squares regression technique.

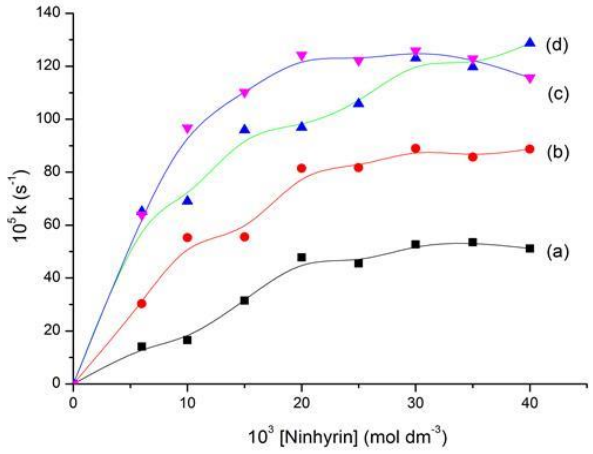

Figure 3. Effect of [ninhydrin] on the reaction rate of ninhydrin with Gly-Ala in the absence (a) and presence of CPC (b), TTAB (c), and CTAB (d). Reaction Conditions: [Gly-Ala] = 2.0 x 10^{-4} mol dm^{-3}, [surfactant] = 20 x 10^{-3} mol dm^{-3}, pH = 5.0, temperature = 70 °C.

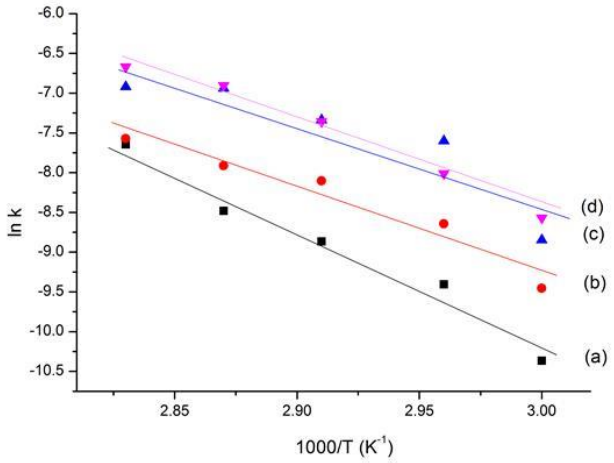

Figure 4. Arrhenius plot for the reaction of ninhydrin with Gly-Ala in the absence (a) and presence of CPC (b), CTAB (c), and TTAB (d). Reaction Conditions: [Gly-Ala] = 2.0 x 10^{-4} mol dm^{-3}, [ninhydrin] = 6.0 x 10^{-3} mol dm^{-3}, [surfactant] = 20 x 10^{-3} mol dm^{-3}, pH = 5.0.

Reaction in Aqueous Medium

On the basis of several studies made on the kinetics of amino acid-ninhydrin (triketohydrindene hydrate) reactions it has been established that the scheme involves oxidation of the amino acid to carbon dioxide and an aldehyde possessing a carbon atom less than the amino acid with the simultaneous reduction of the tri-ketone to hydrindantin and the condensation of the hydrindantin with the ammonia liberated by the oxidation of the amino acid, forming the blue coloured ammonium salt of diketohydrindylidene-diketohydrindamine (DYDA). Further, the amount of the coloured reaction product depends mainly upon temperature, pH and reactant concentrations. In the present case, condensqation between carbonyl group of ninhydrin and amino group of Gly-Ala takes place.[17,18] The reaction starts through the attack of lone-pair of electrons of amino nitrogen (of Gly-Ala) to the carbonyl carbon (of ninhydrin) to give Schiff base A (Scheme 1). This Schiff base is unstable and hydrolyses to give 2-amino indanedione, B, which reacts slowly with another ninhydrin molecule to yield the product P (DYDA).

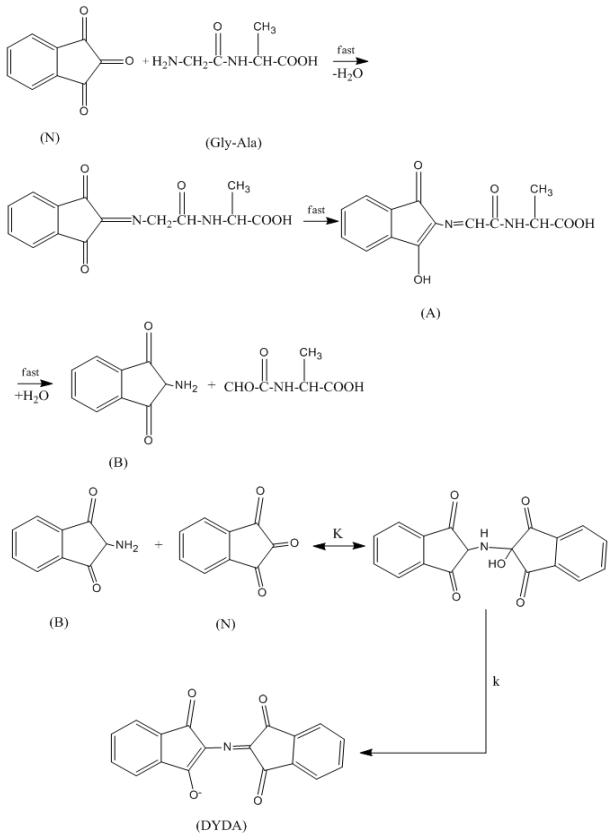

Scheme 1. Gly-Ala-ninhydrin reaction mechanism

On the basis of the observed rate law d[*P*]/d*t*= k_{obs} [Gly-Ala]$_T$ and the proposed mechanism (Scheme 1), the following rate equation is derived

$$k_{obs} = \frac{kK[Nin]_T}{1+K[Nin]_T} \quad (1)$$

where [Nin]$_T$ = total concentration of ninhydrin.

Alternatively,

$$\frac{1}{k_{obs}} = \frac{1}{k} + \frac{1}{kK[Nin]_T} \quad (2)$$

which envisages a straight line between $1/k_{obs}$ and $1/[Nin]_T$ with a positive slope (=$1/kK$) and an intercept (=$1/k$). Indeed it was found so (Figure 5), and thus confirmed the validity of the proposed mechanism. From the intercept and slope, the respective values of *k* and *K* were evaluated, which are: 1.23 x 10^{-3} s^{-1} and 6.87 $mol^{-1}dm^3$ respectively, in aqueous medium.

Reaction in the Presence of Surfactant Micelles

To investigate the surfactant concentration effect on the reaction rate, [TTAB], [CTAB], or [CPC] were varied at constant [ninhydrin] (6.0 x 10^{-3} mol dm^{-3}), [Gly-Ala] (2.0 x 10^{-4} mol dm^{-3}) and pH 5.0 at 70 °C (Table 3). The rate constant (k_Ψ) increased *ca.*4-5x with increase in [surfactant] from (0 to 30 x 10^{-3}) mol dm^{-3}; then the k_Ψ decreased noticeably (Figure 6).

Table 3. Effect of [TTAB] on the pseudo-first-order rate constants (k_Ψ) for the reaction of ninhydrin with Gly-Ala at pH = 5.0, [Gly-Ala] =2.0 x 10^{-4} mol dm^{-3}, [ninhydrin] = 6.0 x 10^{-3} mol dm^{-3} and temperature = 70 °C.

10^3[Surfactant], mol dm^{-3}	10^5 k_Ψ, s^{-1}			10^5 $k_{\Psi cal}$[a], s^{-1}			$(k_\Psi - k_{\Psi cal})/k_\Psi$		
	TTAB	CTAB	CPC	TTAB	CTAB	CPC	TTAB	CTAB	CPC
0	14.1	14.1	14.1						
1.0	15.7	14.0	15.2	14.3	13.0	14.0	+0.09	+0.07	+0.07
3.0	18.7	15.3	17.6	17.6	17.9	16.4	+0.06	+0.07	+0.06
5.0	26.5	34.5	18.4	23.4	31.5	17.4	+0.11	+0.09	+0.05
7.0	33.3	39.1	21.4	26.9	39.4	22.3	+0.19	-0.007	-0.04
10.0	40.5	49.9	26.8	43.9	46.8	27.1	-0.08	+0.06	-0.01
12.0	43.0	52.8	27.7	50.2	50.1	29.4	-0.17	+0.05	-0.06
15.0	47.6	53.2	28.6	56.1	55.1	31.2	-0.16	-0.04	-0.09
20.0	63.9	65.1	30.3	61.1	57.7	34.9	+0.04	+0.11	-0.15
30.0	59.4	63.6	32.6	62.8	62.0	38.2	-0.05	+0.03	-0.17
40.0	48.6	53.2	31.3	63.2	64.3	39.9	-0.30	-0.21	-0.28
50.0	45.3	50.3	31.2	64.3	65.3	40.2	-0.42	-0.29	-0.29
60.0	36.6	49.8	30.7	64.4	68.7	42.1	-0.76	-0.38	-0.37
70.0	30.4	35.9	28.3	65.7	70.1	44.1	-1.16	-0.95	-0.56
90.0	20.9	--	--	66.3			-2.17		
100.0	--	32.9	28.3		72.7	46.9		-1.21	-0.66

[a]calculated values using Eq. (3).

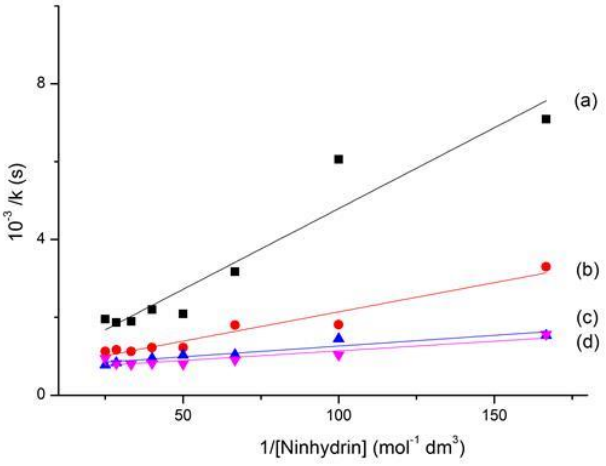

Figure 5. Plots of 1/*k versus* 1/[ninhydrin] for the reaction of Gly-Ala with ninhydrin in the absence (a) and presence of CPC (b), CTAB (c), and TTAB (d). Reaction Conditions: same as in Figure 3.

The existence of maximum in the k_Ψ – [surfactant] profile shape can be explained by considering that in this case, the reaction takes place in the aqueous as well as in the micellar pseudophases. The increase in rate constant at low surfactant concentrations results in an acceleration of the reaction because the organic substrate incorporates into the micelles and the contribution of the reaction occurring in the small volume of the micellar pseudophase (the so-called Stern layer) increases. However, as [surfactant] increases, a diminution in the Gly-Ala ion concentration in the micellar pseudophase is provoked by the greater number of micellar aggregates present in the reaction media. This effect is the one responsible for the decrease in k_Ψ observed at high surfactant concentrations.[19] Another reason for decreasing k_Ψ could be a result of counterion inhibition.

It was mentioned[20,21] that the head group size of the surfactant is one of the factors that decides the packing of the surfactant monomers into a micelle; if so, we would expect difference of packing of the CPC, CTAB and TTAB surfactant monomers. Of course, with aromatic pyridinium ring in CPC, there would be delocalization of charge as well as less charge shielding in comparison to CTAB and TTAB. Additionally, there may be an orientational effect. This effect must be taken into account with the effect of side chain (R) of the dipeptide to describe the reaction rate. The nature of k_Ψ-[surfactant] profile has been found experimentally similar with rate being CTAB ≈ TTAB > CPC (Figure 6).

The same first- and fractional-order kinetics for [Gly-Ala] and [ninhydrin], respectively, was followed in both aqueous and micellar media. Another thing, the absorption band of the product remains unchanged in the presence of TTAB, CTAB, or CPC micelles (Figure 1). Thus, we summarize that the reaction mechanism remains the same in the presence of conventional cationic micelles as that in aqueous medium.

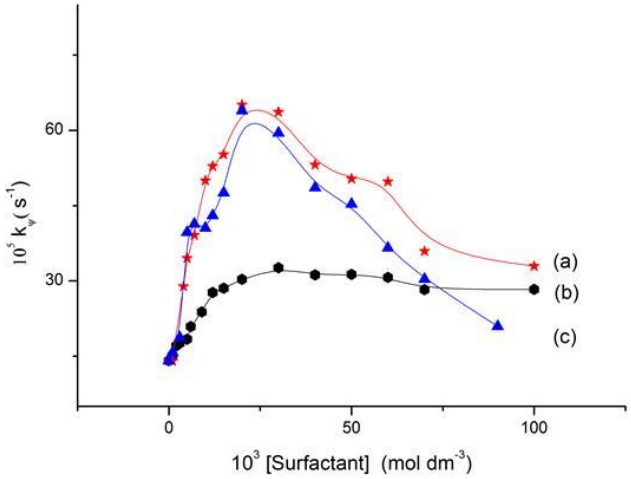

Figure 6. Effect of surfactant structure and concentration on the reaction rate for the interaction of ninhydrin with Gly-Ala. Reaction conditions: [Gly-Ala] = 2.0 x 10^{-4} mol dm^{-3}, [ninhydrin] = 6.0 x 10^{-3} mol dm^{-3}, pH = 5.0, temperature = 70 °C, in the presence of CTAB (a), CPC (b) and TTAB (c).

The rate increase for many reactions upon addition of surfactants has been explained on the basis of the following Scheme, proposed by Menger and Portnoy[22] and developed by Bunton[23] and Romsted.[24]

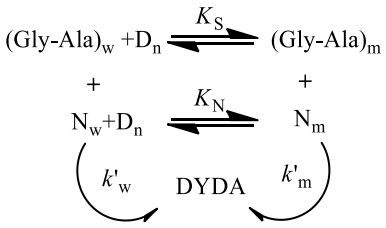

Scheme 2. The pseudo-phase model for the reaction of Gly-Ala with ninhydrin in micellar medium

Although several kinetic equations based on this general Scheme 2 have been developed, the most successful appears to be that of Romsted who suggested Equation (3), which takes into account the solubilization of both the reactants into micelles as well as mass action model

$$k_{\psi}=\frac{k_{w}[\mathrm{Nin}]_{T}+(K_{S}k_{m}-k_{w})M_{N}^{S}[D_{n}]}{1+K_{S}[D_{n}]} \qquad (3)$$

where k_w and k_m are the second order rate constants, referring to aqueous and micellar pseudo phases, respectively, K_S is the binding constant of the Gly-Ala to the cationic micelles, and $[D_n]$ = [surfactant] – CMC. M_N^S is the mole ratio of bound ninhydrin to the micellar head group, given by

$$M_{N}^{S}=\frac{[N_{m}]}{[D_{n}]} \qquad (4)$$

Values of M_N^S were estimated by considering the equilibrium

$$N_{w}+D_{n}\underset{}{\overset{K_{N}}{\rightleftharpoons}}N_{m}$$

$$K_{N}=\frac{[N_{m}]}{[N_{w}]([D_{n}]-[N_{m}])} \qquad (5)$$

and the mass balance

$$[\mathrm{Nin}]_{T}=[N_{w}]+[N_{m}] \qquad (6)$$

Calculation of k_m and K_S requires CMC under kinetic conditions which has been determined conductimetrically. For a given value of CMC, the k_m and K_S were calculated from Equation (3) using the non-linear least squares technique. Such calculations were carried out at different presumed values of K_N. The best value was considered to be the one for which the value of Σd_i^2 (where $d_i = k_{\psi obsi} - k_{\psi cali}$) turned out to be a minimum. The fitting of the evaluated data (K_S, k_m and K_N) to Equation 3 is evident from the calculated values of rate constants, $k_{\psi cal}$, recorded in Table 3.

The observed catalysis is due to the increased concentration of both ninhydrin and Gly-Ala in the Stern layer of micelles. Besides this, micelles also exert a medium effect influencing reactivity (the effect arises from a combination of cage, preorientation, microviscosity, polarity and charge effects).[25]

In order to calculate the dissociation constant of the micellized surfactant back to its components (K_D) and the index of cooperativity (n), the Piszkiewicz model,[26] analogous to the Hill model applied for the enzyme-catalysed reactions, was used. In the micellar systems, the value of n reflects the average number of surfactant molecules associated with each substrate molecule. The Piszkiewicz model relates n and K_D and its contribution to the rate is given by

$$k_{\Psi}=\frac{k'_{m}[D_{n}]^{n}+k'_{w}K_{D}}{K_{D}+[D_{n}]^{n}} \qquad (7)$$

On rearrangement, Equation (7) gives

$$\log\left(\frac{k_{\psi}-k'_{w}}{k'_{m}-k_{\psi}}\right)=n\log[D]-\log K_{D} \qquad (8)$$

According to Equation (8), a plot of $\log((k_{\psi}-k'_{w})/(k'_{m}-k_{\psi}))$ versus log[D] should be a straight line with a positive slope (n). Such a plot has been realized in the CPC, CTAB, and TTAB catalysis of the present study (Figure 7).

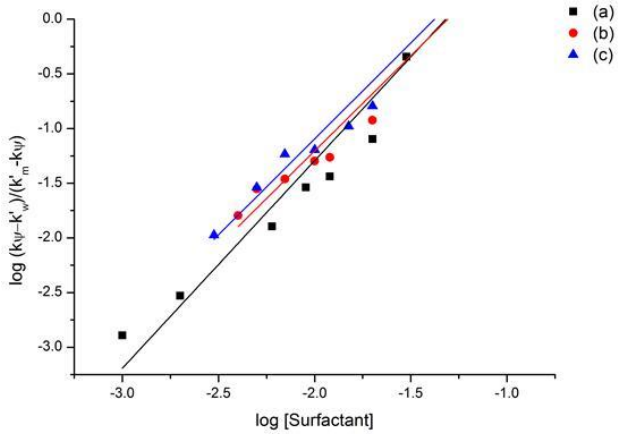

Figure 7. Piszkiewicz plot of log (k_Ψ – k'_w/ k'_m - k_Ψ) vs. log [Surfactant]. Surfactant = [CPC] (a), [CTAB] (b), and [TTAB] (c). Reaction Conditions: same as in Figure 6.

The K_D and n are: 1.29 x 10^{-3}, 1.9 (CPC), 3.49 x 10^{-3}, 1.74 (CTAB), and 1.12 x 10^{-3}, 1.76 (TTAB), respectively. A value of n greater than unity indicates positive cooperativity, i.e., the binding of the first molecule of the substrate makes it easier for subsequent molecules to bind. The advantage of Equation (8) is that it does not require the knowledge of CMC of surfactant used.

 DOI: 10.17628/ecb.2014.3.119-126

Activation parameters such as activation energy (E_a), enthalpy of activation ($\Delta H^{\neq}$) and entropy of activation ($\Delta S^{\neq}$), are summarized in Table 4. Comparing the values with those obtained in aqueous medium we find that the presence of surfactants lowers the $\Delta H^{\neq}$ with a substantial negative $\Delta S^{\neq}$. This lowering occurs not only through the adsorption of both the reactants on the micellar surface but also through stabilization of the transition state. The fitting of the observed k_Ψ at different temperatures to the equation was examined and it was found that the Eyring equation is applicable to the micellar media and the sensitivity of micelle structure to temperature is kinetically unimportant. A meaningful mechanistic explanation of the apparent values of $\Delta H^{\neq}$and $\Delta S^{\neq}$ is not possible because the k_Ψ does not represent single elementary kinetic step; it is a complex function of true rate, binding and ionization constants.

Table 4. Thermodynamic parameters, and k_m, K_S values for the reaction of Gly-Ala and ninhydrin at pH = 5.0 and temperature = 70 °C.

Parameters and constants	Aqueous	TTAB	CTAB	CPC
E_a (kJ mol^{-1})	127	98.1	87.9	90.0
$\Delta H^{\neq}$ (kJ mol^{-1})	124	95.3	85.1	87.2
$\Delta S^{\neq}$ (JK^{-1}mol^{-1})	-306	-297	-299	-305
$\Delta G^{\neq}$ (kJ mol^{-})	216	184	174	178
10^3 k_m (s^{-1})		0.74	8.62	5.54
10^3 k_w (mol^{-1}dm^3 s^{-1})		23.5	23.5	23.5
K_S (mol^{-1}dm^3)		270	214	162
K_N (mol^{-1}dm^3)		45.5	59.1	61.3

Salt Effect

The salt effect on micellar catalysis should be considered in the light of competition between the reactant(s) and counterion for micellar binding sites as well as their effect on the aqueous solubility of substrates. Experimentally, for the title reaction, this effect was explored in the condition of [TTAB] (20 x 10^{-3} mol dm^{-3}), [ninhydrin] (6.0 x 10^{-3} mol dm^{-3}), [Gly-Ala] (2.0 x 10^{-4} mol dm^{-3}), pH (5.0) at 70 °C (Tables 5 and 6). Salts, as additives, in micellar systems acquire a special place due to their ability to modify the systems' properties.[27]

Table 5. Effect of inorganic salts on pseudo-first-order rate constants (k_Ψ) for the reaction of ninhydrin with Gly-Ala at pH = 5.0, [Gly-Ala] = 2.0 x 10^{-4} mol dm^{-3}, [ninhydrin] = 6.0 x 10^{-3} mol dm^{-3}, [TTAB] = 20.0 x 10^{-3} mol dm^{-3}and temperature = 70 °C.

[Salt], mol dm^{-3}	10^5 k_Ψ, s^{-1}		
	$NaNO_3$	Na_2SO_4	Na_3PO_4
0	63.9	63.9	63.9
0.05	67.9	90.4	48.2
0.1	98.1	82.4	23.6
0.2	100	62.2	13.1
0.3	104	48.2	11.4
0.4	106	45.8	8.10
0.5	99.9	43.9	4.30
0.6	99.4	42.9	1.42
0.7	105	42.3	0.08
0.8	98.3	41.4	0.06
0.9	95.9	41.0	0.04

Table 6. Effect of organic salts on pseudo-first-order rate constants (k_Ψ) for the reaction of ninhydrin with Gly-Ala at pH = 5.0, [Gly-Ala] =2.0 x 10^{-4} mol dm^{-3}, [ninhydrin] = 6.0 x 10^{-3} mol dm^{-3}, [TTAB]= 20.0 x 10^{-3} mol dm^{-3}and temperature = 70 °C.

[Salt], mol dm^{-3}	10^5 k_Ψ, s^{-1}			
	NaSal	NaBenz	NaTos	$Na_2C_2O_4$
0	63.9	63.9	63.9	63.9
0.5	75.5	80.2	78.9	67.4
1.0	95.2	112	82.3	72.6
3.0	82.4	106	89.2	83.5
5.0	76.2	97.0	95.3	76.6
7.0	69.2	96.2	80.2	62.4
10.0	66.3	94.6	79.8	57.5
20.0	61.8	90.9	81.7	48.9
30.0	60.9	87.2	81.3	47.8
40.0	52.1	82.1	74.8	33.1
50.0	50.0	62.8	74.8	30.6
80.0	45.3	30.1	56.3	24.7

Figure 8 shows that the rate increases at low concentration of $NaNO_3$, and then becomes almost constant. However, in Na_2SO_4 a slight increase in the rate is observed, then a decrease which becomes almost constant. At low concentration range, the reactant solubility is affected and they are driven off toward the micellar surface. The increased concentration brings about increase in k_Ψ. When the salt concentration is high, the exclusion effect prevails with consequent decrease in k_Ψ. As regards Na_3PO_4, it shows a sharp decreasing effect.

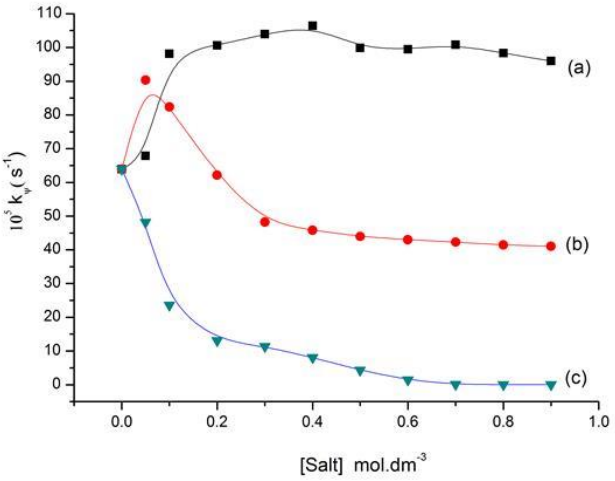

Figure 8. Effect of [inorganic salt] on the reaction rate for the interaction of ninhydrin with Gly-Ala in the presence of surfactant. Reaction Conditions: [Gly-Ala] = 2.0 x 10^{-4} mol dm^{-3}, [ninhydrin] = 6.0 x 10^{-3} mol dm^{-3}, [TTAB] = 20 x 10^{-3} mol dm^{-3}, pH = 5.0, temperature = 70 °C. $NaNO_3$ (a), Na_2SO_4 (b), Na_3PO_4 (c).

The main reason for this is the change in pH which equals ~ 12 which destroys the buffering effect. On the other hand, the biocompatible hydrophobic salts (the so-called *'hydrotropes'*) sodium salicylate (NaSal), sodium benzoate (NaBenz), sodium tosylate (NaTos), and sodium oxalate ($Na_2C_2O_4$) produce marked rate enhancement at low salt concentration, passing through a maximum as the [salt] was increased (Figure 9, Table 6).

 DOI: 10.17628/ecb.2014.3.119-126

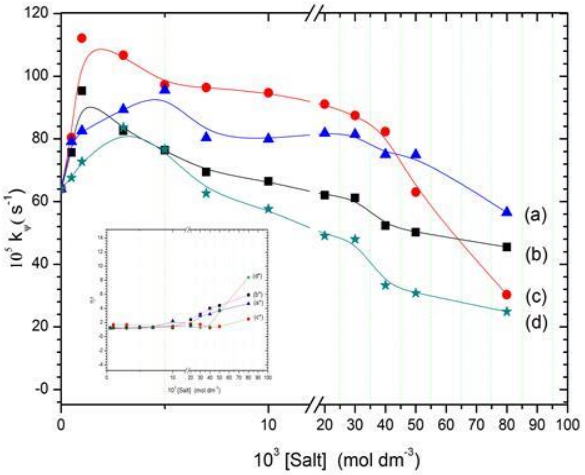

Figure 9. Effect of [organic salt] on the reaction rate (*a*, *b*, *c*, *d*) and on solution viscosity (*a**, *b**, *c**, *d**) (inset) for the reaction of ninhydrin with Gly-Ala in the presence of surfactant. Reaction Conditions: same as in Figure 8. NaSal (*a*,*a**), NaBenz (*b*,*b**), NaTos (*c*,*c**), $Na_2C_2O_4$ (*d*,*d**).

The addition of these organic hydrophobic salts means that we are adding ionic species having hydrophobic character and, therefore, they can interact with micelles both electrostatically and hydrophobically.[28] Therefore, in addition to neutralization of micellar positive charge, they will restrict solubilization sites to hydrophobic substrates. Thus, they catalyse the reaction by virtue of increased concentration of reactants in the Stern layer. The decreased rate observed at relatively higher concentrations of added organic salts is a consequence of the adsorption of hydrophobic anions at the micellar surface and the exclusion of substrate from the micellar surface. The progressive withdrawal of the substrate from the reaction site (micellar surface) would slow down the rate, as was indeed observed. Another factor which could inhibit the rate is the possible micellar growth at higher [salt] as reflected by viscosity data (Figure 9).

In our case the change in morphology from spheroidal micelles to rod-shaped (as inferred by viscosity increase) [29] would have certain changes on the characteristics of the micelle. In rod-shaped micelles the counterions bind more tightly and, therefore, suppress the interactions at the micellar surface.

Conclusions

Kinetic experiments between Gly-Ala and ninhydrin have been performed in aqueous and micellar media by studying the reaction spectrophotometrically at 570 nm. We found that the presence of conventional cationic micelles of TTAB, CTAB, and CPC accelerate the reaction and this is supported by comparing the values of activation parameters in both the media. Finally, we can conclude that interaction of Gly-Ala with ninhydrin in micellar media could successfully be treated using the pseudo-phase and Piszkiewicz models. Quantitative treatment of the kinetic data seems justified as k_ψ and $k_{\psi cal}$ are in close agreement within the experimental error.

Acknowledgement

One of the authors (Adel A. M. Saeed) thanks Aden University for providing financial support.

References

[1]Rosen, M. J., "*Surfactant and Interfacial Phenomena*", Wiley Inc., New Jersey, **2004**.

[2]Khan, M. N., "*Micellar Catalysis*", CRC, Taylor and Francis, USA, **2007**.

[3]Friedman, F., *J. Agric. Food Chem*., **2004**, *52*, 385.

[4]Joullie, M. M., Thompson, T. R. and Nemeroff, N. H., *Tetrahedron*, **1991,** *47*, 8791.

[5]Kabir-ud-Din, Salem, J. K. J., Kumar, S., Rafiquee, M. Z. A. and Khan, Z., *Colloids Surf. A*, **2000**. *168*, 241.

[6]Kabir-ud-Din, Akram, M., Rafiquee, M. Z. A. and Khan, Z., *Colloids Surf. A*, **2001**, *178*, 167.

[7]Kabir-ud-Din, Akram, M. and Khan, Z., *Inorg. React.Mech.*, **2003**, *5*, 1.

[8]Kabir-ud-Din and Fatma, W., *J. Phy. Org. Chem*., **2007,** *20*, 440.

[9]Kabir-ud-Din and Siddiqui, U. S., *Colloid J*., **2010**, *72*, 14.

[10]Khan, I. A., Bano, M. and Kabir-ud-Din, *J. Disp. Sci. Technol.*, **2010,** *31*, 177.

[11]Akram, M., Zaidi, N. H. and Kabir-ud-Din, *Int. J. Chem. Kinet.*, **2006**, *38*, 643.

[12]Akram, M., Zaidi, N. H. and Kabir-ud-Din, *J. Disp.Sci. Technol*., **2008**, *29*, 1.

[13]Akram, M., Kumar, D. and Kabir-ud-Din, *Int. J. Chem. Kinet.*, **2012**, *44*, 800.

[14]Humason, G. L., "*Animal Tissue Techniques*", Freeman, W. H., San Francisco, **1962**.

[15]Mukerjee, P. and Mysels, K. J., "*Critical Micelle Concentrations of Aqueous Surfactant Systems*", NSRDS-NBS 36, *Superintendent of Documents*, Washington, D. C., **1971**.

[16]David, S. L., Kumar, S. and Kabir-ud-Din, *J. Chem. Eng. Data*, **1997**, *42*, 198.

[17]Rafiquee, M. Z. A., Shah, R. A., Kabir-ud-Din and Khan, Z., *Int. J. Chem. Kinet.*,**1997**, *29*, 131.

[18]Akram, M., Kumar, D. and Kabir-ud-Din, *Eur. Chem. Bull.*, **2013**, *2*, 801.

[19]Rodríguez A., Múñoz, M., Graciani M. M. and Moyá M. L., *J. Colloid Interface Sci.*, **2002**, *248*, 455.

[20]Mukerjee, P. and Ray, A., *J. Phys. Chem*., **1966**, *70*, 2144.

[21]Lamothe, P. J. and McCormick, P. G., *Anal Chem.*, **1973**, *45*, 1906.

[22]Menger, F. M. and Portnoy, C. E., *J. Am. Chem. Soc.*,**1967**, *89*, 4698.

[23]Bunton, C. A., *Catal. Rev. -Sci. Eng*., **1979**, *20*, 1.

[24]Romsted, L. S., "*Micellization, Solubilization and Microemulsion*", Vol. 2, Mittal, K. L (ed.), Plenum Press, New York, **1977**.

[25]Tascioglu, S., *Tetrahedron*, **1996**, *52*, 11113.

[26]Piszkiewicz, D., *J. Am. Chem. Soc.*, **1977**, *99*, 1550.

[27]Fendler, E. J. and Fendler, J. H., "*Catalysis in Micellar and Macromolecular Systems*", Academic Press, New York, **1975**.

[28]Kabir-ud-Din, Fatma, W., Khan, Z. A. , and Dar, A. A., *J. Phys. Chem. B*, **2007**, *111*, 8860.

[29]Siddiqui, U.S., Khan, F. A. , Khan, I. A., Dar, A. A. and Kabir-ud-Din, *J. Colloid Interf. Sci.*, **2011**, *355*, 131.

Received: 22.10. 2013
Accepted: 13.12. 2013.

CONVERSION OF SUBSTANCES BY THE APPLICATION OF LASER RADIATION

T. A. Marsagishvili,[a] M. N. Machavariani[a] and G. D. Tatishvili[a]

Keywords: laser radiation; destruction; valence vibrations; chemical bond splitting

Theoretical model of laser destruction process of chemical compounds by laser radiation is proposed in the work. Models for calculation of vibration spectrum of molecule in nonregular condensed medium and for kinetic parameters of electron transfer and photo-transfer process between the particles are presented within the framework of quantum-mechanical approach. In terms of obtained analytic results it is proposed to calculate frequency spectrum for valence vibrations of atoms in molecule and to split corresponding chemical bonds by the help of laser emission. Obtained radicals may be used for formation of other chemical compounds, particularly, with application of laser emission also.

Corresponding Authors*
E-Mail: tamaz.marsagishvili@gmail.com
Fax: 995 32 301830
Tel: 995 32 301830
[a] Iv. Javakhishvili Tbilisi State University R. Agladze Institute of Inorganic Chemistry and Electrochemistry, 11, Mindeli str., Tbilisi, 0186, Georgia

Introduction

Interaction of electromagnetic radiation with condensed medium can be used for purposeful destruction (with break of definite chemical bonds), synthesis or both processes simultaneously.

The processes can be realized by different mechanisms dependent on frequency (or frequencies) of the electromagnetic radiation. Radiation of IR-region can be used for destruction process of some particles in condensed medium or molecules of medium. Synthesis of substances can be realized by two mechanisms at least: 1) transfer of definite reactants in electron-excited state with following forming of a reacting complex and corresponding photochemical reaction; 2) with help of direct out-sphere a charge photo-transfer, leading to forming of purposeful product.

The most interesting processes from the point of view of perspective of their application might be two-photon (or many-photon) processes, when the radiation of one of the sources can be used for dissociation (destruction) of definite particles with the aim of ions obtaining, from which is possible construction (synthesis) of the photochemical products. Several sources of electromagnetic radiation can be used for obtaining of ions from the several different reagents. The subsequent synthesis of products can be conducted with the help of the other source, which will provide realization of one of two out-sphere mechanisms (or both simultaneously).

Schematic picture with brief analytic calculations for explanation of suggested approach is given below.

Model of system

We assume, that we have condensed medium with reacting particles. The Hamiltonian of the system has the form:

$$H^{f} = H^{f}_{m} + H^{f}_{p} + H^{f}_{int} + H_{rad} + H^{rad}_{int} \qquad (1)$$

where H^{f}_{m} is the Hamiltonian of condensed medium, H^{f}_{p} is the Hamiltonian of particles, H^{f}_{int} is the Hamiltonian of interaction of particles with medium, H_{rad} is the Hamiltonian of electromagnetic radiation (of two and more sources), H^{rad}_{int} is the Hamiltonian of interaction of radiation with particles in medium and with medium.

As it was shown by the number of workers, first three components in the first part of the formula (1) can be transformed in frames of the certain model approximations[1,2] and formula (1) for adiabatic "*v*" electronic states of particles will have the form:

$$H^{v} = H_{m} + H^{v}_{p} + H_{int} + H_{rad} + H^{rad}_{int} \qquad (2)$$

where H_{p}^{v} is the Hamiltonian of the particles with "*v*" electronic states.

Vibration spectrum of polarizable diatomic molecule in polar media

The first problem is calculation of the vibration spectra of particles, which should be dissociated. A diatomic particle in polar condensed media will be used as an example for calculation of vibration spectra.

The shift of the vibration levels of the molecules during their transition from gas phase to condensed one is explained in literature by action of Van der Waals forces. Models used in that case are based on Onzager-Betcher theory,[3,4] and doesn't take into account the shift, induced by fluctuation of medium polarization. As a rule, these models

consider medium as structureless dielectric, and doesn't take into account the effects of space dispersion and frequency dispersion of dielectric polarization of medium.

For simplicity we shall consider uncharged diatomic dipole-active impurity particle in polar medium. The Hamiltonian of the system may be written down as:

$$H = H_m + H_p + H_{int} \quad (3)$$

where H_m is the Hamiltonian of medium; H_p is the Hamiltonian of particle; H_{int} is the Hamiltonian of interaction between them.

Interaction H_{int} can be divided into two components[5,6]

$$H_{int} = H_{int}^{(1)} + H_{int}^{(2)} \quad (4)$$

where $H_{int}^{(1)}$ is interaction of impurity with average polarization of medium <*P*> (the task of determination of <*P*> we shall consider as quasi-static):

$$H_{int}^{(1)} = -\int \langle P(r) \rangle E_0(r) dr \quad (5)$$

and $H_{int}^{(2)}$ is interaction of impurity with fluctuations of medium polarization:

$$H_{int}^{(2)} = -\int \delta P(r) E_0(r) dr \quad (6)$$

In formulae (5) and (6) $E_0(r)$ is electric field density, induced by impurity in point *r*.

In frames of the linear response theory the average value of the medium polarization in point *r* in quasi-static approximation can be expressed by Green function (*GF*) of medium polarization operators *P*, which characterizes polar medium, and by tensity of electric field of impurity *E*(*r*), which induces given average polarization of medium:

$$\langle P_i(r) \rangle = -\int G_{p_i p_k}(r, r'; \omega \to 0) E_k(r) dr \quad (7)$$

where $G(r,r',\omega)$ is Fourier representation of the temporal retarded GF of medium's polarization operators. Fourier representation of that GF can be expressed by complex dielectric permeability when ω→ 0, ε(*k*; ω→ 0). Particularly, for homogeneous systems:

$$G_{pp}(k,\omega) = -\frac{1}{4\pi}\left(1 - \frac{1}{\varepsilon(k,\omega)}\right) \quad (8)$$

In formula (5) it is assumed, that average polarization is equal to zero in absence of impurity. Expression analogous to E_0, where instead of gas phase dipole moment $\mu_0(r)$ will be written dipole moment in medium $\mu(r)$.

If impurity molecule is isotropic-polarized, then for dipole moment μ may be used the following expression:

$$\mu(r) = \mu_0(r) + \alpha(r) E(r) \quad (9)$$

where μ(*r*) is polarizability of the molecule; *E* is tensity of the electric field, which affects impurity molecule from medium.

The tensity of the electric field *E* can be expressed through GF of scalar potential operators $G_{\varphi\varphi}$:

$$E_i(r) = grad_{ri} \int dr' \, grad_{r'k} G_{\varphi\varphi}(r, r'; \omega = 0) P_k^{ex}(r') \quad (10)$$

where P^{ex} is polarization of impurity particle, for point dipole approximation $P^{ex}(r) = \mu\delta(r)$.

If intramolecular vibrations of impurity are described in harmonic approximation with frequency ω_s and equilibrium length $Q_0 = 0$, then consideration of interaction $H_{int}^{(1)}$ will bring to change of the square frequency and equilibrium length of this vibration:

$$\Delta\omega^2 = \frac{1}{2}\frac{\partial E_0}{\partial Q} G_{PP} \frac{\partial E}{\partial Q} \quad (11a)$$

$$\Delta Q = \frac{1}{4\omega_S}\left(\frac{\partial E_0}{\partial Q} G_{PP} E + E_0 G_{PP} \frac{\partial E}{\partial Q}\right) \quad (11b)$$

where $\Delta\omega$ is the change of intramolecular frequency of the particle and ΔQ is the change of equilibrium length of vibration.

This change of $\Delta\omega^2$ may be sufficiently large quantity in some cases and endow real contribution in dissociation of the particle.

Let's rewrite Hamiltonian of the system in such form:

$$H = H_{ms} + H_{ps} + H^{(2)}_{int} + F_s \quad (12)$$

where H_{ps} is Hamiltoninan of the particle in polar medium (with parameters ω^2 - $\Delta\omega^2$, *Q*-ΔQ) and F_s has the following form:

$$F_s = -\frac{1}{2} E^0 G_{pp} E \quad (13)$$

Expanding the tensity of electric field $E(r,Q)$ from the expression for $H_{int}^{(2)}$ into series up to linear term we obtain:

$$H_{int} = -\int \delta P E_0(r, Q=0) dr - \int \delta P(r) U(r) Q dr \quad (14)$$

$$U(r) = \left.\frac{\partial E}{\partial Q}\right|_{Q=0}$$

 DOI: 10.17628/ecb.2014.3.127-132

The first component in the right side of the expression results in change of equilibrium polarization of medium, and second one results in change of frequency spectrum of impurity and medium and oscillation damping of impurity.

Calculation method of frequency spectrum of the system, when the interaction of intra-molecular vibrations of impurity particle with fluctuations of medium polarization is taken into account was presented in work.[2] The expression for temperature GF of operators of normal coordinates of intra-molecular vibrations of diatomic dipole-active impurities was obtained in work:[2]

$$G_{QQ}(\omega_n)=\frac{1}{\omega_s^2+\omega_n^2-U(\omega_n)} \qquad (15)$$

$$\omega_n=2\pi nKT,$$
$$n=0;\pm1;\pm2,....,$$

where K is Boltzmann constant; T is Kelvin temperature, and renormalized interaction $U(\omega_n)$ characterized effects of interaction of impurity with medium:

$$U(\omega_n)=\int\frac{\partial E_i(r)}{\partial Q}G_{\delta P\delta P}(r,r';\omega_n)\frac{\partial E(r')}{\partial Q}drdr' \qquad (16)$$

For Green's function $G_{\delta P\delta P}$ we shall use factorization approximation according to space and time dispersion of dependence:

$$G_{\delta P\delta P}(r,r';\omega_n)=G(r,r')f(\omega_n) \qquad (17)$$

where $f(\omega_n)$ is normalization function of frequency dispersion of medium.

Here we'll choose the model, where frequency dispersion of GF of medium's polarization operators has resonance character:

$$f(\omega_n)=-\frac{C}{8\pi}\frac{\Omega_r^2+\gamma_2}{\omega_n}\times\left(\frac{1}{i\omega_n-\Omega_r+i\gamma}-\frac{1}{i\omega_n+\Omega_r+i\gamma}\right) \qquad (18)$$

where C, Ω_r, and γ are experimental parameters.

Equation for vibration spectrum of particle has form:

$$\omega_{1,2}=\omega_s\left[1+k\frac{\Omega_r^2+\gamma^2}{2}\frac{\omega_s^2-\gamma^2-\Omega_r^2}{(\omega_s^2-\gamma^2-\Omega_r^2)^2+4\gamma^2\omega_s^2}\right]-\frac{ik\gamma\omega_s^2(\Omega_r^2+\gamma^2)}{(\omega_s^2-\gamma^2-\Omega_r^2)^2+4\gamma^2\omega_s^2} \qquad (19a)$$

$$\omega_{3,4}=\Omega_r\left[1+k\omega_s^2\frac{2(\Omega_r^2+\gamma^2)(\Omega_r^2-\gamma^2-\omega_s^2)}{2\Omega_r^2\left[(\Omega_r^2-\gamma^2-\omega_s^2)^2+4\gamma^2\Omega_r^2\right]}\right]-i\gamma\left[1-\frac{k\omega_s^2(\Omega_r^2+\gamma^2)}{(\Omega_r^2-\gamma^2-\omega_s^2)^2+4\gamma^2\Omega_r^2}\right] \qquad (19b)$$

where, k is parameter of coupling with medium.

Depending on correlation of parameters ω_n, ω_s, Ω_r and k solutions of equation (19) describe vibrations with attenuation or pure attenuations. We'll cite solutions of equation (19) for most realistic model – when constraint force with medium is weak, when $k<<1$. In that case:

$$F(\omega)=-\omega^4-2i\gamma\omega^3-(\Omega_r^2+\omega_s^2+\gamma^2)\omega^2-2i\omega_s\omega+\omega_s^2(\Omega_r^2+\gamma^2)(1-k)=0 \qquad (20)$$

It is obvious, from obtained expressions, that consideration of interaction $U(\omega_n)$ brings to frequency shift and appearance of attenuation of these vibrations. It's easy to see that when $\omega_n<\omega_s$ one of the proper frequencies of the system shifts aside high energies.

The calculations of the vibration spectrum can be carried out in an analytical form for polyatomic particle also.

Electron transfer and photo-transfer processes

The second problem for photo-induced processes is a problem of an absorption spectrum of system in electronic region of the frequencies. It is possible to receive a correlation between kinetic parameters of chemical reactions and curve shape of light absorption in this region of frequencies.

The correlation function of GF formalism is one of the most general techniques for research of electron non-adiabatic charge-transfer processes in condensed media. It permits the development of a general theory capable of describing, from common point of view, charge-transfer processes in condensed homogeneous and heterogeneous systems; that is optical processes including charge-transfer processes in condensed media. This technique sets up different correlations between kinetic characteristics of dark processes and corresponding optical processes and makes it possible to analyze the kinetics of charge-transfer processes by means of the absorption curves.[2]

 DOI: 10.17628/ecb.2014.3.127-132

The rate constant for *n* particles of an electronic, non-adiabatic transition is:[5]

$$K_n = \frac{\beta V^{n-1}}{i\hbar}\exp(\beta F_i)\int d\theta Sp\left[e^{-\beta(1-\theta)H_i}Le^{-\beta\theta H_f}L^+\right]$$
$$\beta \equiv \frac{1}{k_B T} \qquad (21)$$

where H_i and H_f are the Hamiltonians for the ingoing and outgoing channels, F_i is the initial-state Gibbs energy, V is volume of the system, L is the electronic resonance integral; the integration contour, C_A, for the variable θ is parallel to the imaginary axis in the planar strip when $0 \le \mathrm{Re}\,\theta \le 1$; k_B is Boltzmann constant and T is the absolute temperature.

The rate constant, K_n within the Condon approximation can be represented in the form:

$$K_n = \int\prod_{i=2}^{n}\frac{d\rho_i\prod_\alpha d\varphi_{i\alpha}}{\Omega_0}\Phi_i(\rho,\varphi)\left|L_{fi}(\rho,\varphi)\right|^2 \times$$
$$\frac{\beta}{i\hbar}\int_{C_\theta} d\theta\exp\left[-\beta\theta\Delta F_m(\rho,\varphi)-\Psi_m(\theta)\right]\left\langle e^{\beta\theta H_i^v}e^{-\beta\theta H_f^v}\right\rangle \qquad (22)$$

where the angular brackets denote quantum-statistical averaging, ρ_i is the radius-vector of the center of gravity of the *i*-th particle with respect to the first particle, φ_α are three angles determining the orientation of the particle with respect to the first particle (as $\varphi_{\omega\alpha}$ can be used, for example, Euler's angles); Ω_0 is normalization factor, which is $8\pi^2$, or $4\pi^2$, or 1 (depending upon the particle symmetry); $\Phi_i(\rho,\varphi)$is the reactants distribution function which has the form:

$$\Phi_1(\rho,\varphi) = \left[\frac{\exp\left[-\beta F_1(\rho,\varphi)\right]}{\prod_{i=2}^{n} d\rho_1 \frac{1}{V\Omega_0}\int\prod_\alpha d\varphi_{1\alpha} e^{-\beta F_1(\rho,\varphi)}}\right] \qquad (23)$$

Here $F_i(\rho, \varphi)$ is the Gibbs energy of the system in the initial state with fixed value of reactants' coordinates ρ and φ.

In eq. (22) $\Delta G_m(\rho,\varphi)$ is the Gibbs energy change of the medium during the process at fixed values of reactant coordinates ρ and φ. Similarly, L_{fi} is the matrix element of the electronic resonance integral, H_i^v and H_f^v are vibrational Hamiltonians of the reactants and products, and the function $\Psi_m(\theta)$has the form:

$$\Psi_m(\theta) = (\pi\hbar)^{-1}\int\int dr dr'\Delta E_\alpha(r)\Delta E_\beta(r')\times$$
$$\int_{-\infty}^{\infty} d\omega \mathrm{Im}G^R(r,r';\omega)\,sh\frac{\beta\hbar\omega\theta}{2}\,sh\frac{\beta\hbar\omega(1-\theta)}{2}\left[sh\left(\frac{\beta\hbar\omega}{2}\right)\omega^2\right]^{-1} \qquad (24)$$

In eq. (24) $\Delta E(r)$ is the electronic field strength change of the reactants during the process and $G^R(r,r',\omega)$ is retarted Green function of the medium polarization operators. By using, for the factorization approximation,

$$\mathrm{Im}G^R(r,r';\omega) = \pi f(\omega)G^R(r,r';\omega=0) \qquad (25)$$

we obtain the following expression for $\Psi_m(\theta)$:

$$\Psi_m(\theta) = \frac{2E_r^m}{\hbar}\times$$
$$\times\int_{-\infty}^{\infty}\frac{d\omega}{\omega^2}f(\omega)\frac{sh\left(\frac{\beta\hbar\omega\theta}{2}\right)sh\left[\frac{\beta\hbar\omega(1-\theta)}{2}\right]}{sh\left(\frac{\beta\hbar\omega}{2}\right)} \qquad (26)$$

where E_r^m is reorganization energy of the medium

$$E_r^m = \frac{1}{2}\iint dr dr'\Delta E_\alpha(r)\Delta E_\beta(r')G^R_{\alpha\beta}(r'r';\omega=0) \qquad (27)$$

The function $f(\omega)$ can be determined from the experimental data of the frequency dependence of the dielectric constant of the system, considering different correlations between the Green functions and dielectric properties of the medium.[7]

The integration with respect of φ in eq. (22) is carried out in various ways. The simplest results are obtained for the case of strong coupling with the medium, when the integral can be calculated by the saddle-point method.

It must be noted that the expression in the angular brackets can also make allowance for such effects as ionic atmosphere fluctuation around the reactants (i.e. whatever can be described by vibrational degrees of freedom) in addition to the reactant vibrations.

For adiabatic processes it is essential to allow the interaction between the reactant electronic state and the vibrational degrees of freedom, which have been ignored so far. In particular, for limiting adiabatic processes, the allowance for additional low frequency relaxation degrees of freedom of the medium leads to the dependence of the pre-exponential factor in the rate constant expression on the characteristic relaxation time τ.[5]

$$K \approx (A/\tau)\exp(-\beta E_a) \qquad (28)$$

The Green function technique makes possible to analyze the kinetics of the elementary act of charge photo-transfer processes in detail.

According to the Lambert-Beer law, the optical density for absorption of the electromagnetic radiation is

$$D = \chi d \qquad (29)$$

 DOI: 10.17628/ecb.2014.3.127-132

where d is the thickness of the adsorbing layer and χ is related to the extinction coefficient ε, by the equation (29).[6-11]

$$\chi = \varepsilon_a c_a + \varepsilon_{ab} c_a c_b + \ldots \quad (30)$$

where c_a is the concentration of particle a and ε are the extinction coefficients. The first term in eq. (30) describes light absorption by isolated particles, both with transition into an excited state and with charge transfer from one part of a particle to another. The second term characterizes light absorption by reactants, which leads to charge photo-transfer between reactants.

The result of microscopic calculation of the extinction coefficient in the more complicated second term is given below. As for the first term, the expression for ε_a can be easily obtained from the expression for ε_{ab}.

If the absorption at the frequency ω_k, leading to a photo-transfer between n particles, occurs in the system with the volume V, then the extinction coefficient has the form

$$\varepsilon_n = \left(\frac{2\pi\hbar\omega_k}{c}\right) V^{n-1} \times \times \int_{C_\theta} d\theta e^{\beta\theta\hbar\omega_k} \left\langle e^{\beta\theta H_i} d_{fi}^{k\Lambda} e^{-\beta\theta H_f} d_{fi}^{k\Lambda} \right\rangle \quad (31)$$

where L is the absorbed photon polarization, H_i and H_f are initial- and final-state nuclear Hamiltonians of the system with no photons and $d_{fi}^{K\Lambda}$ is the dipole matrix element projection on the photon polarization vector.

Comparing the latter expression with that of the rate constant of the dark n-particle reaction, one can see, that the extinction coefficient can be derived from the rate constant of the dark reaction by the formal substitution in eq. (21)

$$L_n \to \sqrt{\frac{2\pi\hbar\omega_k}{c d_{fi}^{k\Lambda}}} \quad (32a)$$

$$\Delta F \to \Delta F - \hbar\omega_k \quad (32b)$$

If an exchange of heavy fragments does not occur during the charge transfer process, the medium can be represented by the linear approximation and a translational and rotational reactant motion can be represented by the classical approximation, then it is not difficult to obtain, for the extinction coefficient in the Condon's approximation,

$$\varepsilon_n = (2\pi\omega_k/3c) \int \prod_{i=2}^{n} d\rho \frac{\prod_x d\varphi_{i\alpha}}{\Omega_0} \Phi_i(\rho,\varphi) \frac{\beta}{i} \times \times \int_{C_\theta} d\theta \left\langle e^{\beta\theta[H_i(\rho,\varphi)+\hbar\omega_k]} d_{fi} e^{-\beta\theta H_f(\rho,\varphi)} d_{fi} \right\rangle_i \quad (33)$$

where $\theta_i(\rho,\varphi)$ is the reactant distribution function, ρ and φ are the coordinates of the i-th particle, determining the position ρ and the orientation φ with respect to the first particle. The expression in the angular brackets includes contributions to the extinction coefficient, both of the intra-molecular vibration degrees of freedom of the reactants and the vibration degrees of freedom, describing ionic atmosphere fluctuations around the reactants.

While the expression in the angular brackets in formula (33) is computed, the harmonic approximation allows this function to be calculated precisely. In so doing we obtain the following expression for the extinction coefficient

$$\varepsilon_n = (2\pi\beta\omega_k/3ic) \int \prod_{i=2}^{n} d\rho_i \frac{\prod_x d\varphi_{i\alpha}}{\Omega_0} \Phi_i(\rho,\varphi) |d_{fi}(\rho,\varphi)|^2 \times \int_{C_\theta} d\theta \exp\left\{\beta\theta[\hbar\omega_k - \Delta J(\rho,\varphi)] - \Psi(\theta)\right\} \quad (34)$$

where $\Delta J = \Delta F_m + \Delta J_v$; $\Psi(\theta) = \Psi_m(\theta) + \Psi_v(\theta)$; ΔJ_v is the difference between the minimal vibration energies and the function $\Psi_v(\theta)$ resembles the function $\Psi_m(\theta)$ in structure. To make it simple we take its form for the case when there is no mixture of normal coordinates in the beginning and at the end of the reaction. In this case

$$\Psi_v(\theta) = \prod_l \frac{2\exp\left[\theta\left(x_l^f - x_l^i\right)\right] sh x_l^i}{\left\{4sh^2\left[x_l^i\lambda + x_l^f\theta\right] - (1 - \frac{x_l^i}{x_l^f}) sh\left[2x_l^i\lambda sh(2x_l^f\theta)\right]\right\}^{1/2}} \times \exp\left\{-\frac{x_l^f (Q_{l0}^f - Q_{l0}^i)^2}{x_l^f cth x_l^i (1-\theta) + x_l^i cth x_l^f \theta}\right\} \quad (35a)$$

$$x_l^{i(f)} = \frac{\beta\hbar\omega_l^{i(d)}}{2} \quad (35b)$$

$$\lambda = 1 - \theta \quad (35c)$$

where ω_l^i and ω_l^f are the frequencies of vibrations in the initial and final states, and Q_{l0}^i and Q_{l0}^f are the equilibrium meanings of normal coordinates in the initial and final states.

In the case of strong coupling with the medium, when the integral over θ can be calculated by the saddle-point method,

$$\varepsilon_n = \frac{(2\pi)^{3/2}\beta\omega_k}{3c|\Psi_{\theta\theta}''|^{1/2}} \int \prod_{i=2}^{n} d\rho_i \frac{\prod_\alpha d\varphi_{i\alpha}}{\Omega_0} \Phi_i(\rho,\varphi) |d_{fi}(\rho,\varphi)|^2 \times \exp\left\{\beta\theta^*[\hbar\omega_k - \Delta J(\rho,\varphi)] - \Psi(\theta^*)\right\} \quad (36)$$

where the saddle-point θ^* can be determined from the equation

$$\beta(\hbar\omega_k - \Delta J) - \Psi_\theta'(\theta) = 0 \quad (37)$$

The expression for the extinction coefficient related to the absorption by isolated particles can be easily obtained from eq. (36), if we omit the factor $\Phi_i(\rho,\varphi)$, and integrals ρ, φ and the normalization factor Ω_0.

Discussion

In case when the initial substance is toxic, toxicity of some complex particles may be connected with presence of some functional groups. The reconstruction of exactly these functional groups is necessary for change of toxic properties. Thereto at the first stage it is necessary to break certain chemical bonds.

As obtained results have shown, selection of polar solvent is enough sometimes for dissociation of the particles see form. (11) and (19). If in this case the dissociation of the particles will not take place at least the change of vibration frequency will occur, in the direction of frequency decrease as a rule. Concentration of vibration energy on exact chemical bonds, e.g. of toxic molecules (nonequilibrium processes) is more effective method of particles destruction. Radiation exposure of given frequency on the systems (formula (19)) is necessary for this. Transfer of the particles in electron-excited state where dissociation of particle takes place is effective method as well. Extinction coefficient for these processes has the form (36).

Products obtained during destruction may recombine or take part in chemical processes thermally with other particles. To ensure passing of purposeful chemical processes probably is necessary to provide destruction of other molecules. Fragments of dissociated toxic molecule will interact with fragments of these molecules. Meanwhile it is necessary to influence the system by two sources of radiation at least.

The most interesting case is when photo-synthesis of new particles is realized from fragments of disrupted toxic molecules and fragments of other particles. Meanwhile it is necessary to use additional radiation source, which will ensure photosynthesis. The processes of direct out-sphere photosynthesis of new complex particles are described by formula (35), synthesis processes via electron-excited particles appropriately by expression of ε_a (formula (30)).

Conclusion

It is evident from the results of the investigations, that selection of polar solvent is enough sometimes for dissociation of the particles. Analytic expressions describing the processes of direct out-sphere photosynthesis of new complex particles, synthesis processes via electron-excited particles, extinction coefficient for transfer of the particles in electron-excited state have been obtained. Use of laser emission for splitting of specified chemical bonds and for formation of other chemical compounds is proposed as well.

References

[1]Dogonadze, R. R., Marsagishvili, T. A., *Methods of quantum field theory in electrodynamics of solvation*. "The chemical physics of solvation", Part A, chap. 2. "Elsevier", Amsterdam, **1985**, 39.

[2]Dogonadze, R. R., Marsagishvili, T. A., *Quantum theory of electronic and vibrational spectra of impurity molecules in polar media*. "The chemical physics of solvation", Part B, chap. 5. "Elsevier", Amsterdam, **1986**, 189.

[3]Onsager, L., *J. Am. Chem. Soc.*, **1936**, *58*, 1485.

[4]Buckingham, A., *Proc. Roy. Soc.*, **1956**, *A238*, 235.

[5]Zaqaraya, M. G., Marsagishvili, T. A., Khoshtaria, D. E., *Elementary processes in condensed media* (in Russian), "Mecniereba", Tbilisi, **1989**, 260.

[6]Marsagishvili, T. A., Machavariani, M. N., *Phys. Stat. Sol. (b)*, **1989**, *154*, 97.

[7]Platzman, P. M., Wolff, P. A., *Waves and interactions in solid state plasmas.* Academic press, N.Y. –London, **1973**.

[8]Khoshtariya, D. E., Kjaer, A. M., Marsagishvili, T. A., Ulstrup, J., *J. Phys. Chem.*, **1991**, *95*, 8797.

[9]Marsagishvili, T. A., *J. Electroanal. Chem.* **1998**, *450*, 47.

[10]Marsagishvili, T. A., *Kinetics of the elementary act of the processes of a charge transfer and phototransfer in irregular condensed systems* (in Russian). Chemistry and Chemical Technology, "Mecniereba", Tbilisi, **2001**, 191.

[11]Marsagishvili, T. A., *Russ. J. Electrochem.*, **2003**, *39*, 21.

Received: 31.10.2013.
Accepted: 14.12.2013.

AQUEOUS AND ALCOHOLIC EXTRACTS FROM *GLYCYRRHIZA GLABRA* AND THEIRS ACTIVITY AGAINST BACTERIA AND RHABDOMYO SARCOMAS

Omar Hamad Shehab Al-Obaidi[a]

Keywords: *Glycyrrhiza glabra* extracts, antibacterial and anticancer activity, extraction, isolation, Rhabdomyo sarcoma

Active substances such as Saponins (41.1 %), volatile oils (2.5 %) and Tannins (13.2 %) are isolated from *Glycyrrhiza glabra* plant, and some mineral elements such as sodium (203 ppm), calcium (176 ppm) and potassium (181 ppm) respectively from the *Glycyrrhiza glabra* seeds. The concentration of the mineral elements was measured by using Flame Spectrometer. Also a study of anti-bacterial activity of the extracts was made using two types of pathogenic bacteria viz., Escherichia Coli and aurous Staphylococcus showed the ability of inhibition for all different extracts by vary inhibition diameters for different active substances, concentrations and bacteria. One type of cancer cellular line used to study the effect of *Glycyrrhiza glabra* extracts were studied on the growth of *Rhabdomyo sarcomas* (RD) cell line in human by using *in vitro* system and compared with anticancer drug cisplatin (cis-pt) as a positive control. The cancer cell were treated with different concentration for each of the three treatments and cis-pt after 72 h exposure time. The cytotoxic activity was tested by inhibition rate as parameter. The results showed significant differences ($p < 0.05$) for each three treatments when the inhibition rates were increased. There was strong correlation between the three treatments and the different concentrations in comparison with cisplatin.

* Corresponding Authors
Fax:
E-Mail:
[a] Department, Women Education College, Al-Anbar University, Anbar, Iraq

Introduction

Liquorice or licorice is the root of *Glycyrrhiza glabra* from which a somewhat sweet flavor can be extracted. The liquorice plant is a legume (related to beans and peas) that is native to southern Europe and parts of Asia. It is not botanically related to anise, star anise, or fennel, which are sources of similar flavouring compounds.

Figure 1. Glycyrrhiza glabra

The source of scent of liquorice root is from a complex and variable combination of compounds present in the root, of which anethole is a minor component (0-3 % of total volatiles). Much of the sweetness in liquorice, which is obtained by boiling liquorice root and evaporating most of the water, is due to glycyrrhizin, which has 30–50 times the sweetness of sugar. The sweetness is very different from that of sugar, being less instant and longer lasting. Liquorice extract is marketed both in solid and syrup form.

The isoflavene glabrene and the isoflavane glabridin, found in the roots of liquorice, are xenoestrogens. [1]

***Glycyrrhiza glabra* from Koehler's Medicinal-Plants**

The compound glycyrrhizic acid, found in liquorice, is now routinely used throughout Japan for the treatment and control of chronic viral hepatitis, and there is a possible transaminase-lowering effect.[2] Hepatoprotective mechanisms have been demonstrated in mice.[3] Recent studies indicated that glycyrrhizic acid disrupts latent Kaposi's sarcoma (also demonstrated with other herpesvirus infections in the active stage), exhibiting a strong anti-viral effect.[4] The Chinese use liquorice to treat tuberculosis.[5]

Liquorice affects the body's endocrine system as it contains isoflavones (phytoestrogens). It might lower the amount of serum testosterone slightly [6], but whether it affects the amount of free testosterone is unclear. Consuming liquorice may prevent the development of hyperkalemia in persons on hemodialysis.[7] Large doses of glycyrrhizinic and glycyrrhetinic acid in liquorice extract can lead to hypokalemia and serious increases in blood pressure, a syndrome known as apparent mineralocorticoid excess. These side effects stem from the inhibition of the enzyme 11-hydroxysteroid dehydrogenase (type 2) and subsequent increase in activity of cortisol on the kidney. Cortisol acts at the same receptor as the hormone aldosterone in the kidney and the effects mimic aldosterone excess, although aldosterone remains low or normal during liquorice overdose. To decrease the chances of these serious side effects, deglycyrrhizinated liquorice preparations are available. The disabling of similar enzymes in the gut by glycyrrhizinic acid and glycyrrhetinic acid also causes increased mucus and decreased acid secretion.

As it inhibits *Helicobacter pylori*, it is used as an aid for healing stomach and duodenal ulcers, and in moderate amounts may soothe an upset stomach. Liquorice can be used to treat ileitis, leaky gut syndrome, irritable bowel syndrome and Crohn's disease as it is antispasmodic in the bowels.[8]

The compound carbenoxolone, derived from liquorice, indicated that it inhibited 11-hydroxysteroid dehydrogenase (type 1), an enzyme that is highly expressed in liver and fat tissues, which plays a role in metabolism, and in the brain, where the same enzyme is involved in stress response that has been associated with age-related mental decline.[9]

Excessive consumption of liquorice or liquorice candy is known to be toxic to the liver[10] and cardiovascular system, and may produce hypertension[11] (acquired pseudohyperaldosteronism) and edema.[12] In occasional cases, blood pressure has increased with excessive consumption of liquorice tea, but such occasions are rare and reversible when the herb is withdrawn.[13] Most cases of hypertension from liquorice were caused by eating too much concentrated liquorice candy.[14] Doses as low as 50 grams (2 oz) of liquorice daily for two weeks can cause a significant rise in blood pressure.[15]

Experimentals

(Cis-platin) (10 mg/20ml) was provided by Ebew (Austria). *Glycyrrhiza glabra* was obtained from the local market. *Glycyrrhiza glabra* was grounded and kept at a laboratory temperature until use. 40 g of powdered *Glycyrrhiza glabra* was placed in a conical flask containing 200 mL of distilled water and stirred with a magnetic blender for 30 minutes and then centrifuged for 15 minutes. The supernatant liquid was kept at 35 ℃ in an electric furnace until the extract was obtained hich was the suitably diluted to give 5, 10, 15, 20 and 25 % solutions,

Alcoholic extract was obtained from putting 50 g of *Glycyrrhiza glabra* powder in an extraction unit (Soxhlet) and 350 ml of 80 % ethanol was added and boiled at 40 ℃ for 12 hours . The alcoholic extract was then obtained by using Vacuum Rotary Evaporator at 35 °C.[16] The extract was the diluted to desired dilutions with 80 % ethanol.[17]

Isolation of active components

A: Tannins

Tannins were isolated from *Glycyrrhiza glabra* by adding 75 ml of distilled water to 0.5 g of *Glycyrrhiza glabra* powder. The mixture was placed in the boiling water bath for 30 minutes. It was then centrifuged at 200 cycle min^{-1} for a period of 20 minutes .The solution was next transferred to a 100 mL flask and made up to the mark with distilled water. A 20 mL of of 4 % lead acetate was added and the mixture was continuously shaken for some time before filtering it. The sludge was dried at 70 °C in an electric furnace.[18]

B: Saponins

To 10 g of *Glycyrrhiza glabra* powder was added (50 mL of 20 % ethanol and then heated at 55 °C using a water bath for half an hour with constant stirring. It was then filtered and the filtrate was added to 100 ml of ethanol. This solution was then heated at 90 ºC in a water bath till the final volume was reduced to about 40 mL. It was then filtered and the filtrate was transferred to 20 mL of ether in a separating funnel. The ether mixture was shaken for some time and allowed to stand till the water and ether layers separated. The water layer was separated and added to 10 mL of n-butanol and shaken vigourously. The n-butanol was then evaporated in the water bath. The resulting solution was dried to get saponins.[17,18]

C: Volatile oils

Volatile oils were extracted from 5 g of *Glycyrrhiza glabra* powder mixed with 150 ml of ether in a Soxhlet flask. The extraction process was carried out for a period of 24 hours when the volatile oils were separated from the ether solvent.[19]

D: Determination of ash content

Ash content was estimated by burning 2 g of *Glycyrrhiza glabra* powder in an oven at 550 °C till a the powder turned into a gray italics white and then the weight of the form a second time to calculate the percentage of ash.[20]

E: Determination of moisture

The percentage of moisture was estimated from 2 g of *Glycyrrhiza glabra* powder which was heated at 60 ℃ in an electric furnace for a period of 24 hours. It was then taken out and weighed again to estimate the proportion of moisture.[20]

F: pH measurement

10 g of *Glycyrrhiza glabra* powder was blended with 100 ml of distilled water using magnetic stirrer for 10 minutes. The pH of the supernatant liquid wasmeasured using pH-Meter.

G: Qualitative detection of components

The components of *Glycyrrhiza glabra*, such as semi-alkaloids, carbohydrates, saponin and flavonoids, lipids, proteins, and tannins, were qualitatively detected from the extract of Glycyrrhiza glabra as follows.[20,21]

Study of the activity against bacteria

The sensitivity of bacteria, *Escherichia Coli* and *Aurous Staphylococcus* bacteria (isolated from *Glycyrrhiza glabra* and diagnosed in the culture laboratory of Children's Hospital in Ramadi) was measured using the Agar-well diffusion method as described by Kirby Baauer.[22] We also used the Mueller Hinton agar to test the sensitivity of bacteria from *Glycyrrhiza glabra* extracts, prepared using the process as per instructions of the company. It was then placed in Petri dishes which were put in an incubator at 37 °C for 24 hours. The inhibition diameter was then measured (inhibition zone)[22] in each hole by a ruler.

Preparation of standard solutions of isolated substances from *Glycyrrhiza glabra*:

A series of solutions containing 5%, 10%, 15% 20% 25% mg mL^{-1} of different extracts were prepared.

 DOI: 10.17628/ecb.2014.3.133-137

Study of cytotoxic effect on cancer cell line

One type of cancer cell lines was used to study the impact of the extracts from *Glycyrrhiza glabra* powder on the growth of cells in laboratory to know the specifications of extracts to act as an antitumor (work was carried out at the Department of Cancer Research in Biotechnology Research Center, University of Nahrain).

All solutions were prepared at the same center and culturing tissues were studied in vitro under optimum conditions by the same center. The growth media used in tissue culture technique was MEM (Minimum Essential Media), provided by Fetal Calf Serum (10 %) to form a confluent monolyer, then Subculture to discard the previous growth medium and the cell washed with sterilized phosphate buffer solution (PBS) by autoclave at 121 ºC for 15 min and addition 2-3 min and moving the culture flask kindness. The trypsin-versene solution to discard and cells incubated at 37 ºC until the cell separation from ground flask, added new growth media and redistribution of cells at the microtiter and incubated at 37 ºC.[23]

Statistical Analysis

Data were analyzed by ANOVA. Investigation of differences between cis-platin and the relation with other groups by toward using the statistical program (SPSS) within significant level ($p<0.05$) [24].

Result and discussion

The results of the phytochemical (screening of plant materials) studies of the *Glycyrrhiza glabra* are presented in Table 1.

Table 1. Chemical substances effective in *Glycyrrhiza glabra*

Active Compounds	Reagents	Indicators	Results
Alkaloids	Draggendorff	orange	+
Tannins	$FeCl_3$, Lead acetate	Greenish blue solution, ge-latinous ppt.	+
Intense Tannins	Lead acetate	Light Brown ppt.	+
Flavonoids	Ammonia solution	Yellow solution	+
Amino acids	Alnhidran	purple	+
Phenols	Potassium ferrocyanide	Greenish blue ppt.	+
Resins	Aq. HCl	Turbid	-
Terpenoids	Salkowski	dark red	+
Saponins	$HgCl_2$	white ppt.	+
Carbohydrates	α-naphthol	Purple	+
Loco antho-cyanidins	Aq. HCl	Red ppt.	+
Steriods	Terpenoids reagent after 1 d	Blueish solution	+
Glycosides	Benedict	red precipitate	+

(+) indicate the positive test; (-)indicate the positive test

According to the results shown in Table 1. the aqueous extract of *Glycyrrhiza glabra* plant contains flavonoids, phenols, terpenoids and tannins, etc.

Table 2 and Fig. 1 show the percentage of active contents that were isolated from *Glycyrrhiza glabra* and the percentage of saponins, tannins and volatile oils are (41.1 %, 2.5 % and 13.2 %) respectively, where it is noted that the percentage of moisture (2.1 %) , ash (1.6 %) and pH (6.35).

The percentage values in the plant depend on several factors, including climatic related to different temperatures and different seasons of the year as the high temperature leads to the loss of more water, and that the decline reduces the loss of water from the plant.[17]

Total carbohydrates = 100 - (% moisture +% crude protein

+% crude fat +% ash content)

The percentage of protein and carbohydrates about 96.3%. which is consistent with the calculated ratios of previous studies.[25]

Table 2. Percentage of active combatants in Glycyrrhiza glabra

Active combatants	Percentage
Volatile oils	2.5 %
Tannins	13.2%
Saponins	41.1%
Moisture	2.1%
PH	6.35
Ash	1.6%

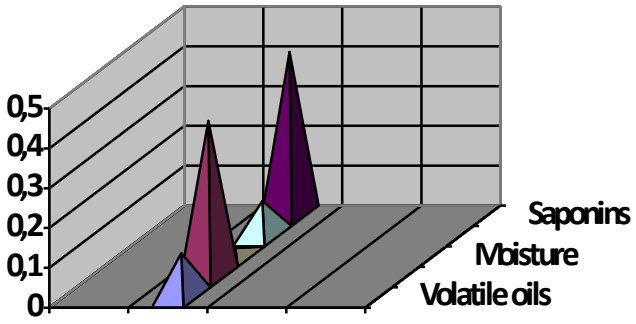

Fig. 1. The percentage of extracted material

Table 3 and Fig. 2. show the amount of mineral elements in *Glycyrrhiza glabra* where the result showed that contains sodium (203) ppm, calcium (176) ppm and potassium (181) ppm, all are important functional and metabolic metals for body.[24]

Table 3. The amount of mineral elements in *Glycyrrhiza glabra* measured by Flame Spectrometer.

Concentration (ppm)	Symbol	Element
Sodium	Na	203
Calcium	Ca	176
Potassium	K	181

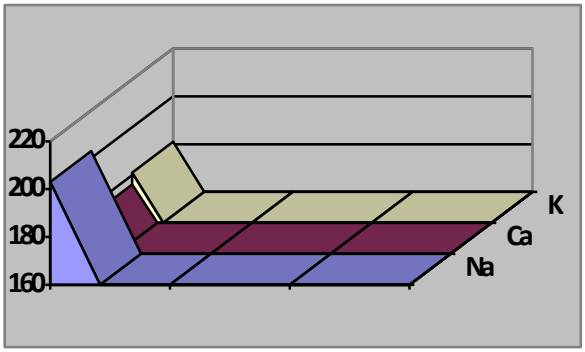

Figure 2. Shows the percentages of elements in the extract of *Glycyrrhiza glabra*

Tables 4 and 5 shows a the anti-bacterial activity results of *Glycyrrhiza glabra* extracts. The activity have been studying for these extracts separately, in different concentrations and using two types of pathogenic bacteria *Escherichia Coli* and *Aurous Staphylococcus*. The water extracts of *Glycyrrhiza glabra* shown higher activity at 25 mg ml^{-1}, where inhibition diameter was 15 mm for *Staphylococcus aurous* and 12 mm for *Escherichia Coli*, followed by the rest of the varying concentrations and rates Table 4.

The inhibition action of alcohol extract is due to it contained *Glycyrrhiza glabra*, flavonoids, tannins, and include some of phenolic compounds which have a biological influence on many bacteria races due to the presence of hydroxyl groups ($-OH^-$), as it have the ability to form hydrogen bonds between hydroxyl group in these compounds and water molecules in bacterial cell, were water is (90 %) of weight and that will disables dynamic actions in bacterial cell.[26] These compounds as phenolic compounds have the ability to coagulation the bacterial cell proteins and destroy enzymes involved in the manufacture of necessary amino acids to increase cell division.[27]

Table 4. Effect of aqueous extract of *Glycyrrhiza glabra* in different concentrations on growth of pathogenetic bacterial races

Conc. in mg ml^{-1}	Inhibition diameter	
	Aurous Staphylococcus	*Escherichia Coli*
25	12	13
20	11	10
10	9	9
10	7	7
5	4	5

Table 5. Effect of alcoholic extract of *Glycyrrhiza glabra* in different concentrations on growth of pathogenesis bacterial races

Conc. in mg ml^{-1}	Inhibition diameter	
	Aruginosa Pseudomonas	*Escherichia Coli*
25	12	15
20	10	12
10	8	10
10	7	8
5	5	6

In general, from Tables 4 and 5 for all extract and in all prepared concentrations the influence almost equal against bacteria *Aurous Staphylococcus* and *Escherichia Coli*. It found that inhibition diameter for aqueous extract is bigger than for the rest of the extracts of other due to the varying rate of active materials in different extracts.

Study of Cytotoxic Effect

Cancer cell lines were used to study the effect of Glycyrrhiza glabra extracts on the growth of cells in laboratory to know the specifications of extracts as anti-tumors. Cancer cell line type mice transformed cell line (RD) used with different concentrations comparable with anticancer drug cisplatin as a positive control after 72 h. exposure time.[30]

In this method, we calculate the proportion of cells number within the optimal conditions for growth without the addition of extracts so the output is the control group (control). Then extracts are added for the purpose of knowing their effects on cell growth in elected lines.

Extracts were divided into three groups, first group included a hot water extract, second group included hot alcoholic extract, third group Cis-Pt.

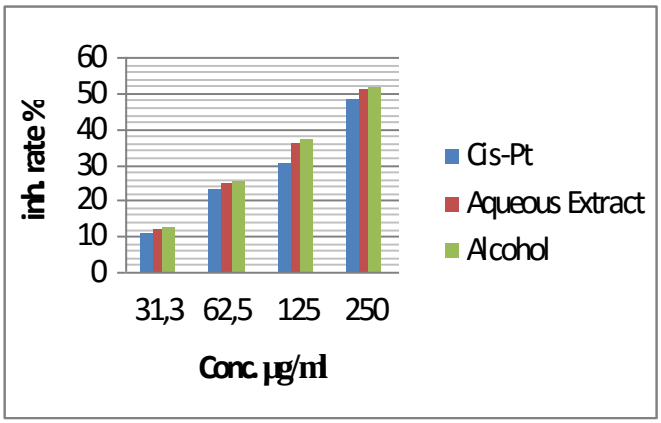

Figure 3. The comparison of inhibition rates between three treatments with cis-pt drug in cell line (RD)

Table 6. Inhibition effect on cancer line (RD) with different concentrations of extract and cis-pt after 72 h exposure time.

Treatment conc. µg ml^{-1}	Inhibition rates %		
	Cis-Pt	Aqueous Extract	Alcohol Extract
31.25	10.55	11.98	12.10
62.5	22.95	24.88	25.49
125	30.1	35.65	36.99
250	47.97	50.76	51.45

The result statistically analyzed by one way ANOVA. the following results as Fig. 3. which demonstrates the impact of compounds on cells number ratio when using cell line (RD), it is clear that hot alcoholic extract have the greatest influence on the proportion of growth cell number and the effect was significantly (p <0.05). This result is identical to those published in literature.[28,29]

 DOI: 10.17628/ecb.2014.3.133-137

Also the effect of aqueous extract was significant effect (P <0.05) but the percentage of inhibition - as in the scheme 4- less effect than alcoholic extract Table (6).

REFERENCES

[1]Tamir, S., Eizenberg, M., Somjen, D., Izrael, S. and Vaya, J., *J. Steroid Biochem. Mol. Biol.*, **2001**, *78(3)*, 291-298.

[2]Shibata, S., *Yakugaku Zasshi*, **2000**, *120(10)*, 849–62.

[3]Lee, C. H., Park, S. W., Kim, Y. S., Kang, S. S., Kim, J. A., Lee, S. H. and Lee, S. M., *Biol Pharm Bull*. **2007** , *30(10)*,1898-904

[4]Curreli, F., Friedman-Kien, A. E., Flore, O., *J. Clin. Invest.*, **2005,** *115(3)*, 642-652.

[5]Ferrell, V., Archbold, E. E., Cherne, H. M., 'Natural Remedies Encyclopedia' Fourth Edition, 2004, 412.

[6]Yokota T., Nishio, H., Kubota, Y., Mizoguchi, M., *Pigment Cell Res*., **1998,** *11(6)*, 355-61 .

[7]Farese, S., Kruse, A., Pasch, A., Dick, B., Frey, B. M., Uehlinger, D.E., Frey, F.J., *Kidney Intern.*, **2009,***76 (8)*, 877–84.

[8]Winston, D., Steven, M., *Adaptogens: Herbs for Strength, Stamina and Stress Relief*. Healing Arts Press., **2007.**

[9]Sandeep, T. C., Joyce, L.W., Yau Alasdair M., MacLullich, J., Noble, J., Deary, I. J., Walker, B. R. and Seckl, J. R., *Proc., Natl. Acad. Sci.*, **2004**, *101 (17)*, 6734–6739.

[10]*The Nurse's Guide To Herbal Remedies from Salisbury University*.

[11]*Liquorice and hypertension*. Editorial in *The Neth. J. Med.*, **2005.**

[12]*A Guide to Medicinal and Aromatic Plants from Purdue University*.

[13]Dharmananda, S., Ph.D., Safety Issues Affecting Herbs: Herbs that May Increase Blood Pressure, **2010.**

[14]*Woman 'overdoses' on liquorice*, BBC News online, **2004**.

[15]Sigurjnsdttir, H. A., Franzson, L., Manhem, K., Ragnarsson, J., Sigurdsson, G. and Wallerstedt, S., *J. Human Hypertension*, **2001**, *15*, 549-552.

[16]Harborne, T. B., *Phytochemical methods*. Halasted Press. John Wiley & Sons, New York., **1973**, 178.

[17] Ba-Angood, S. A., Ermel K. and Schumutterer H., *Univ. Aden J. Natural Appl. Sci.*, **1996**, *1*, 13-25.

[18]Francis, G., Kerem, Z., Makkar, H. P. S. and Becker, K., *Brit. J.f Nutr.*, **2002**, *88*, 587–605.

[19]Dewar, M. J. S., Zoebisch, E. G., Healy, E. F., Stewart, J. J. P., *J. Am. Chem. Soc.*, **1990,** *107*, 3902.

[20]Sageska, Y. M. and Uemura, T., *Yaugaku Zasshi*, **1997**, *116(3)*, 238.

[21]Pavia, D. L., Lampman, G. M. and Kriz, G. S., *Organic Chemistry*, Mason, Ohio, **2004,** *3*, 653.

[22]Vandpitte, J. and Verhaegen, J., *Basic laboratory procedures in clinical bacteriology*, WHO, Geneva, **1991**, 78-110.

[23]Freshney, R. I., *Cultured of Animal Cells: A manual for Basic Techniques*, Inc. Publication, New York, **2000**, 64-69.

[24]Al-Mohammed, N. T., Al-Rawi, K. M., Younis, M. R. and Al-Morani, W. K., *Principles of Statistics*, Al-Mousl Univ., **1986,** *7*, 50-52.

[25]Herrera, E., Barbas, C., *J. Physiol. Biochem.*, **2001**, *57(2)*, 43–56.

[26]Allan, G., Robert, A., Denis, St. J., Michael, J. S. and James, S., *An illustrated colour text clinical biochemistry*, 2nd ed., UK, **1999** , 106 -114.

[27]Grimshow, J., *Depsides, Hydrolysable Tannins, Lignans, Lignin and Humic Acid.* **1976**, *vol. 111*, Part D. Amsterdam: Elsevier Science Publishing Co.

[28]Yin, F., Giuliano, A. E., Van Herle, A. J., *Thyroid*, **1999**, *9(4)*, 369–76.

[29]Jing, Y., Waxman, S., *Anticancer Res.*, **1995**, *15(4)*, 1147–52.

Received: 10.11.2013.
Accepted: 14.12.2013.

STUDIES ON THE LEVEL OF HEAVY METALS IN THE ANTARCTIC FISH

M. Sjahrul

Keywords: Antarctic fish; accumulation of heavy metals; *Pagothenia borchgrevinki*

The level concentration of metallic elements (Hg, Cd, and Fe, Mn, Zn, Cu, Pb, and Ni) in muscles and liver tissue, which have a tendency to accumulate different metals, of marine fish (*Pagothenia borchgrevinki*) in the Antarctic ocean is investigated. With the view that it may lead to a further investigation of the quality of the Antarctic ocean environment.

* Corresponding Authors
E-Mail: eddievedder_jie@yahoo.com
[a] Department of Inorganic Chemistry, Faculty of Sciences, University of Hasanuddin Makassar, Indonesia

Introduction

Heavy metals and other trace elements in aquatic environment are generally natural constituents.[1] They occur in these media as result of the weathering of soils and rocks, from volcanic eruptions, and from a variety of human activities such as the mining, processing, or use of metals or substances that contains metal contaminants[2] and from the atmospheric input of many substances into the oceans.[3]

Metals in the ocean have a specific biological response[4] and a tendency to attach themselves to the marine organisms and undergo bioaccumulation.[5]. Although some metals such as Mn, Fe, Cu and Zn are essentials micronutrients necessary to promote the growth of marine organisms. However, an accumulation of these metals and Hg, Cd and Pb even in small amounts become hazardous to marine lives. Because fishes accumulate trace metals from their environment, they are excellent organisms for the study of long term changes in trace elements in the envionment.[6] Therefore, the concentrations of heavy metals in various tissues and organs of marine fish, *Pagothenia borchgrevinki* from the Antarctic ocean were investigated.[8] The analysis of the concentrations of trace elements in individual organisms of fish showed that the metallic elements are concentrated in particular organs. [7] The level composition of metal ions in tissues of marine fish (*Seriola grandis*) from New Zealand (North Island) followed the order : Zn>Fe>Cu>Mn>Pb>Ni>Cd.[8] The liver tissue of arctic cod (*Boreogadus saida*) from Strathcona sound, northern Baffin Island were found to have a level of metal concentration in the order: Zn>Fe>Cu>Cd. Previously it was shown that concentration of Mn, Fe and Zn decreased with size[9] as do concentration of Cu and Zn in whole striped bass fingerlings (*Morone saxatilis*) for wet weights less than 15 gram.[10] For striped bass ranging from 15 to 60 gram, concentration of Cu and Zn were constant with weight.

Muscle tissue of fish is one of the means for investigating the amount of heavy metals entering the human body by consumption of the fish as food chain, and has therefore been investigated more than other organs. On the basis of the varying affinities of the metals for the in individual organs, the fish muscle tissue proves not to be suitable for determining the extent of the heavy metal contamination of the entire organism. The absolute increase of heavy metals in muscle tissue of contaminated fish is often much lower than other organs.[11] In addition, the ability of organisms to concentrate trace elements is one of very great complexity and little information's is known concerning physiological processes that regulate the concentrations of trace metals in marine organisms. There are no reports about the relation between the bioaccumulation of metallic elements in individual tissue and size of antartict marine fish.

Materials and Methods

Materials

Twenty two Antarctic fish (*Pagothenia borchgrevinki*) were caught during 22nd Japanese Antarctic Research Expedition (JARE). The fish were collected around syowa station (69º00 S, 39º35'E) Antarctica.

All specimens appeared to be in good healthy conditions, with no macroscopic pathological symptoms. All of them were kept frozen at about 20 ºC until analysis. Body organs were dissected and excided. Samples of skin, muscle, liver, testis, ovary and other organs were separated and wrapped in plastic pocket and weighed and then frozen until next analysis.

Determination of Heavy Metals

For analysis of the heavy metals, homogenized samples of tissue and organ (0.2-5 g in wet weight) were digested in a nitric, perchloric and sulfuric acid mixture, and other organs (bone and muscle mixture) samples in nitric, and perchloric acid mixture. The resultant solutions were then diluted to a known volume with deionizer water, and the concentrations of Fe, Zn and Mn were directly measured by atomic absorption spectrophotometry (AAS). The concentrations of Hg was determined by Flameless AAS after adding $SnC1_2.H_2SO_4$ solution. The Cu, Pb, Ni and Cd, were extracted with methyl isobutylketon (MIBUK) and determined after chelation with sodium diethyl-dithiocarbamate (DDTC) using ASS.[12]

Results and Discussions

Levels of Heavy Metal Concentrations

The concentration of Fe, Mn, Zn, Cu, Pb, Ni, Cd and Hg distributed in individual tissues and organs of fish (*Pagothenia borchgrevinski*) are shown in Fig,1, which showed that affinities of metals for the individual tissue and organ of fish is different.

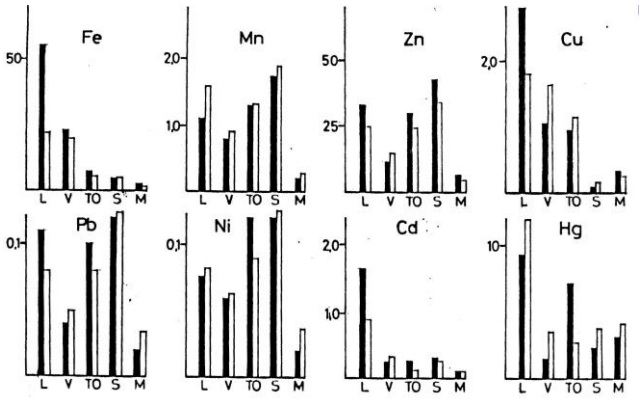

Figure 1. Comparison of heavy metal concentrations (μg g^{-1}, wet weight) in liver, other viscera, gonads, skin and muscle tissue of *Pagothenia borchgrevinki*. L-liver; V-viscera except for liver; T-testis; O-ovary; S-skin; M-muscle: ■ male □ female

The highest concentration ratios of (Mn, Zn, Pb and Ni) (Hg) : (Fe, Cu, Cd, and Hg) : (Cu, Pb, and Cd) : (Fe, Cu and Cd), and (Ni) are found in the skin, muscle, liver, ovary or testis, other organs, and bone and muscle mixture respectively. Among the tissues and organs of fish only in the lowest area except the mercury (Hg). It is also to be noted that the highest percentage of Fe, Mn, Zn, Cu, Pb and Ni, about 49-70% is present in bone and muscle; cadmium is present in liver tissue in about 42 %, whereas mercury is present in muscle tissue in about 44 % (Fig.2).

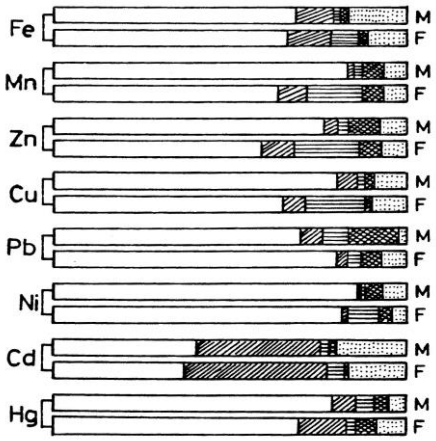

Figure 2. Percentage of tissue burden to body burden of heavy metals in *Pagothenia borchgrevinki*,

▭: muscle+bone; ▨: liver; ▬: testis (ovary); ▩: skin ▭: other viscera; M-Male, F-Female

This fact is evident from the tendency of metals to accumulate in different tissues and organs, and that the accumulation is different for different metals. The differences in the distribution of heavy metals in body organs are probably due to the differences of constituent composition in the tissue and organ of fish, such as protein lipids, blood content etc.

Distribution of Heavy Metals in Tissues and organs

The results of the variations of the concentration of Fe, Mn, Zn, Cu, Cd, Pb, Ni and Hg in muscle, liver tissue and whole body of fish (*Pagothenia borchgrevinki*) from Antarctic ocean are discussed here. As seen in table 2 fish (*Pagothenia borchgrevinki*) caught in the Antarctic ocean averaged lower concentration of Fe, Mn, Zn, Cu, Cd, Pb, Ni and Hg in the muscle than in the liver tissue. These results are same as observations for seven species of (*Chondrichtyes*) and that the concentration of Cu, Cd and Zn metals was higher in liver than in muscle tissue.[13,14] The mean concentration of cadmium and iron from seven individual arctic cod (*Boreogadussaida*) was also found higher in liver than in the muscle.[15] The highest values of Zn, Cu, Cd, Pb, and Hg metals were found to have a greater variation coefficient in the liver than in the muscle in 42 black marlin (*Macaira indica*) from unpolluted water of Northeast Australia.[11]In order to confirm further this tendency, determination of the ratio of metal concentration levels in liver to muscle tissue were carried out; it was found for Fe 15.22 : 1, Mn 5.42 : 1, Zn 4.97 : 1, Cu 5.74 : 1, Pb 2.42 : 1 Ni 2.38 : 1 Cd 47.22 : 1 and for Hg 2.0 : 1. These findings appeared to indicate that liver has great ability to accumulate these eight metals when compared with muscle tissue. The similar ratio for Cu 1600 : 1 and Zn 47 : 1 were found in (*Epinephelus striatus*) by Taylor and Bright.[16]

It is further necessary to know the level of chemical composition of metallic elements present in muscle and liver tissue of fish (*Pagothenia borchgrevinki*) because both muscle and liver tissue lare mostly edible parts, which are r possibly unfit for human consumption from a toxicological point of view[17-22] considered using the fish tissue as indicator organisms for the heavy metals pollution.. As shown in the Table 1, the chemical composition of mean concentration level of each metal combined in muscle and liver tissue of fish (*Pagothenia borchgrevinki*) are such as summarized as follows :

Muscle Zn > Hg > Fe > Cu > Mn > Pb > Ni > Cd

Liver Fe > Zn > Hg > Cu > Mn > Cd > Pb > Ni

The next case indicated that in muscle tissue, range coefficient variation are 0.155 for Zn and 0.652 for Cu, while in liver tissue it was found 0.123 for Zn and 0.875 for Ni. These results are in agreement with the range of 0.1 – 1.0 which is of the same range of coefficient of variation of various components in organisms as pointed out by Eberhardt.[23]

The results mentioned above are explained on the basis that the concentration of metals differ greatly between different parts of fish organs in particular in muscle and liver tissue of the same fish.

Table 1. Metal concentrations (μg g^{-1} wet weight) in muscle, liver, and whole body of *Pagothenia borchgrevinki*

Metal	Muscle			Liver			Whole Body		
	n*	**Mean**	**Range**	***n****	**Mean**	**Range**	***n****	**Mean**	**Range**
Fe	(22)	2.07±0.98	(1.04-4.34)	(18)	31.5 ± 19.6	(7.30–83.3)	(22)	4.99 ± 1.65	(2.52–10.65)
Cv		0.474			0.621			0.332	
Mn	(22)	0.24 ± 0.07	(0.10–0.46)	(18)	1.30 ± 0.60	(0.42–2.94)	(22)	0.65 + 0.16	(0.33-1.03)
Cv		0.307			0.463			0.251	
Zn	(22)	5.65 ± 0.88	(4.27–8.15)	(18)	28.1 ± 3.46	(22.4-34.2)	(22)	11.21 + 1.72	(8.73–14.92)
Cv		0.155			0.123			0.154	
Cu	(22)	0.43 ± 0.28	(0.17–1.39)	(18)	2.47 ± 1.58	(0.92–5.88)	(22)	0.75 ± 0.33	(0.38–1.73)
Cv		0.652			0.64			0.448	
Pb	(22)	0.12 ± 0.06	(0.02–0.28)	(18)	0.29 ± 0.24	(0.04–0.96)	(22)	0.13 ± 0.05	(0.02–0.29)
Cv		0.558			0.833			0.423	
Ni	(22)	0.08 ± 0.04	(0.02–0.23)	(18)	0.19 ± 0.17	(0.04–0.66)	(22)	0.08 ± 0.02	(0.05–0.17)
Cv		0.55			0.875			0.278	
Cd	(22)	0.02 ± 0.01	(0.01–0.04)	(18)	0.85 ± 0.52	(0.30–2.46)	(22)	0.07 ± 0.03	(0.02–0.12)
Cv		0.451			0.606			0.494	
Hg**	(22)	5.2 ± 1.9	(2.3–8.7)	(18)	10.4±5.52	(5.0–26.3)	(22)	2.69 ± 0.85	(0.9–4.7)
Cv		0.356			0.533			0.317	

* Number of samples analyzed; ** Ng/g, wet weight Cv = Coefficient variation

These concentrations difference in the tendency of metals to bind to the various molecular groups is found within the cells of each fish, as well as to the degree of the exposure to the metal as influenced by its metabolic characteristic.[2]

Conclusions

The experimental fish (*Pagothenia borchgrevinki*) was collected from the 22nd Japanese Antarctic Research Expedition (JARE). The concentrations of Fe, Mn, Zn, Cu, Ni, Pb, Cd, and Hg were determined by atomic absorption spectrophotometry. It was found that the tendency of metal to accumulate in the individual tissue and organs of the fish is different for each metal. Mean concentration of these metals in twenty two of fish are found higher in the liver than muscle tissue. The concentration rations of these metals in liver to muscle tissue are found for Fe 15.22 : 1, Mn 5.42 : 1,Zn 4.97 : 1, Cu : 5.74 : 1 Pb, 2.42 : 1, Ni 2.38 : 1, Cd 47.22 : 1 and Hg 2.0 : 1.

Acknowledgments

The author wishes to acknowledge his indebtedness to Professor Dr. R. Tatsukawa, chairman of Department of Environmental conservation, faculty of Agriculture, Ehime University, for his kindness, guidance and valuable support during the two years of study in his Department.

The author also expresses gratitude to Associate Professor T. Wakimoto, and to Mr. S. Tanabe and to Mr. M. Kawano and to Mr. K. Honda, Department of Environmental Conservation, for their assistance and direct guidance in the conduct of this work.

The author wishes to express his thanks to Associate Professor M. Azuma, Nagasaki University, for his helpful suggestion and cooperation with respect to the identification and collection of biological samples, and to Mr. H. Hidaka, Department of Environmental Conservation, Ehime University who collected the Antarctic samples during JARE 22

The author would also like to acknowledge Dr. Z Kawabata for his kind supervision of the manuscript.

The author also thanks Mr. K Maruyama, Mr. N Oka and many students in the laboratory of the Department of Environmental conservation for their assistance with the sample collection and chemical analysis and preparation of some figures and data processing.

The author also likes to express his grateful thanks to the local public officials of Kohyogi town, Nagasaki prefecture, who extended us their kind assistance and support.

Finally, my genial thanks are also extended to all members of the Department of Environmental conservation, for their Kindness and cooperation during two most enjoyable and meaningful years..

References

[1]Murphy, B. C. Jr., Spiegel, S. J., *J. Water Pollut. Control Fed*., **1982**, *54(6)*, 849.

[2]Laws, E. A., *Aquatic pollution*, John Willey & Sons, New York, **1981**, 301-36

[3]Zoller W. H.,E.S Gladney, *Atmospheric concentrations and source metals at the South Pole*, Science **1974,** *183*,198-200.

[4]Leland, H. V., Copenhaver, E. D., Corriill, L. S., *J. Water Pollut. Control Fed*., **1974,** *46, II*, 1452

[5]Goldberg, E.D., *Minor elements in seawater*, In J.P, Riley and G. Skirrow (Ed) Chemical oceanography, Academic Press, London,**1965**, *1* ,163 – 196

[6]Lucas, H. F., Jr., Edgington, D. N., Col, P. J., *J. Fish Res. Board Can*.,**1970,** *27*, 4.

[7]Horne, A. R., *Marine chemistry*, John Wiley & Sons, Inc, New York,**1969,***3*, 282 – 287

[8]Brooks, R. R., Rumsey, D., *New Z. J. Marine Freshwater Res.*, **1974,** *8*, 155–166

[9]Cross, F. A., Brooks, J. H., Proc. 3rd Natl. Symp. Radioecology (Nelson, D. J. as Ed.), Oak Ridge, USA, **1973,** 769-775.

[10]O'Rear, C. W. Jr., *Some environmental influences on the zinc and copper content of striped bass (Moronesaxatilis)*, (Walbaum) Ph.D Thesis, Virginia Polytechnic and State University, Blacksburg Va ,*70P*, **1971**

[11]Forstner U., Wittmann, G. T. W., *Metal pollution in the aquatic environment*, Springer–Verlag, Berlin Heidelberg, New York, **1981,** 306 – 308

[12]Fujiyama T., *Studies on the levels of organoxhlorine compounds and heavy metals in the marine organisms*, University of the Ryukyus, Okinawa, Japan,**1981**, 13-23

[13]Windom, H. Stickney, R., Smith, R., White, D., Taylor, F., *J. Fish Res. Board Can*., **1973,** *30*, 275 – 279

[14]Honda K, Matsuda, M., Tatsukawa, R., *Nippon Nogei Kagaku Kaishi*, **1979,** *53(6)*, 177 –182.

[15]Bohn., A., McElroy, R. O., *J. Fish Res. Board Can*., **1976,** *33*, 2836-2840.

[16]Taylor, D. D., Bright, T. J., *The distribution of heavy metals in reef dwelling groupers in the Gulf of Mexico and Bahama Island* , Rep. Dep. Oceanogr , Texas A. and M. Univ, College Station , Tex.,**1973,** 249.

[17]Johnels, A. G., Westermark, T., Berg, W., Person, P. I., Sjostrand, B., *Oikos*, **1967**, *18*, 323 – 333.

[18]Uthe, J. H., Bligh. E. G., *J. Fish. Res. Board Can.*, **1971,** *28*, 786 – 788.

[19]Ui, J., Kitamura, S., *Marine Pollut. Bull*., **1971**, *2*, 56 – 58.

[20]Lovett, R. J., Geteman, W. H., Pakkala, I. S., Youngs, W. D., Lisk, D. J., Burdick, G. E., Harris E. J., *J. Fish. Res. Board Can*., **1972**, *29*, 1283 – 1290.

[21]Dworsky, R., Ebher, F., Gams, H., Ottendorfer, L. J., *Osterr. Abwasserrundsch*., **1973**, *18*, 2227.

[22]Kreger, K., Nieper L., Auslitz, H. J., *Arch. Lebensmittelhyg*., **1975**, *26*, 201-207

[23]Patel B., *Management of environment*, Wiley Eastern Limited New Delhi, **1980**, 409-416

[24]Atchison, G. J., Murphy, B. B., Bishop, W. E., McIntosh, A. W., Mayes, R. A., *Trans. Am. Fish. Soc.*, **1977**, *106*, 6,637 – 640

[25]Giesy J., Wienner, P., *Trans. Am. Fish. Soc.*, **1977**, *106(4)*, 393 – 403

[26]Kelso, J. R., Frank, M. R., *Trans. Amer. Fish. Soc*.,**1974**, *103*, 577 -581

[27]Hattula, M. L., Sarkka, J., Janatuinen, J., Pasivirta, J., Roos, A. *Environ. Pollut.*, **1978,** *17*, 19-29.

[28]Boyden, C. R., N*ature*, **1974**, *251*, 311-314.

[29]Cross, F. A., Hardy, L. H., Jones, N. Y., Barber, R. T., *J. Fish Res. Board. Can*., **1973**, *30*, 1287–1291

[30]Guthrie, F. E., Perry, J. J., *Introduction to environmental toxicology*, Elsevier New York, **1980**, 34 - 42

Received: 04.12.2013.
Accepted: 18.12.2013.

LOW - TEMPERATURE ELECTROLYTE (MELT) FOR THE PREPARATION OF CORROSION AND HEAT-RESISTANT ELECTROPLATINGS BY ALUMINUM

Nodari Gasviani[a], Gulnara Kipiani[a], Lia Abazadze[a], Sergo Gasviani[a] and Raul Kokilashvili[a]

Keywords: Low-temperature electrolysis, halide melt, aluminum electroplating.

The composition of the melt was described in which, primarily the preparation of aluminum electroplatings at low - temperatures: 95-110 ^{0}C is possible on hardware and steels such as: ST-3, Cr-18 and ST-40, as well as on screw like hardware (bolts, nuts), manufactured from steels 25CrMoFe and 35MoFe. Optimum conditions of the process of plating preparation and electrochemical parameters were also determined. The effect of various metal-modifier (Pb, Sn, Bi, Mn, Zr, Cr) on plating process and quality of the melt has also been studied.

Corresponding Authors
Tel: +995 (032) 2 30 14 30
E-Mail: nodargasviani@mail.ru
[a] R. Agladze Institute of Inorganic Chemistry and Electrochemistry of Ivane Javakhishvili Tbilisi State University, Georgia, Tbilisi, Mindeli str. 11, 0186

INTRODUCTION

The service period of hardware, machines-plants, constructions and others etc. depends upon corrosion-resistance and heat stability of the metals. Unfortunately, most of them are not characterized by these properties. All over the world the annual losses, caused by corrosion, estimated as 20 million tons in terms of pure metals in the form of machines-plants, equipment, constructions and others etc. The replacement of these old ones with new material requires the enormous expenses. The losses, caused by corrosion, comprise 2.5-4 % of annual national income in industrially developed countries. For example, in USA this estimated value is about 3.1 % (276 million dollars, annually, by the data of the year 2011), in Germany – 2.8 % and etc. Therefore, all over the world it's a matter of great importance to search the new methods of corrosion prevention and improvement of existing ones. Comprehensive development of electro-deposition is of considerable importance for metal protection against corrosion by efficient methods.

Preparation of electroplatings is possible by electrolysis of aqueous solutions, non-aqueous solutions and of the melts. From aqueous solutions the production of the majority of metals and their platings is impossible because of high electronegative potential (for example, E=-1,7 V for Al). The use of organic compounds is limited because of their instability, toxicity and high costs.[1,2] The preparation of more than a half of the metals and, respectively, of their electroplatings is possible from the molten electrolytes. High temperature, huge power consumption and costly materials used for the corrosion resistance are the difficulties faced during the implementation of such processes. Despite of above mentioned difficulties there is no alternative for the preparation of the platings of the majority of the metals and their alloys from molten electrolytes. Prepared platings are characterized by high adhesion with a base metal which, every so often, is due to the surface diffusion of plated metal into base metal or to the formation of intermetallides. Although in some cases an existence of intermetallides on the base surface is harmful (for example, $FeAl_3$, formed on iron surface, impairs iron properties).

Protective coatings on the basis of organic (paints-varnishes, polymeric materials and etc.) and inorganic (metals, oxides and etc.) compounds occupies an important place in unified system of corrosion control of hardware and other construction etc.

Protection of metals by metals (Zr, Sn, Ni, Cr) plating against corrosion is used since centuries. Due to this world reserves of these metals are to be exhausted. Availability of aluminum resources in the world is the specific reason to use it for plating for corrosion world wide. Aluminized metals are corrosion-resistance and heat stabile also, they are unaffected by corrosion even at high temperatures. The surface of aluminized iron is unchanged at 470 ^{0}C and is characterized by 85 % reflection of heat and light. It is corrosion – resistant at 700 ^{0}C over several thousand hours. Sulfur-containing hot gases also have no effect on aluminum plating even at high temperatures.

Aluminum platings protect the base metals not only mechanically but also electrochemically (anodic). In the case of mechanical damage of aluminum plated surface the corrosion "couple" is formed where the base metal becomes a cathode and is not oxidized.

Presently various methods are used for the plating of aluminum such as: high-temperature spraying; obtaining of aluminum electroplatings from organic solutions; colorizing (hot aluminizing) – immersion of large size hardware iron sheets in molten aluminum at 700-800 ^{0}C for some time. These methods are characterized by considerable disadvantages. They are unsuitable for aluminizing of complex-profile hardware as well as of screw-surface bolts and nuts, on which the durability of various constructions as well as of the masts of high-voltage line is highly dependent. Thus there is a huge demand of these materials.

The preparation of aluminum electroplatings is possible from cryolite - containing melts at the temperatures of 1000-1070 ^{0}C, in fluoride-chloride melts at 800-900 ^{0}C.[3-6] The use of chloride melt allows performing the process at relatively low (~200 ^{0}C) temperatures.[7-9]

On the basis of available literature data, it is observed that high volatility of $AlCl_3$ and the formation of large quantities of sludge – Al_2O_3 is the main hurdle in promoting the present process in industries.

Our main aim is to create some eco-safe and techno-friendly electrolyte, melting at low temperatures, for preparation of aluminum electroplatings on hardware. Molten chloride system is proposed in which, usually the preparation of mentioned platings is possible at "unusual" low (95-105 ^{0}C) temperatures. Low-temperature processes are characterized by less technological difficulties, there is no need in the use of heat-stable materials, evidently, power consumption is significantly less and etc. At ~100 ^{0}C the volatility of $AlCl_3$ is sharply decreased what is more important from ecological viewpoint. In proposed electrolyte one of the cations is a powerful acceptor of oxygen-ions[10] which hinders the formation of sludge - Al_2O_3. It should be also noted that at preparation of aluminum electroplatings on hardware in such conditions the above-mentioned undesirable inter-metallide – $FeAl_3$ is not formed.

Proposed electrolyte allows obtaining aluminum electroplatings at hardware (steels) which are widely used in power engineering, agriculture, food, chemical and oil - refineries etc.

Galvanic aluminizing for metals of strategic importance (Pb, Ti, Zr, Hf, Ta, Nb, Mo, W and etc.) is topical for use on various fields of engineering. These metals are heat-resistant at high temperatures (400-1500 ^{0}C) and have load bearing capacities also. As a result they become corrosion-resistant at the temperatures of (400-1500 ^{0}C). Previously, aluminizing of mentioned metals was carried out in the melts at the temperatures of (800-1070 ^{0}C).

Because of thermal in-stability of plastic materials their plating by aluminum is not possible at high – temperature. In low-temperature (~100 ^{0}C) melt, proposed by us, in a usual practice, the galvanic aluminizing of various plastic materials was made possible with heat stability up to more than 100 ^{0}C.

The results of the investigations, performed on the present problems, strongly suggest possible solutions in proposed electrolyte by galvanic aluminizing.

In present paper the results of the investigation of low-temperature galvanic aluminizing of hardware are given.

EXPERIMENTAL

The experiments were performed in the beakers of glass, corundum or porcelain. An electrolyte was prepared by fusion of chemically pure and preliminary dehydrated salts. In the beaker an anode of aluminum and metal-modifier were hung. The properly treated plates of low-grade steels, including steel-3 (thickness: 0.2-2 mm) as well as screw-profile hardware (bolts and nuts, manufactured from the steels 25KhMF and 35MF) were used as the cathodes (base). Temperature was controlled by contact thermometer with an accuracy of ±1 ^{0}C. Cathode current density was varied in the range from 0.01 to 0,05A·cm^{-2}, electrolysis duration: 15-35 min; temperature (105-110 ^{0}C±1^0).

The preparation of the surface of a base metal is of a significant importance at obtaining of plating. The surface of the metal for aluminum plating was prepared by two ways: a)-mechanically, b)-electrochemically – by anodic treatment in a solution: H_2SO_4 150-200 g L^{-1}; NaCl 20-40 g L^{-1}; temperature: 20-25 ^{0}C, anode -- plated hardware, cathode - lead plate, anode current density – 0.02-0.1 A·cm^{-2}, electrolysis duration: 5-10 minutes. Plated hardware was washed by water and acetone. Thereafter their aluminum electroplating was performed in selected melt.

Structure and composition of obtained platings were determined by metallographic, X-ray crystallographic and chemical analyses. Plating thickness was measured by weight increment too.

Detection of the microstructure of aluminum and its alloys is very difficult because of high plasticity and relatively low – hardness of pure aluminum. The surface of the samples has pale color after grinding-polishing. For its elimination the sample was brushed with 0.5 % acid (HF) moistened cotton. Thereafter the sample was placed in 5-20 % aqueous solution of NaOH over 30-60 seconds for "pickling". Dark color, formed after pickling, was removed by concentrated nitric acid. Thereafter the sample was washed by hot distilled water and was dried. The presence of diffusion layer was determined by microscope MIM-7. Micro-hardness was measured by device PMT-3.

RESULTS AND DISCUSSION

The experiments have shown that the reasonable aluminum electroplatings were obtained at the following conditions: temperature: 100-110 ^{0}C, electrolysis duration: 25-45 minutes, cathode current density 0.03-0.1 A·cm^{-2}. In this conditions the light, silvery platings were obtained with a good adhesion with a base; a thickness comprises 20-30 μm. Dependence of current efficiency on current density is shown in Fig. 1.

The experiments were also performed for aluminizing of other complex-profile hardware. Angle-bars, manufactured from low-grade steels and other small – size complex- shape hardware were used as a cathode. The results are identical (Picture 1).

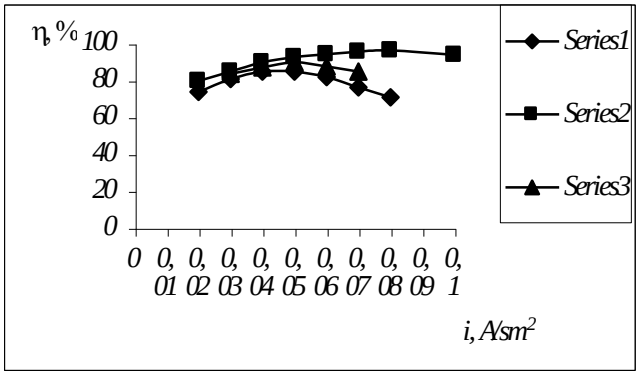

Figure 1 Dependence of current efficiency of the process of preparation of aluminum electroplating on the cathode current density without modifier. 2. modified by Pb. 3. modified by Zr.

Since the dendrites are formed at a cathode in a course of long-term electrolysis, therefore in many cases the preparation of the plating of desirable thickness has not met with success. For this reason metals – "modifiers" were added to a melt.

Picture 1. Various aluminized complex-profile hardware.

There are three reasons about the mechanism of the effect of small amounts of metals ions-additives on the process of aluminum electroplating:[8-11]

- In the course of electrolysis the atoms of metals-additives are deposited on active centers of a cathode, cause their passivating and in doing so are favorable for the formation of new crystallization centers;

- Because of mixing of separated atoms of metals-additives with aluminum the surface energy of crystalline formations is reduced, increasing the probability of their generation;

Metal ions positively affect on plating quality if the potentials of separation of metal-additive and main metal are closely related or their separation proceeds in equilibrium (quasi - equilibrium) regime. Along with it the sizes of the atoms of metals-additives must differ significantly from the sizes of the atom of main metal or it must form a chemical compound with it. Two or more metals, separated in quasi-equilibrium regime, in many cases form inter-metallides.[10-11]

The effect of the ions of metals-modifiers (Pb-1,75 Å, Sn-1.27 Å, Bi-1,82 Å, Mn-1,30 Å, Zr-1,60 Å, Cr-1,27 Å) on the process of preparation of aluminum electroplatings and on plating quality in proposed melt was studied.

Ionic compounds of the metals (0,01-0,1 wt. %) were used as the additives in terms of existing aluminum halide or metals ions were introduced into a melt by anodic dissolving of a metal. Current strength on anode-modifier was smaller by a factor 500-600 than cathode current strength and varied with increase of the amount of metal ions-additives, when the occasion requires. By this way their concentration was controlled in molten electrolyte in the course of the overall process.

Experimental results have shown that the small additives of the metals (10^{-6}-10^{-5} g. at. mol^{-1}) improve considerably the plating quality. The plating of better quality is obtained with the use of Pb and Zr, in comparison with other similar metals. The thickness increases to 60-70 μm. The plating is dense, smooth and is characterized by high adhesion.

At the use of lead auxiliary electrode at electrode surface an interaction of absorption type takes place between aluminum growing crystals and lead additives. The small amount of lead additives acts as a surfactant allowing increase the plating thickness. Lead amount in the plating does not exceed 1 %.

The use of Cr and Mn made possible not only to increase a plating thickness but reduced the electrolyte volatility too, decreased dendrites amount and the rate of sludge formation respectively. These facts increase the electrolyte stability very considerably.

It was also established that Mn content in the plating comprises no more than 2 %. The plating of such type is used in chemical and food industries and etc. They replace success- fully the items of scarce tin in an industry.

At co-deposition of aluminum-tin the plating is smooth, but porous. In the case of small additives of bismuth the dendrites are formed, the plating is not thick and hard. Mechanical strength increases in series: Bi, Sn, Mn, Pb, Zr, Cr.

Literature reveals that the greater is the difference between the values of atomic radius of main metal and metal-additive, the plating is obtained by good mechanical strength. This observation is not always true, as in the case of Bi.

It was established that the grip of aluminum platings on ST-3 is reasonably large. Doping of the plating by chromium and manganese at the same base increases an increase in the grip and comprises 70-77 kg cm^{-2} and at a steel Kh-18: 55-60 kg cm^{-2}. The said grip of aluminum platings, doped by lead, comprises 50 kg cm^{-2}.

Also the high-quality and corrosion-resistant platings are obtained on screw hardware (bolts and nuts) which are manufactured from the steels – 25KhMF, 35MF.

Table 1. Characteristics of aluminum platings

№	Base material	Anode-modifier	Ratio I_C/I_A	Current density, *i*, Acm^{-2}	Plating thickness, μm	Current efficiency, η%
1	ST-3	-	-	0,02	16	74
2	Kh-18	-	-	0,04	25	85,5
3	ST-40	-	-	0,06	22	82
				0,08	18	72
4	ST-3	Pb	1/1000	0,02	20	80
5		Pb	1/1000	0,06	60	96
6		Zr	1/500	0,03	35	84
7		Zr	1/500	0,05	49	90
		Mn	1/500	0,04	52	89,5
		Cr	1/250	0,03	55	80,0
8	Kh-18	Pb	1/1000	0,04	27	90
9		Pb	1/1000	0,06	63	94
10		Zr	1/500	0,07	54	85
		Mn	1/500	0,04	55	91,5
11	ST-40	Pb	1/1000	0,08	68	96,5
12		Zr	1/500	0,05	57	90,0
13		Mn	1/500	0,05	60	91,0

Hardware, aluminized in various regimes as well as non-aluminized ones (bolts and nuts), were tested on corrosion resistance in humid atmosphere and in 5-10 % aqueous solution of NaOH (over 25-30 days). Un-plated hardware was subjected to strong corrosion but some aluminized hardware remained unchanged. This fact also became a reference point for selection of electrolysis conditions. Some characteristics of aluminum platings on the metals are presented in Table 1.

Thus the investigation, performed in proposed electrolyte, has shown that a high-quality aluminum electroplatings are obtained on above-listed base-metals. Doping of aluminum by other metals - modifiers allows to increase the current density, current efficiency and plating thickness.

The additives of selected metals have an encouraging effect on plating adhesion among which Cr and Mn additives must be marked off.

References

[1]Spiridonov, B. A. *Galvanotechn. Obrab. Poverkh.*, **2009**(2)**,** 214-218.

[2]Titova, V. N., Kazakov, V. A., Iavich, A. A., Petrova, N. V. *Korrozia, Metally, Zashch.*, **2006**(9), 1721-1723.

[3]Belyaeva, G. I., Anfinogenov A. I., Solomatin, V. E., Tlyushchenko, N. G., *Trudy Inst. Elektrokhim. UF AN SSSR*, **1966(**8), 79-84.

[4]Anfinogenov, A. I., Ilyushchenko, N. G., Belyaeva, G. I., Shurov, N. I., *Trudy Inst. Elektrokhim. UF AN SSSR*, **1966(**13), 56-62.

[5]Ryabinov, N. A., Andreev, Yu. A., Fokin N. M., *"Electrokhimicheskie pokritiya splavami"*. **1975** M. Mashinostroenie, p. 159.

[6]Bradley, E. F., Rausch, J. J., *US306289.*

[7]Delimarskii, Yu. K. Chetverikov, A. V., Makogon, V. F., *SU 178257*

[8]Delimarskii, Yu. K., Kuzmovich, V. V., *Zh. Fiz. Khim.*, **1972**, *46(10)*, 2567-2571.

[9]Kuzmovich, V. V., Makagon, V. F., Kazakov, Yu. B. *Ukr. Khim. Zh.*, **1969,** *35(3)*, 258-265.

[10]Gasviani, N. Avtoreferat doktorskoi dissertatsii . **2006**. Tbilisi.

[11]Baraboshkin, A. N. *Elektrokristallizatsia metallov iz rasplavlennikh solei*, M**,** Nauka, **1972**, 280.

Received: 31.10.2013.
Accepted: 15.12.2013.

RELOOK ON MERCUROUS NITRITE AND SOME EXOTIC GOLD AND PLATINUM COMPOUNDS

D. Banerjea

Keywords: Mercurous nitrite; Gold and platinum clusters

Evidences seem to indicate that existence of stable mercurous nitrite, reported by P. C. Ray, is doubtful. Ray also reported a number of subnormal compounds of platinum and gold, for which he proposed astounding constitutions, which are most likely to be metal cluster compounds; the plausible structures of a few of these are proposed. Their investigations by X-ray crystallography to determine their structures and thus establish their identity would be fruitful.

* Corresponding Authors
E-Mail: banerjeas2005@yahoo.co.in
[a] Former Sir Rashbehary Ghose Professor of Chemistry, Calcutta University, 92, A. P. C. Road, Kolkata – 700009, India

INTRODUCTION

In the year 1896 P. C. Ray reported[1,2] preparation of mercurous nitrite, $Hg_2(NO_2)_2.H_2O$, and during the next few years published a few papers on its preparation and properties.[3-6] He also reported hyponitrites of Hg(I) and Hg(II).[7-10] Although the reported discovery of mercurous nitrite was highly acclaimed, we hardly notice any mention of this in the advanced level treatises on Inorganic Chemistry published in the following years.

DISCUSSION

In the year 1966 Potts and Allred[11] reported that they failed to isolate the mercurous nitrite reported by Ray. Subsequent attempt by the present reporter to make the said compound also ended in failure. On the basis of an estimate of the enthalpy of formation of mercurous nitrite, $Hg_2(NO_2)_2$, using thermochemical data available in literature, it was concluded that the compound should be highly endothermic, which explains its instability.[12]

In the year 2009 Hancock and coworkers[13] reported a stable crown-ether complexed mercurous perchlorate, but the corresponding nitrite was too unstable and disproportionated forming the crown-ether complexed mercury(II) nitrite.

However, Ray reported[6] that his 'mercurous nitrite' was quite stable and could be crystallized out in a pure form from a hot concentrated aqueous solution, in which it suffered only ca. 20 per cent decomposition (disproportionation) indicating this to be a slow process even in hot water; the recovery of major part of the salt from the solution in a pure form showed that it also did not suffer any hydrolytic transformation. From our knowledge on the behavior of Hg_2^{2+} and Hg^{2+} ions in solution it seems that the reported hydrolytic stability would suggest the compound to be a basic salt of mercury. Analytical data on the Hg and N contents as reported by Ray[1-6] agree reasonably well (particularly because of the crude method used in the estimation of Hg) with those expected in basic salts of compositions such as $Hg^{I}_6O(NO_3)_4.2NO_2$, $Hg^{I}_8O(NO_3)_6.2NO_2$, $Hg^{I}_2Hg^{II}_2(OH)_2(NO_2)_4$, $Hg^{I}_3Hg^{II}(OH)(NO_2)_4$ etc.

In view of the aforesaid information and findings the reported determination of the structure of the mercury(I) nitrite of Ray by X-ray crystallography,[14-16] without chemical characterization of its identity, needs reinvestigation after proper chemical characterization of the sample. One group[16] reported the species as unstable requiring work at 100 K; this contradicts what was reported by Ray.[6]

It is worth noting in this connection that the hyponitrites of mercury reported by Ray[7-10] are even more unlikely to exist.[17]

P. C. Ray also reported a series of compounds of platinum and of gold in very abnormal/subnormal valence states for which he proposed astonishingly absurd constitutions.[18-24] However, a proper investigation of their structures by sophisticated methods as are available now, including X-ray crystallography, may reveal their true nature, possibly as metal cluster compounds.[25-28]

Thus, for the compound of stoichiometry $2AuCl_3.3C_2H_4S$ (arrived at from analytical data on Au, S and Cl) Ray proposed the constitution shown in Figure 1 in which Ray considered the Au to be in pentavalent state (+5 oxidation state).[19]

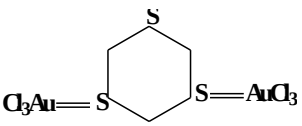

Figure 1.$2AuCl_3.3C_2H_4S$, as proposed by Ray (see text)

However, the proposed constitution is short of 6H from the stoichiometric composition (which of course will not be

distinguishable by analytical data on Au, S and Cl only, due to high molar mass of the species). But assuming that the compound formed was as shown in Figure 1, the S to Au bond would be a coordinate bond with the Au in +3 (and not +5) oxidation state. In fact the compound might be a dinuclear compound of Au^{III} as shown in Figure 2 and Figure 3 having coordination number 5 and 6 respectively for Au(III), examples of which are known[29] though rare.

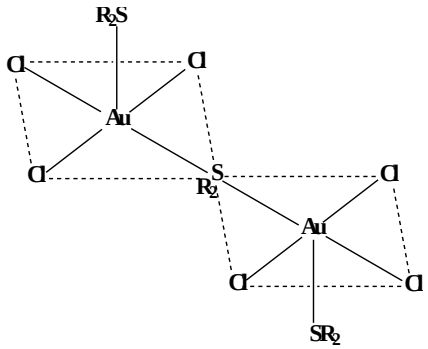

Figure 2. One plausible structure of $2AuCl_3$. $3R_2S$ ($R_2 = C_2H_4$)

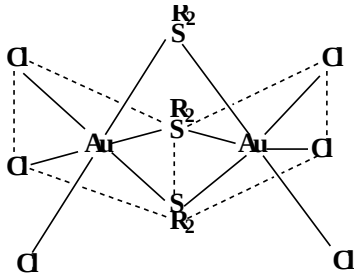

Figure 3. Another plausible structure of $2AuCl_3$. $3R_2S$ ($R_2 = C_2H_4$)

Similarly, the compound $Au_2Cl(SCH_2CH_2S)_2$ reported by him,[19] for which he proposed the constitution shown in Figure 4 with one Au in bivalent and another Au in trivalent states, is more likely to be a Au-centered trigonal bipyramidal Au_5 cluster with a Cl bound to each of the three Au in the trigonal plane with an $^-SC_2H_4S^-$ ligand bridging two Au along each of six edges of the trigonal bipyramid (Figure 5).

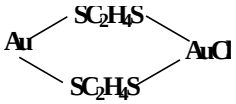

Figure 4. $Au_2Cl(SC_2H_4S)_2$, as proposed by Ray (see text)

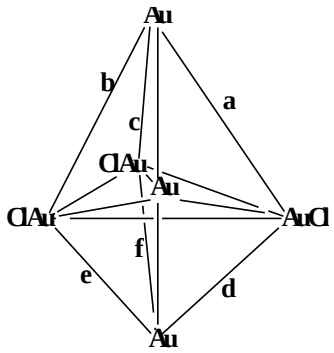

Figure 5. Plausible structure of $\{Au_2Cl(SCH_2CH_2S)_2\}_3$, i.e. $Au_6Cl_3(SCH_2CH_2S)_6$. The six $^-SCH_2CH_2S^-$ ligands are bridging along the edges a-f of the trigonal bipyramid

Likewise, the compound $Pt_5Cl(Et_2S_2)_4(Et_2NH)_2$ [22] is likely to be a Cl-centered trigonal bipyramidal Pt_5 cluster with the Et_2S_2 and Et_2NH present as bridging ligands along the edges of the trigonal bipyramid (Figure 6).

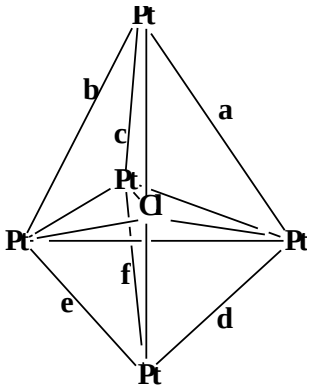

Figure 6. Plausible structure of $Pt_5Cl(Et_2NH)_2(Et_2S_2)_4$. The two Et_2NH ligands may be bridging along the edges b and d, while the four Et_2S_2 ligands may be bridging along the edges a, c, e and f.

Elucidation of the structures of all these compounds by X-ray crystallography would be worthy of investigation to establish their true nature. If the last two mentioned compounds are thus shown as metal cluster species, then that would establish P. C. Ray as a pioneer in the field.

ACKNOWLEDGEMENT

Thanks are due to Dr. Sanchita Goswami, Assistant Professor of Chemistry, Calcutta University, for her assistance in preparing the manuscript in the format required by the publisher.

REFERENCES

[1]Ray, P. C., *J. Asiatic Soc. Bengal*, **1896**, *65* (Part II), 1.

[2]Ray, P. C., *Z. Anorg. Chem.*, **1896**, *12*, 365.

[3]Ray, P. C., *J. Chem. Soc.(London)*, **1897**, *71*, 337.

[4]Ray, P. C., *J. Asiatic Soc. Bengal*, **1900**, *69*, 476.

[5]Ray, P. C., *Ann. Chem.*, **1901**, *115*, 250.

[6]Ray, P. C., *J. Chem. Soc.(London)*, **1905**, *87*, 171.

[7]Ray, P. C., *Proc. Chem.. Soc.(London)*, **1896**, *12*, 217.

[8]Ray. P. C., *J. Chem. Soc.(London)*, **1897**, *71*, 348.

[9]Ray. P. C., *J. Chem. Soc.(London)*, **1897**, *71*, 1105.

[10]Ray. P. C., *J. Chem. Soc.(London)*, **1907**, *81*, 1404.

[11]Potts, R. A., Allred, A. L., *Inorg. Chem.*, **1966**, *5*, 1066.

[12]Banerjea, D., *J. Indian Chem. Soc.*, **2004**, *81*, 1018.

[13]Williams, N. J., Hancock, R. D., Riebensples, J. H., Fernandes, M., de Sousa, A. S., *Inorg. Chem.*, **2009**, *48*, 11724.

[14]English, R. B., Rohm, D., Schutte, C. J. H., *Acta Cryst.C.*, **1985**, *41*, 997.

[15]Ohba, S., Matsumoto, F., Ishihara, M., Saito, Y., *Acta Cryst.C*, **1986**, *42*, 1.

[16]Samanta, S., Goswami, S., Chakravorty, A., *Indian J. Chem. A*, **2011**, *50*, 137.

[17]Aylett, B. J., in: *Comprehensive Inorganic Chemistry*, Eds. Bailar, Jr., J. C., Emeleus, H. J., Nyholm, R. S., Trotman-Dickerson, A. F., vol. 3, chapter 30, Pergamon Press, Oxford, **1973/1975,** 293.

[18]Ray, P. C., *J. Chem. Soc.(London)*, **1923**, *123*, 133.

[19]Ray, P. C., *J. Indian Chem. Soc.*, **1924**, *1*, 63.

[20]Ray, P. C., Bose Ray, K. C., *J. Indian Chem. Soc*., **1925**, *2*, 178.

[21]Ray, P. C., Bose Ray, K. C., *Z. Anorg. Allgem. Chem*., **1929**, *178*, 329.

[22]Ray, P. C., Sengupta, S. C., *Z. Anorg. Allgem. Chem*., **1930**, *187*, 33.

[23]Ray, P. C., Ghosh, N. N., *Z. Anorg. Allgem. Chem*., **1933**, *215*, 201.

[24]Ray, P. C., Ghosh, N. N., *Z. Anorg. Allgm. Chem.*, **1934**, *220*, 247.

[25]Cotton, F. A., *Acc. Chem. Res.*, **1978**, *11*, 225.

[26]Cotton, F. A., *J. Chem. Educ*., **1983**, *60*, 713.

[27]Mingos, D. M. P., Wales, D. J., *Introduction to Cluster Chemistry*, Prentice-Hall, Englewood Cliffs, NJ, **1990**.

[28]Shriver, D. F., Kaesz, H. D., Adams, R. D., *The Chemistry of Metal Cluster Complexes*, VCH, Weinheim, **1990**.

[29]Cotton, F. A., Wilkinson, G., Murillo, C. A., Bochmann, M., *Advanced Inorganic Chemistry*, 6th Edition, John Wiley, New York, **1999**, 1085.

Received: 09.11.2013.
Accepted: 18.12.2013.

POLYMERIZATION REACTION OF STARCH-PHENOL FOR THE PREPARATION OF LINSEED OIL EPOXY PS-PMMA COPOLYMER BLEND AND TRANSITION METAL BASED COORDINATION POLYMER

Nahid Nishat,[a]* Ashraf Malik[a] and Akhilesh Kumar[a]

Keywords: use the Keywords style for the list of keywords, separating with a comma each items.

Starch-Phenol based polymer synthesized by the process of polycondensation which further is modified into two different branches. In one case with Linseed Oil Epoxy and PS-PMMA co-polymer by melt blending method for the preparation of biodegradable blend and in another case by transition metals Mn(II), Co(II), Ni(II), Cu(II) and Zn(II) for synthesizing coordination polymer. The type of modified starch used in the composition inherently affects the properties and also play a role in the biodegradability of the developed material. All the synthesized polymeric ligands were characterized by Fourier transform infrared spectroscopy (FT-IR), ^{1}H NMR spectroscopy, ^{13}C NMR spectroscopy, UV-visible spectra, magnetic moment measurements, thermogravimetric analysis (TGA), Differential Scanning Calorimetry (DSC), Scanning electron microscopy (SEM) and Biodegradation studies. Thermal data revealed that Polymer metal complexes are lesser in thermal strength than blend and that the biodegradation rates of blends and polymer metal complexes are somewhat similar.

Corresponding Authors
Tel.: +91-112-682-3254;
Fax: +91-112-684-0229
E-Mail: nishat_nchem11@yahoo.com
[a] Department of Chemistry, Jamia Millia Islamia New Delhi, 110025, India

INTRODUCTION

Advanced technologies in petrochemical polymers have brought about many benefits to mankind. However it is becoming more and more obvious that the ecosystem is considerably disturbed and damaged as a result of the non-degradability of disposal items.[1] Much effort has recently been made to develop biodegradable materials because of the worldwide environmental and resources problems, resulted from petroleum-derived plastics. The synthesis of polymers or copolymers based on renewable resources has attracted considerable attention from polymer scientists throughout the world because of their potential attributes as substitute for petrochemical derivatives.[2-4] Starch, a natural renewable polysaccharide obtained from a great variety of crops, is one of the promising raw materials for the production of biodegradable plastics. It is a versatile and cheap, and has many uses as thickener, water binder, emulsion stabilizer and gelling agent. Starch based plastics are mainly harvested from wheat, potatoes, rice, and corn. Of these four starches, corn is the most commonly used and is the least expensive starch. Most sales of starch come from the United States, which makes about $1.8 million annually. Being an extremely versatile product, about 20 % of starch is used for non-food items. Starch is used for many non-food items such as making paper, cardboard, textile sizing, and adhesives ("Green Plastics" 2004). Starched plastics have already been processed into eating utensils, plates, cups and other products. Besides the uses of phenol are also manyfold as is in the production of phenolic resins, which are used in the plywood, construction, automotive, and appliance industries. Phenol is also used in the production of caprolactam and bisphenol A, which are intermediates in the manufacture of nylon and epoxy resins, respectively. Other uses of phenol include as a slimicide, as a disinfectant, and in medicinal products such as ear and nose drops, throat lozenges, and mouthwashes. Phenolic adhesives manifest good adhesion to materials such as wood, leather, rubber, plastics, synthetic fibers, glass, ceramics, cements and metals.[5-7] Other important phenolic starting materials are the alkyl-substituted phenols, hydro- quinone, resorcinol and catechol.[8] It is becoming extremely important to find durable plastic substitutes, especially for short-term packaging and disposable applications.[9] A variety of biomedical applications, has also been in consideration by making use of starch based biodegradable polymers. Starch-based materials have also been projected for incorporation into orthopedic implants[10], as a bone replacements[11]and for controlled drug delivery.[12-13] Polymer blends play an important role in the technological field since they allowed improvements in material characteristics by combining selected properties of the original polymers.[14-15] Most polymeric blends are multiphase systems and, therefore their properties largely depend on their morphologies.The use of biodegradable packaging is considered a partial solution for solid waste accumulation problems.This part of research work aims at dual mode for making a biodegradable material by synthesizing plastic blend that combines a low cost starch and thermoplastic polystyrene–polymethylmethacrylate, which uses naturally abundant renewable resource based linseed oil epoxy as a compatabilizer and the starch phenol based polymer modified into a transition metal based coordination polymer, which in a course of scientific innovation is characterized by readily available techniques such as FTIR, NMR, Electronic Spectroscopy, TGA, DSC, SEM and CO_2 evolution based ASTM method of biodegradability.

EXPERIMENTAL

Materials

Starch, phenol, ethanol MERCK (Mumbai), sodium hydroxide were used without further purification. Oil was extracted from linseed (obtained from local market) through Soxhlet apparatus. Petroleum ether (b.p. 60-80 ^{0}C) was used as a solvent. MMA (350,000) and S (140,000) were procured from Aldrich chemical company USA. Hydrogen peroxide (30 % w/w) sulphuric acid, maleic anhydride, benzoil peroxide, glacial acetic acid. All the chemicals were of analytical grades .Solvents such as acetone, DMF, DMSO and (S.d fine chemicals) methanol were purified by standard procedure before use. Manganese(II) acetate tetrahydrate [$Mn(CH_3COO)_2.4H_2O$], copper(II) acetate monohydrate [$Cu(CH_3COO)_2.H_2O$], nickel(II) acetate tetrahydrate [$Ni(CH_3COO)_2.4H_2O$], cobalt(II) acetate tetrahydrate [$Co(CH_3COO)_2.4H_2O$] and zinc(II) acetate dihydrate [$Zn(CH_3COO)_2.2H_2O$] were used without further purification. All the microorganisms for biodergradable studies were provided by A.M.U. Agricultural and Microbiology Department, Aligarh.

SYNTHESIS

Synthesis of polymeric resin

Polycondensation polymerization method was adopted for the synthesis of polymeric ligand (Poly-SPhe) by the reaction of phenol and starch in alkaline medium in 2:1 molar ratio (Scheme 1). 250 mL three-necked round-bottomed flask, equipped with a condenser 1.94 g, 0.02 mol of phenol and 1.62 g, 0.01 mol of starch dissolved in a 70 mL distilled water were placed, and then it was stirred with high speed stirrer in a constant temperature water bath at 90 ^{0}C for 4 h. A very little amount of sodium hydroxide pellet was used to pH being stablised at 8. The reaction was monitored by thin layer chromatography (TLC) using ethanol as an eluent. The product of the polymerization reaction was a colorless highly viscous product which was washed with ethanol and acetone several times and then was dried in a vacuum oven under reduced pressure at 60 ^{0}C for 15 h. The off white powder of starch based polymer modified by phenol (Poly-SPhe) was obtained in 82 % yield. The synthesized product was found to be soluble in distilled water and DMSO and insoluble in some common organic solvents.

Synthesis of metal complexes

Metal complexes of poly-SPhe were prepared by using molar ratio (1:1) of poly-SPhe and metal salts. (Scheme 1). A typical procedure for the preparation of the Cu(II)-complex is carried out as 2.61 g, 0.01 mol of poly-SPhe was dissolved in a hot DMSO solvent (30 mL) and 1.99 gm, 0.01 mol of Cu(II) salt was also dissolved in hot DMSO (35 mL) separately. Both the solutions were mixed in hot condition under constant stirring. Then the whole reaction mixture was refluxed at 60 ^{0}C under constant stirring for 3-4 h. A dark green colored product was obtained which was reprecipitated in distilled water. The product was filtered and washed several times with alcohol, acetone and dried in a vacuum desiccator on calcium chloride, yield 79 %. A series of similar procedure was also adopted for the synthesis of the other metal complexes such as poly-SPhe-Mn(II), poly-SPhe-Co(II), poly-SPhe-Ni(II) and poly-SPhe-Zn(II), and their respective yields were between 79-83 %. All the obtained metal complexes product were found to be soluble in DMSO and insoluble in other common organic solvents and distilled water.

Synthesis of copolymer of PS-PMMA

Synthesis of copolymer was carried out using the methods reported earlier. Monomers are freed from inhibitor. Styrene 0.01 mol, 20 g and MMA 0.01 mol, 20 g in the ratio (1:1) with benzoyl peroxide 0.50 gm taken in a three necked round bottom flask equipped with a mechanical stirrer, condenser, dropping funnel and thermometer. The temperature of reaction mixture was kept at 50– 60 ^{0}C during the reaction. The reaction time was 45 minutes.[16] After completion of reaction, the reaction mixture was washed with solvents in which the synthesized polymer was found to be non-soluble in with, and was finally dried at room temperature in vaccum desiccator over calcium chloride.

Synthesis of linseed oil epoxy

Synthesis of linseed oil epoxy (LOE) was carried out using the methods reported earlier. Linseed oil 40 g (I.V 180) equivalent to 0.2899 mol of unsaturation, 40 mL of benzene, 7.995 mL (0.1326 mol) of glacial acetic acid, and 1 mL of concentrated sulphuric acid diluted to 50% with water were taken in a three necked round bottom flask equipped with a mechanical stirrer, dropping funnel and thermometer. The flask was then immersed in a cold water bath, 48.5 mL, 0.427 mol of hydrogen peroxide was added drop wise with continuous stirring. The temperature of the reaction mixture was kept at 45 ^{0}C during the addition of hydrogen peroxide.The temperature was then raised to 60 ^{0}C, which was maintained till the end of reaction.[17]

Synthesis of blend

Modified starch, PS-PMMA and linseed oil epoxy blend were prepared by melt method. 25g solution PS and PMMA were mixed with 75 g solution of LOE separately in different reaction vessels under vigorous stirring at room temperature. The solvent was evaporated slowly in a fuming cupboard under exhaust till the product become dry. Different concentration of the two were tried for reaction and finally 2.5 g of modified starch, 7.5 g PS-PMMA -LOE complex with 1 wt.% of a maleic anhydride were mixed with benzoil peroxide (in the range of 0-1 wt %) taken in reaction vessels under vigorous stirring at 80 ^{0}C for 1 h, and it worked out with good results. After the complete homogenegization of the mixture, the blend was prepared and then dried in vacuum oven at 20 ^{0}C for 24 h. The phase separation was checked under hot and cold condition.

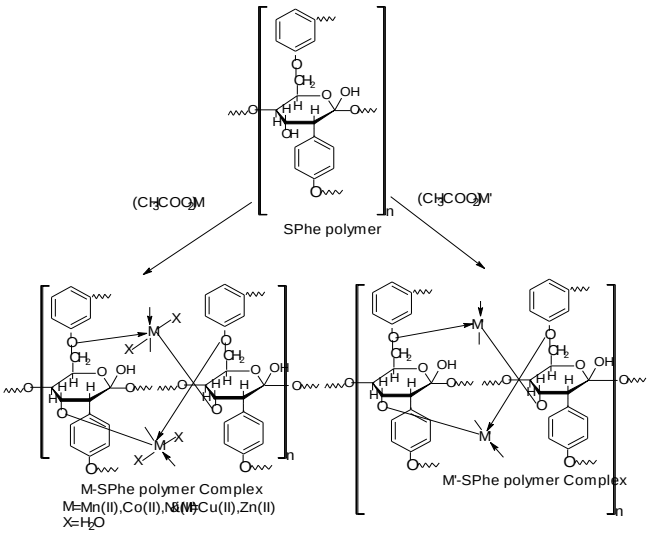

Scheme 1. Synthetic route of the polymer metal complex of (SPhe)

Measurements

Perkin-Elmer infrared spectrometer model 621 by using KBr pellets was used to record the functionality of the synthesized polymer in the infrared (IR) regions. The ^{1}H-NMR spectra were recorded on a JOEL-FX-100 FT NMR instrument in dimethylsulfoxide (DMSO) solution and tetramethylsilane (TMS) as an internal standard. The elemental analysis of carbon, hydrogen and nitrogen was carried out on a Perkin-Elmer model-2400 elemental analyzer (CDRI Lucknow). The percentage of metals was determined by complexometric titration against EDTA after decomposing with concentrated nitric acid (HNO_3). The solubility of polymeric ligand and its metal polychelates were checked at room temperature in different solvents. The thermal stability of polymer and its metal polychelates have been evaluated for recording thermograms by TA analyzer 2000 at a heating rate of 20 ^{0}C per minute under Nitrogen atmosphere.. The electronic spectra of the metal complexes were recorded on a Perkin-Elmer Lambda-EZ 201 and magnetic susceptibility measurements were done with vibrating sample magnetometer. The *T*g and *T*m of the synthesized polymeric resin and its blend have been evaluated by PYRES DIAMOND DSC instrument. The morphological changes have been evaluated by using the instrument JEOL JSM840 SEM. The biodegradable testing were carried out through CO_2 evolution method in the laboratory itself. The solubility of polymeric ligand and its polymer metal complexes were checked at room temperature in different solvents.

RESULTS AND DISCUSSIONS

The polymeric resin (poly-SPhe) was prepared by the polycondensation process in the molar ratio of 1:1 in alkaline medium, according to Scheme 1, and metal complexes were prepared by the reaction of poly-SPhe with metal acetate in 1:1 molar ratio, and the polymer blend were prepared by the reaction of poly-SPhe with PS-PMMA copolymer and Linseed oil epoxy in different molar ratio till compatibilization. All the products were obtained in good yields. The polymeric resin was found to be soluble in distilled water and DMSO while all the metal complexes were soluble in DMSO only, and insoluble in common organic solvents like methanol, ethanol, THF, DMF, $CHCl_3$, CCl_4 etc. The elemental and spectral analysis provide good evidence that the compounds are polymeric and these data are also in agreement with the molecular structure given in scheme 1. The results of elemental analysis and yields of the synthesized compounds are given in Table 1.

FT-IR spectra

The FT-IR spectral bands of the important groups with their respective range of frequencies of all the polymeric compounds and their polymer metal complexes are given in Table 2. The IR spectral analysis of poly- SPhe observed the vibrational band for νOH in the region 3412 cm^{-1}. Stretching frequencies of νC-O and CH_2 scissoring appeared at 1081 cm^{-1}, 1458 cm^{-1} for poly- SPhe respectively. The bands observed at 2926-2865 cm^{-1} for CH_2 asymmetric and symmetric stretching vibrations. The stretching frequencies for aromatic νC=C appeared at 1553 cm^{-1} in the benzene ring of phenol. Vibrational band for νC-H bending and νCH_2 wagging appeared at 1023 cm^{-1} and 1157 cm^{-1} for poly-SPhe. Polymer metal complexes of poly-SPhe observed a vibrating band of νC-O shifted to the lower frequencies from 1081 cm^{-1} to 1051 cm^{-1} and suggested the occurrence of coordination at oxygen to metal ion and this can be explained by the sharing of electrons from oxygen as dative bond to metal atom, and more supportively by the appearance of (M-O) band at a stretching frequency of 620-613 cm^{-1}. In the polymer metal complexes of poly-SPhe the loss of a proton from the OH group leads to the shifting of νC-O band by coordination with metal ion. Another band at a stretching frequency of 865 cm^{-1} appeared in metal complexes of manganese, cobalt and nickel, which may be assigned to M-H_2O. The νO-H also registered lowering in frequency.[18-21]

^{1}H-NMR spectra

The ^{1}H NMR band ranges of polymeric resin and its metal complex with Zn(II) are given in Fig 1 and Fig 2. In the spectrum of poly-SPhe a sharp and intense vibration band at 4.389 ppm appeared which may be attributed to CH_2–O protons.[22] Vibrational bands at 5.451, 5.090, 4.484, 4.456 and 3.408 ppm is assigned to protons of the pyranose ring of starch for poly-SPhe.[24-25] A vibration band of CH-OH was observed in the polymeric resin at 4.01 ppm. In the spectrum of poly- SPh -Zn(II) complex, the bands for CH_2 –O was shifted, due to coordination by the free electron of oxygen in the group.

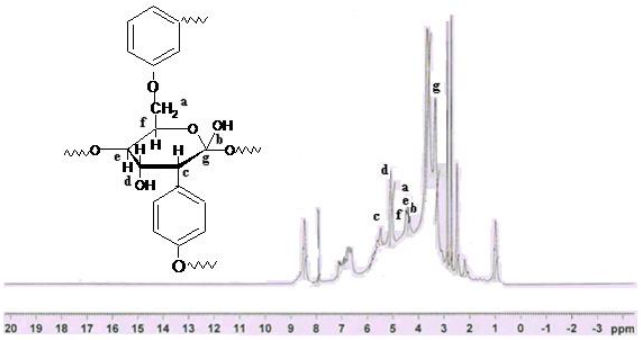

Figure 1. ^{1}H-NMR spectrum of polymeric ligand (SPhe)

 DOI: 10.17628/ecb.2014.3.149-156

Table 1. Elemental analysis and yields of the synthesized polymeric compounds

Compounds	Yield, %	d.p., °C	Elemental analysis			
			C, %	H, %	O, %	M, %
Poly-SPhe	82	252	63.50	8.29	28.19	…..
			63.10	8.540	27.105	…..
Poly- SPhe -Mn(II)	83	292	52.34	7.26	29.73	12.76
			52.390	7.00	28.450	12.22
Poly- SPhe -Co(II)	81	294	49.77	7.19	26.46	13.56
			48.770	7.110	25.97	12.210
Poly- SPhe -Ni(II)	80	299	49.80	7.19	29.48	13.517
			48.10	7.360	27.970	12.108
Poly- SPhe -Cu(II)	79	298	53.65	6.97	23.82	15.77
			52.100	6.01	22.77	15.12
Poly- SPhe -Zn(II)	79	296	53.40	6.72	23.712	16.15
			53.700	6.200	22.880	16.33

In the band of CH-OH, the proton was lost, and that too again for coordination and, so the shifting was occurred. Protons of pyranose ring also observed a slight shifting to lower values of chemical shift.

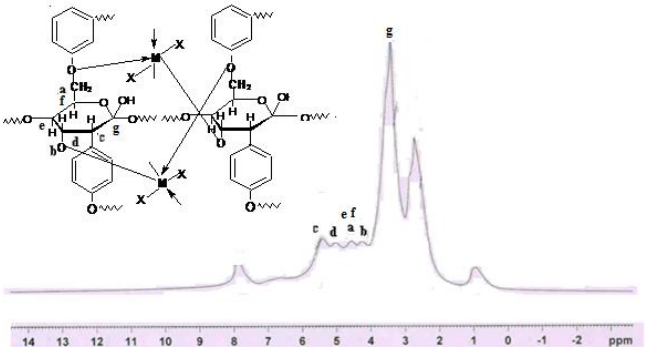

Figure 2. ^{1}H-NMR spectrum of polymer metal complex of SPhe-

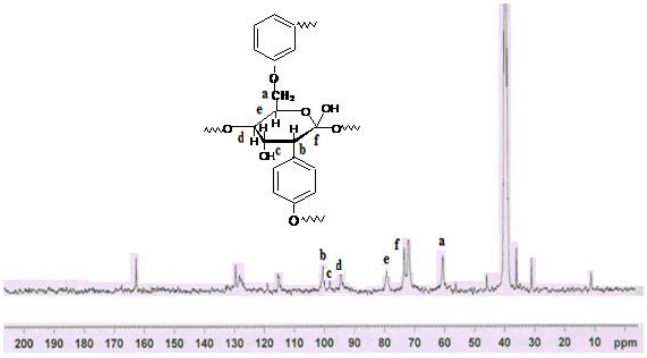

Figure 3. ^{13}C-NMR spectra of polymeric ligand (SPhe)

^{13}C-NMR spectra

The ^{13}C NMR band ranges of polymeric resin of (poly-SPhe) and its metal complexes with Zn(II) are given in Fig 3 and Fig 4. Singlet peak of vibrational band at 62.90 ppm appeared due to CH_2–O carbon of methylene group in poly-SPhe.[23] Pyranose carbons of Starch molecules for poly-SPhe registered bands in the region 100.28, 96.94, 94.444, 79.06 and 76.51 ppm.[23] In case of metal complex of poly-SPhe bands showed shifting in comparison with the corresponding bands observed in polymeric resin and the band due to carbon of CH_2–O group was assigned at 58.16 ppm. This was due to involvment of oxygen atom in coordination which is well supported by M-O bond in IR spectra.

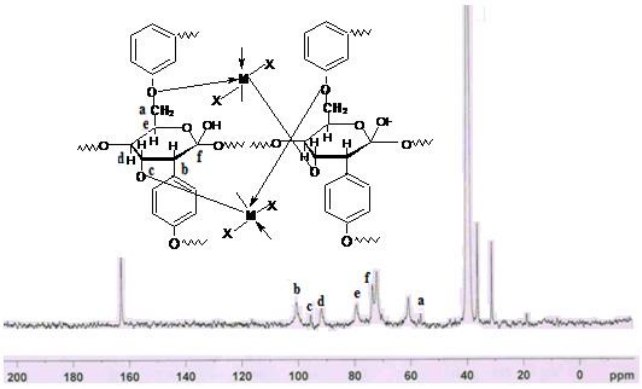

Figure 4. ^{13}C-NMR spectra of polymer metal complex of SPhe-Zn(II)

Pyranose ring carbons also observed a little shifting and were observed at 100.10, 95.17, 93.57,78.112 and 75.75 ppm .

UV Visible Spectra and Magnetic Moment

Polymer metal complexes were recorded in DMSO for the electronic spectral observation. Table 3 depicts all the electronic spectral bands and their magnetic moment measurement and other parameters. Polymer metal complex SPhe-Mn(II) in the electronic spectrum exhibited three bands at 14947, 21186, 26455 which may reasonably correspond to $^{4}T_2g(D) \leftarrow {}^{6}A_1g(G)$, $^{4}T_2g(G) \leftarrow {}^{6}A_1g(G)$ and $^{4}A_2g(G) \leftarrow {}^{4}T_2g(P)$ transitions, respectively. Using these data we can calculate crystal field parameter and the values of 10*Dq*, *B*, β^0 and β% were found to be 17742.7, 810, 0.843 and 15.7% respectively. The polymer metal complex SPhe-Mn(II) has a magnetic moment value 5.82 BM, which is close to the calculated value of high spin state of the metal ion. An octahedral geometry is proposed for polymer metal complex SPhe -Mn(II) on the basis of μ_{eff} value and electronic spectral bands observed data.

 DOI: 10.17628/ecb.2014.3.149-156

Table 2. IR Spectra of polymeric ligand (SPhe) and its polymer metal complexes

Compounds	O-H	CH bending	C=C	CH_2 asym-sym	$CH_{2\ wag}$	CH_{2sci}	C-O	M-O
SPhe	3412	1023	1553	2926-2865	1157	1458	1081	-
SPheMn(II)	3411	1018	1548	2926-2865	1153	1453	1050	620
SPheCo(II)	3410	1017	1547	2926-2865	1154	1452	1051	618
SPhe-Ni(II)	3409	1016	1552	2926-2865	1152	1457	1053	615
SPheCu(II)	3408	1022	1549	2926-2865	1155	1454	1055	617
SPhe-Zn(II)	3409	1017	1551	2926-2865	1151	1456	1058	613

Table 3. Electronic spectra, magnetic moment and ligand field parameters of polymer metal complexes.

Abbreviation	Magnetic moment, B.M.	Electronic spectral data		10Dq	*B*	β^0	$\beta^{\%}$
		Electronic transition, cm^{-1}	Assignment				
SPhe-Mn(II)	5.82	26445	$^4T_2g(D) \leftarrow {}^6A_1g(G)$	17742.7	810	0.843	15.7
		21186	$^4T_2g(G) \leftarrow {}^6A_1g(G)$				
		14947	$^4A_2g(G) \leftarrow {}^4T_2g(P)$				
Sphe-Co(II)	5.04	25445	$^4T_{2g}(F) \leftarrow {}^4A_{2g}(F)$	16291	775.7	0.799	20.1
		18416	$^4T_1g(F) \leftarrow {}^4T_1g$				
		15082	$^4T_1g(G) \leftarrow {}^4A_2g(G)$				
Sphe-Ni(II)	2.95	24450	$^3T_1g(P) \leftarrow {}^3A_2g(F)$	4285.01	840.19	0.77	22.3
		16420	$^3A_2g(F) \leftarrow {}^3T_1g(P)$				
		13351	$^3T_1g(F) \leftarrow {}^3A_2g(F)$				
Sphe-Cu(II)	1.98	15320	$^2A_{1g} \leftarrow {}^2B_{1g}(F)$				
		25108	Charge transfer				
Sphe-Zn(II)	diamagnetic	No transitions					

SPhe-Co(II) has a magnetic moment value 5.04 BM. due to four unpaired electrons and showed three bands at 25445, 18416.2, 15082.9 which were assigned to $^4T_2g(F) \leftarrow {}^4A_2g(F)$, $^4T_1g(F) \leftarrow {}^4T_1g$ and $^4T_1g(G) \leftarrow {}^4A_2g(G)$ transition respectively, and suggested octahedral environment around the Co(II) ion. The calculated values of 10Dq, B, β^0 and β% are 16291,775.7, 0.799, 20.1. 24449.8, 16420.3, 13351.1 are the three bands that has been observed for SPhe-Ni(II) which possess a transition $^3T_1g(P) \leftarrow {}^3A_2g(F)$, $^3A_2g(F) \leftarrow {}^3T_1g(P)$ and $^3T_1g(F) \leftarrow {}^3A_2g(F)$ respectively. Through these data the calculated values of 10*Dq*, *B*, β^0 and β% are found to be 4285.01, 840.19, 0.77, 22.3% respectively. The observed magnetic moment value for this compound is 2.95 BM and this suggested an octahedral structure. The above discussion very strongly indicates an octahedral geometry around the central metal ion in all polymer metal complexes and the making of octahedral geometry is supported by the occupation of two coordinating sites by H_2O out of six. This series of the study also defines the electronic spectra of the SPhe-Cu (II) ,which exhibits the transition of $^2A_{1g} \leftarrow {}^2B_{1g}$ and charge transfer spectra for the bands at 15320 cm^{-1} and 25108 cm^{-1} respectively, which indicate square-planar geometry.[26-31] 1.98 BM was the magnetic moment value of SPhe-Cu(II) which accords well with the square planar geometry. Tetrahedral geometry has been shown by the diamagnetic SPhe-Zn(II).

Thermogravimetric analysis

The thermal decomposition of poly-SPhe and its transition metal complexes and its blend is studied by the thermogravimetric method. The thermogravimetric curves of poly-SPhe and its transition metal complexes for a comparative analysis are depicted in Fig 5, and between SPhe and blend is given in Fig 6 and the thermal analytical weight loss % list of data are listed in Table 4.

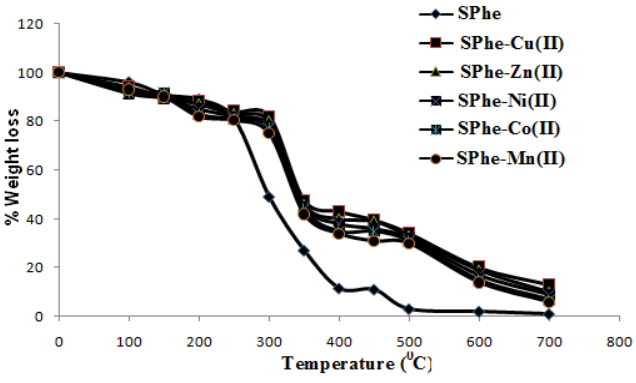

Figure 5. TGA curve of SPhe, SPhe-M(II)

 DOI: 10.17628/ecb.2014.3.149-156

Table 4. Thermal behaviors of SPhe , Blend and their polymer metal complexes

Compound/Temperature, ^{0}C	Weight Loss(%)								
	100	**150**	**200**	**250**	**300**	**400**	**500**	**600**	**700**
SPhe	4	5	2	8	32	26.5	8.5	1	1
Sphe-Mn(II)	6	4	2	4	2	39	10	14	7
Sphe-Co(II)	4	4	4	6	6	34	9	8	5
Sphe-Ni(II)	6	5	3	2	2	37	11	5	6
Sphe-Cu(II)	3	1	1	5	5	34.5	8	4	3
Sphe-Zn(II)	2	2	5	3	6	36	7	5	9
Blend	1	0.8	7.7	2	16	20.5	11.1	7.5	14.1

The poly-SPhe showed weaker thermal resistance as far as comparison to its metal polymer complex is concerned and started to decompose with weight loss from 4-6 % at 100 °C and this weight loss is mainly absorbed solvent loss and then futher mass loss from 100 °C to the higher temperature was related to the decay of crosslinked polymeric resin.

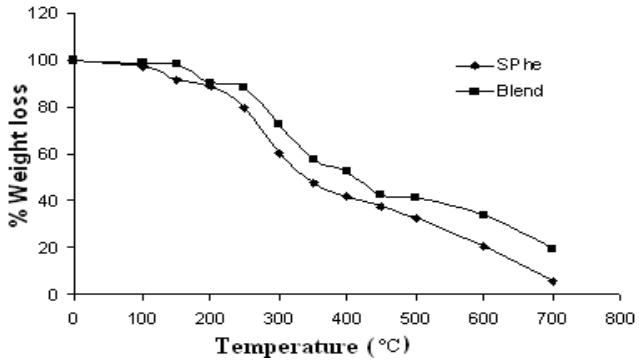

Figure 6. TGA curve of SPhe, Blend

The decomposition of poly-SPhe was less in the initial stage but above 250 °C wt loss showed a very fast steep downward mass loss. The thermal data indicate that the thermal stability of the poly-SPhe upto 250 °C, and then fast decaying, however its transition metal complexes showed lesser decreases in mass losses and decomposition and reduced mass loss at that particular increasing temperature.

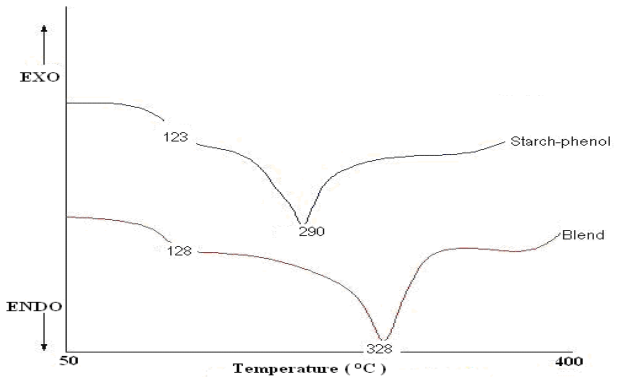

Figure 7. DSC curves of SPhe and it's Blend

The volatility of the poly-SPhe -metal complexes was reduced because of the formation of coordination bond with the metal. Metal complex started to decompose with weight loss 7-8 % at 100 °C and this loss can be mainly ascribed to attached coordinated water molecule. Although decomposition rate of polymer metal complexes was very slow up to 300 °C, but above 300 °C weight loss became fast. This result revealed that all the polymer metal complex show better heat resistant characteristics than the poly-SPhe due to the coordination of metal ions and chelation. Blend was slow at its decomposition initially and less mass is reduced as compared to SPhe. The volatility of the blend was reduced because of the formation of physical bonding while in the formation of blend. Polymer blend started to decompose with weight loss 1-2 % at 150 °C and the decomposition rate of blend was very slow upto 250 °C, but while reaching at temperature of 300 °C weight loss became fast. This pattern of data revealed that the blend show better heat resistant characteristics than the polymeric resin due to the enhanced stability, and these results are very well in correlation with the synthesis of blend.

Differential Scanning Calorimetry (DSC)

The DSC measurement has been done to create the comparison between the thermal points of SPhe and Blend and is given in Fig 7. The DSC measurements served to determine the glass transition temperature, *T*g and melting behavior. The melting temperature scattered typical range of 290 °C for Starch phenol, and the *T*g scattered in the range of 123 °C for starch phenol polymer, this evolution could be ascribed to the interactions between the starch and phenol. The strong H-bond formed between starch and phenol, which decrease starch chain mobility and consequently increased the matrix glass transition. Meanwhile, as compared to the starch phenol polymer, the melting temperature and *T*g of the blend is increased. The melting temperature scattered typical range for a blend at 328.73 °C. The *T*g scattered in the range of 128.49 °C. This indicate that the copolymer and linseed oil epoxy affect the thermal stability and glass transition of polymer blends. The single peaks of thermogram show the no phase separation in starch–phenol polymer blend.

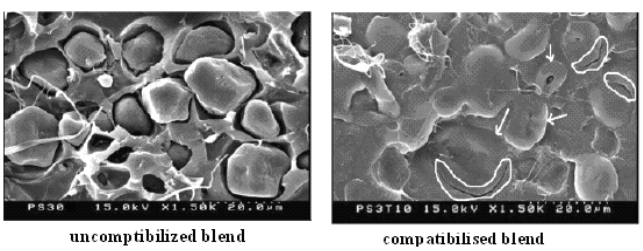

Figure 8. SEM micrograph of uncompatiblized and compatiblized blend

 DOI: 10.17628/ecb.2014.3.149-156

Scanning Electron Microscopy (SEM)

Figure 8 shows an electron micrograph of a blend with and without in the state of being compatibilized for the case of uncompatiblized and compatiblized blend. Clearly distinct phases are visible in the uncompatibilised blend. Where as, a more evenly distributed polymer, results from the compatibilised blend. The increase in homogeneity can be explained through the phobicity of the molecules in the blend. Starch is hydrophilic and PS-PMMA copolymer is hydrophobic, this causes repulsions throughout the uncompatibilised blend that are dramatically diminished by the well-dispersed copolymer addition and compatiblizer. When an uncompatibilised starch/copolymer blend is produced the two phases do not integrate well and stay as two distinct phases in a state of low interfacial adhesion. This causes the blend to be mechanically weak. By using suitable compatiblizer homogenization with greater extent occurred in these copolymer molecules throughout the starch/phenol matrix, a significant improvement in the properties was encountered as a result of this decreased repulsion and hence increased interfacial adhesion. Developing a blend with satisfactory overall physic-mechanical behaviors depends on a proper interfacial tension to generate a small phase size and strong interfacial adhesion to transmit an applied force effectively between the component phases.

BIODEGRADABLE ACTIVITY

Laboratory respirometeric method as a biotic function (ASTM- D5338-93) that uses compost pile inocula was used to evaluate the biodegradable activity of SPhe their polymer metal complexes and blend against some selected microorganism[32].

Table 5. % CO_2 mineralization of starch, SPhe, SPhe-M(II) and Blend

Time	% CO_2 mineralization			
	Starch	SPhe	SPhe-M(II)	Blend
24		0.3	0.25	
44	1.6	0.7	0.55	0.35
68	2.2	1.3	1.15	0.45
92	3.7	2.65	2	1.65
110	5	3.7	3.85	2.23
136	9	4.8	4.1	3.25
160	15	6.6	6.1	4.75
187	18.5	7.5	6.1	5.4
200	18.6	7.8	6.15	6.6

All the synthesized polymers show promising biodegradable activity against the given microorganism. Conveniently designed flask has been used for this purpose. Water or soil may be used in the test method but here soil is used. Although in both cases a suitable volume of activated sludge to obtain complete mineralization of the sample in about a month is used. It is recommended to use 10 cm^3L^{-1} for aqueous system but we have used 5 cm^3 50 g^{-1} with cold medium successfully. The inoculums must be kept aerated until used and it should be used on the same day as collected. Urea and potassium hydrogen phosphate (0.1 and 0.05 % of weight of polymer substrate) are added for the further growth of microbes and for the fortification of the medium. The biodegradation rates of starch, polymeric resin (SPhe)and polymer metal complexes (SPhe -Cu(II), SPhe -Mn(II), SPhe -Ni(II), SPhe -Zn(II), SPhe -Co(II) and Blend are shown in Fig.9.

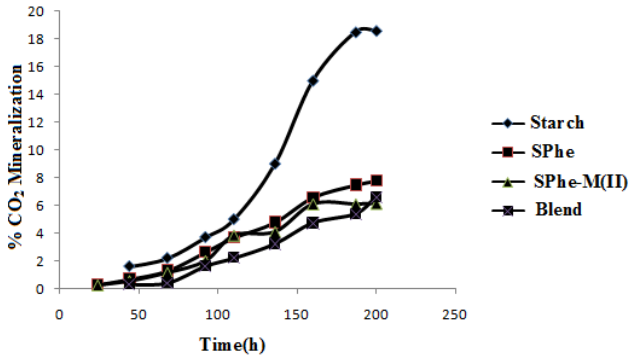

Figure 9. % CO_2 mineralization of starch , SPhe, SPhe-M(II) and Blend

From these figure and Table, it is clear that polymer metal complexes of poly-SPhe degrade at a slower rate than starch polymer after 200 hrs, and that the biodegradation rates of polymer metal complexes and Blends are comparatively similar, at regular interval of time.

REFERENCES

[1]Schwach. E., Averous. L., *Polym. In.*, **2004**, *54*, 2115.

[2]Glass. J.E., *ACS Symp. Ser.*, **1990**, *433*, 52.

[3]Narayan. R., Rowell. R. W., Schultz. T. P., Narayan. R., *ACS Symp. Ser.*, **1992**, *476*, 1.

[4]Braun. D., Cherdron. H., Ritter. H., *Polymer synthesis: theory and practice*, Berlin: Springer-Verlag, **2001**.

[5]Campbell. J. M., *Introduction to Synthetic Polymers*, Oxford Science, Oxford, **1994**.

[6]Knop. A., Pilato. L. A., *Phenolic Resins*, Springer Verlag, Berlin, **1985**.

[7]Feldman. D., *Polymeric Building Materials*, Elsevier, London, **1989**.

[8]*Kirk-Othmer Encyclopedia of Chemical Technology*, John Wiley & Sons, *New York*, **1985**, 628.

[9]Mori. F., *Jpn Kokai Tokkyo Koho, JP 08323949 A2* 961210 Hesei, **1996**.

[10]Mendes. S.C., Reis. R. L., Bovell. Y. P., Cunha. A. M., Van Blitterswijk. C. A., De Bruijn J. D., *Biomaterials*, **2001**, *22*, 2057.

[11]Leonor. I. B., Ito. A., Onuma. K., Kanzaki. N., Reis. R. L., *Biomaterials*, **2003**, 24,579.

[12]Duarte. M. G., Brunnel. D., Gil. M. H., Schacht. E., *J. Mater. Sci. Mater. Med.*, **1997**, *8*, 321.

[13]Elvira. C., Mano. J. F., San Roman. J., Reis. R. L., *Biomaterials*, **2002**, *23*, 1955.

[14]Scott, G. and Gilead, D., *Polym. Degrad. Stab.*, **2000**, *68*, 1 .

[15]Scott, G. and Gilead, D., *Degradable polymers principls and applications*, Chapman and Hall: London, UK , **1995**,15, 247.

[16]Resis, R. L., Cunha, A. M., Bevis, M. J., *Adv. Polym. Technol.*, **1997**, 16.

[17]Sharmim. E., Ashraf. S. M., Ahmad. S., *Int. J. Biol. Macromol.*, **2007**, *40*, 407 .

[18]Mohamed. G. G., Omar, M., Hindy. A. M., *Turk. J. Chem.*, **2006**, *30*, 361.

[19]Bakiler. M., Akyuz. S., *Bull. Chem. Technol. Macedonia*, **2002**, *21*, 35.

[20]Harvest Collier, L., Cho, Y., *Korean Polym. J.*, **1997**, *5*, 185 .

[21]Topacli, C., Topacli. A., *J. Mol. Struct.*, **2003**, *644*, 145 .

[22]Kumar, H., Tripathi, S. K., Mistry, S. and Bajpai, G., *E-J. Chem.*, **2009**, *6*, 1253 .

[23]Pajua, J., Pehkb, T., Christjansonc, P., *Proc. Estonian Acad. Sci.*, **2009**, *58*, 45 .

[24]Mounika, K., Anupama, B., Pragathi, J. and Gyanakumari, C., *J. Sci. Res*., **2010**, *2*, 513 .

[25]Pasanphan, W., Buettner, G. R., Chirachanchai. S., *Carbohydrate Res.*, **2010**, *345*, 132.

[26]Agwara. M. O., Yufanyi, M. D., Foba-Tendo, J. N. , Atamba, M. A., Derek, T. N., *J. Chem. Pharm. Res*., **2011**, *3*, 196.

[27]Bailey, R. A., Peterson, T. R., *Can. J. Chem.*, **1969**, *47*, 1681 .

[28]Chandra, S., Sharma, A. K., *Res. Lett. Inorg. Chem.*, **2009**, Article ID 945670, 4 pages .

[29]El-Moshaty, F. I., El-Zweay, R. S., El-Ajaily, M. M., Jerboa, A. M., *E-J. Chemistry*, **2011**, *8*, 19.

[30]Prasad, N. R. and Gupta, N., *J. Serb. Chem. Soc*., **2003**, *68*, 455.

[31]Sonmez, M., *Turk. J. Chem.*, **2011**, *25*, 181.

[32]Bellia, G., Tosin, M., Floridi, G., Degli-Innocenti, F., *Polym. Degrad. Stab.*, **1999**, *66*, 79.

Received: 13.11.2013.
Accepted: 18.12.2013.

SPARK PLASMA SINTERING OF PLASMA SYNTHESIZED NANOSIZED SiC POWDER

Zoltán Károly[a]*, Szilvia Klébert[a] , Eszter Bódis[a], István E. Sajó[a] and János Szépvölgyi[a]

Keywords: Sintering, silicon carbide, SPS, porosity, plasma synthesis

Spark Plasma Sintering (SPS) of thermal plasma synthesized nanosize powders were studied without removing the free carbon impurities. Instead, SiC was mixed with silicon powder to react with the free carbon during sintering with boron as sintering aids. Density of the resulted disc samples found to be increased with the applied temperature and achieved a maximal 93 % of relative density at 1950 °C after 5 minutes holding time. The obtained samples composed of β-SiC along with a few per cent of un-reacted graphite.

Corresponding Authors
Tel.: +(36).(1).4381100
Fax: +(36).(1).4381147
E-Mail: karoly.zoltan@ttk.mta.hu (Z. Károly)
[a] Institute of Materials and Environmental Chemistry, Research Centre for Natural Sciences HAS, Budapest, H-1025, Hungary

Introduction

Silicon carbide is an advanced ceramic material that has found widespread application both for structural and electrical purposes.[1] The enhanced mechanical properties and other outstanding features associated with nanosize particles and nanostructured bulk materials has directed an increased interest in manufacturing and sintering of nanosize powders. Several methods for the synthesis of nanosize powders have been developed over the last decades including sol-gel processes,[2] pyrolysis of silicon-bearing polymers,[3] CVD methods,[4] plasma synthesis[5-6] rapid carbothermal reductions,[7] etc. Nanosize powders require, however, special sintering treatment to retain the nanostructure. During conventional sintering substantial grain coarsening can occur on the account of the relatively prolonged sintering process at high temperatures. Spark plasma sintering (SPS) method is a newly developed technique that enables the compacted powder to be fully densified at a comparatively low temperature, and in a very short time intervals.[8-12] Several reports have already been published recently on the successful sintering of nanosize SiC by SPS retaining the nano-structured characteristic.[13,14] In these reports SiC was sintered with addition of various sintering aids in minor amounts. One of the main drawbacks of nanoparticle synthesis methods is that the primary products usually contaminated with carbon and unreacted silica.[15-16] These impurities are usually removed prior to sintering. Carbon is commonly eliminated by heating the sample in a furnace between 600-700 °C under oxidizing atmosphere. Even though SiC is considered to be an oxidation resistant material, during this process oxidation of the surface of silicon carbide particles is inevitable in thermodynamic point of view. In addition, due to the high specific surface area of the nanoparticles the oxygen contamination can also be increased. The formed oxide layer along with unreacted silica particles are easily eliminated by a subsequent acidic washing. The whole process, however, may lead to substantial yield loss. On the other hand, pure SiC is difficult to sinter due to its highly covalent nature, which results in very slow atomic diffusion. To promote sintering various sintering additives are used. Carbon is routinely employed when solid phase sintering mechanism is aimed. This may pose the question if carbon really has to be completely removed before sintering. In the practice of conventional SiC sintering there are well-developed methods for sintering SiC without removing the carbon. In these cases the compacted form is getting into contact with molten silicon. This way is not viable in advanced sintering methods such as SPS, or at least not in that form.

There has not been any study reported yet on the sintering of carbon contaminated SiC by SPS. In the present work we investigated the sintering behavior of nanosized SiC powders synthesized by thermal plasma processing without removing the free carbon content, which remained in the product after synthesis as an impurity. Unlike conventional sintering technique, silicon is initially mixed into the SiC powder to react with the free carbon remained in the powder. At the high temperature of sintering (>1800 °C) the reaction between silicon and carbon is thermodynamically favored. We investigated the completeness of the above reaction after sintering as well as the porosity of the obtained specimens.

Experimental

Nanosized SiC powder (marked as IMEC powder) was prepared by RF thermal plasma synthesis from solid precursors, namely fine powders of silica and carbon. Experimental details of the procedure were published elsewhere.[17] It was found that the SiC particles were contaminated with non-reacted silica and carbon precursors. The silica was leached out with hydrofluoric acid but the carbon wasn't burnt out for fear the fine silicon carbide may also be oxidized. In this way the starting SiC powder, which was used for sintering had lower oxygen contamination (3 wt. %) but had free carbon content as much as 20 wt.%. Reference tests were also performed using commercial SiC powder (Carborex F1200, Washington Mills). Main characteristics of the tested SiC powders are detailed in Table 1.

Table 1. Specifications of SiC powders used in sintering tests

SiC Powder	Phases	Specific area, $m^2 \cdot g^{-1}$	Mean size, μm	Purity (wt%)				
				SiC	Free C	Si	O_2	Fe
Commercial	α	0.6	3	98.3	0.25	0.35	0.60	0.10
IMEC	β	54	0.035		~20	<0.1	3.1	0.17

Boron (H.C.Starck) and silicon (Aldrich) additives were mixed with SiC powders in a ball mill using ethanol. The mechanism by which boron facilitates sintering is still under discussion[18-19] but its beneficial effect is indisputable, while carbon has the role to remove the oxygen from the surface of SiC particles. The additives and their ratio in particular tests are given in Table 2. Finally the mixtures were dried by infrared heating for 1 hour.

The SPS consolidation was carried out using a HP D5 apparatus (FCT GmbH, Germany). 3 grams from each mixture were put into a cylindrical graphite die having an inner diameter of 20 mm. A vacuum of 3 Pa was maintained in the chamber. The powders were uniaxial pressed throughout the sintering process with 30 MPa up to 600 °C, above that it was increased to 50 MPa. A degassing treatment was performed at 600 °C for 5 minutes. The maximum sintering temperatures were selected to be 1850 °C and 1950 °C with a heating rate of 100°C min-1. A soaking time of 5 minutes were applied at the sintering temperature. In one test an extra holding time was applied at 1600 °C for 5 minutes. It is reasoned by our previous tests that showed an increased densification rate at this temperature. In each case, pressure was released at the end of the holding time and specimens were cooled down to room temperature in the die. The experimental parameters including temperature, applied load and sample displacement were measured continuously during sintering. The temperature was controlled by an infrared pyrometer that focused to a hole drilled in the upper graphite punch thereby only a few millimetres from the sample surface. Linear shrinkage of the powder compacts during the SPS process was continuously monitored by displacement of the punch rod.

The sintered samples were cleaned by grit blasting then analyzed for microstructure by scanning electron microscopy (SEM Hitachi HR-SEM S4800 and Philips XL30 model a) and phases by X-ray powder diffraction (XRD, Siemens D5000 diffractometer) using CuKα radiation. Density of the specimens was measured by Archimedes method in distilled water.

Results

Figure 1. shows the linear shrinkage of the different SiC disc samples against temperature during SPS treatment. The starting temperature of reduction can be assessed from the diagram. However, it was determined more precisely using the differentiation of the deformation curves (Table 2). It can be noticed that without sintering aids densification started at much higher temperature (TS) as compared to the other tests. This temperature (TS) considerably decreased by addition of boron and carbon to SiC powder. Using the plasma synthesized nanopowders (IMEC) the densification shifted down at even lower temperatures. From Fig. 1 one can also compare the sintering tests with respect to their final shrinkage. Maximum reduction was determined at the end of the soaking time at the highest sintering temperature. Analyzing these values it can be observed that tests carried out at 1850 °C had almost the same reduction, while the best densification was obtained using nanosized powder at 1950 °C.

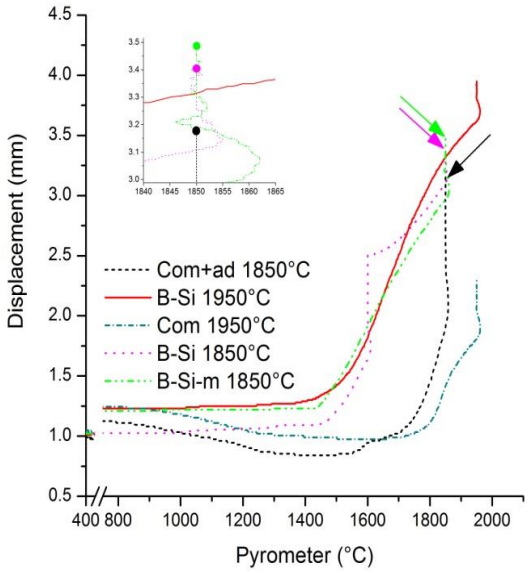

Figure 1. Linear shrinkage of the sintered samples against temperature.

X-ray diffraction plots of commercial and IMEC powders sintered at different temperatures are shown in Fig. 2. No phase changes occurred in any sample during sintering.

The commercial powder that composed of α-polytypes (6H and 12H) no any phase change was presumed. However, the plasma synthesized SiC powder composed of β-polytypes. The β to α phase formation is common at high temperatures especially in the presence of traces of α-polytypes that facilitate this transformation as nuclei. Even though, in tests No 3-5 using IMEC powder no such β-to- α transformation was detected. Similar observations were reported in other papers,[20-22] as well.

According to Suzuki[20] for obtaining pure β-SiC ceramics the powder has to be free of stacking faults. During SPS the applied lower temperature and shorter sintering time was not sufficient for such a phase change. Other studies also confirm this observation. Beyond SiC, graphite was present in minor amount, too, while silicon was not detected in the XRD plot at all.

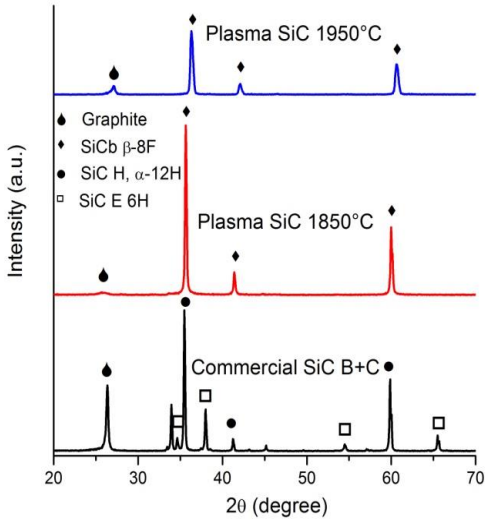

Figure 2. XRD plots of the sintered disc samples.

Discussion

The relative densities of the sintered products are listed in Table 2. These are in good agreement with the maximum values of the reduction curves in Fig. 1. It is apparent that the commercial SiC without additives hardly sintered in particular conditions; the final density was close to the green density. The difficulties in sintering pure SiC are well known. Pressure-less sintering can be hardly viable without sintering aids. Even using the conventional pressurized techniques such as hot pressing or hot isostatic pressing high sintering temperatures (T≥2100 °C) and long soaking times (*t*≥30 min) are required. There are, however, reports [13-14] of achieving almost full density SiC without sintering aids using SPS owing to the increased surface diffusion and plastic deformation caused by the electric discharges between particles. Applying the same conditions in our test, intensive densification of pure SiC began above 1760 °C. However, the shrinkage finished after 5 min of soaking at 1950 °C. The commercial SiC was failed to achieve similar densification probably because of its micron sized character. The SEM image (Fig. 3.a) of the sintered body of commercial SiC shows a rather porous structure. In this stage of sintering only neck formation began among particles.

Boron and carbon addition to commercial SiC reduced the starting temperature of densification to 1540 °C. In addition, the sintering temperature also decreased to 1850 °C and the sintered body achieved significantly much higher final shrinkage. The relative density obtained under these conditions is in line with other reports.[13] Indeed, SEM image of the sintered product (Fig. 3.b) shows that although neck formation has been finished, pores can be still observed in the microstructure.

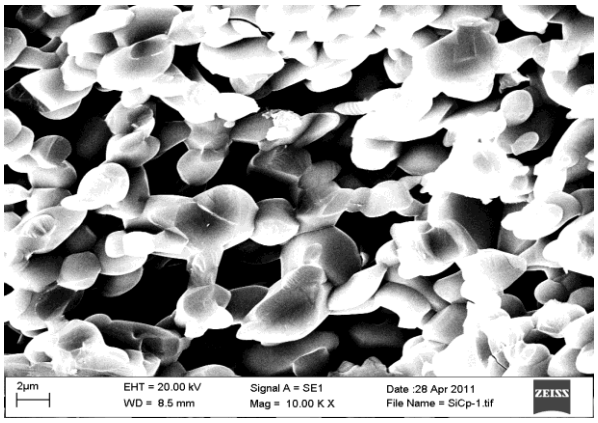

Figure 3a. SEM images of the fracture surface of sintered samples (a) commercial SiC sintered at 1950 °C.

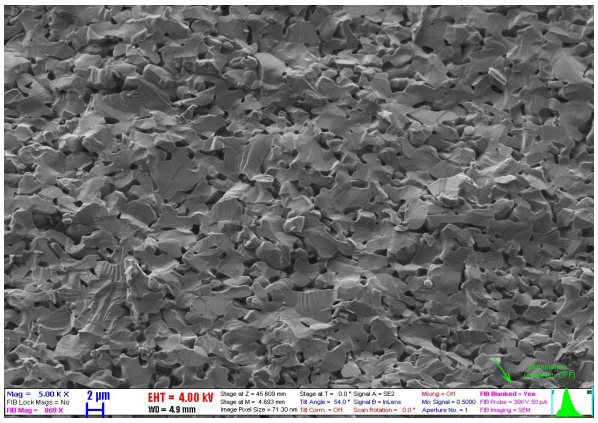

Figure 3b. SEM images of the fracture surface of sintered samples, (b) commercial SiC with B and C sintering aids sintered at 1850 °C.

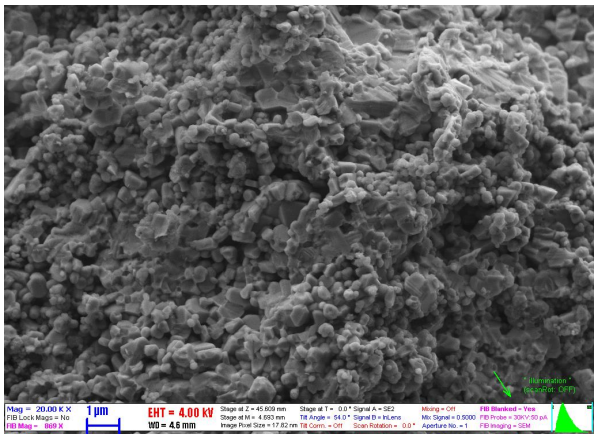

Figure 3c. SEM images of the fracture surface of sintered samples (c) nanosized SiC with B and Si sintering aids sintered at 1850 °C.

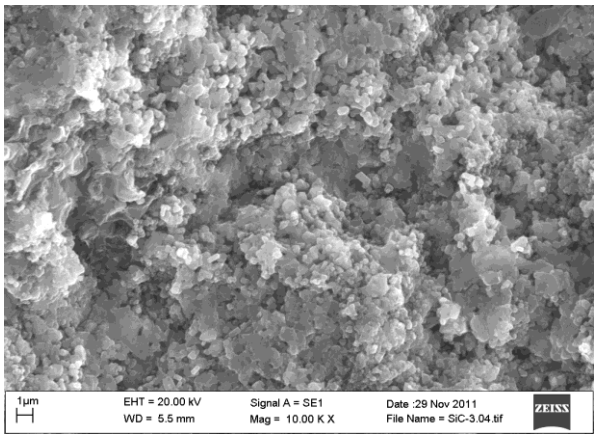

Figure 3d. SEM images of the fracture surface of sintered samples, (d) nanosized SiC with B and Si sintering aids sintered at 1950 °C.

In sintering experiments using IMEC nanopowders, densification started at still lower temperatures of 1420-1440 °C. Interesting, however, that final reduction of IMEC powder sintered at 1850 °C did not exceed that of commercial SiC mixed with additives (Fig. 1). Even the relative densities of the sintered bodies were similar for the commercial and the IMEC powders. It is because of the excess carbon that was not completely reacted with the silicon in experiment No. 3. Comparing the SEM images of these samples (Fig. 3.b-c) great difference can be observed in the grain size. Although the porosity of the disc samples was identical, the nanosize structure could be retained on sintering of plasma synthesized IMEC powders. Variation in the heating schedule during sintering by inserting a new holding step at 1600 °C corresponding to the temperature of highest densification rate did not lead to higher overall densification either.

Table 2. Sintering conditions and relative densities of the SPS sintered ceramics

SiC powder	Additives, wt%	Sintering temperature, °C	Relative density, %
Commercial	no	1950	64
Commercial	B-0.6 C-3	1850	85
IMEC	B-0.6 Si-10	1850	84
IMEC	B-0.6 Si-10	1600	81
IMEC	B-0.6 Si-10	1950	94

The highest relative density was obtained on sintering the nanosized powder at 1950 °C (Test No. 5). Densification started similarly to the previous two tests at 1420 °C, but it had a more distinctive peak above 1600 °C. The lack of silicon in the XRD plot suggests that it reacted with the free carbon in the starting powder and formed SiC. It also revealed that silicon additives did not cause any lag in sintering time due to the reaction between silicon and the free carbon. The SEM image of the sample (Fig. 3.d) exhibits a dense product seemingly free of pores.

Conclusion

In the present study nanosized monolithic SiC ceramic was prepared by SPS method using plasma synthesized SiC nano-powders containing considerable amount of carbon as an impurity. We found that the silicon powder initially added to SiC along with some boron reacted with the free carbon to form SiC. According to this way a 93 % relative density was obtained after 5 minutes of sintering at 1950 °C. The sintered disc sample composed of β-SiC phase and minor amounts of free carbon. As compared to micro sized commercial SiC powder with 0.25 wt.% of free carbon similar densities were achieved with nanosized SiC powder. However, in the latter case nanosized microstructure was formed. The result showed that instead of removing the excess carbon from the nanosized powders, they could be sintered by SPS in short time by adding silicon powder.

Acknowledgements

This work was supported by the National Office for Research and Technology (NKTH) (Project No: REG-KM-09-1-2009-0005).

References

[1]Lee, W. E., Rainforth, W. M., *Ceramic Microstructures, Property Control by Processing*. London: Chapman & Hall; **1994.**

[2]Cerovic, L., Milonjic, S. K., Zec, S. P., *Ceram Int.*, **1995**, *21(4)*, 271.

[3]Narisawa, M., Shimoda, M., Okamura, K., Sugimoto, M., Seguchi, T., *Bull. Chem. Soc. Jpn.*, **1995**, *68(4)*, 1098.

[4]Cao, L. Z., Jiang, H., Song, H., Li, Z. M., Miao, G. Q., J Alloy Compd., **2010**, 489(2), 562.

[5]Kong, P., Huang, T. T., Pfender, E., *IEEE Trans Plasma Sci*,. **1986**, *14(4)*, 357.

[6]Stachowicz, L., Singh, S. K., Wender, E., Girshick, S.L., *Plasma Chem. Plasma Process*., **1993**, *13(3*), 447.

[7]Pan, S., Zhang, J., Yang, Y., Song, G., *Ceram Int.*, **2008**, *34(2)*, 391.

[8]Zhang, Z. H., Wang, F.C., Lee, S.K., Liu, Y., Cheng, J. W., Liang, Y., *Mater. Sci. Eng. A*, **2009**, *523(1-2)*, 134.

[9]Orru, R., Licheri, R., Locci, A. M., Cincotti, A., Cao G., *Mater. Sci. Eng. R.*, **2009**, *63(4-6)*, 127.

[10]Anselmi-Tamburini, U., Garay, J. E., Munir, Z. A., *Scr. Mater.*, **2006**, *54(5)*, 823.

[11]Chen, W, Anselmi-Tamburini, U, Garay, J. E., Groza, J. R., Munir, Z. A., *Mater. Sci. Eng. A*, **2005**, *394(1-2)*, 132.

[12]Trombini, V., Pallone, E. M. J. A., Anselmi-Tamburini, U., Munir, Z. A., Tomasi, R., *Mater. Sci. Eng. A*, **2009,** *501(1-2)*, 26.

[13]Zhang, Z. H., Wang, F. C., Luo, J., Lee, S. K., Wang, L., *Mater. Sci. Eng. A*, **2010**, *527(7-8)*, 2099.

[14]Maitre, A., Vande Put, A., Laval, J. P., Valette, S, Trolliard, G., *J. Eur. Cer. Soc.*, **2008**, *28(9)*, 1881.

[15]Moshtaghioun, B. M., Monshi, A., Abbasi, M. H., Karimzadeh, F., *Int. J. Ref. Met. Hard Mat.*, **2011**, *29(6)*, 645.

[16]Nayak, B. B., Mohanty, B. C., Singh, S. K., *J. Am. Ceram. Soc.*, **1996**, *79(5)*, 1197.

[17]Károly, Z., Mohai, I., Klébert, Sz., Keszler, A., Sajó, I. E., Szépvölgyi, J., *Powder. Tech.*, **2011**, *214*, 300.

[18]Shinoda, Y., Yoshida, M., Akatsu, T., Wakai, F., *J. Am. Ceram. Soc.*, **2004**, *87(8)*, 1525.

[19]Datta, M. S., Bandyopadhyay, A. K., Chaudhuri, B., *Bull. Mater. Sci*., **2002**, *25(3)*, 181.

[20]Suzuki, H., *Mater. Chem. Phys*. **1995**, *42*, 1.

[21]Noviyanto, A., Yoon, D. H., *Mat. Res. Bull.* **2011**, *46(8)*, 1186.

[22]Lara, A., Ortiz, A. L., Munoz, A., Dominguez-Rodriguez, A., *Ceram. Int*., **2012**, *38(1)*, 45.

Received: 07.12.2013.
Accepted: 19.12.2013.

ELECTROCHEMICAL GOLD EXTRACTION FROM THE RESIDUES OF VACUUM-THERMAL TREATMENT OF GOLD-CONTAINING ANTIMONY ORES

Tsisana Gagnidze,[a] Jondo Bagdavadze,[b] Rusudan Chagelishvili,[a] Manana Mamporia,[a] Aleksi Kandelaki,[b] and Zurab Tsiskaridze[b]

Keywords: electrochemical processing, gold-containing antimony ores, gold extraction

The method for gold extraction from the residues of vacuum-thermal treatment of the concentrate of gold-containing antimony ore of Zopkhito (deposit) has been established by eco-friendly electrochemical method. The effect of main technological parameters on the process of electrochemical leaching of the residues has been studied in the presence of a selective ligand, thiourea, in chloride system and optimal conditions of leaching have been established providing for the gold extraction from gold-containing residues by 82-90 % in the conditions of so-called "soft" oxidation without release of molecular chlorine at the anode and eco-contamination. Continuous technological process of electrochemical leaching of the residues of gold-containing antimony ore and electrochemical reactor for realization of this process are proposed.

Corresponding Authors
Tel: **+ 995 593 74 08 43**
E-Mail: **ts.gagnidze@mail.ru**
[a] I. Javakhishvili Tbilisi State University, R. Agladze Institute of Inorganic Chemistry and Electrochemistry, Georgia, Tbilisi, Mindeli str.11, 0182.
[b] F. Tavadze Institute of Metallurgy and Materials science, Georgia, Tbilisi, Kazbegi str. 7.

INTRODUCTION

The most important way to meet the increasing demand for non-ferrous, noble and rare metals is to enhance the efficiency of the processing of the raw materials. To achieve this, it is necessary not only to improve the existing technologies but also to find new, atom-efficient and eco-freindly metallurgical processes. Complete extraction of valuable components from gold-containing antimony ores and their concentrates of Zopkhito deposit (Mountainous Racha) poses a serious challenge.

Most of gold-containing antimony ores are resistant to the common process of gold extraction-treatment with cyanide. One of the reasons of this resistance is a presence of finely-impregnated gold in sulfide mineral of arsenic and antimony. Further, antimonite sulfide destroys cyanide.

The goal of our research involves development of a process for the recovery of gold from the resistant antimony ores of Zopkhito deposit (Mountainous Racha)

In Table 1, chemical composition of the concentrate of Zopkhito ore is presented.

The concentrates of Zopkhito deposit was subjected to vacuum-thermal process at high-temperature vacuum plant (10^{-5} MPa, 400-600 ^{0}C), in F. Tavadze Institute of Metallurgy and Materials Science. As a result of vacuum – thermal treatment of the concentrate, antimony sulfide (Sb_2S_3) and high-purity antimony are produced and whole of gold (already shorn of protective sulfide layer) remained in the cinder. Gold-extraction to a high extent from the gold-containing cinder of this type is possible by hydro-metallurgical methods.

Hydrometallurgical cyanide process[1,2] has been widely used in to extract precious metals from gold-containing raw material. The method is characterized by high toxicity, high costs and low selectivity. Further, the disposal of cyanide solutions presents serious environmental problems.

Hydrochlorination method[3] is considered as one of the real alternatives of the cyanide process of treating of the residues of vacuum-thermal treatment of gold-containing antimony ore. It was shown[4] that in concentrated chloride solutions, the normal potential of Cl_2/Cl^- electrode is more positive (1.242 V) than that of Au^{3+}/Au electrode (1.012 V) which allows metallic gold to be oxidized by molecular chlorine, dissolved in the solution:

$$2Au+3Cl_2+2HCl \rightarrow 2HAuCl_4 \quad (1)$$

The system Cl_2-NaCl-HCl-H_2O, which contains 0.5 M HCl and is characterized by the highest value of redox potential, was used by us to treat gold-containing quartzites by the method of electrochlorination leaching.[5] The process of electrochemical leaching of gold-containing raw material proceeds at the anode by generation of molecular chlorine which oxidizes gold with the formation of an anionic complex $[AuCl_4]^-$ with dissociation constant value of K=1.2x10^{-12} (pK=11.2).[6] Because of negative charge, the complex cannot migrate to the catholyte and consequently is unable to discharge at the cathode with the formation of metallic gold and remains in the anolyte. Therefore the process of gold extraction from the solution by this method requires the additional operations which hinder the leaching process. Another disadvantage lies in the necessity of high redox potential (higher power consumption) and environmental contamination by excess molecular chlorine, separated at the anode in the course of leaching.

Table 1. Chemical composition of the concentrate of Zophito gold-containing ore

Au, g ton^{-1}	Ag, g ton^{-1}	Sb, %	Fe, %	Al, %	Cu, %	As, %	SiO_2, %	Pb, %	Ni, %
4.5	1.2	6.0	5.0	5.0	0.2	1.5	75	0.1	0.1

Table 2. Chemical composition of the residue of vacuum-thermal treatment of the concentrate of gold-containing antimony ore of Zopkhito deposit

Au, g ton^{-1}	Ag, g ton^{-1}	Sb, %	Fe, %	Al, %	Cu, %	As, %	Si, %	Pb, %	Ni, %
5.5	2.0	1.0	2.0-5.0	5.0	0.02	0.7	67-70	0.1	0.1

Investigations were carried in aqueous solutions containing chlorides of alkali metal and ligands which form strong complexes with gold with an aim to enhance the efficiency of the electrochemical process and to make it more eco-friendly. It has been reported[7] that lower is the standard redox potential of the aqueous solutions of gold-complex, stronger is the gold-complex. The thermodynamic ease of the oxidation of gold is indicated by the reduction in the redox potential of the complex-forming ligand on its addition to the system. The ease of oxidation finally depends on the kinetic parameters of the process.

On the basis of experiments,[8] thiourea was chosen as selective ligand for complexation with gold. Thiourea is characterized by penetration into internal sphere of complex compounds of some heavy metals with the formation of new strong complex compounds.[9] By the addition of thiourea in chloride system redox potential of the solution is reduced from 1.0 to 0.4 V. Such low redox potential of the system leads to electrochemical leaching of gold from ores under the so-called "soft" oxidative conditions and does not involve release of chlorine at the anode and consequent environmental contamination,[8,10] Under the experimental conditions, polarization of gold and its passage into the solution phase take place in the anode area. As a result a cationic complex with thiourea, $[Au(Thiourera)_2]^+$ is formed with a dissociation constant, $K = 10^{-23}$ ($pK = 22$)[7] by the reaction:

$$Au + 2Thiourea + Cl^- = [Au(Thiourea)_2]^+Cl^- + e^- \quad (2)$$

The cationic complex of gold with thiourea is considerably more stable than the anionic chloride one which is due to low (0.38 V) standard potential of the reaction (2). Along with it, due to the presence of positive charge, migration of the cationic gold complex into cathode area and its discharge at the cathode results in the formation of metallic gold. The above-mentioned process of electrochemical leaching considerably simplifies the passage of gold from the ore to the solution and its subsequent extraction since these processes are performed in the same electrochemical apparatus.

EXPERIMENTAL

The main components of the samples of the residues of vacuum-thermal treatment of the concentrate of gold-containing antimony ore of Zopkhito deposit, which were subject of this study, are given in Table 2.

The process was carried out at pilot plant of our elaboration (Fig. 1).

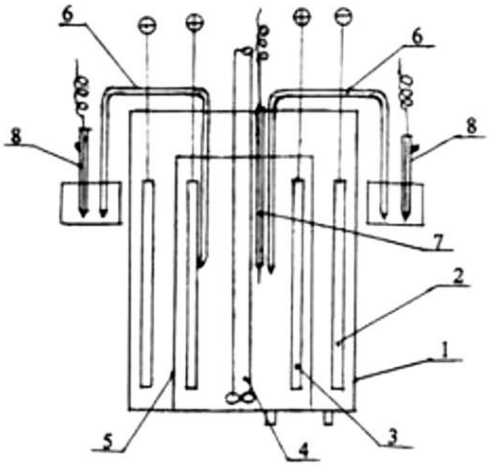

Figure 1. Scheme of stationary electrolyzer

1-electrolyzer body; 2-cathode; 3-anode; 4-mixer; 5-diaphragm; 6-electrolytic key; 7-Pt-electrode; 8-Ag/AgCl reference electrode

The anode cell is located at the center of the plant. Graphite was used as the anode and carbon-fiber material, which is characterized by high reaction surface, was used as the cathode. The diaphragm consists of thermally treated perchlorovinyl cloth. In the anode cell, the suspension was the intensively agitated. The process proceeded under potentiostatic regime. Redox potential, anode potential (φ_a), temperature and electrolysis conditions were controlled. Silver chloride electrode was used as a reference one. The potentials were recalculated in terms of potential of normal hydrogen electrode. At the end of the experiment the spent suspension was filtered, the sediment was washed by plumping, dried and the gold content was determined by atomic-absorption spectrometer.

The experiments were performed to establish the effect of electrolyte composition and of process parameters on the indexes of gold extraction by electrochemical method from the residue of vacuum-thermal treatment of the concentrate of gold-containing antimony ore.

 DOI: 10.17628/ecb.2014.3.161-165

RESULTS AND DISCUSSION

Experimental results are given in Table 3. It was observed that with an increase in the concentration of thiourea in the electrolyte, the degree of gold extraction enhances and attains a maximum in the concentration range of 0.5- 0.6 M, which corresponds to the lowest redox potential of the system.

Experimental results (Table3-III) indicated that at the absence of KCl anodic extraction of gold is characterized by low indexes and an addition of 0.5 M of KCl to the solution resulted in considerable increase of gold extraction. Addition of small amounts of Na_2SO_3 and Na_2S, which exerts the catalytic influence on the process[11], caused further increase in the degree of gold extraction.

Temperature has a pronounced effect on the indexes of the gold extraction. It is well-known[3] that thiourea-containing solution is stable at 25-30 ^{0}C, therefore, the experiments were performed in this temperature range. As is seen from Table 3-IV, the temperature variation in the range of 22-27 ^{0}C has a negligible effect on the indexes of gold extraction but attains a value of ~90 % at 30-32 ^{0}C.

It has also been observed (Table 3-VI-VII) that the size of ore particles and ratio between solid and liquid phases has a pronounced effect on the index of gold extraction. In particular, in the case of large-size particles (0.16 mm) the index of gold extraction is greater (~86 %). Similarly, smaller is the solid: liquid ratio, greater is the degree of gold extraction (Table 3-VI). This observation may be explained by current distribution in pulp area during the course of electrochemical process.

It is well-known[12] that thiourea system is stable at anode potential of ~0,6 V. At higher potential the anodic oxidation of thiourea takes place. Therefore electrochemical process of ore leaching was carried out in potentiostatic regime where a rigid control of anode potential was maintained. As the experiments show (Table 3-VIII), the indexes of gold extraction attain maximum value at anode potential = 0.5±005 V and is ~84 %.

Thus the optimum condition for the maximum extraction of gold (82-90 %) from the concentrate is the use of solution containing 0.5 M KCl + 0.5 M Thiourea + 0.03 M Na_2S, in potentiostatic regime, φ_a=0.5±0.05 V, T=22-32 ^{0}C, grinding degree = 0.16 mm and pH<1.

Based on the experimental results, a continuous technological process for the extraction of gold from the residue (or ore concentrate) of vacuum-thermal treatment of gold-containing antimony ore of Zopkhito deposit was developed and an electrochemical reactor was created. The electrodes for the reactor were made of highly-developed surface carbon-fiber material, which are characterized by high efficiency especially in solutions containing electro-active components in low concentration (Fig. 2).

The reactor operates in the following manner: the pulp is supplied to the reactor and immediately after switching of a mixer the catholyte is fed to cathode cell. When anode and cathode cells are filled by the solutions, constant current of optimal parameters is supplied to the reactor. After a definite time the control of the composition of anolyte and catholyte drain is carried out. On attaining of optimal composition an adjustment of maximum rate of the solutions supply is carried out by corresponding control. Thus putting of the reactor into stationary regime of operation is completed.

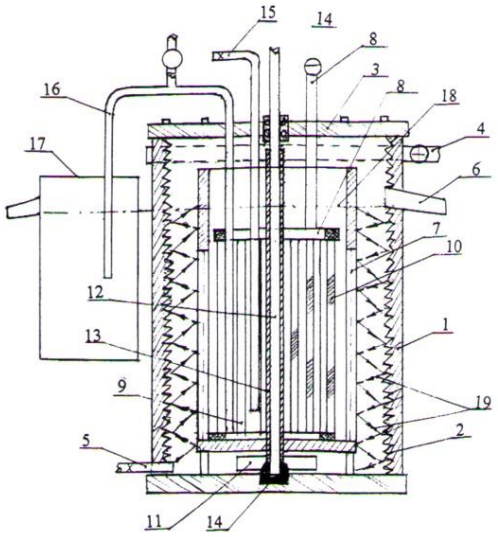

Figure 2. Electrochemical reactor

1-reactor body-graphite anode; 2-anode operating surface; 3-reactor cover; 4-current leading rim; 5-pulpsupplying branch pipe; 6-pulp discharging chute; 7- diaphragm-cathode cell; 8-cathode cassette with current lead; 9-cathodes; 10-carbon material tightly reeled up on the cathode; 11-pump-mixer; 12-pump driving shaft; 13-pump shaft isolating pipe enclosure casing; 14-pump shaft bearings; 15-catholyte supplying pipe; 16-siphon drain for spent catholyte; 17-inter-mediate vessel; 18- solution level; 19-trajectory of pulp circular movement

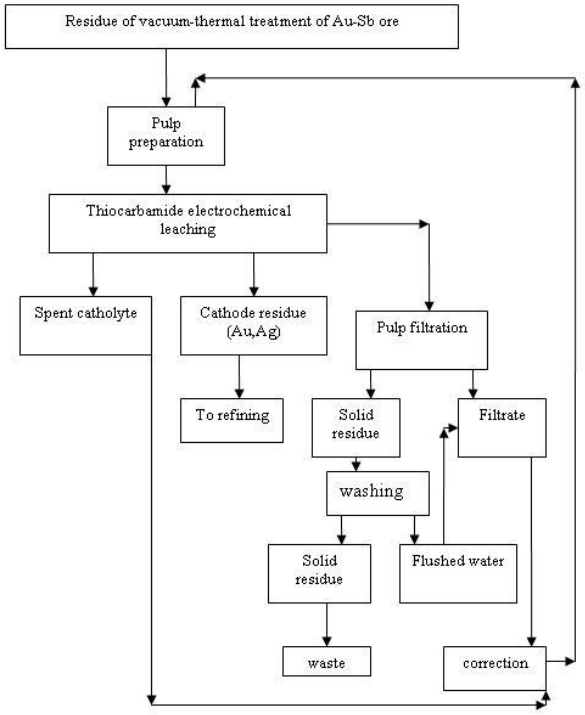

Figure 3. Basic technological scheme of electrochemical leaching of the residue of vacuum-thermal treatment of gold-containing antimony ore

 DOI: 10.17628/ecb.2014.3.161-165

Table 3. Research of technological process of gold extraction by electrochemical method from the residue of vacuum-thermal treatment of gold-containing antimony ore of Zopkhito deposit

#	Composition	Red/Ox potential, V	φ_a, V	T, °C	τ, hours	pH	Solid:Liquid ratio	σ, mm	I, A	U, V	W, Vt	Au recovery %	Remarks
I	0.5 M KCl + 0.35 M ThiO	0.435	0.4±0.05	25 °C	4	<1	1 : 3	-0.063	0.007	0.7	0.0049	77	potentiostatic regime
	0.5 M KCl + 0.5 M ThiO	0.421	0.4±0.05	25 °C	4	<1	1 : 3	-0.063	0.012	1.1	0.0132	81.8	potentiostatic regime
	0.5 M KCl + 0.65 M ThiO	0.419	0.4±0.05	25 °C	4	<1	1 : 3	-0.063	0.017	0.75	0.0075	81.2	potentiostatic regime
II	0.5 M KCl + 0.5M ThiO	0.423	0.4±0.05	25 °C	4	<1	1 : 3	-0.063	0.012	1.1	0.0132	81.8	potentiostatic regime
	0.9 M KCl + 0.5M ThiO	0.450	0.4±0.05	25 °C	4	<1	1 : 3	-0.063	0.01	0,9	0.009	79.8	potentiostatic regime
	1.3 M KCl + 0.5M ThiO	0.466	0.4±0.05	25 °C	4	<1	1 : 3	-0.063	0.0081	0.8	0.0065	70.9	potentiostatic regime
III	0.5 M ThiO	0.454	0.4±0.05	25 °C	4	<1	1 : 3	-0.063	0.031	1.83	0.057	63.6	potentiostatic regime
	0.5 M NaCl + 0.5 M ThiO	0.431	0.4±0.05	25 °C	4	<1	1 : 3	-0.063	0.006	0.85	0.05	76.1	potentiostatic regime
	0.5 M KCl + 0.5 M ThiO+ 0.024 M Na_2SO_3	0.453	0.4±0.05	25 °C	4	<1	1 : 3	-0.063	0.017	1.57	0.027	83.2	potentiostatic regime
	0.5MKCl + 0.5 M ThiO + 0.03 M Na_2S	0.438	0.4±0.05	25 °C	4	<1	1 : 3	-0.063	0.04	1.75	0.07	82.9	potentiostatic regime
IV	0.5 M KCl + 0.5 M ThiO	0.422	0.4±0.05	22 °C	4	<1	1 : 3	-0.063	0.012	1.1	0.0132	81.8	potentiostatic regime
	0.5 M KCl + 0.5 M ThiO	0.427	0.4±0.05	27 °C	4	<1	1 : 3	-0.063	0.012	1.1	0.0132	81.8	potentiostatic regime
	0.5 M KCl + 0.5 M ThiO	0.461	0.4±0.05	30-32 °C	4	<1	1 : 3	-0.063	0.016	1.1	0.0176	89.9	potentiostatic regime
V	0.5 M KCl + 0.5 M ThiO	0.420	0.4±0.05	25 °C	2	<1	1 : 3	-0.063	0.057	1.25	0.071	80.4	potentiostatic regime
	0.5 M KCl + 0.5 M ThiO	0.427	0.4±0.05	25 °C	4	<1	1 : 3	-0.063	0.011	0.9	0.01	81.8	potentiostatic regime
	0.5 M KCl + 0.5 M ThiO	0.430	0.4±0.05	25 °C	5	<1	1 : 3	-0.063	0.012	1.1	0.0132	81.8	potentiostatic regime
VI	0.5 M KCl+0.5 M ThiO	0.426	0.4±0.05	25 °C	4	<1	1 : 3	-0.063	0.012	1.1	0.0132	81.8	potentiostatic regime
	0.5 M KCl+0.5 M ThiO	0.415	0.4±0.05	25 °C	4	<1	1 : 5	_"_"_	0.012	1.1	0.0132	72.7	potentiostatic regime
VII	0.5 M KCl + 0.5 M ThiO	0.42	0.4±0.05	25 °C	4	<1	1 : 3	-0.05	0.01	0.95	0.0151	81.8	potentiostatic regime
	0.5 M KCl + 0.5 M ThiO	0.429	0.4±0.05	25 °C	4	<1	1 : 3	-0.063	0.012	1.1	0.0132	81.8	potentiostatic regime
	0.5 M KCl + 0.5 M ThiO	0.458	0.4±0.05	25 °C	4	<1	1 : 3	-0.16	0.141	1.79	0.25	85.5	potentiostatic regime
VIII	0.5 M KCl + 0.5 M ThiO	0.426	0.4±0.05	25 °C	4	<1	1 : 3	-0.063	0.012	1.1	0.0132	81.8	potentiostatic regime
	0.5 M KCl + 0.5 M ThiO	0.518	0.5±0.05	25 °C	4	<1	1 : 3	_"_"_	0.0136	1.65	0.022	83.6	potentiostatic regime

Thio=Thiourea

DOI: 10.17628/ecb.2014.3.161-165

In the course of ore leaching in anode area the gold dissolving and the formation of the cathionite complex with thiourea takes place. The complex after migration through filtering, thermally treated perchlorovinyl diaphragm enters in cathode area where gold is discharged at the cathode, manufactured from carbon-fiber material and free ligand-containing solution is returned to anode area for pulp preparation.

The continuous technological scheme of the process of electrochemical leaching of the residue of vacuum-thermal treatment of the concentrate of gold-containing antimony ore is presented (Fig.3).

Thus on the basis of experimental results it may be concluded that the efficient processing of residue of vacuum-thermal treatment of gold-containing antimony ore of Zopkhito deposit is possible by 82-90 % gold extraction by electrochemical method using chloride electrolyte to which thiourea - selective complex former with gold is added. The process proceeds in the conditions of so-called "soft" oxidation without release of molecular chlorine and environmetal contamination.

References

[1]*Izvlechenie zolota iz upornikh rud i concentratov*. Pod. red. Lodeishchikova, V. V. M.: Nedra, **1968**, 287.

[2]*Tekhnika i tekhnologia izvlechenia zolota za rubezhom*. Pod. red. Lodeishchikova, V. V., M.: Metallurg. **1973**, 246-252.

[3]*Gidrometallurgia Zolota*. Pod red. Laskorina, I. V., M.: Nauka, **1980**, 198.

[4]Gagnidze, T., Gvelesiani, J., Gvelesiani, G., Lezhava, T., Mamporia. M., *Sak. Mets. Akad. Matsne. Khimii ser*. **2000**, *26(3-4)*, 35-39.

[5]Gvelesiani, J., Lezhava, T., Gagnidze, T., Mamporia, M., Adamia, T. *Sak. Mets. Akad. Matsne. Khimii Ser*. **2006**, *32(1-2)*, 167-175.

[6]Winand, R., *Hydrometallurgy*, **1991**, *27*, 285-316.

[7]Paddefet, I., *Khimiya Zolota*. M.: Mir, **1982**, 259.

[8]Gagnidze, T., Gvelesiani, J., Mamporia, M., Khsnari okroshemtsveli sulfiduri nedleulis gadamushavebisatvis. *Sakpatenti*, **2011**, 5220(1).

[9]Sorokin, I., *Elektronnaya Technika*. **1974**, *14(1)*, 20.

[10]Gagnidze, T., Gvelesiani, J., Mamporia, M., *Sak. Metsn. Akad. Matsne, Khimii ser*. **2011**, *37(1-2)*, 2005-20012.

[11]Bek, R. and Shuraeva, L., *Elektrokimiya*, **2006**, *42(4)*, 340-346.

[12]Zhang, H., Ritchie, J., Labrooy, R. *J. Electrochem. Soc.*, **2001**, *148(10)*, 146.

Received: 31.10.2013.
Accepted: 21.12.2013.

STUDY ON THERMOPHYSICAL PROPERTIES OF BINARY MIXTURES OF BUTYL PROPIONATE AND KETONES AT 303.15 AND 313.15 K

M. V. Rathnam,[a]* M. S. S. Kumar,[b] Reema T. Sayed,[a] and D. R. Ambavadekar[a]

Keywords: butyl propionate; cyclohexanone; cyclopentanone; 3-pentanone; acetophenone; density; viscosity; speed of sound; binary mixture

Densities, viscosities and speeds of sound for the binary systems of butyl propionate with cyclopentanone, 3-pentanone, cyclohexanone and acetophenone have been determined as a function of composition at (303.15 and 313.15) K and atmospheric pressure. The excess volume (V^E), excess Gibbs free energy of activation of viscous flow (ΔG^{*E}), deviation in speeds of sound (Δu), isentropic compressibility (K_S), deviation in isentropic compressibility (ΔK_S), and intermolecular free length (L_f) were derived from the experimental data. These binary data were correlated as a function of the mole fraction by using the Redlich- Kister Polynomial equation to determine the fitting parameters and the standard deviations.

* Corresponding Authors
E-Mail: mvrathnam58@rediffmail.com
[a] Physical Chemistry Research Laboratory, B. N. Bandodkar College of Science, Thane- 400601-India
[b] Department of chemistry, Zulal Bhilajirao Patil college, Deopur, Dhule – 424002 – India

Introduction

Thermodynamic, transport and ultrasonic studies have created a great deal of interest amongst physical chemists and chemical engineers. Such studies have great relevance in many areas of applied and theoretical research.

Ketones are organic compounds that contain a carbonyl group and two aliphatic or aromatic substituents. The reactivity of the carbonyl group is influenced considerably by steric effects. Thus a study on thermophysical properties data of binary liquid mixtures containing ketones has attracted considerable interest in the literature.[1-10] Cyclopentanone, 3-pentanone are used in fragrances. Acetophenone is commonly used as a flavouring in many cherry flavoured sweets and drinks, as it costs far less and proves as satisfying to consumers this way. While butyl propionate is used for high solid coatings, enamels and printing inks.

The selected components have reached wide applicability in various industrial process due to their special properties. With this aim, in continuation of our earlier work[11-14] we report the experimental densities, viscosities and speeds of sound for binary mixtures of butyl propionate with cyclopentanone, 3-pentanone, cyclohexanone and acetophenone at (303.15 and 313.15) K over the entire range of composition. From these measurements, excess volume (V^E) excess Gibbs free energy of activation of viscous flow (ΔG^{*E}), deviation in speeds of sound (Δu), isentropic compressibility (K_S), deviation in isentropic compressibility (ΔK_S), and intermolecular free length (L_f) and excess intermolecular free length (L_f^E) were determined.

Experimental

Materials

High purity analytical grade samples of cyclopentanone (Fluka), cyclohexanone and 3-pentanone procured from Merck, butyl propionate and acetophenone procured from Sigma Aldrich were used. Before measurements all the liquids were carefully dried over 0.4 nm molecular sieves and stored in dark bottles. These samples were distilled just before use. The purity of these liquids was ascertained by Gas Chromatography (HP 8610) using a FID detector and the analysis indicated a mole percent purities > 99.5 %.

Methods

A set of nine compositions in the mole fraction range from 0.1 to 0.9 were prepared by weighing each component in specially designed airtight bottles. The mass measurements accurate to $\pm$ 0.01 mg were performed on a digital electronic balance (Mettler AE-240, Switzerland). The possible uncertainty in the mole fraction was estimated to be less than $\pm$ $1x10^{-4}$. The densities of pure liquids and their binary mixtures were determined with a densitymeter (DMA 35 Anton Paar). The reproducibility of the density measurements was $\pm$ 0.0005 g cm^{-3}. The uncertainty in the density measurements was estimated to be $\pm$ 4 x 10^{-4}. The viscosities of pure liquids and their mixtures were determined using an Ubbelohde viscometer with an uncertainty of $\pm$ 0.007 mPa s. The speed of sound of pure liquid and liquid mixtures was measured with a single crystal variable path interferometer (Model F-81) supplied by Mittal Enterprises, New Delhi, India operating at a frequency of 2 MHz. The details and calibration procedures of all the methods have been described elsewhere.[11] The uncertainty in speed of sound was found to be $\pm$0.02 %. In all property measurements, the temperature was controlled within $\pm$ 0.01 K using a constant low temperature bath (INSREF model IRI 016C, India) by circulating water from thermostat.

Table 1. Experimental density (ρ), excess volume (V^E), viscosity (η), excess free energy of activation (ΔG^{*E}), speed of sound (u), isentropic compressibility (K_S), intermolecular free length (L_f) for the binary mixtures of butyl propionate.

x_1	ρ, g.cm^{-3}	V^E, cm^{3}mol^{-1}	η, mPa.s	ΔG^{*E}, J mol^{-1}	u, m.s^{-1}	K_S, TPa^{-1}	L_f x 10^{-8} cm
	Butyl propionate(1) + Cyclopentanone(2)						
	***T* =303.15 K**						
0.0000	0.9394		0.998		1371	566	0.4939
0.0618	0.9331	-0.089	0.975	17.2	1354	585	0.5018
0.1298	0.9262	-0.132	0.948	27.2	1336	605	0.5105
0.2025	0.9193	-0.164	0.921	37.0	1316	628	0.5202
0.2832	0.9121	-0.174	0.894	48.8	1296	653	0.5303
0.3716	0.9048	-0.170	0.864	52.0	1276	679	0.5408
0.4710	0.8973	-0.153	0.837	66.8	1256	706	0.5517
0.5808	0.8898	-0.125	0.808	72.5	1237	734	0.5625
0.7040	0.8823	-0.096	0.776	68.7	1219	763	0.5732
0.8412	0.8748	-0.049	0.741	53.3	1201	793	0.5843
1.0000	0.8672		0.696		1180	828	0.5973
x_1	***T* =313.15 K**						
0.0000	0.9299		0.861		1333	605	0.5198
0.0618	0.9238	-0.109	0.843	21.0	1315	626	0.5287
0.1298	0.9170	-0.164	0.823	42.7	1296	649	0.5384
0.2025	0.9101	-0.195	0.801	54.1	1276	675	0.5489
0.2832	0.9030	-0.218	0.779	67.4	1256	702	0.5599
0.3716	0.8956	-0.200	0.755	76.2	1237	730	0.5708
0.4710	0.8881	-0.181	0.731	86.9	1217	760	0.5826
0.5808	0.8806	-0.152	0.706	92.3	1198	791	0.5944
0.7040	0.8731	-0.120	0.677	80.5	1180	823	0.6060
0.8412	0.8656	-0.070	0.647	60.9	1163	854	0.6176
1.0000	0.8579		0.607		1144	891	0.6306
x_1	**Butyl propionate (1) + 3-pentanone (2)**						
	***T* =303.15 K**						
0.0000	0.8054		0.419		1188	879	0.6156
0.0734	0.8114	0.026	0.443	56.6	1190	870	0.6123
0.1496	0.8174	0.035	0.467	100.5	1192	861	0.6090
0.2317	0.8237	0.014	0.492	138.0	1193	853	0.6062
0.3217	0.8302	-0.011	0.520	165.9	1191	849	0.6048
0.4137	0.8364	-0.033	0.548	182.5	1188	847	0.6041
0.5146	0.8427	-0.048	0.579	193.6	1186	844	0.6029
0.6226	0.8489	-0.050	0.611	186.8	1184	840	0.6017
0.7387	0.8550	-0.036	0.645	166.7	1182	837	0.6005
0.8624	0.8610	-0.017	0.675	115.6	1181	833	0.5989
1.0000	0.8672		0.696		1180	828	0.5973
x_1	***T* =313.15 K**						
0.0000	0.7967		0.376		1156	939	0.6476
0.0734	0.8025	0.046	0.397	64.7	1158	929	0.6441
0.1496	0.8085	0.047	0.419	117.1	1160	919	0.6406
0.2317	0.8148	0.018	0.441	155.4	1161	911	0.6376
0.3217	0.8212	0.003	0.465	185.6	1158	908	0.6368
0.4137	0.8273	-0.019	0.487	196.9	1155	906	0.6361
0.5146	0.8335	-0.027	0.515	213.3	1153	902	0.6348
0.6226	0.8397	-0.038	0.544	208.7	1150	900	0.6341
0.7387	0.8458	-0.034	0.572	197.7	1148	987	0.6329
0.8624	0.8517	-0.006	0.596	138.4	1146	894	0.6318
1.0000	0.8579		0.607		1144	891	0.6306

x_1	Butyl propionate(1) + Cyclohexanone(2)						
	T =303.15 K						
0.0000	0.9375		1.817		1388	554	0.4884
0.0721	0.9314	-0.111	1.613	-115.7	1364	577	0.4986
0.1486	0.9248	-0.167	1.429	-226.8	1342	600	0.5086
0.2298	0.9180	-0.199	1.280	-229.9	1320	625	0.5190
0.3170	0.9111	-0.224	1.158	-336.7	1300	649	0.5289
0.4090	0.8041	-0.225	1.061	-329.8	1280	675	0.5393
0.5104	0.8868	-0.206	0.985	-271.7	1260	702	0.5501
0.6183	0.8895	-0.174	0.915	-199.7	1241	730	0.5608
0.7349	0.8821	-0.123	0.849	-113.4	1222	759	0.5719
0.8612	0.8747	-0.067	0.782	-25.5	1202	791	0.5839
1.0000	0.8672		0.696		1180	828	0.5973
x_1	T =313.15 K						
0.0000	0.9290		1.476		1352	589	0.5128
0.0721	0.9230	-0.135	1.340	-75.4	1326	616	0.5245
0.1486	0.9163	-0.192	1.199	-179.2	1305	641	0.5349
0.2298	0.9095	-0.237	1.081	-251.0	1283	668	0.5461
0.3170	0.9024	-0.248	0.987	-282.2	1263	695	0.5569
0.4090	0.8953	-0.247	0.909	-278.9	1242	724	0.5686
0.5104	0.8879	-0.226	0.845	-234.4	1223	753	0.5798
0.6183	0.8805	-0.190	0.788	-169.4	1204	783	0.5915
0.7349	0.8730	-0.135	0.731	-99.2	1185	816	0.6035
0.8612	0.8655	-0.073	0.679	-12.0	1165	851	0.6165
1.0000	0.8579		0.607		1144	891	0.6306
x_1	Butyl propionate(1) + Acetophenone(2)						
	T =303.15 K						
0.0000	1.0198		1.508		1459	461	0.4455
0.0801	1.0057	-0.138	1.415	-1.3	1434	484	0.4564
0.1642	0.9911	-0.234	1.320	-9.6	1407	510	0.4686
0.2519	0.9765	-0.329	1.230	-14.7	1381	537	0.5810
0.3434	0.9618	-0.411	1.146	-13.5	1355	566	0.4939
0.4387	0.8467	-0.431	1.067	-6.7	1329	598	0.5076
0.5404	0.9312	-0.430	0.989	2.8	1303	633	0.5220
0.6468	0.9154	-0.373	0.917	16.1	1276	671	0.5376
0.7518	0.8996	-0.296	0.846	28.7	1248	714	0.5545
0.8755	0.8834	-0.148	0.774	30.2	1216	766	0.5743
1.0000	0.8672		0.696		1180	828	0.5973
x_1	T=313.15 K						
0.0000	1.0130		1.266		1425	486	0.4659
0.0801	0.9978	-0.044	1.190	-2.5	1397	514	0.4788
0.1642	0.9829	-0.137	1.113	-12.4	1370	542	0.4920
0.2519	0.9680	-0.228	1.041	-16.4	1343	573	0.5057
0.3434	0.9530	-0.303	0.973	-15.8	1317	605	0.5197
0.4387	0.9379	-0.354	0.909	-10.0	1291	640	0.5347
0.5404	0.9222	-0.357	0.846	-2.4	1264	679	0.5505
0.6468	0.9064	-0.331	0.788	15.1	1237	721	0.5647
0.7518	0.8903	-0.237	0.730	27.1	1210	768	0.5855
0.8755	0.8741	-0.119	0.670	24.9	1278	824	0.6067
1.0000	0.8579		0.607		1144	891	0.6306

Results and discussion

The densities (ρ), excess volumes (V^E), viscosities (η), excess free energy of activation (ΔG^{*E}), speed of sound (u), isentropic compressibility (K_S), and intermolecular free length (L_f) of the mixtures of butyl propionate with cyclopentanone, 3-pentanone, cyclohexanone and acetophenone at 303.15 and 313.15 K along with the mole fraction of ester are given in Table 1.

The excess volumes (V^E, in cm^3 mol^{-1}) have been evaluated from density using the following relation

$$V_E = \frac{x_1M_1 + x_2M_2}{\rho} - \frac{x_1}{M_1\rho_1} - \frac{x_2}{M_2\rho_2} \quad (1)$$

where ρ is the density of the mixture, x_1, v_1, M_1 and x_2, v_2, M_2 are the mole fraction, molar volume and molecular weight of pure components 1 and 2 respectively.

The excess Gibbs free energy of activation of viscous flow ΔG^{*E} is obtained by the equation

$$\Delta G^{*E} = RT[\ln\eta v_m - \{x_1 \ln\eta_1 v_1 + x_2 \ln\eta_2 v_2\}] \quad (2)$$

The deviations in speed of sound Δu, isentropic compressibility ΔK_S, and excess intermolecular free length L_f^E have been calculated from the results of u, K_S and L_f (Table 1) using the general equation

$$\Delta y = y_m - y_1x_1 - y_2x_2 \quad (3)$$

where Δy refers to Δu, ΔK_S or L_f^E and y_m is the respective mixture property. The isentropic compressibility K_S has been calculated from the experimental density and speed of sound data using the relation.

$$K_S = \frac{1}{u^2\rho} \quad (4)$$

The intermolecular free length L_F has been obtained using the relation

$$L_f = K(K_S)^{1/2} \quad (5)$$

where K is the temperature dependent Jacobson constant. The values of ΔG^{*E}, Δu, ΔK_S and L_f^E have been graphically represented in Figs. 2-5, respectively. Each set of these excess functions has been fitted by the method of non-linear least squares to a Redlich-Kister type Polynomial:[15]

$$\Delta Y = x_1(1-x_1)\sum_{i=0}^{m} A_i(2x_1-1)^i \quad (6)$$

where i is the number of estimated parameters and A_i the polynomial coefficients obtained by fitting the equation to the experimental results. The standard deviations σ has been obtained by using the equation

$$\sigma = \left[\frac{\sum(Y_{exptl} - Y_{cal})^2}{(n-m)}\right]^{0.5} \quad (7)$$

where 'n' represents the number of data points and 'm' is the number of coefficients alongwith their standard deviations σ are given in Table 2. Excess volumes for mixtures of butyl propionate with cyclopentanone, 3-pentanone, cyclohexanone and acetophenone at (303.15 and 313.15) K are represented in Figure 1.

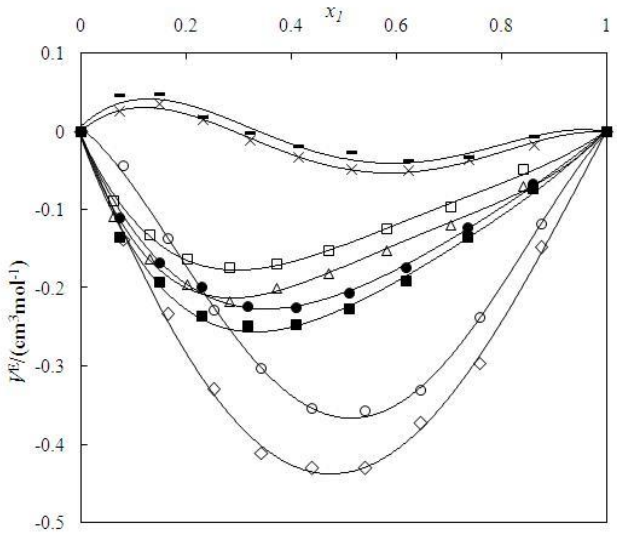

Figure 1. Curves of excess molar volume (V^E) Vs mole fraction for the binary mixtures of (butyl propionate + cyclopentanone) □, at 303.15 K; Δ, at 313.15 K, (butyl propionate + 3-pentanone) x, at 303.15 K; -, at 313.15 K, (butyl propionate + cyclohexanone) ●, at 303.15 K; ■, at 313.15 K and (butyl propionate + acetophenone) ◊, at 303.15 K; O, at 313.15 K

It is observed that for mixtures cyclopentanone, cyclohexanone, acetophenone the V^E values are completely negative. However for mixtures of 3-pentanone the V^E curves show a sigmoidal trend with sign inversion from positive to negative occurring at about x_1= 0.3 further it is found that with increasing size of ketones from cyclopentanone to acetophenone (except 3-pentanone) the negative magnitude of V^E values at the studied temperatures increase systematically indicating the dispersion type interactions involving in these mixtures. Thus it is evident that the size of a second component plays an important role in deciding the type of interactions in the mixtures. The ΔG^{*E} values (Figure 2) are positive for mixtures cyclopentanone and 3-pentanone, while for cyclohexanone mixtures these values are negative over the entire range of composition at both the studied temperatures. However for mixtures of acetophenone the ΔG^{*E} values exhibit both negative and positive deviations. The sign inversion from negative to positive occurs at x_1 = 0.55.The dependence of Δu, on the mole fraction of butyl propionate x_1 is shown in Figure 3.

 DOI: 10.17628/ecb.2014.3.166-172

Table 2. Values of parameters by Redlich Kister equation for excess properties and their standard deviations

Function	*T*/K	A_0	A_1	A_2	A_3	σ
	Butyl propionate (1) + Cyclopentanone(2)					
V^E	303.15	-0.5848	0.4142	-0.3525	0.3091	0.003
	313.15	-0.6962	0.4846	-0.5564	0.3106	0.005
ΔG^{*E}	303.15	267.43	148.33	104.34	-81.602	2.3
	313.15	350.45	96.770	100.39	-59.446	2.3
Δu	303.15	-99.372	25.160	34.812	-12.499	0.219
	313.15	-107.48	23.385	19.294	-2.8553	0.318
ΔK_s	303.15	6.7437	-0.4400	-4.6437	-0.4505	0.019
	313.15	8.3397	0.1075	-3.4845	-0.2873	0.035
$L_f{}^E$	303.15	0.0369	0.0034	-0.0223	-0.0190	0.000
	313.15	0.0428	-0.0094	-0.0092	0.0166	0.000
	Butyl propionate (1) + 3-pentanone (2)					
V^E	303.15	-0.1875	-0.2033	0.4832	-0.1519	0.002
	313.15	-0.1372	-0.1575	0.5188	-0.3423	0.008
ΔG^{*E}	303.15	764.42	85.033	229.24	64.201	1.1
	313.15	851.33	186.09	380.97	-31.116	2.9
Δu	303.15	9.8523	-37.013	22.548	16.241	0.104
	313.15	12.768	-35.319	25.672	12.314	0.178
ΔK_s	303.15	-4.0363	5.7071	-3.0752	-2.3712	0.016
	313.15	-4.7598	6.0313	-3.8292	-2.1454	0.028
$L_f{}^E$	303.15	-0.0143	0.0169	-0.0128	-0.0041	0.000
	313.15	-0.0158	0.0186	-0.0111	-0.0045	0.000
	Butyl propionate (1) + Cyclohexanone (2)					
V^E	303.15	-0.8296	0.4152	-0.2225	0.3018	0.005
	313.15	-0.9064	0.4786	-0.3641	0.4488	0.006
ΔG^{*E}	303.15	-1143.4	1233.5	239.17	-336.67	5.4
	313.15	-988.24	1059.4	406.62	-431.99	9.5
Δu	303.15	-87.375	40.182	-4.4333	10.964	0.263
	313.15	-91.877	39.140	-13.403	20.248	0.715
ΔK_s	303.15	3.4038	-2.3514	-0.8833	-0.8002	0.026
	313.15	4.0545	-2.3872	-0.0892	-1.2187	0.069
$L_f{}^E$	303.15	0.0235	-0.0154	0.0009	0.0073	0.000
	313.15	0.0287	-0.0127	-0.0029	-0.0067	0.000
	Butyl propionate (1) + Acetophenone (2)					
V^E	303.15	-1.7454	0.1671	0.2953	0.1332	0.009
	313.15	-1.4629	-0.0761	0.8607	-0.1753	0.005
ΔG^{*E}	303.15	-9.2659	226.64	203.99	-17.055	1.4
	313.15	-20.044	236.97	182.27	-61.293	1.6
Δu	303.15	-25.074	46.638	18.764	-18.628	0.261
	313.15	-39.620	42.514	4.9344	-1.3823	0.350
ΔK_s	303.15	-10.323	-5.2242	-3.1125	0.8375	0.027
	313.15	-10.160	-5.0275	-1.8226	-0.0914	0.041
$L_f{}^E$	303.15	-0.0210	-0.0177	-0.0095	0.0047	0.000
	313.15	-0.0160	-0.0150	-0.0045	-0.0028	0.000

It is observed that the values of Δu for mixtures of cyclopentanone and cyclohexanone are negative over the entire composition range at (303.15 and 313.15) K. While for mixtures of 3-pentanone the Δu values are completely positive. However the Δu for mixtures of acetophenone are negative in the low regions of butyl propionate concentration (x_1<0.9), and positive in the high regions of butyl propionate concentration (x_1>0.9). The variation of

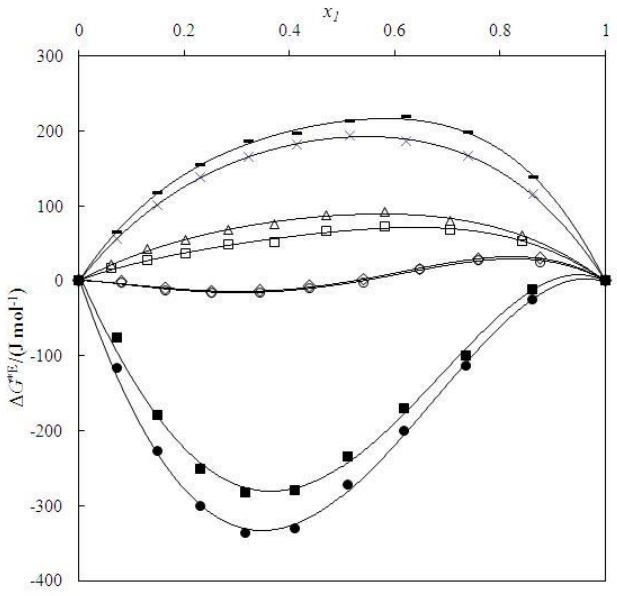

Figure 2. Curves of excess free energy of activation (ΔG^{*E}) Vs mole fraction for the binary mixtures of (butyl propionate + cyclopentanone) □, at 303.15 K; Δ,at 313.15 K,(butyl propionate + 3-pentanone) x, at 303.15K; -, at 313.15K, (butyl propionate + cyclohexanone) ●, at 303.15 K; ■, at 313.15 K and (butyl propionate + acetophenone) ◊, at 303.15 K; O, at 313.15 K.

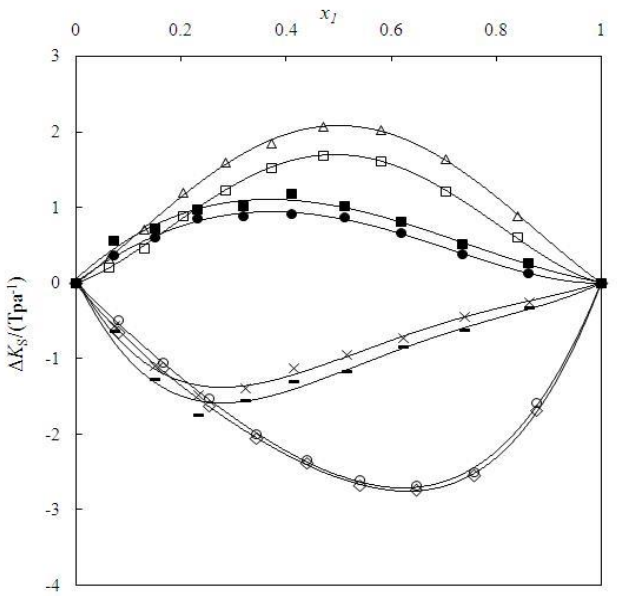

Figure 4. Curves of deviations in isentropic compressibilities (ΔK_S) Vs mole fraction for the binary mixtures of (butyl propionate + cyclopentanone) □, at 303.15 K; Δ, at 313.15 K, (butyl propionate + 3-pentanone) x, at 303.15 K; -, at 313.15 K,(butyl propionate + cyclohexanone)●, at 303.15K; ■, at 313.15 K and (butyl propionate + acetophenone) ◊, at 303.15 K; O, at 313.15 K.

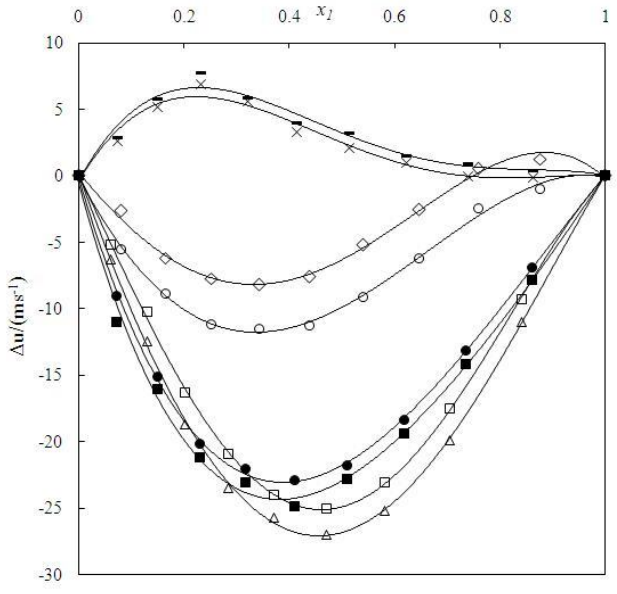

Figure 3. Curves of deviations is speed of sound (Δu) Vs mole fraction for the binary mixtures of (butyl propionate + cyclopentanone) □, at 303.15 K; Δ, at 313.15 K,(butyl propionate +3-pentanone) x, at 303.15K; -, at 313.15 K, (butyl propionate + cyclohexanone) ●, at 303.15 K; ■, at 313.15 K and (butyl propionate + acetophenone) ◊, at 303.15 K; O, at 313.15K.

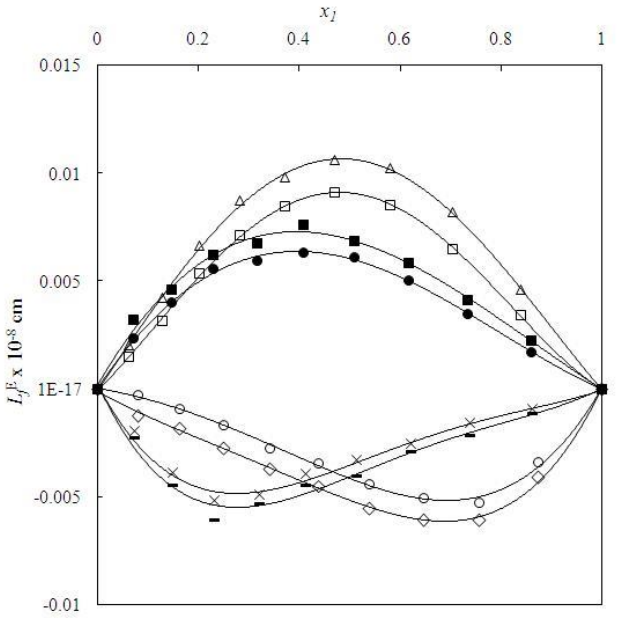

Figure 5. Curves of excess intermolecular free length ($L_f{}^E$) Vs mole fraction for the binary mixtures of (butyl propionate + cyclopentanone) □, at 303.15 K, Δ, at 313.15 K, (butyl propionate + 3-pentanone) x, at 303.15 K; -, at 313.15 K, (butyl propionate + cyclohexanone) ●, at 303.15 K; ■, at 313.15 K and (butyl propionate + acetophenone) ◊, at 303.15 K; O, at 313.15 K.

ΔK_S vs. mole fraction of butyl propionate is shown in Figure 4. The ΔK_S values are found to be positive for mixtures of cyclopentanone and cyclohexanone. While for mixtures of 3-pentanone and acetophenone the ΔK_S values are negative over the entire range of composition. Further it is observed that the maxima and minima of the isotherms are not identical in each case. Figure 5 shows the variation of excess intermolecular free length $L_f{}^E$ Vs mole fraction of butyl propionate x_1. It is observed that the isotherms of $L_f{}^E$ almost exhibit the identical behaviour as in case of ΔK_S values. The positive deviation of $L_f{}^E$ for mixtures of cyclopentanone and cyclohexanone may be attributed to the weaker interactions between these components and improper interstitial accommodation due to more or less the same molar volumes

of the components, while the negative value of L_f^E in case of 3-pentanone and acetophenone mixtures may be due to the existence of strong molecular interactions between the components of the mixtures. Comparing the present data of V^E and Δu with our earlier published data of butyl propionate + ether mixtures[16], it is found that the values almost exhibit same trends except for the mixtures of butyl propionate + 3-pentanone for which both V^E and Δu are found to be positive. The probable explanation for this may be the difference in the molecular size between the two mixing solvents, where the dipole–dipole interactions between the like molecules predominate.

Conclusions

The density, viscosity and speed of sound for the binary mixtures of butyl propionate with cyclopentanone, 3-pentanone, cyclohexanone and acetophenone have been determined over the entire range of composition at the temperatures (303.15 and 313.15) K. From the experimental data excess volume V^E, excess Gibbs free energy of activation for viscous flow ΔG^{*E}, isentropic compressibility K_S, intermolecular free length L_f, deviations in speeds of sound Δu, deviations in isentropic compressibility ΔK_S and excess intermolecular free length L_f^E have been calculated for analyzing the molecular interactions between molecules.

The reported excess functions showed both positive and negative deviations. These excess functions were correlated by the Redlich-Kister Polynomial equation to derive the coefficients and standard deviations.

References

[1]Nayak, J. N., Aralaguppi, M. I., Aminabhavi, T. M., *J. Chem. Eng. Data*, **2003**, *48*, 628.

[2]Jyostna, T. S., and Satyanarayana, N., *Indian. J. Pure Appl. Phys.*, **2005**, *43*, 591.

[3]Gonzalez, C., Resa, J. M., Concha, R. G., Goenaga, J. M., *J. Food Eng.*, **2007**, *79*, 1104.

[4]Alonso, I., Mozo, I., Dela Fuente, I. G., Gonzalez, J. A., Cabos, J. C., *J. Mol. Liq.*, **2011**, *160*, 180.

[5]Comelli, F., Francesconi, R., *J. Chem. Eng. Data*, **1994,** *39*, 108.

[6]Pereiro, A. B., Rodriguez, A., J. Canosa, and J. Tojo, *J. Chem. Eng. Data*, **2005**, *50*, 481.

[7]Pereiro, A. B., Tojo, E., Rodriguez, A., J. Canosa, J. Tojo, *J. Chem. Thermodyn.*, **2006**, *38*, 651.

[8]Pereiro, A. B., Rodriguez, A., J. Canosa, and J. Tojo, *Fluid Phase Equilibria*, **2005**, *235*, 83.

[9]Iloukhani, H., and Rostami, Z., *J. Chem. Eng. Data*, **2007,** *52*, 921.

[10]Iloukhani, H., Rostami, Z., *J. Chem. Thermodyn.*, **2007**, *39*, 1231.

[11]Rathnam, M. V., Reema, T. S., Kavita, B. R., Kumar, M. S. S., *J. Mol. Liq.*, **2012**, *166*, 9

[12]Rathnam, M. V., Mohite, S., Kumar, M. S. S., *J. Mol. Liq.*, **2011**, *163*, 170.

[13]Rathnam, M. V., Mohite, S., Kumar, M. S. S., *J. Chem. Eng. Data*, **2010**, *55*, 5946

[14]Rathnam, M. V., Mohite, S., Kumar, M. S. S., *J. Serb. Chem.* Soc, **2012**, 77, 507.

[15]Redlich, O., Kister, A. T., *Ind. Eng. Chem.*, **1948**, *40*, 345.

[16]Rathnam, M. V., Ambavadekar, D. R., Nandini, M., *Eur. Chem.Bull.*, **2013**, *2(9)*, 642.

Received: 04.12.2013.
Accepted: 26.12.2013.

SYNTHESIS AND X-RAY CRYSTAL STRUCTURE OF 3,3,6,6-TETRAMETHYL-9-(3,4-DIMETHYLPHENYL)-3,4,6,7,9,10-HEXAHYDROACRIDINE-1,8- DIONE

Dalbir Kour[a], D. R. Patil[b], Madhukar B. Deshmukh[b], Vivek K. Gupta[a] and Rajni Kant[a]*

Keywords: Acridinediones, Crystal structure, Direct methods, N-H…O hydrogen bonding.

The title compound 3,3,6,6-tetramethyl-9-(3,4-dimethylphenyl)-3,4,6,7,9,10-hexahydroacridine-1,8-dione ($C_{25}H_{31}NO_2$) crystallizes in the monoclinic space group $P2_1/c$ with unit cell parameters: a=18.616(3), b=9.9747(13), c=11.8093(15) Å, β=91.89(13)º, Z=4. The crystal structure was solved by direct methods and refined by full-matrix least-squares procedures to a final *R*-value of 0.075 for 3088 observed reflections. The central ring of the acridinedione system adopts a *boat* conformation. The four essentially planar atoms (C10/C11/C13/C14) of this ring [maximum deviations = 0.2047(3) Å] forms dihedral angles of 87.32º(13) with the benzene ring. The two outer rings of the acridinedione system adopt *sofa* conformations. The crystal packing is stabilized by intermolecular N-H…O interactions.

* Corresponding Authors
Fax: +91 191 243 2051
E-Mail: rkvk.paper11@gmail.com
[a] X-ray Crystallography Laboratory, Post-Graduate Department of Physics & Electronics, University of Jammu, Jammu Tawi - 180 006, India.
[b] Department of Chemistry, Shivaji University, Kolhapur - 416 004 (MS), India.

Introduction

Acridines, the earliest known antibiotics, are toxic towards bacteria and some of its derivatives show good inhibition against the pathogen Vibrio isolate-I.[1] Certain acridine-1,8-diones exhibit fluorescence activities[2] and a few acridinedione derivatives also show photophysical[3] and electrochemical properties.[4] The nucleus containing 1,4-dihydropyridine (DHP) ring act as a versatile intermediate for the synthesis of several pharmaceuticals together with those of cardiovascular drugs and as a calcium channel modulators, laser dyes and photo initiators.[5-7]

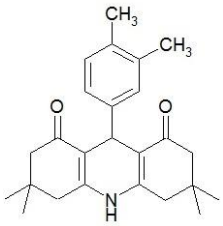

Scheme 1. Structure of 3,3,6,6-tetramethyl-9-(3,4-dimethylphenyl)-3,4,6,7,9,10-hexahydroacridine-1,8- dione

It has also been further revealed that DHP heterocyclic ring is a common feature of various bioactive compounds such as vasodilator, bronchodilator, anti-atherosclerotic, anti-tumor, and anti-diabetic agents.[8-10] Thus, the accurate description of crystal structures of substituted acridinediones are expected to provide useful information on the role of substituents in influencing molecular conformation which has a direct relationship to biological activity. This paper deals with the crystal structure of a 3,4-dimethylphenyl substituted tetramethyl acridinedione (**1**).

Experimental

Synthesis

In a 50 ml rounded bottom flask, a mixture of dimedone (2 mmole), 3,4-dimethyethylbenzaldehyde (1 mmole) and ammonium acetate (1.2 mmole) in mixture of aqueous ethanol (2.5ml : 2.5ml, v/v) (5 ml) was stirred at room temperature for 5 min. To this [CMIM][HSO_4] (20 mol %, CMIM = 3-(carboxymethyl)-1-methyl-1H-imidazol-3-ium) was added and the reaction mixture heated at 85 °C till reaction complete. The progress of reaction was monitored by TLC. After completion of reaction, the mixture was gradually cooled to room temperature and poured onto ice water under stirring, when a solid were precipitated out. The solid product was filtered off and dried (at 50 °C for 120 min.) well. The crude product was recrystallized from ethanol. M.P.: >300 ^{0}C, Yield: 86 %. ^{1}H-NMR (300MHz, DMSO-D_6): δ 7.91 (s, 1H, NH); 6.92–6.61 (m, 3H, Ar-H); 5.13 (s, 1H, CH); 2.19 (s, 3H, CH_3); 2.17 (s, 3H, CH_3); 2.33–2.21 (m, 8H, CH_2);1.01 (s, 6H, CH_3); 0.92 (s,6H,CH_3).

Crystal Structure Determination and Refinement

The X-ray intensity data of a well defined crystal (0.30 x 0.20 x 0.10 mm) were collected at room temperature (293 K) by using a CCD area-detector diffractometer (*X'calibur system – Oxford diffraction, 2010*) which is equipped with graphite monochromated MoKα radiation (λ=0.71073 Å). The cell dimensions were determined by the least-squares fit of angular settings of 2511 reflections in the θ range 3.98 to 28.82º. A total number of 8802 reflections were collected of which 3088 reflections were treated as observed ($I > 2\sigma(I)$). Data were corrected for Lorentz, polarization and absorption factors.

Table 1. Crystal data and other experimental details for **1.**

CCDC	962911
Crystal description	White block
Crystal size	0.30x0.20x0.10
Emperical Formula	$C_{25}H_{31}NO_2$
Formula weight (g mol-1)	377.51
Radiation, Wavelength (Å)	Mo *K*α, 0.71073
Unit cell dimensions	*a*=18.616(3), *b*=9.9747(13), *c*=11.8093(15) Å, β=91.887(13)º
Crystal system, Space group	monoclinic, $P2_1/c$
Unit cell volume ($Å^3$)	2191.7(5)
No. of molecules per unit cell, *Z*	4
No. of parameters refined	279
Absorption coefficient (mm^{-1})	0.071
F(000)	816
θ range for entire data collection (º)	3.49<θ < 26.00
Limiting indices	$-22 \le h \le 14$, $-12 \le k \le 8$, $-11 \le l \le 14$
Reflections collected / unique	8802/4294
Reflections observed (I > 2σ(I))	3088
Final R-factor	0.075
$wR(F^2)$	0.1941
R_{int}	0.0435
R_{sigma}	0.0562
Goodness-of-fit	1.067
$(\Delta/\sigma)_{max}$	0.001
Final residual electron density ($eÅ^{-3}$)	-0.226< Δρ < 0.229

The structure was solved by direct methods using SHELXS97.[11] All non-hydrogen atoms of the molecule were located from the E-map. Full-matrix least-squares refinement was carried out by using SHELXL97 software.[11] The geometry of the molecule is determined by PLATON.[12] All the hydrogen atoms were positioned geometrically and were treated as riding on their parent C/N atoms, with C-H distances of 0.93-0.99 Å and N-H distance of 0.99 Å; and with U_{iso}(H)=1.2U_{eq}(C/N), except for the methyl groups where U_{iso}(H)=1.5U_{eq}(C). The final refinement cycles yielded an *R*-factor of 0.075 ($wR(F^2)$=0.1249) for the observed data. The residual electron density ranges from -0.226 to 0.229 $eÅ^{-3}$.

Atomic scattering factors were taken from International Tables for X-ray Crystallography (1992, Vol. C, Tables 4.2.6.8 and 6.1.1.4). The crystallographic data are summarized in Table 1. CCDC – 962911 contains the supplementary crystallographic data for this paper.

Results and discussion

An ORTEP view of the title compound with atomic labeling is shown in Figure 1.[13] The geometry of the molecule was calculated using the PLATON[12] and PARST[14] software. Bond lengths and angles have normal values (Table 2) and correspond to those observed in related structures.[15,16] The central ring (C9/C10/C11/N12/C13/C14) of the acridinedione moiety adopts a *boat* conformation (ΔCs (C9-C12) = 0.89 & ΔCs (C10-C11) = 11.62) and the four essentially planar atoms (C10/C11/C13/C14) of this ring (maximum deviation 0.2047(3) Å for C9) form a dihedral angle of 86.57(8)º with benzene ring. In this ring, N12 and C9 deviate from C10/C11/C13/C14 plane by 0.1370(3) and 0.2047 (3) Å, respectively. Both the outer rings adopt *sofa* conformations (ΔCs (C3-C10) = 6.74; ΔCs (C6-C14) = 5.847).[17] The atoms C3 and C6 deviate from the mean planes defined by C1, C2, C4, C11, C10 and C5, C7, C8, C14, C13 by 0.3118(4) and 0.3352 (3) Å, respectively.

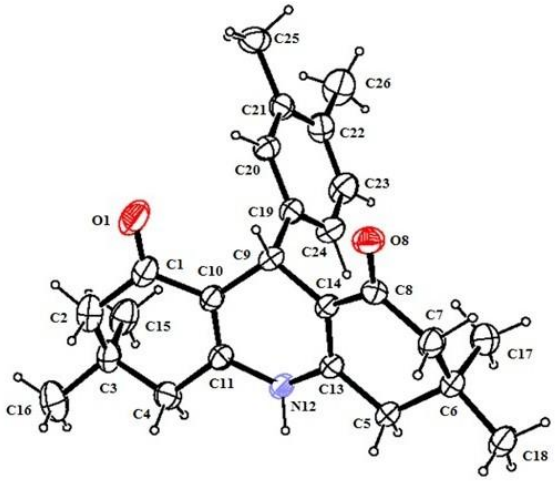

Figure 1. ORTEP view of the molecule with displacement ellipsoids drawn at the 50 % probability level. H atoms are shown as small spheres of arbitrary radii

Packing of the molecules in the unit cell down the b-axis is shown in Figure 2. The crystal packing is stabilized by intermolecular N-H…O interactions (Table 3).

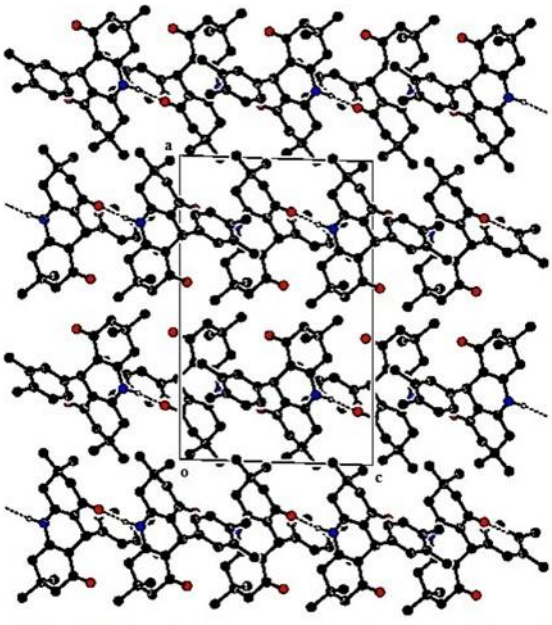

Figure 2. The packing arrangement of the molecule viewed done the b-axis. The dashed lines show intermolecular N-H....O hydrogen bonds.

 DOI: 10.17628/ecb.2014.3.173-175

Table 2. Selected bond lengths (Å) and angles (°) for non hydrogen atoms (e.s.d.'s are given in parentheses) for (**1**)

Bond lengths		**Bond angles**	
O1- C1	1.223(4)	C13- N12- C11	120.8(3)
O8- C8	1.240(3)	O1- C1- C10	121.2(3)
N12-C13	1.379(4)	O1- C1- C2	121.2(3)
N12- C11	1.398(4)	O8- C8- C14	122.5(3)
C10- C11	1.353(4)	O8- C8- C7	118.3(3)
C13- C14	1.365(4)	C10- C11- N12	120.2(3)
C22- C25	1.515(5)	N12- C11- C4	116.1(3)
C21-C26	1.512(4)	C14- C13- N12	120.1(3)
		N12- C13- C5	116.0(2)

Table 3. Geometry of inter molecular hydrogen bonds for (**1**)

D-H…A	D-H (Å)	H…A (Å)	D…A (Å)	θ[D-H…A(°)]	Symmetry code
N1-H12…O8	0.99 (4)	1.82 (4)	2.79 (3)	165(3)	x,-y+3/2,+z+1/2

Acknowledgements

One of the authors (Rajni Kant) acknowledges the Department of Science & Technology for single crystal X-ray diffractometer as a National Facility under Project No. SR/S2/CMP-47/2003.

References

[1]Josephrajan, T., Ramakrishnan, V. T., Kathiravan, G., Muthumary, J., *ARKIVOC*, **2005**, 124.

[2]Murugan, P., Shanmugasundaram, P., Ramakrishnan, V. T., Venkatachala-pathy, B. , Srividya, N., Ramamurthy, P., Gunasekaran, K., Velmurugan, D., *J. Chem. Soc. Perkin Trans. 2*, **1998**, 999.

[3]Srividya, N., Ramamurthy, P., Ramakrishnan, V. T., *Spectrochim. Acta Part A*, **1998**, *54*, 245.

[4]Srividya, N., Ramamurthy, P., Shanmugasundaram, P., Ramakrishnan, V. T., *J. Org. Chem.*, **1996**, *61*, 5083.

[5]Tu, S., Miao, C., Gao, Y., Fang, F., Zhuang, Q., Feng, Y., Shi. D. *Synlett*, **2004,** 255.

[6]Fan, X., Li, Y., Zhang, X., Qu, G., Wang, *Heteroatom Chem*, **2007,** *18*, 7.

[7]Leon, R., Rios, C., Contelles, J. M., Lopez, G. M., Garcia A. G., Villarroya, M., *Eur. J. Med.Chem.*, **2008,** *43*, 668.

[8]Mager, P. P., Coburn, R. A., Solo, A. J., Triggle, D. J., Rothe, H., *Drug Res. Discov*, **1992**, *8*, 273.

[9]Mannhold, R., Jablonka, B., Voigdt, W., Schoenafinger, K., Schravan, K., *Eur. J. Med. Chem.*, **1992**, *27*, 229.

[10]Godfraid, T., Miller, R., Wibo, M., *Pharmacol. Rev.*, **1986**, *38*, 321.

[11]Sheldrick, G. M., *Acta Cryst*., **2008**, *A64*, 112.

[12]Spek, A. L., *Acta Cryst*., **2009**, *D65*, 148.

[13]Farrugia, L. J., *J. Appl. Cryst.*, **2012**, *45*, 849.

[14]Nardelli, M., *J. Appl. Cryst*., **1995**, *28*, 659.

[15]Kant, R., Gupta, V. K., Kapoor, K., Patil, D. R., Patil, P. P., Deshmukh, M. B., *Acta Cryst*., **2013a**, *E69*, o100.

[16]Kant, R., Gupta, V. K., Kapoor, K., Patil, D. R., Jagadale, S. D., Deshmukh, M. B., *Acta Cryst*., **2013b**, *E69*, o101.

[17]Duax, W. L., Norton, D. A., *Atlas of Steroid Structures*, New York: Plenum Press, **1975**, 1.

Received: 23.12.2013.
Accepted: 27.12.2013.

MYCO-ECOLOGICAL STUDY OF HISTORICAL SANDSTONE MONUMENTS, WITH SPECIAL REFERENCE TO MAMA BHANJA TEMPLE OF CHHATTISGARH

Sanjay Prasad Gupta,[a]* K. S. Rana,[a] D. N. Sharma,[b] and G. K. Chandrol[b]

Keywords: Degradation; deterioration; sandstone monuments; myco-ecological; biofilm.

Historical sand stone monuments, is subjected to degradation induced by diverse mycoflora. Fungi are among the most active microorganisms in these processes. Fungal ability in production of pigments and organic acids have crucial role in discoloration and degradation of different types of sandstone in historical monuments. This investigation focuses on myco-ecological analyses of microbial bio-film from Mama Bhanja temple of Chhattisgarh State. The seven (07) fungal organisms with specific distribution on sandstone monuments were isolated. Fungi from Ascomycotina as well as Deuteromycotina were more frequent. The most frequent isolated fungal species from these historical sandstone monuments are *Aspergillus niger, Curvularia lunata, Rhizoctonia solani* and *Aspergillus flavus. Aspergillus niger* was common in almost all the sandstone structures of this monument. The frequency and relative frequency of these fungal organisms associated with deteriorated sandstone monuments site provides valuable data for future studies.

* Corresponding Authors
E-Mail: guptasanjayprasad@gmail.com
[a] Archaeological Survey of India, Dehradun, Uttrakhand, India
[b] Kalyan P. G. College, Bhilainagar (Durg), Chhattisgarh, India

INTRODUCTION

Chhattisgarh is the land of ancient culture where a lot of ancient monuments, temples and forts etc. are located. Every nook and corner of Chhattisgarh has traditional heritage. There are numerous monuments in Bastar Division of Chhattisgarh state. One of such monuments, the Mama Bhanja temple is located in geographical area of Dantewada district of Chhattisgarh state and in the forested terrain which is highly affected by Naxlite (Terrorist) activities. The temple dedicated to Lord Shiva is built on a moulded base. The building of the temple is attributed to the two family members (Mama or uncle and Bhanja or nephew) of the Naga dynasty. The mandapa of the temple, however, has succumbed to the ravages of time. There is an image of Ganesh on the lalatabimba (lintel). The adhishthana and the door jambs are decorated with excellent carvings of foliage, lotuses etc. It is 16 meter in height with a well preserved imposing curvilinear Sikhara over the sanctum. An inscription in Telgu characters datable to the 13th Century A.D. is found on the temple platform[1-2]. This temple has several sculptures. The patches on monuments pertain to fungi that are part of the total vegetational growth over their surface.

Numerous factors affect the stone durability. Stone surfaces are continuously exposed to physical, chemical and biological degradation. Physical, chemical, and biological agents act in co-association, ranging from synergistic to antagonistic, leading to the deterioration. Among biological agents microorganisms have critical importance, in stone deterioration. They can cause various damages on the stone surface, such as: formation of bio-film, chemical reactions with substrate, physical penetration into the substrate as well as pigments production. Fungal ability in production of pigments and organic acids have crucial role in discoloration and degradation of monuments. The microbial metabolites of bio-films are responsible for the deterioration of the underlying substratum and may lead to physical weakening and discoloration of sandstone[3].

a b

Figure 1. Mama Bhanja temple, Barsoor. a-Lateral view; b-front view

The aim of this work is to study the micro fungi community on monuments by using myco-ecological parameters and microscope observations in order to evaluate the variety richness and potential damage caused by fungal species.

MATERIAL AND METHODS

Sampling and Isolation of fungi

Totally 10 Samples were collected from various places of Mama Bhanja temple of Bastar (Chhattisgarh State) and brought to the laboratory under aseptic conditions. The isolation of microorganisms was done by culturing the

Table 1. The isolated fungi

Isolated fungi/Moss	S_1	S_2	S_3	S_4	S_5	S_6	S_7	S_8	S_9	S_{10}	*F*, %	*RF*, %	$d=S/\sqrt{N}$
Aspergillus niger	+	+	+	-	+	+	+	+	+	+	90	25.0	
Aspergillus flavus	-	+	+	+	-	+	+	-	-	-	50	13.8	
Chaetomium piluliferum	-	-	-	+	-	-	-	+	-	-	20	05.5	
Curvularia lunata	-	+	+	-	+	-	+	+	+	+	70	19.4	**0.70**
Fusarium oxysporum	+	-	-	+	+	-	-	-	+	-	40	11.1	
Rhizopus vigricans	-	-	-	-	-	+	+	+	-	-	30	08.3	
Rhizoctonia solani	+	-	+	+	-	+	-	-	+	+	60	16.6	
Total											**360**	**99.7**	

samples and by direct incubation of samples in moist chamber. The purified fungal cultures were identified by using mycological techniques and were compared with the available authentic literature, reviews and mycological manuals[4-7].

Calculations

Various myco-ecological characters have been calculated using the following formulae:

$$F = 100 \times \frac{N_1}{N_2}$$

Where

F is the total frequency of organism in %,

N_1 is the number of samples in which specific organism occurred

N_2 is the total number of samples examined

$$RF = 100 \times \frac{F_i}{F}$$

where

RF is the relative frequency in %

F_i is the frequency (in %) of individual organism

$$d = \frac{S}{\sqrt{N}}$$

where

d is the variety richness index

S is the total number of species.

N is the value of total relative frequencies of all fungal species.

RESULTS AND DISCUSSION

During screening for search of mycoflora, total seven species of fungal organisms were isolated from Mama Bhanja temple (Table 1). Composite result indicate that all the ten (10) samples were mainly dominated by different species of *Aspergillus niger*, *Aspergillus flavus*, *Curvularia lunata and Rhizoctonia solani* due to their high percentage frequency.

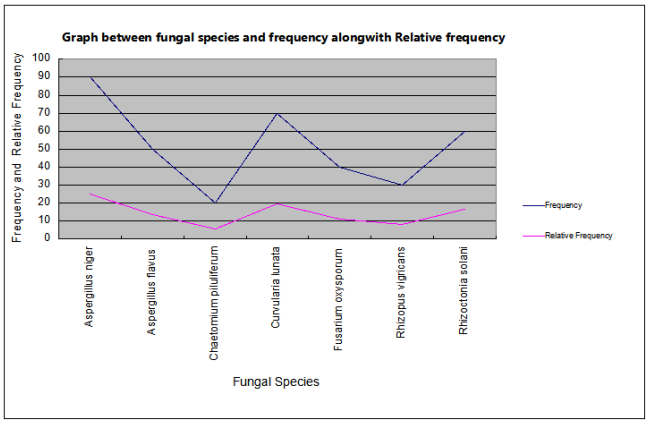

Figure 2. Frequency and relative frequency of the fungal species

Aspergillus niger shows maximum frequency followed by *Curvularia lunata and Rhizoctonia solani.*. Some of the fungal species are confined to particular area. These confinements of fungal species depend on environmental conditions of the area, which varies from geographical area to area. In the present study *Aspergillus* species are the most common species found in the sites. The grey and black colour of the stone surfaces is not only due to dematiceous fungi but very frequently it is due to the endolithic phototrophic microorganisms like cyanobacteria and algae. As in the case of fungi the dark pigments protect algal cells against UV radiation besides other stress factors[8].

Value of index of variety richness i.e. 0.70 revealed that the studied fungal community was significant. In each fungal community all the species are not equally important. There are relatively only few of these, which determine the nature of the community[9]. These few species exert a major controlling influence on the community and also play important role in deterioration of various substrates.

The variation in the composition of fungal organism depends upon biochemical nature of host, degree of competition between the fungal organisms and the prevailing environmental conditions. The frequency and relative frequency are directly or indirectly correlated with meteorological data and climatic conditions[10].

 DOI: 10.17628/ecb.2014.3.176-178

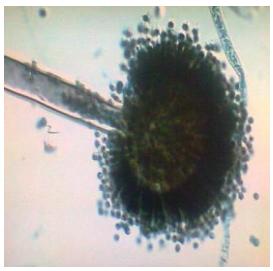

Aspergillus niger

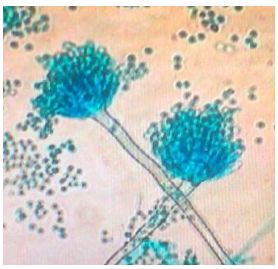

Aspergillus flavus

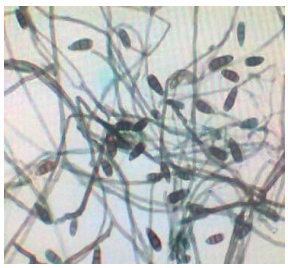

Curvularia lunata

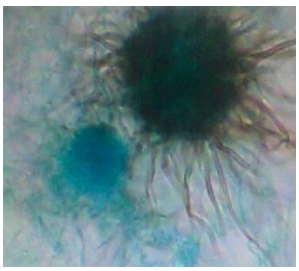

Chaetomium piluliferum

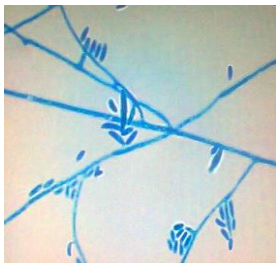

Fusarium oxysporum

Rhizopus vigricans

Rhizoctonia solani

It has also been shown in the laboratory that fungal species such as *Aspergillus niger* were able to solubilize powdered stone and chelate various minerals in a rich glucose medium because they produce organic acids such as gluconic, citric, and oxalic acids[11]. The toxic metabolites produced by various species of fungal organisms function as chelating agents that can leach metallic cations, such as Iron, Magnesium etc. from the stone surface. Laboratory experiments have demonstrated that basic rocks are more susceptible to fungal attack than acidic rocks. In the present study *Aspergillus* are the most common species found in the sites. *Aspergillus niger* releases certain metal ions from the rock samples[12].

ACKNOWLEDGEMENT

Authors are grateful to Principal Kalyan PG College, Bhilainagar for providing laboratory facilities for identification of fungal species.

REFERENCES

[1]Mishra, P. K., Shriwastava, K. C., Khamari, D. K., and Yadav, S. N., *Samsmriti (Protected monuments of Raipur circle at a glance).* Archaeological Survey of India, Raipur Circle, Chhattisgarh, India. **2012 ,** 27.

[2]Mitra, S., *Chhattisgarh full of surprises*. Good Earth Publ., New Delhi for Chhattisgarh Tourism Board, Raipur. Chhattisgarh, India, **2008**, 1-120.

[3]Gupta, S. P., Sharma, K., Chhabra, B. S., Sharma, D. N. and Chandrol, G. K., *Int. J. Curr. Res.,* **2012,** *4 (6)*, 045-047.

[4]Alexopoulos, C. J., *Introductory mycology (2nd ed.).* Wiley Estern Ltd. New Delhi, Banglore, Bombay. **1978.**

[5]Barnett, H. C., and Hunter, B. B., *Illustrated genera of important fungi.* Macmillan Publishing Company. New York and Collier. Macmillon Publishers, London. **1987.**

[6]Ellis, B. M., *More Dematiaceous Hyphomycetes*. CMI, Kew, England. **1976.**

[7]Gilman, C. J., *A Manual of Soil Fungi*. Print well publication, Jaipur (India). **1995.**

[8]Salvadori, O. O., *Characterisation of endolithic communities of stone monuments and natural outcrops.* Kluwer Academic Publishers, New York. **2000,** 89-101.

[9]Simpson, E. H., *Nature*, **1949,** 163 – 688.

[10]Chandel, D. S., Studies of Phylloplane interaction of fungi from Soybean and Pigeon pea. *Ph.D. Thesis.* Pt Ravishankar University, Raipur, **1990**.

[11]Lapidi, A. A. and Schipa, G., Some aspects of the growth of chemotrophic and heterotrophic bacteria from decayed stone. *In: Proc. 5th Int. Congr. Deterior. Conserv. Stone.* (Ed) G.Felix Lausanre, Switzerland. **1973,** 633-640.

[12]Boyle, J. R. and Voight, G. K., *Plant and Soil.* **1973,** *38*, 191-201.

Received: 07.11.2013.
Accepted: 27.12.2013.

SOURCE DISTRIBUTION OF POLYCYCLIC AROMATIC HYDROCARBONS OF AN OIL SPILL IMPACTED SITE IN NIGER DELTA, NIGERIA

M. C. Onojake,[a]* J. O. Osakwe[b] and Omokheyeke, O[c]

Keywords: Polycyclic aromatic hydrocarbons; Petrogenic; Bodo city; oil spillage and distribution ratios

Soil samples were collected from an oil spilled polluted site in the Niger Delta, Nigeria. The polycyclic aromatic hydrocarbon content was determined using gas chromatography. Results indicated that 1,2-benzanthracene was the most abundant with concentration of 11.90 mg kg^{-1} for surface and 8.10 mg kg^{-1} for subsurface. Benzo[*b*]fluoranthene followed closely with concentrations of 2.15 mg kg^{-1} for surface and 2.02 mg kg^{-1} for subsurface. There was low concentration of phenanthrene in the samples (0.01 mg kg^{-1}) which indicate that the samples suffered from mild evaporation caused by weather. Various ratios such as the Σ3-6 ringed PAHs/Σ5-alkylated PAHs of 2.77; fluoranthene/pyrene of 7.89; benz[*a*]anthracene/chrysene of 9.79 were far greater than unity (>1) indicating petrogenic source; phenanthrene/anthracene ratio is 0.10 depicted that the area under study was unexposed to bush burning.

Corresponding Authors
Tel: +234- 8035404696
E-Mail: *ononed@yahoo.com*, mudiaga.onojake@uniport.edu.ng,
[a] Department of Pure and Industrial Chemistry, University of Port Harcourt, P.M.B 5323, Choba, Port Harcourt, Nigeria
[b] QA/QC Laboratory, Notore Chemical Industries Ltd., Onne, Rivers State, Nigeria
[c] Centre for Marine Pollution Moritoring and Seafood Safety,University of Port Harcourt, P.M.B 5323, Choba, Port Harcourt, Nigeria

Introduction

Polycyclic aromatic hydrocarbons (PAHs) are a large group of compounds with two or more fused aromatic rings thatoccur either naturally in fossil fuels (coal and petroleum) or released from combustion of fossil fuels and degradation of manufactured materials such as lubricating oils, dyes, detergents and plastics.[1] Terrestrial PAHs are predominantly formed via pyrolysis, dehydrogenation and incomplete combustion of biogenic materials, and constituted a class of organic compounds that include potent mutagenic and carcinogenic compounds. They are often associated with combustion processes and exist under ambient environmental conditions as gases, volatile liquids, semi volatile substances and solids.[2]

PAHs are made of condensed aryl rings with hydrocarbons of very low molecular masses including methane which may act as precursors for the polycyclic aromatic compounds.[3] PAHs can be classified into two major groups consisting of alkylated homologous PAHs (naphthalene, phenanthrene, dibenzothiophenes, fluorene and chrysene) and EPA priority (Fig. 1) PAHs (acenaphthalene, acenapthene, anthracene and pyrene etc). The high molecular weight PAHs (three–six ringed) are known as pyrolytic (product of pyrolysis) PAHs while the low molecular weight PAHS (two-ringed) are known as fossil PAHs.[4]

Polycyclic aromatic hydrocarbons that are environmental contaminants are mainly derived from incomplete combustion of organic matter, emissions of non-combustion related petrogenic (from petroleum) process and crude oil spillages.[5] These compounds can be point source pollutants (e.g. oil spill) or non–point source pollutants (e.g. atmospheric deposition) and are part of the most widely spread organic pollutants.[6]

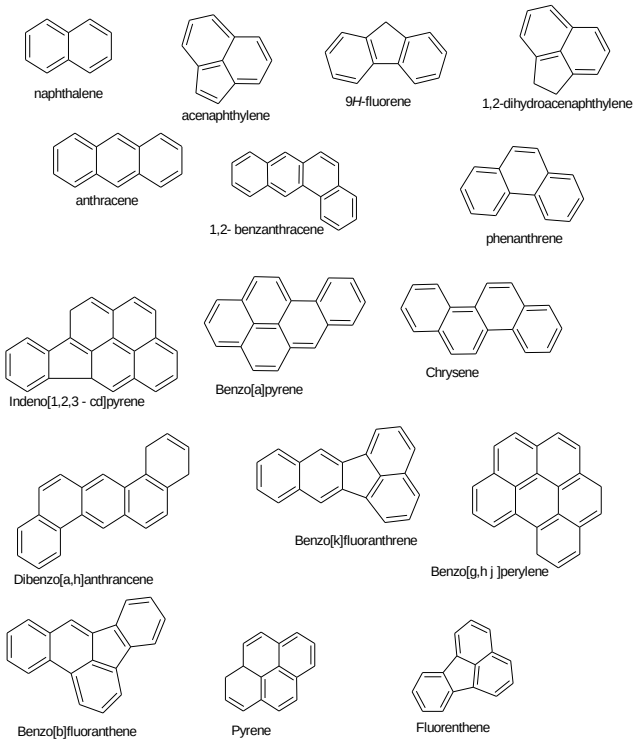

Figure 1. Chemical structures of sixteen (16) EPA PAHs.

They gain access into the environment through a number of pathways such as leakages from crude oil pipelines, sabotage, and accidental discharges such as blowouts, petroleum refining, cracking of crude oil, incineration of industrial and domestic wastes and chemical

manufacturing.[7-9] Since they are classified as carcinogenic compounds, these are monitored worldwide in a wide range of environmental substances including drinking water, waste water, furnace emissions, soil, hazardous waste leachates and in air over major cities.[10] Contamination of our environment by PAHs and how they reach our ecosystem is receiving a serious attention in society because of their impact on human health.[11] High molecular mass PAHs are mainly adsorbed into particulate matter and reach the hydrosphere and geosphere by dry and wet deposition.[5,12]

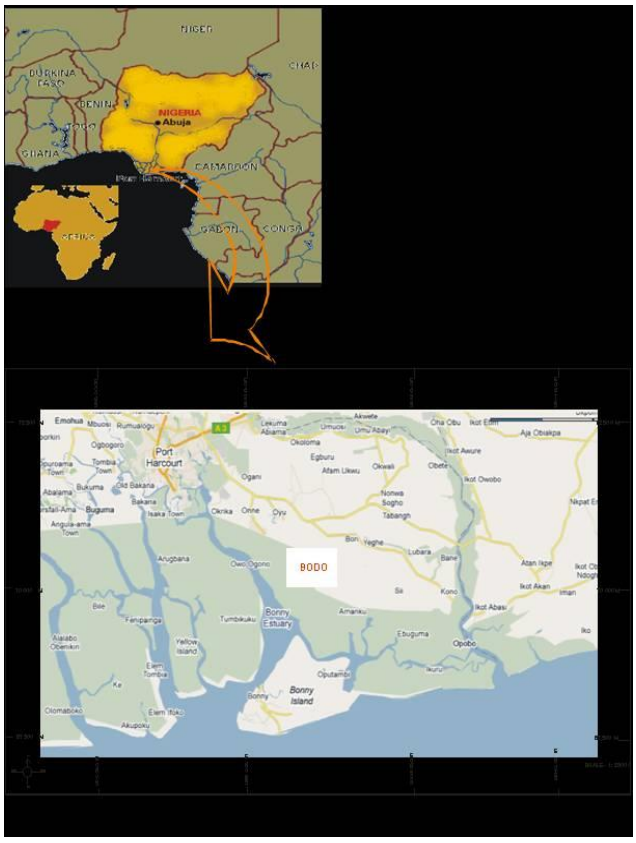

Figure 2. Map of study area showing Bodo city in Niger Delta, Nigeria.

The fate of PAHs and how they reach our ecosystem is receiving serious attention because of their impact on human health. Some of these compounds have carcinogenic, mutagenic and teratogenic effects on organisms and humans who consume these organisms.[6,13]

The incessant oil spillage, which led to the contamination of the environment in the area under investigation, initiated the interest in determining and quantifying the source of PAHs in the environment.

Experimentals

Description of study site

The Bodo city (Fig. 1) is within latitude 6° 73′ N and longitude 5° 32′ - 5°34′ E in Gokana local Government Area of Rivers State, Nigeria. Bodo creek complexes are vulnerable to crude oil pollution due to the network of oil pipelines in the area (Fig.3).

Figure 3. A section of the oil spill site showing superficial patches on the vegetation

Chromatographic Analysis

Soil samples from surface and sub surface at the depth of 0 to 15 cm and 15 to 30 cm were collected from the oil spilled area, air dried, crushed and sieved to obtain a uniform particle size. 5g of the homogenized sample was weighed into clean and dry beakers. 10 ml of hexane/dichloromethane mixture was added and thoroughly mixed with the soil sample, and filtered. The extracts were injected into a capillary gas chromatograph, HP 6890 series GC system equipped with a flame ionization detector (FID). The column used was a HP-5, 30m × 0.25mm × 0.25µm (HP Part No. 1909IS -433). Hydrogen (10.2 psi) was used as carrier gas at 1.5 ml min^{-1}. The column was kept at 80°C for 1 min. It was programmed to first reach 280 °C at the rate of 20 °C min^{-1}, and then to 300 °C at the rate of 2.5 °C min^{-1}. Temperature of the FID was kept at 325 °C. The GC recorder was interfaced to a Hewlett (HP) Computer software (6207AA Kayak XA PIT/350) for recording the chromatographic output.

Results and Discussion

The results of the concentration of PAHs are shown in Table 1. The mean of the results is also graphically represented in Fig 4. The results show that the concentration of PAHs is more on the surface samples indicating their petrogenic origin.

Table 1. Concentration of PAHs in mg kg^{-1} of an oil spill polluted soil in Niger Delta Nigeria.

Compound	Sample 1		Sample 2		Sample 3		Sample 4		Sample 5	
	surface	subsurface	surface	subsurface	surface	subsurface	surface	subsurface	surface	subsurface
Acenapthene	0.63	0.35	3.57	3.68	0.42	0.11	0.03	0.22	0.13	0.42
Acenapthylene	0.04	0.02	0.56	0.62	0.32	0.26	0.19	0.12	0.20	0.30
Anthracene	0.06	0.06	0.17	0.17	0.15	0.14	0.24	0.15	0.23	0.10
1,2-Benzanthracene	11.90	8.10	0.91	0.91	1.00	1.00	0.27	0.20	0.63	0.34
Benzo[*a*]pyrene	0.71	0.71	0.24	0.32	0.41	0.23	0.01	0.01	0.38	0.52
Benzo[*b*]fluoranthene	2.15	2.02	0.02	0.01	0.29	0.29	0.03	0.02	0.54	0.63
Benzo[*g,h,j*]perylene	2.07	1.68	0.03	0.04	0.36	0.32	0.30	0.36	0.19	0.21
Benzo[*k*]fluoranthene	0.52	0.48	0.28	0.22	0.12	0.12	0.11	0.11	0.12	0.10
Chrysene	0.03	0.03	0.02	0.13	0.46	0.39	0.38	0.40	0.22	0.52
Dibenzo[*a,h*]anthracene	2.00	1.98	0.27	0.32	1.14	1.23	2.04	1.04	1.23	0.25
Fluoranthene	0.01	0.01	0.03	0.03	0.01	0.01	0.01	0.01	0.01	0.01
Fluorene	0.11	0.13	0.08	0.12	0.15	0.41	0.03	0.05	0.21	0.13
Indeno[1,2,3-*c,d*]pyrene	2.29	2.31	0.30	0.30	1.04	0.97	0.07	0.04	0.04	0.31
Naphthalene	0.14	0.11	2.66	2.12	0.53	0.53	0.23	0.30	0.31	0.23
Phenanthrene	0.01	0.01	0.06	0.01	0.01	0.01	0.01	0.01	0.01	0.01
Pyrene	0.01	0.01	0.01	0.04	0.04	0.03	0.01	0.01	0.01	0.01

Crude oils and refined products from different sources can have different PAH distribution. PAHs are resistant to weathering than their saturated hydrocarbon counterparts (n–alkanes and isoprenoids) and volatile alkylbenzene compounds, thus making them one of the most valuable classes of hydrocarbons for oil spill identification.[14,15] The distribution patterns of PAHs in the early stages of oil spillage can be used to identify sources of crude oils and petroleum products. Table 1 shows clearly the concentrations for the various PAHs in Bodo city oil spillage. The low molecular weight PAHs such as naphthalene and phenanthrene are susceptible to biodegradation and are not reliable indices for oil spill source analysis. The high molecular weight PAH containing 4, 5, and 6 rings are more stable and are therefore useful as diagnostic constituents of petroleum.[7]

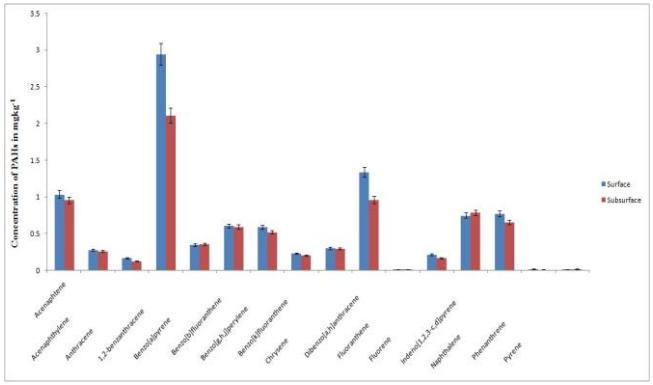

Figure 4. Graphical representation of mean of PAHs for surface and subsurface ± S. E

1,2-Benzanthracene is the most abundant with concentration of 11.90 mg kg^{-1} for surface and 8.10 mg kg^{-1} for subsurface (Table 1). Benzo[*b*]fluoranthene closely follows with concentrations of 2.15 mg kg^{-1} surface and 2.02 mg kg^{-1} for subsurface. The concentration of Phenanthrene in the samples is low (0.01 mg kg^{-1}) which further indicated that the samples suffered from mild evaporation from the weather.

The concentrations of the high molecular weight PAHS (three–six ringed PAHs) are also low. These low values indicated that the area of the oil spillage was not exposed to bush burning after the spill incidence since high values of PAHs is an indication of bush burning and combustion.[16] Numerous quantitative diagnostic ratios have been defined to differentiate pyrogenic PAHs from other hydrocarbon sources including phenanthrene/anthracene (Ph/An), fluoranthene/pyrene (Fl/Py), benz[*a*]anthracene /chrysene (BaA/Ch), etc The ratio of the sum of the three to six ringed PAHs to the sum of five alkylated PAHs is 2.77.[17] The ratio greater than unity (>1) depicted petrogenic source of PAHs.[15] The higher value of the ratio shows that though the spilled oil is from a petrogenic source, the surface of the land would have been exposed to combustion or bush burning prior to the oil spilling incidence.[16]

Benlahcen reported a method using the ratio of phenanthrene/anthracene <10 and fluoranthene/pyrene>1 to identify contamination sources of PAHs.[18] Result also showed that phenanthrene/anthracene ratio is 0.10 and fluoranthene/pyrene ratio is 7.89 for soil samples. These values also support that combustion process had taken place just before the spill.

On the other hand, the ratio of benz[*a*]anthracene to chrysene, 9.79, also affirmed the initial argument that there was combustion/bush burning before the spilling incident.

Fig. 4 is a graphical representation of the mean concentrations of the PAHs for surface and subsurface soil samples. The higher concentrations of PAHs at surface depth may be attributable to the fact that PAHs are resistant to biodegradation and may remain at the surface depth for years.

Conclusion

Studying PAHs distribution has made it possible to identify the probable sources of these hydrocarbons in the environment. The diagnostic ratios can equally be used to

distinguish between pyrolytic and petrogenic sources. The PAHs from Bodo city oil spillage were more of petrogenic source. It was also confirmed that the area was exposed to combustion prior to the spill incident and that there was no bush burning after the spill.

Acknowledgements

The authors are sincerely grateful to Professor Leo C. Osuji for proofreading this article and his constructive criticism that brought this research article to fruition.

References

[1]Giorgi, A., Khatuna, B., Witold, B., Tea, D., Osman, G., Nodar, L. and Erna, L., *Mater. Sci.*, **2010,** *16(2)*, 1392–1320.

[2]Nauss, K. M., *Expos. Health Effect*, **1995,** 11-61.

[3]Manaham, S. E., *Enivironmental chemistry*, 3rd Edition, CRC LLC USA **2005**.

[4]Cinta, B., Dolors, P., Monstserrat, S. and Joan, A., *Env. Sci. Technol.*, **2000,** *34(9)*, 5067 – 5075.

[5]Harvey, R. G., *Polycyclic Aromatic hydrocarbons.* New York: Wiley, **1996.**

[6]Osuji, L. C., Erondu, E. S. and Ogali, R. E., *Chem. Biodiv.*, **2010,** *7*, 116 – 128.

[7]Osuji, L. C., Iniobong, D. I. and Ojinnaka, C. M., *Environ. Forens.*, **2006,** *7*, 259 – 265.

[8]Osuji, L. C. and Onojake, M. C., *Chem. Biodiv.*, **2004,** *1*, 1708 – 1715.

[9]Xiao –Jun, L., She –Jun, C., Bia- Xian, M., Qing- Shu, Y., Guo – Ying, S. and Jia – Mo, F., *Environ. Pollut.*, **2006,** *139*, 9-20.

[10]Considine, T., Robbatt, J., *Environ. Sci. Technol.*, **2008,** *42*, 1213 – 1220.

[11]Okafor, E. C. and Opuene, K., *Int. J. Env. Sci. Technol.*, **2007,** *4(2)*, 233 – 240.

[12]Hites, R. A., Laflame, R. E. and Farrington, J. W. J., *Science*, **1997,** *198*, 829 – 831.

[13]ATSDR. *US Department of Health and Human Services*, Atlanta, **1995.**

[14]Brassell, S. C., Eglinton, G., Albaiges, J., *Analytical Techniques in Environmental Chemistry*, Oxford, Pergamon Press, **1980.**

[15]Zhendi, W., Marv, F., David, S. P., *J. Chromy.*, **1999.** 843, 369 – 411.

[16]Osuji, L. C. and Inimfo, A. U., *Environ. Monit. Asses.*, **2008,** *141*, 359– 364.

[17]Colombo, J. C. E., Pelletier, C., Brochu, M., Khalil, J. A., *Environ. Sci. Technol.*, **1988,** *23*, 888–894.

[18]Benlahcen, K. T. A., Chaoui, H., Budzinski, H., Bellocq, J., Garrigues, P., *Mar. Pollut. Bull.*, **1997,** *34*, 298–305.

Received: 01.12.2013.
Accepted: 27.12.2013.

SYNTHESIS, CHARACTERIZATION AND CRYSTAL STRUCTURE OF 3'-[(4-FLUOROPHENYL)CARBONYL]-5'-(HYDROXYMETHYL)-4'-PHENYLSPIRO[INDOLE-3,2'-PYRROLIDIN]-2(1*H*)-ONE

Ratika Sharma [a], M. Sapnakumari[b], B. Narayana[b], B. K. Sarojini[c], Vivek K. Gupta[a], Rajni Kant [a]*

Keywords: spiro[indole-3,2'-pyrrolidine], 1-(4-fluorophenyl)-3-phenylprop-2-en-1-one, isatin; crystal structure, intermolecular and intramolecular hydrogen bonds

The title compound 3'-[(4-fluorophenyl)carbonyl]-5'-(hydroxymethyl)-4'-phenylspiro[indole-3,2'-pyrrolidin]-2(1*H*)-one is synthesized by the straightforward multicomponent reaction of 1-(4-fluorophenyl)-3-phenylprop-2-en-1-one, isatin and serine, and is crystallises in monoclinic space group C2/c.The molecule is essentially planar except one of the pyrrolidin ring which adopts normal envelope conformation. The supermoleular assembly is consolidated by π–π interactions [centroid- centroid distance= 3.7983(18)]. The crystal structure is stabilized by one C-H…O intra-hydrogen bond, two N-H…O and one O-H…N inter-hydrogen bonds, and these interactions links the molecules into chain extending along the b-axis.

* Corresponding Authors
Fax: +91 191 243 2051
E-Mail: rkvk.paper11@gmail.com
[a] Department of Physics& Electronics, Jammu University, Jammu Tawi-180 006, India
[b] Department of Studies in Chemistry, Mangalore University, Mangalagangotri-574 199, India
[c] Department of Studies in Chemistry-Industrial Chemistry Section, Mangalore University, Mangalagangotri-574 199, India

Introduction

The indole ring system is present in a number of natural products, many of which are found to possess antibacterial,[1] antitumour,[2] antidepressant,[3] antimicrobial[4,5] and anti-inflammatory activities.[6,7] The derivatives of indole are important chemical materials, because they are excellent drug intermediates for many pharmaceutical products.[8] As part of our interest in the synthesis and structural characterization of such materials, we report here the crystal structure of the title compound $C_{25}H_{21}N_2O_3F$ (Figure 1).

The spiroindole-pyrrolidine ring system is a commonly encountered structural design in many biologically important alkaloids. Compounds with an oxindole framework shows potential biological activities. The derivatives of spirooxindole ring systems are used as antimicrobial, antitumor agents and as inhibitors of the human NKI receptor.[9] Several natural alkaloids and pharmacological agents, contain spiro-oxindole system e.g., spirotryprostatin A, isopteropodine and pteropodine, which have shown important biological activity with potential use in antibacterial, antiprotozoal, and anticancer activities.[10,11] Such new heterocyclic scaffolds can be prepared by the intermolecular 1,3-dipolar cycloaddition reaction of azomethine ylide with olefinic and acetylenic dipolarophiles.[12,13,14]

Experimental

Materials and Method

Melting point was taken in open capillary tube and was uncorrected. The purity of the compound was confirmed by thin layer chromatography using Merck silica gel 60 F_{254}-coated aluminium plates using ethyl acetate:n-hexane (1:3, v/v) as solvent system. LCMS was obtained using Agilent 1200 series LC and Micromass zQ spectrometer. Elemental analysis was carried out using VARIO EL-III (Elementar Analysensysteme GmBH).

Procedure for the synthesis of 3'-[(4-fluorophenyl)carbonyl]-5'-(hydroxymethyl)-4'-phenylspiro[indole-3,2'-pyrrolidin]-2(1*H*)-one

A mixture of 1-(4-fluorophenyl)-3-phenylprop-2-en-1-one **1** (0.01 mol, 2.26 g), isatin **2** (0.01 mol, 1.4 g**)** and serine (0.01 mol, 1.05 g) in ethanol was refluxed for 24 h. After the completion of reaction, as indicated by TLC, the reaction mixture was cooled to room temperature and quenched with ice cold water. The resulting precipitate was filtered and recrystallized from methanol. The crystals were grown by the slow evaporation method. Colourless crystals obtained with 67 % yield. M.p. 175–177 °C; Analytical data: Found (Calcd): C %:72.07 (72.10); H %: 5.11 (5.08); N %: 6.71 (6.73). A schematic reaction scheme is given below.

X-Ray Structure determination

X-ray intensity data of a crystal (dimensions:0.20 X 0.10 X 0.10 mm) were collected at room temperature (293(2)K) using *X'calibur* CCD area-detector diffractometer equipped with graphite monochromated MoKα radiation (λ=0.71073 Å).

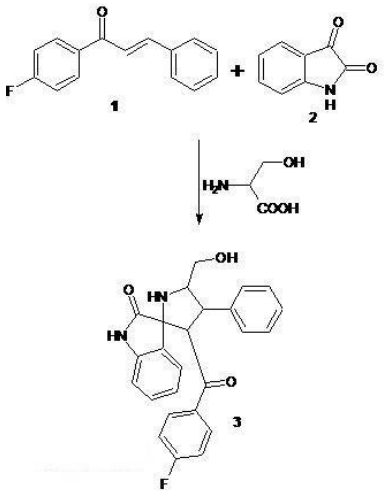

Scheme 1. Synthesis of title compound

The intensities were measured by scan mode (θ ranges 3.53 to 29.12º).A total number of 10427 reflections were collected of which 5181 were found to be unique and 2476 reflections were treated as observed ($I > 2\sigma(I)$). Data were corrected for Lorentz and polarization factors. The structure was solved by direct methods using SHELXS97.[15] All non-hydrogen atoms of the molecule were located in the best E-map. Full-matrix least-squares refinement was carried out using SHELXL97.[15] The hydrogen atoms were geometrically fixed(except N1-H8, N2-H7, H12-O3, H11-C11, C10-H10) and allowed to ride on the corresponding non-H atoms with C-H= 0.97 Å, and $1.2U_{eq}$ for H atoms. The final refinement cycles converged to an R = 0.0602 and w$R(F2)$ = 0.1400 for the observed 2476 reflections. Residual electron densities ranged from -0.198 to 0.151 eÅ^{-3}. Atomic scattering factors were taken from International Tables for X-ray Crystallography (1992, Vol. C, Tables 4.2.6.8 and 6.1.1.4). The crystallographic data are summarized in Table 1. Selected bond lengths, bond angles and torsion angles are given in Table 2. Inter- and intramolecular interactions are shown in Table 3 and π–π interaction is given in Table 4. An ORTEP[16] view of the title compound with atomic labelling is shown in Figure 2. The geometry of the molecule was calculated using the PLATON[17] and PARST software.[18]

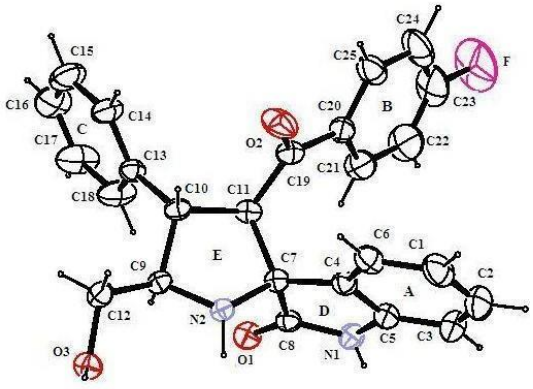

Figure 1. ORTEP view of the molecule with displacement ellipsoids drawn at the 40 % probability level. H atoms are shown as small sphere of arbitrary radii.

Result and Discussion

In the title compound $C_{25}H_{21}N_2O_3F$, the molecule is composed of three six membered rings labeled as A, B and C, and two five membered rings labeled as D and E. All the rings in the molecule is almost planar except ring E which adopts normal envelope conformation with single mirror plane of symmetry passing through the bond N2-C7, with asymmetry parameter ΔC_s = 7.0544. The atom N2 and C7 are situated at -0.1271, 0.1918Å. The bond distances and bond angles, by and large, are in agreement with the values observed for some analogous indole derivatives.[19, 20]

Table 1. Crystal data and other experimental details

CCDC Number	**976498**
Crystal description	block
Crystal size	0.20 x 0.10 x 0.10 mm
Empirical formula	$C_{25}H_{21}N_2O_3F$
Formula weight	416.44
Radiation, Wavelength	Mo *K*α, 0.71073 Å
Unit cell dimensions	*a* = 25.5894(16), *b* = 7.8863(4), *c* = 23.2184(14) Å, γ=103.704(7)º
Crystal system, Space group	Monoclinic, *C*2/*c*
Unit cell volume	4552.2(5)Å^3
No. of molecules per unit cell, *Z*	8
Absorption coefficient	0.086 mm^{-1}
F(000)	1744
θ range for entire data collection	3.53< θ < 29.12º
Reflections collected / unique	10427 / 5181
Reflections observed $I > 2\sigma(I)$	2476
Range of indices	*h*= -32 to 29, *k*= -10 to 9, *l*= -17 to 31
No. of parameters refined	300
Final *R*-factor	0.0602
w*R*(*F*2)	0.1400
R_{int}	0.0448
R_{sigma}	0.0914
Goodness-of-fit	0.947
(Δ/σ)max	0.001
Final residual electron density	-0.198< Δρ >0.151 eÅ^{-3}

Table 2. Selected bond lengths (Å), bond angles (º) and endocyclic torsion angle (º) about the ring junction for non hydrogen atoms (e.s.d.'s are given in parentheses)

Bond lengths, Å		**Bond angles, °**	
O1 -C8	1.233(2)	C3-C5-N1	127.8(2)
O2 -C19	1.216(2)	C4-C5-N1	109.9(2)
O3 -C12	1.428(2)	N2-C9-C12	111.78(16)
N2 -C9	1.479(3)	N2-C9-C10	101.27(17)
N2 -C7	1.483(2)	C22-C23-F1	117.9(4)
C23-F1	1.363(4)	C24-C23-F1	118.4(4)
N1-C5	1.407(3)	O3-C12-C9	111.54(17)
		O1-C8-N1	125.4(2)

Endocyclic torsion angle (º) about the ring junction

	Atoms	**Angle,º**	**Atoms**	**Angle,º**
A/D	C6-C4-C5-C3	-2.0	C7-C4-C5-N1	-1.6

 DOI: 10.17628/ecb.2014.3.183-186

Table 3. Geometry of intra- and intermolecular hydrogen bonds

D-H…A	D-H, Å	H…A, Å	D…A, Å	θ[DH…A, º]
C10-H10…O2	0.98(2)	2.40(2)	2.823(3)	105
O3- H12…N2^{i}	0.94(3)	1.86(2)	2.784(2)	166
N2-H7…O1^{ii}	0.90(2)	2.16(2)	3.050(2)	171
N1-H8…O3^{ii}	0.91(2)	1.87(2)	2.781(3)	178

Symmetry codes: (i) –*x*+1/2+1, -*y*-1/2, -*z*+1 (ii) –*x*+1/2+1,-*y*+1/2, -*z*+1

Table 4. Geometry of π–π interaction

CgI…CgJ	CgI…CgJ, Å	CgI…P, Å	α, º	β, º	Δ, Å
Cg5-Cg5	3.798(2)	3.771	4.54	6.93	0.45

Mean bond distances viz. C(sp^3)-C(sp^3)=1.5345(3), C(sp^2)-C(sp^3) = 1.5195(3), C(sp^2)-C(sp^2)=1.3905(4), C(sp^2)-C(sp^2)=1.3741(5), C(sp^2)=O=1.2245(2), C(sp^2)-O= 1.428(2) are within expected value.[21] The bond distances between the C(sp^3)-N = 1.481(3) and C(sp^2)-N = 1.3795(3), is typical and is in agreement with the various related compounds.[19,20]

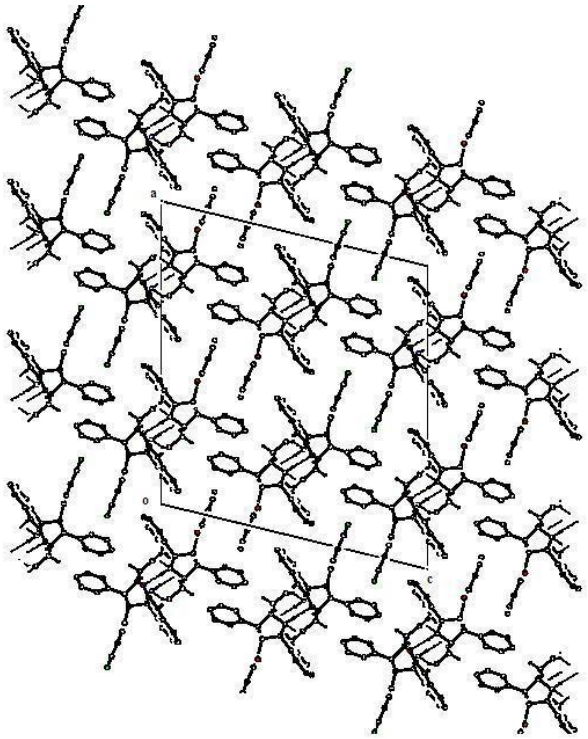

Figure 2. Packing diagram viewed down the b-axis

In the molecule (Figure 1), the indole ring is almost planner with maximum deviation for ring atoms = 0.0244(15) Å. Indole ring is almost perpendicular to the ring E with dihedral angle 89.54(7)º. Ring A and ring B are almost planar with dihedral angle = 3.11(7)º. The packing of the molecule (Figure 2) reveals π–π stacking between the rings D with symmetry operation 1-X, Y, ½-Z and centeriod separation 3.7983(18) Å; interplanar angle 4.54º. Each adjacent pair of the molecule is linked by the π–π stacking interaction. The crystal structure is stabilised by one C-H...O intra-hydrogen bonds, two N-H...O and one O-H...N inter-hydrogen bonds and these interactions link the molecules into layers extending along *b*-axis.

Acknowledgement

One of the authors (Rajni Kant) acknowledges the Department of Science and Technology for single crystal X-ray diffractometer as a National Facility under Project No. SR/S2/CMP-47/2003. The authors are thankful to the Director, IISc, Bangalore for NMR data. BN thanks the UGC for financial assistance through BSR one time grant for the purchase of chemicals. MS thanks DST for providing financial help for the research work through INSPIRE Fellowship.

References

[1]Okabe, N., Adachi, Y. *Acta Cryst*., **1998**, *C54*, 386–387

[2]Schollmeyer, D., Fischer, G., Pindur, U., *Acta Cryst.*, **1995**, *C51*, 2572–2575.

[3]Papenstasion, Z.W., Newmeyer, J. L., US Patent No. 36748 09; *Chem. Abstr.*, **1972,** *77*, 126425

[4]El-Sayed, K., Barnhart, D. M., Ammon, H. L. & Wassel, G. M., *Acta Cryst.*, **1986**, *C42*, 1383–1385.

[5]Gadaginamath, G. S., Patil, S. A., *Indian J. Chem. Sect. B*, **1999**, *38*, 1070–1074.

[6]Rodriguez, J. G., Temprano, F., Esteban Calderon, C., Martinez-Ripoll, M. Garcia-Blanco, S., *Tetrahedron*, **1985**, *41*, 3813–3823.

[7]Papanastassiou, Z. B., Neumeyer, J. L., *US 3674809*, 1972.

[8]Kunzer, A. R., Wendt, M. D., *Tetrahedron*, **2011,** *52*, 1815–1818.

[9]Sundar, J. K., Rajesh, S. M., Sivamani, J., Perumal, S., Natarajan, S., *Chem. Cent. J*., **2011**, *5*, 45.

[10]Alcaide, B., Almendros, P., Alonso, J. M., Aly, M. F., *J. Org. Chem*., **2001**, *66*, 1351–1358.

[11]Chen, G. Yang, J., Gao, S., He, H., Li, S., Di, Y., Chang, Y., Lu, Y., Hao, X., *Mol. Divers.*, **2012**, *16*, 151–156.

[12]Dondas, H. A., Fishwick, C. W. G., Grigg, R., Kilner, C., *Tetrahedron*, **2004**, *60*, 3473–3485.

[13]Kawashima, K., Kakehi, A., Noguchi, M., *Tetrahedron*, **2007**, *63*, 1630–1643.

[14]Huang, Z., Zhao, Q., Chen, G., Wang, H., Lin, W., Xu, L., Liu, H., Wang, J., Shi, D., Wang, Y., *Molecules*, **2012**, *17*, 12704-12717.

[15]Sheldrick, G. M., *Acta Cryst*., **2008**, *A64*, 112.

[16]Farrugia, L. J., *J. Appl. Cryst*., **1999**, *32*, 837.

[17]Spek, A. L. *Acta Cryst*., **2009,** *D65*, 148.

[18]Nardelli, M., *J. Appl. Cryst.*, **1995,** *28*, 659.

[19]Sakthivel, P., Sethusankur, K., Jaisankar, P., Joseph, P. S., *Acta Cryst*., **2006**, *E62*, o1199-o1201.

[20]Hua Ge, Y., Zhang, G. G., Luo, Y. H., *Acta Cryst*., **2012**, *E68*, 073.

[21]Allen, F. H., Kennard, O., Watson, D. G., Brammer, L., Orpen, A. G., Taylor, R., *J. Chem. Soc., Perkin Trans-II*, **1987**, S1.

Received: 26.12.2013.
Accepted: 28.12.2013.

HETEROGENEOUS CATALYSTS BASED ON SULPHONATED PHTHALOCYANINE MACROHETEROCYCLES AND SOLID MATRIXES

Alena Voronina[a], Ilya Kuzmin[a], Artur Vashurin[a]*, Svetlana Pukhovskaya[a], Natalya Futerman[a] and Maxim Shepelev[a]

Keywords: water-soluble porphyrins and metallophthalocyanines, polymer matrix, surface modification.

Hybrid materials containing sulfo-substituted cobalt(II) phthalocyanines and various pre-treated solid organic and inorganic matrixes (poly(methyl methacrylate), polypropylene, silicon dioxide) have been obtained. It is shown that the plasma chemical activated polypropylene matrix results 85-90 % attachment of the macrocycles. Attaching the sulphonated cobalt(II) phthalocyanines to silicon dioxide matrix, ~65 % of the macrocycles were found to be bound.

* Corresponding Authors
E-Mail: asvashurin@mail.ru
[a] Ivanovo State University of Chemistry and Technology, Ivanovo, 15300 Sheremetevsky str. 7, Russia

Introduction

Water-soluble porphyrins and metallophthalocyanines are of great scientific interest nowadays due to their usage as efficient catalysts and photocatalysts in different oxidation processes[1,2] Recently a number of papers devoted to the use of macroheterocyclic compounds in photodynamic therapy of cancer[3-5] and as antiviral agents have been published.[6] However, such compounds have a number of disadvantages restricting their use. Phthalocyanines are prone to self-association in a solution[7] and have a narrow range of photoactivation.[8]

One of the promising areas in the chemistry of porphyrins and metallophthalocyanines is their immobilization in a solid matrix of organic and inorganic nature[9,10] eliminating a self-association of macroheterocycles and significantly extending a range of photoactivation. This approach provides additional thermal and morphological properties of a polymer matrix maintaining the desired properties of macrocyclic compounds.

Numerous investigations[11,12] deal with the oxidation processes which are catalyzed by the metal complexes held on the surface of polymers or mineral carriers. The advantage of using a heterogeneous catalyst is the ability of its separation from the oxidation products and its further usage. However deactivation due to the sorption of polar products and a solvent in pores in the case of frequently used zeolite continues to be a serious factor decreasing the effectiveness of a catalyst.

Heterogenization of tetrapyrrol macroheterocyclic compounds on a polymer matrix surface is considered in this article.

Material

Cobalt complexes of tetra-4-sulfophthalocyanine ($Co(SO_3H)_4Pc$), tetra-4-[(6'-sulfo-2-naphthyl)oxy]-phthalocyanine ($CoPh(SO_3H)_4Pc$) and tetra-4-[(6',8'-disulfo-2-naphthyl)oxy]phthalocyanine ($CoPh(SO_3H)_8Pc$) were prepared from the corresponding phthalonitriles and anhydrous cobalt chloride by template synthesis on heating according to known methods.[13] The structure of the product compounds was characterized by IR and electronic absorption spectroscopy and elemental analysis.[14]

$Co(SO_3H)_4Pc$ (Sigma-Aldrich) were used without additional purification, the purity of reagent being controlled by spectral methods (H^1 NMR, electron absorption and IR-spectra and elemental analysis).

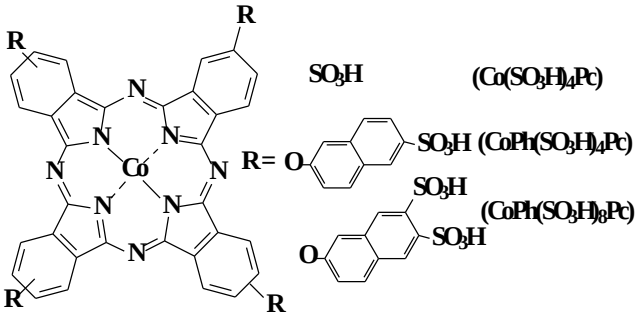

The organic supports used were commercial nonwovens made from poly(ethylene terephthalate)–poly(methyl methacrylate) (PMMA) and polypropylene (PP). The PMMA has an average molecular mass of 20000 and a density of 203 g m^{-2}. The PP has density of 400 g m^{-2} and 4 mm thickness.

Cobalt phthalocyanine complexes were immobilized onto the copolymer by deposition from aqueous solutions with a concentration of ~ $5 \cdot 10^{-5}$ mol L^{-1}. A nonwoven sample of 5×5 cm in size was immersed into 100 ml of a phthalocyanine solution, held for 2–4 h at 298 K, and freed of the solvent by evaporation. The sample was washed by

holding it for 40 min in 100 ml of distilled water and then slowly dried at 313 K. The amount of an immobilized complex was monitored by following electronic absorption spectra of the washing solutions.

An inorganic support used was a silicon dioxide matrix. A modified sol–gel technique was used to synthesize polymeric SiO_2 matrix.[15,16]

Tetraethoxysilane (TEOS) was used as a precursor. The following molar ratio of reactants: TEOS:H_2O:C_2H_5OH, 1:4.5:10 was used in the synthesis. Triethylamine was gradually added drop wise to the reaction mixture after its homogenization as a polycondensation catalyst. The resulting hybrid material was dried under vacuum by gradually raising the temperature up to 353 K. Drying was stopped after reaching a constant mass of the sample, the yield of the hybrid material being 22 %. After drying the hybrid material, it was washed 3 times with water: the amount of solvent in each of the washes was 20 ml; the suspension was stirred for 5 min, centrifuged and the solution was separated from the sediment.

Results and discussion

In holding the macrocycles on the surface of a polymer sample for preliminary preparation of a carrier results in the formation of functional groups on inert materials surface, which is of great importance.

During the immobilization of tetrapyrrol macroheterocyclic compounds the bonding of a macrocycle with a polymer carrier can proceed due to covalent and ionic bonds with active functional groups which are on a polymer matrix surface and due to the coordinative integration of a central metal cation with an electrodonor polymer group.[17,18]

The activation of an organic polymer matrix has been carried out by two methods: 1) by the action of a microwave emission on a PMMA sample, 2) by preliminary treatment in a gas discharge on a PP sample.

In the process of a polymer matrix, the activation of PMMA by a microwave emission equal to 750 W, friability of its structure and the appearance of polarization groups on the surface takes place.[19,20] Changing the time of preliminary activation of a sample it is possible to obtain a hybrid material possessing different degree of phthalocyanine fixation.

The experimental data (Fig. 1, 2) show the possibility of obtaining a hybrid material by the immobilization of phthalocyanines ($Co(SO_3H)_4Pc$, $CoPh(SO_3H)_4Pc$, $CoPh(SO_3H)_8Pc$) onto the activated surface of PMMA. It should be underlined that a definite part of an immobilized macrocycle is connected with the carrier surface by means of weak non-specific interactions. In order to define the immobilization quality the samples of a heterogenic catalyst were washed many times with some portions of a distilled water till the appearance of colorless extracts.

According to UV–Vis (Fig. 1) spectra of aqueous extracts it seems that 65-70 % of a catalyst is fixed on a polymer surface; it corresponds to ~ $3.25 \cdot 10^{-6}$ mol g^{-1} of phthalocyanines on PMMA. According to the same method phthalocyanines were fixed on PP.

In the following experiments the activation was carried out by the action of a plasma discharge on the polymers. Under the action of a gas discharge on the polymers the oxidation of the surface and the appearance of acid containing functional groups take place.[17,18] This fact can be taken as an initiation stage for the processes of a radical grafting copolymerization on a material surface with an inclusion of a macrocyclic component.

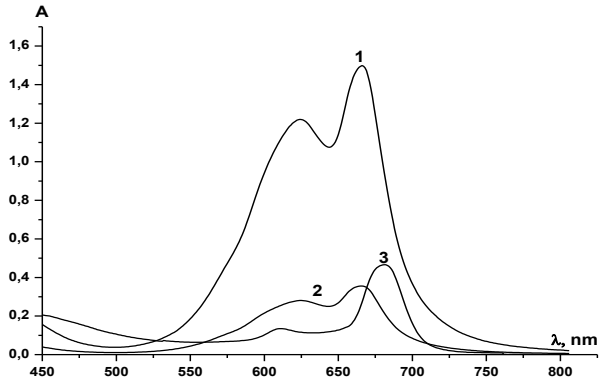

Figure 1. UV-VIS spectra of water solution of $Co(SO_3H)_4Pc$ – 1, UV-VIS spectra of washing solution – 2, UV-VIS spectra of hybrid material in quinoline – 3.

Firstly a polymer matrix treatment was carried out in a gas discharge excited in a solution volume ("end face" discharge) at pH values of the solutions equal 5-12, the time of discharge burning being changed from 5 to 25 minutes ($I_{discharge}$ = 1 A).

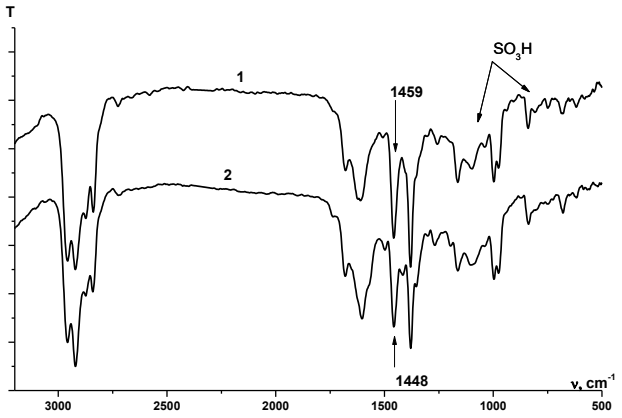

Figure 2. IR-spectra of hybrid material $Co(SO_3H)_4Pc$-Polypropylene obtained by mechanical activation matrix discharge: 1) pH 6, 2) pH 10. The time of discharge 20 minutes.

IR–spectra of hybrid materials obtained at different pH values coincide (Fig. 2). The bands in 1032-1039 cm^{-1} region which are responsible for the vibrations of sulpho-groups which are in the structure of a phthalocyanine molecule undergo the process of transformation.

 DOI: 10.17628/ecb.2014.3.187-189

Table 1. Effective constants of diethyl dithiocarbamate oxidation rate by the oxygen of air at 298.15 K, pH 8.

Macrocycle	$k_{eff} \times 10^4$, s^{-1}		
	PPMA microwave activation	PP plasma activation	SiO_2
$Co(SO_3H)_4Pc$	2.3	25 – glow discharge 8 – "end face" discharge	0.88
$CoPh(SO_3H)_4Pc$	3.2	42 – glow discharge 14 – "end face" discharge	1.43
$CoPh(SO_3H)_8Pc$	4.6	28 – glow discharge 12 – "end face" discharge	0.99

A band in 1465 cm^{-1} region which characterizes the linking of sulpho-groups with surface polymer groups has different position as well.

During a plasma-chemical treatment of PP surface in an acid solution and further immobilization of a macrocycle the given band is displaced into the region of 1459 cm^{-1}. In a similar treatment in an alkaline solution the displacement is greater, it proceeds to the region of 1448 cm^{-1}.

In the next working stage the activation of a polymer material was carried out by a glow discharge ($I_{dischsrge}$ = 10-50 mA). An aqueous – alkaline solution at pH 10 was used as an electrolyte. The control of macrocycles immobilization was done with the help of IR and UV-VIS spectra. The fixation degree is 85–90 %. It was established that the optimum time of discharge burning was 17 min, discharge current being 45 mA.

Polymer samples with metallophtalocyanines on their surface possess catalytic activity in the model reaction of sodium diethyl dithiocarbamate soft oxidation[21] (effective rate constants for the oxidation are presented in Table 1).

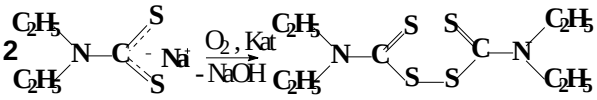

Further the macroheterocycles fixation was carried out in an inorganic matrix of silicon dioxide. The degree of a complex fixation in a matrix was established to be 63-65 %. During the combined polymerization of orthosilicic acid and a macrocycle the latter is covalently fixed in the polymer matrix volume and it averts its washing out later.[16,22] A hybrid material on the base of phthalocyanines ($Co(SO_3H)_4Pc$) and polymer matrix of a silicon dioxide possesses as well a catalytic activity during the oxidation of sodium diethyl dithiocarbamate but in this case the activity is increased only two times as compared with homogenic version of catalysis in the presence of $Co(SO_3H)_4Pc$.[16] Hybrid material on the basis of macrocycle displays a photocatalytic activity in the process of oxidation of Rhodamin 6G.[22]

Acknowledgment

The reported study was partially supported by RFBR (research project No. 13-03-00615_a).

References

[1]Ozoemena, K., Kuznetsova, T., *J. Photochem. Photobiol. A Chem.*, **2001,** *139*, 217.

[2]Barrera, C., Zhukov, I., Villagra, E., *J. Electroanal. Chem.*, **2006,** *589*, 212.

[3]Bohm, F. *J. Photochem. Photobiol.*, **2005,** *80*, 1.

[4]Lang, K., Mosinger, D., Wagnerova, M., *Coord. Chem. Rev.*, **2004,** (248), 321.

[5]Jiang, Z., Shao, J., Yang, T., Wang, J., Jia L., *J. Pharm. Biomed. Anal.*, **2014,** *87*, 98.

[6]Smetana, Z., Ben-Hur, E., Mendelson, E., Salzberg, S., Wagner, P., Malik, Z., *J. Photochem Photobiol. B: Biol.*, **1998,** *44*, 77.

[7]Lebedeva, N., Kumeev, R., Al'per, G., Parfenyuk, E., Vashurin, A., Tararykina, T., *J. Solution. Chem.*, **2007,** *36*, 793.

[8]Iliev, V., Alexiev, V., Bilyarska, L. *J. Mol. Catal. A Chem.* **1999,** *137*, 15.

[9]Trytek, M., Fiedurek, J., Lipke, A., Radzki, S, *J. Sol-Gel Sci. Technol.*, **2009,** *51*, 272.

[10]Rezaeifard, A., Jafarpour, M., Naeimi, A., Mohammadi, K., *J. Mol. Catal. A: Chem.*, **2012,** *357*, 141.

[11]Tao, Y., Kanoh, H., Abrams, L., Kaneko, K., *Chem. Rev.*, **2006,** *106*, 896.

[12]Bennur, T. H., Srinivas, D., Sivasanker, S. *J. Mol. Catal. A: Chem.*, **2004,** *207*, 163.

[13]Kulinich, V. P., Shaposhnikov, G. P., Badaukaite, R. A. *Macroheterocycles,* **2010,** *3*, 23.

[14]Vashurin, A. S., Badaukaite, R. A., Futerman, N. A., Puhovskaya, S. G., Shaposhnikov, G. P., Golubchikov, O. A., *Petrol. Chem.*, **2013,** *53*, 197.

[15]Hench, L., West, J. *Chem. Rev.*, **1990,** *90*, 33.

[16]Marfin, Y. S., Vashurin, A. S., Rumyantsev, E. V., Puhovskaya, S. G., *J. Sol-Gel Sci. Technol.*, **2013,** *66*, 306.

[17]Titov, V. A., Rybkin, V. V., Shikova, T. G., Ageeva, T. A., Golubchikov, O. A., Choi, H.-S., *Surf. Coat. Technol.*, **2005,***199*, 231.

[18]Choi, H.-S., Kim, Y.-S., Zhang, Y., Tang, S., Muyng, S.-W., Shin, B.-C., *Surf. Coat. Technol.*, **2004, 182**, 55.

[19]Vashurin, A. S., Voronina, A. A., Kuzmin, I. A., Kuzmicheva, L. A., Pukhovskaya, S. G., Golubchikov O. A. *Izv. Vyssh. Uchebn. Zaved., Khim. Khim. Tekhnol.*, **2012**(56), 74.

[20]Koifman, O. I., Ageeva, T. A. *Polymer Sci.: C,* **2004,** *46*, 2187.

[21]Vashurin, A. S., Pukhovskaya, S. G., Semeikin, A. S., Golubchikov, O. A., *Macroheterocycles,* **2012,** *5*, 72.

[22]Vashurin, A. S., Gubarev, Yu. A., Lebedeva N. Sh., Vyugin, A. I., *Adv Mater.*, **2013**(7), 5.

Received: 19.12.2013.
Accepted: 01.01.2014.

SYNTHESIS, STRUCTURE AND MAGNETIC BEHAVIOR OF $[Cu_2$(2-AMINO-5-TRIFLUOROMETHYLPYRIDINE)$_4(OH)_2](ClO_4)_2\cdot$ BIS(2-AMINO-5-TRIFLUOROMETHYLPYRIDINE) ADDUCT

R. Louise Forman,[a] Christopher P. Landee,[b] Jan L. Wikaira[c] and Mark M. Turnbull[a]*

Keywords: Copper(II) complexes, magnetic susceptibility, X-ray structure

The reaction of $Cu(ClO_4)_2\cdot 6H_2O$ with 2-amino-5-(trifluoromethyl)pyridine (5-TFMAP) in 1-propanol/water solution gave the product $[Cu_2(5\text{-TFMAP})_4(OH)_2](ClO_4)_2\cdot(5\text{-TFMAP})_2$. The complex forms as a dihydroxide briged Cu(II) dimer with two coordinated 5-TFMAP on each copper ion and two non-coordinated 5TFMAP molecules in the asymmetric unit. Although hydroxide bridged Cu(II) dimers generally exhibit strong magnetic exchange, the compound shows only very weak antiferromagnetic interactions (~ -1.7 K) which is attributed to the Cu-O-Cu bridging angles.

*Corresponding Authors
Fax: +1-508-793-2014
E-mail: mturnbull@clarku.edu
[a] Carlson School of Chemistry and Biochemistry, Clark University, 950 Main Street, Worcester, Massachusetts 01610
[b] Department of Physics, Clark University, 950 Main Street, Worcester, Massachusetts 01610
[c] Department of Chemistry, University of Canterbury, Private Bag 4800, Christchurch, New ZealandChapters

INTRODUCTION

In the field of molecular magnetism, there is an interest in copper(II) complexes because the Cu(II) ion possesses a single unpaired electron, regardless of its geometry, as well as a g-factor of approximately 2.00.[1] These two properties of copper make it of particular interest for the study of quantum magnetism and allow for observation of the effects of the ligands on magnetic exchange within the complexes and how the steric and electronic properties of the ligand influence the molecular complex as a whole.[2-5]

Our research in this field has led us to investigate a wide variety of ligands, each one of which affects the magnetic superexchange and crystal lattice in a unique way. In this field, we focus on complexes involving copper halide complexes and copper(II) salts, such as those involving copper(II) perchlorate which has yielded magnetically interesting and significant 2-dimensional quantum Heisenberg antiferromagnets (2D-QHAF), as well as a highly isolated 2-dimensional layer.[6] It has been observed that 2-amino-5-substituted pyridines have a tendency to form such 2-dimensional magnetic layers.[4] One particularly interesting ligand for such study is 2-amino-5-trifluoromethylpyridine (5-TFMAP), which has a similar structure to that of the corresponding methyl-substituted compound, but with significant electronic differences. We have previously reported the synthesis, structure and magnetic properties of two tetrahalocuprate salts of 5-TFMAP which occurred as a magnetic ladder and a honeycomb-like lattice.[2] We were particularly interested in the effect of replacing the halide ions with non-coordinating anions, and as such examined the reaction of 5-TFMAP with $Cu(ClO_4)_2\cdot 6(H_2O)$. The resulting compound, $[Cu_2$(2-amino-5-(trifluoromethyl)pyridine)$_4(OH)_2]$ $(ClO_4)_2\cdot$ (2-amino-5-(trifluoromethyl)pyridine)$_2$, is an unusual example of a hydroxide bridged Cu(II)-dimer which exhibits only very weak antiferromagnetic interactions . It has lead us to a family of di-μ-hydroxo-copper(II) dimers in which the Cu−O−Cu angle, along with the Cu...Cu distance is significant in the magnetic exchange. The synthesis, structure, and magnetic properties of this compound are reported.

EXPERIMENTAL

Copper perchlorate hexahydrate and 1-propanol were purchased from Aldrich Chemical Company and used without further purification. 2-Amino-5-(trifluoromethyl)-pyridine (5-TFMAP) was purchased from Matrix Scientific and used without further purification. IR spectra were recorded as KBr pellets on a Perkin-Elmer Spectrum 100.

Synthesis of $[Cu_2(5\text{-TFMAP})_4(OH)_2](ClO_4)_2\cdot(5\text{-TFMAP})_2$ (1)

A solution of $Cu(ClO_4)_2\cdot 6H_2O$ (0.182g, 1.0 mmol) in 15 mL of 50 % water/1-propanol was added slowly with stirring to a solution of 5-TFMAP (0.353 g, 2.2 mmol) in 15 mL of 50 % water/1-propanol resulting in a pale blue solution which was left for slow evaporation at room temperature. Dark blue crystals formed at the bottom of the beaker after seven days and were recovered by vacuum filtration, washed with t-butanol and allowed to air dry to yield 0.062 g (12.5 % yield). IR (KBr, ν in cm^{-1}): 3461 (m), 3371 (m), 1651 (s), 1627 (m), 1573 (w), 1559 (w), 1529 (w), 1425 (w), 1330 (s), 1283 (w), 1115 (s), 1081 (s), 930 (w), 832 (w), 624 (w), 517 (w), 463(w).

X-ray Structure Analysis

Data for **1** was collected on an Agilent Technologies diffractometer using the CrysAlisPro software with CuKα radiation (λ = 1.54184 Å) with ω-scans at 120.01(10) K employing a mirror monochomator. Cell parameters were refined using CrysAlisPro[7] and absorption corrections using spherical harmonics were made using SCALE3 ABSPACK scaling algorithm.[7] The crystal structure was solved and refined via least-square analysis using SHELX97-2.[8] All non-hydrogen atoms were refined anisotropically. Hydrogen atoms bonded to carbon atoms were added in calculated positions and refined using a riding model with fixed isotropic thermal parameters. Hydrogen atoms bonded to N- or O-atoms were located in the difference map and their positions refined using fixed isotropic thermal parameters. Crystallographic information and collection details can be found in Table 1.

Magnetic Susceptibility of Data Collection

Magnetic susceptibility data for **1** were collected using a Quantum Design MPMS-XL SQUID magnetometer. A sample of the crystal was finely ground and packed into a gelatin capsule. The moment was measured using magnetic fields from 0 to 50 kOe at 1.8 K. Several data points were collected as the field returned to 0 kOe to check for hysteresis effects; none were observed. Magnetization was then measured from 1.8 to 310 K in a 2kOe field. Data were corrected for the background signal of the gelatin capsule and sample holder. The data was also corrected for the temperature independent paramagnetism of the copper(II) ion (60×10^{-6} emu/mol·Oe) as well as the diamagnetism of the constituent atoms (-500×10^{-6} emu/mol·Oe) which was estimated using Pascal's constants.[1]

Table 1. X-ray data for **1**.

Empirical Formula	$C_{36}H_{32}N_{12}O_{10}F_{18}Cl_2Cu_2$
Formula weight, g mol^{-1}	1332.68
T, K	120.01(10)
Wavelength, Å	1.54184
Crystal System, Space Group	Monoclinic, P2(1)
a, Å	9.59889(18)
b, Å,	27.0705(5)
c, Å	10.0702(2)
α , °	90.0
β, °	94.3818(17)
γ, °	90.0
V, A^3	2609.05(9)
Z	2
Crystal size (mm)	0.23 × 0.12 × 0.07
Absorption coefficient (mm^{-1})	3.12
F(0,0,0)	1332.0
θ_{min}, θ_{max}	4.412, 73.7720
Index Ranges	$-10 < h < 11$ $-33 < k < 33$ $-12 < l < 12$
Reflections collected	16931
Independent reflections	9808
Restraints/parameters	21/813
Final *R* index [$I > 2\sigma(I)$]	0.0605
R index (all data)	0.0645
Largest peak/hole (e/A^3)	2.066 (near C33)/-0.605

RESULTS AND DISCUSSION

Reaction of two equivalents of 5-TFMAP and one equivalent of copper(II) perchlorate in a 50 % water /1-propanol solution over a week produced dark blue crystals of $[(5\text{-TFMAP})_4Cu_2(OH)_2](ClO_4)_2\cdot(5\text{-TFMAP})_2$ (**1**) in 12.5 % yield.

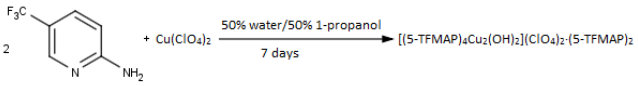

Scheme 1. Preparation of compound **1**.

Attempts to prepare the complex in either pure water or pure 1-propanol proved to be ineffective. This is most likely due to the necessary insertion of a hydroxyl group which bridges the two copper ions and the deprotonation of the hydronium-like ion formed by coordination of a water molecule to the Cu(II) ions. The propyl group may act as a hydrophobic buffer which reduces the hydrogen bonding occurring in a pure water solution and the OH-groups in both the water and 1-propanol can act as a proton donor or acceptor.[9]

Crystal Structure Analysis

Compound **1** crystallizes in the monoclinic space group $P2_1$. The asymmetric unit is shown in Figure 1. A non-symmetric hydroxide-bridged dimer was formed. The six 5-TFMAP molecules are numbered with successive addition of 10 (N11, N21, N31…) to facilitate comparisons between them.

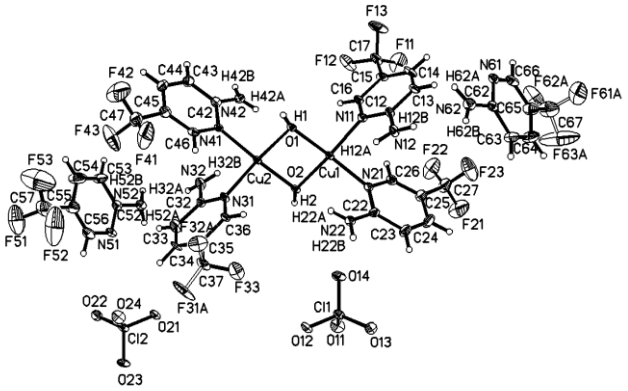

Figure 1. Thermal ellipsoid plot of the asymmetric unit of **1** showing 50% probability ellipsoids. Only H-atoms whose positions were refined are labeled. Only the major occupancy fluorine atoms are shown.

Both Cu1 and Cu2 have a geometry that is tetragonal. Cu1 and Cu2 are each coordinated to two 5-TFMAP ligands and two bridging OH ions, with two long Cu…O contacts to the ClO_4^- ions occupying the Jahn-Teller elongated positions. Selected bond lengths and angles are given in Table 2. The largest deviation from the plane observed for the four 5-TFMAP ligands and two uncoordinated 5-TFMAP molecules is 0.016 Å indicating the degree of planarity of the molecules and is comparable to previously reported work using 5-TFMAP.[2] The planes of the N11 and N21 rings are at 35.3° to one another whereas the planes of the N31 and N41 rings are only canted at an angle of 25.3°. The

N21 and N31 rings are virtually perpendicular with a canting angle of 90.3° as are the N11 and N41 rings which display a canting angle of 81.4°. The Cu1…Cu2 coordination plane has a maximum mean deviation of 0.091Å with a fold angle of 1.4°.

The trifluoromethyl groups on five of the 5-TFMAP molecules (in the 21, 31, 41, 51, and 61 number sequence) exhibit disorder in the position of the fluorine atoms. This disorder was resolved on ligands 30 and 60, as seen in Figure 2A and Figure 2B, respectively. Attempts to resolve the disorder in the remaining trifluoromethyl groups failed to converge and did not improve the overall refinement; these groups were treated as non-disordered and exhibit large thermal ellipsoids in the final refinement.

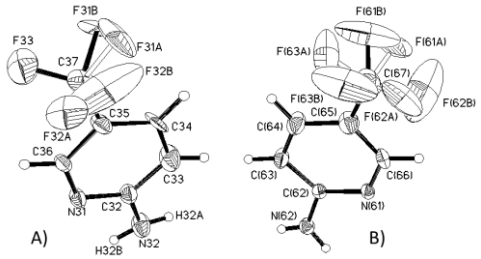

Figure 2. Thermal ellipsoid plot of disordered 5-TFMAP molecules of **1** showing 50% probability ellipsoids. H atoms placed in calculated positions are not labeled.

(A) Ligand 30**.** The major F occupancy atoms are labeled A and the minor F occupancy are labeled B with a refined occupancy for F31 and F32 of 0.72 and 0.50 respectively. Attempts to resolve the disorder of F33 were unsuccessful.

(B) Ligand 60. The major occupancy F atoms are labeled A and the minor occupancy of F atoms are labeled B. The refined occupancy of the major component was 0.64. Attempts to refine a three-site disorder model were unsuccessful and not used in the final refinement.

Table 2. Selected bond lengths (Å) and angles (°) for **1**.

Bond lengths, Å		**Bond angles, °**	
Cu1-O1	1.934(3)	Cu1-O1-Cu2	97.22(16)
Cu1-O2	1.925(3)	Cu1-O2-Cu2	96.48(15)
Cu1-N11	2.023(4)	O1-Cu1-O2	83.35(14)
Cu1-N21	2.016(4)	O1-Cu2-O2	82.94(14)
Cu2-O1	1.922(3)	O1-Cu1-N11	92.65(16)
Cu2-O2	1.953(3)	O1-Cu1-N21	169.3(17)
Cu2-N31	2.001(4)	O2-Cu1-N11	174.1 (17)
Cu2-N41	2.028(4)	O2-Cu1-N21	95.04(16)
Cu1…Cu2	2.8936(8)	O1-Cu2-N31	174.88(18)
		O1-Cu2-N41	94.70(16)
		O2-Cu2-N31	92.57(16)
		O2-Cu2-N41	168.64(17)

The crystal structure of **1** is stabilized by multiple hydrogen bonds (see Table 3). The hydroxide ions form hydrogen bonds to the pyridine nitrogen atoms of the free 5-TFMAP molecules in the adjacent unit cell which generates a chain of dimers and may explain the presence of the uncoordinated 5-TFMAP molecules in the structure. There is also significant hydrogen bonding between three of the amino groups to oxygen atoms of the perchlorate ions and from N42 to one bridging hydroxide ion. These contacts can be observed in Figure 3. Hydrogen bonds are further displayed in Figure 4 where the packing structure of the compound is viewed parallel to the *c*-axis. The hydrogen bonded chains are well isolated parallel to the *b*-axis and a zigzag pattern parallel to the *b*-axis is observed.

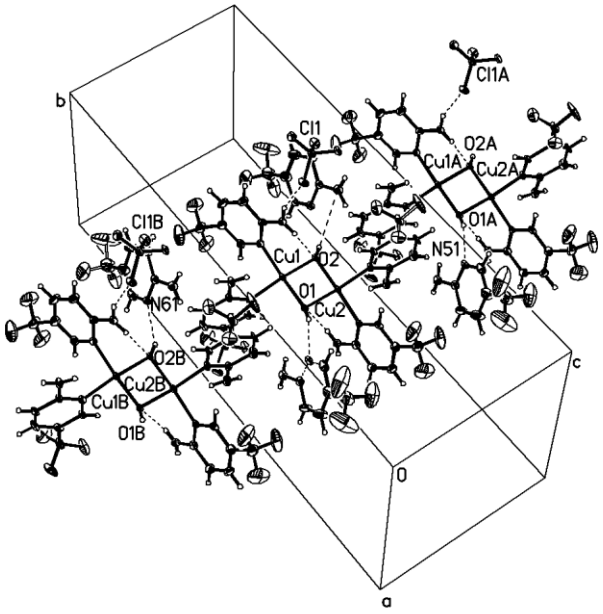

Figure 3. Chain packing of **1**. There are no significant interactions along the *a* or *c* axis. The perchlorate ions are removed for clarity. Dashed lines represent hydrogen bonds.

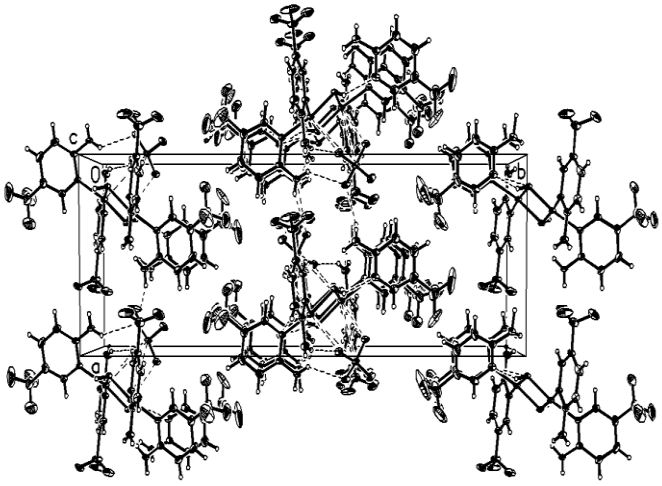

Figure 4. Packing structure of **1** viewed parallel to the *c* axis. Only the major occupancy F atoms are shown. Dashed lines represent hydrogen bonds.

 DOI: 10.17628/ecb.2014.3.190-194

Table 3. Significant hydrogen bond lengths (Å) and angles (°) for **1**.

D - H	A	*d*(D-H)	*d*(H···A)	*d*(D···A)	<(DHA)	Symmetry code
O1 - H1	N51	0.82(7)	2.16(7)	2.904(6)	151(7)	x, y, z-1
O2 - H2	N61	0.88(7)	2.26(7)	2.976(6)	139(6)	x, y, z+1
N12 -H12A	O21	0.88(8)	2.20(8)	3.007(6)	153(7)	
N22 - H22A	O21	0.86(2)	2.08(4)	2.868(6)	153(7)	
N22 - H22B	O14	0.84(2)	2.19(3)	2.988(6)	157(6)	x-1, y, z
N32 - H32B	O12	0.84(9)	2.24(9)	3.024(6)	156(8)	
N42 - H42A	O1	0.81(8)	2.31(8)	2.918(6)	133(7)	

Magnetic Study

Magnetization of **1** as a function of applied field showed a uniform increase with increasing field reaching a value of approximately 8000 emu-Oe mol^{-1} at 5.0 T and 1.8 K. This value is approximately two-thirds of the saturation magnetization for two Cu(II) ions and agrees well with the predicted value for a copper dimer with weak antiferromagnetic interactions.[1] Magnetic susceptibility data were collected for compound **1** from 1.8 to 310 K in a 0.2 T field (Figure 5).

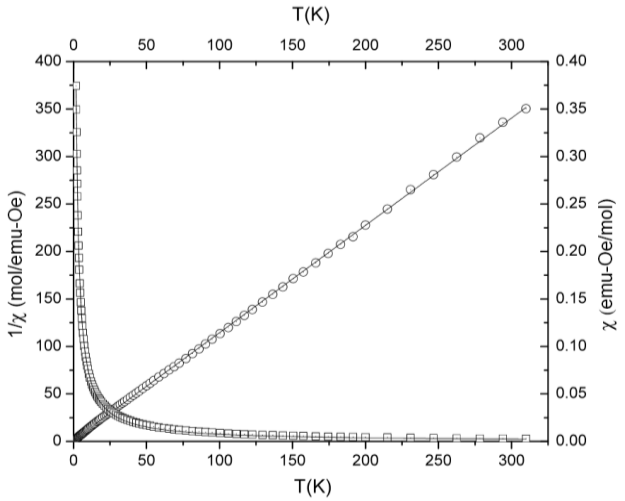

Figure 5. χ_m vs. *T* (□) and $1/\chi_m$ vs. *T* (○) for **1** in a 0.2 T field. The solid line represents the best fit to a dimer antiferromagnet model with an R^2-value of 0.99971 (for χ_m vs. *T*) and the Curie-Weiss model (for $1/\chi_m$ vs. *T*) with an R^2-value of 0.99999.

No maximum is found in the susceptibility above 1.8 K. $\chi_m(T)$ was fit with the Bleaney-Bowers equation (where ρ represents a paramagnetic impurity, and *N*α represents the temperature independent paramagnetism, eqn 1). The best fit yielded, 2*J*=-1.69(5) K, *g*=2.160 again in agreement with a weak antiferromagnetic interaction. Attempts to fit the percent paramagnetic impurity led to unphysical results as is common for very weakly interacting antiferromagnetic materials. No impurity was detected in the powder X-ray diffraction pattern of the material used for magnetic data collection, so the impurity fraction was fixed at 1 % (ρ=0.01)in the final fitting, a value below that detectable via our powder diffraction experiment.

$$\chi_m = \frac{2N\beta^2 g^2}{3kT}\left[1+\frac{1}{3}\exp\left(-\frac{2J}{kT}\right)\right]^{-1}(1-\rho)+\frac{\left(N\beta^2 g^2\right)}{4kT}\rho+N\alpha \quad (1)$$

A fit of the $1/\chi_m$ vs. *T* data (Figure 5) to the Curie-Weiss expression (Eqn 2) yielded C=0.8852(1) mol emu-Oe^{-1} and θ =-1.3982(1)° in good agreement with the Bleaney-Bowers fitting results.

$$\frac{1}{\chi m} = \frac{T-\theta}{C} \quad (2)$$

A wide variety of bis-hydroxide bridged Cu(II) dimers have been prepared using pyridine-derived ligands such as di(3-pyridyl)amine,[10] 2,2'-bypyridine[11] and phenanthroline,[12] but there are no structures available where the ancillary ligands are simple substituted pyridine compounds for comparison with **1**. The closest analogues are those of dipyridylamine with perchlorate,[13] or bipyridine with tetrafluoroborate as the counter ions.[14] In the μ-OH Cu(II) dimer family, it is typical for the exchange to exhibit strong antiferromagnetic, and ferromagnetic interactions.[15-17] However, in a study done by Crawford *et al.*, the relationship between the Cu−O−Cu bridging angle, Cu…Cu distance, and the magnetic exchange value for hydroxide-bridged Cu(II) dimers was reported.[17] It was shown that between the angles of 97.0 and 99.5, the interactions switch from ferromagnetic exchange to antiferromagnetic exchange as seen. Their 2*J* values respectively +49 and -130 cm^{-1} with a paramagnetic exchange intermediate.[18,19] The calculated crossover angle was calculated to be 97.5°. The bond angle of the Cu−O1−Cu in $[(5\text{-TFMAP})_4Cu_2(OH)_2](ClO_4)_2\cdot(5\text{-TFMAP})_2$ is 97.22(16)° which lies in the region of where it was predicted to cross between ferromagnetic and antiferromagnet exchange. The Cu-O2-Cu angle is 96.48(15)° is similar and suggests that the contributions from the two superexchange pathways are either nearly zero, or serve to cancel the exchange via each pathway. Either option provides a viable explanation of the lack of strong exchange in **1**. Further work is in progress to extend this family of compounds through the use of additional substituted 2-aminopyridine ligands.

ACKNOWLEDGEMENTS

The MPMS-XL SQUID magnetometer was purchased with the assistance of funds from the National Science Foundation (IMR-0314773) and the Kresge Foundation. The Bruker D8-Advance powder X-ray diffractometer was purchased with the assistance of Funds from the Kresge Foundation and PCISynthesis, Inc.

APPENDIX A. SUPPLEMENTARY DATA

CCDC (974812) contains the supplementary crystallographic data for 1, respectively. These data can be obtained free of charge via http://www.ccdc.cam.ac.uk/conts/retrieving html, or from the Cambridge Crystallographic Data Centre, 12Union Road, Cambridge CB2 1EZ, UK; fax: (+44) 1223-336-033; or e-mail: deposit@ccdc.cam.ac.uk.

REFERENCES

[1]Carlin, R. L., *Magnetochemistry*, Springer-Verlag, **1986**.

[2]Gale, A. J., Landee, C. P., Turnbull, M. M., Wikaira, J. L., *Polyhedron*, **2013**, *52*, 986.

[3]Zhao, J. P., Hu, B. W., Sanudo, E., Yang, Q., Zeng, Y.F,. Bu, X. H., *Inorg. Chem*. **2009**, *48*, 2482.

[4]Abdalrahhman, M., Landee, C. P., Telfer, S. G., Turnbull, M. M., Wikaira, J. L., *Inorg. Chem. Acta* **2012**, *389*, 66.

[5]Solomon, B. L., Landee, C. P., Jasinski, J. P., Turnbull, M. M., *Eur. Chem. Bull.* **2013**, 2, 845.

[6]Selmani, V., Landee, C. P., Turnbull M. M., Wikaira, J. L., Xiao, F., *Inorg. Chem. Comm*. **2010**, *13*, 1399.

[7]CrysAlisPro Oxford Diffraction Ltd., Version 1.171.35.19 (release 27-10-2011 CrysAlis171.NET).

[8]Sheldrick, G. M., *Acta Cryst. A* **2008**, *64*, 112.

[9]Hossen, S. M. M., Islam, S., Hossain, M. M.,Hoque, M. E., Akteruzzaman, G., *Der Pharma Chemica*, **2012**, *4*, 1375.

[10]a)Youngme, S., Chailuecha, C., van Albada, G. A., Pakawatchai, C., Chaichit, N., Reedijk, J., *Inorg. Chim. Acta*, **2004**, *357*, 2532. b) Allen, J. J., Hamilton, C. E., Barron, A. R., *Dalton Trans.*, **2010**, *39*, 11451. c) Wu, L., Keniry, M. E., Hathaway, B., *Acta Crystallogr., Sect.C: Cryst. Struct. Commun.*, **1992**, *48*, 35.

[11]a)Castro, I., Faus, J., Julve, M., Bois, C., Real, J. A., Lloret, F., *J. Chem. Soc., Dalton Trans.*, **1992**, 47. b) Doyle, R. P., Julve, M., Lloret, F., Nieuwenhuyzen, M., Kruger, P. E., *Dalton Trans.*, **2006**, 2081. c) Figgis, B. N., Mason, R., Smith, A. R. P., Verghese, J. N., Williams G. A., *J. Chem.Soc., Dalton Trans.*, **1983**, 703.

[12]a)Maldonado, C. R., Quiros, M., Salas J. M., *Inorg. Chem. Commun.*, **2010**, *13*, 399. b) Zheng, Y., Sun, J., Lin, J., *Z. Anorg. Allgem. Chem.*, **2000**, *626*, 613.

[13]Youngme, S., van Albada, G.A., Kooijman, H., Roubeau, O., Somjitsripunya, W., Spek, A. L., Pakawatchai, C., Reedijk, J., *Eur. J. Inorg. Chem.*, **2002**, 2367.

[14]Prescimone, A., Sanchez-Benitez, J., Kamenev, K. K., Moggach, S. A., Warren, J. E., Lennie, A. R., Murrie, M., Parsons, S., Brechin, E. K., *Dalton Trans.*, **2009**, *39*, 113.

[15]Massoud, S. S., Louka, F. R., Xu, W., Perkins, R. S., Vicente, R., Albering, J. H., Mautner, F. A., *Eur. J. Inorg. Chem.*, **2011**, *50*, 3469.

[16]Cvetkovic, M., Batten, S. R., Moubaraki, B., Murray, K. S., Spiccia, L., *Inorg. Chim. Acta*, **2001**, *324*, 131.

[17]Crawford, V. H., Richardson, H. W., Wasson, J. R., Hodgson, D. J., Hatfield, W. E., *Inorg. Chem*., **1976**, *15*, 2107.

[18]Barnes, J. A., Hodgson, D. J., Whillans, F. D., *Inorg. Chem*., **1972**, *74*, 144.

[19]Hoskins, B. F., Whillans, F. D., *J. Chem. Soc., Dalton Trans.*, **1975**, 1267.

Received: 16.12.2013.
Accepted: 05.01.2014.

SPECTROPHOTOMETRIC DETERMINATION OF AMINOPHENOL ISOMERS USING 9-CHLOROACRIDINE REAGENT

Theia'a N. Al-Sabha,[a] Shireen O. Ismael[b] and Suzan A. Ali[b]

Keywords: spectrophotometric determination; o-aminophenol; m-aminophenol; p-aminophenol; 9-chloroacrididne

A simple, sensitive and accurate spectrophotometric method is developed for the quantitative determination of aminophenol isomers, i.e. *o*-aminophenol, *m*-aminophenol and *p*-aminophenol. The method is based on the interaction between these amines and 9-chloroacridine reagent (9-CA). The spectra of the products show maximum absorption at 436 nm. Beer's law is obeyed in the concentration range of 0.25-12, 0.2-10 and 0.0-10 µg mL^{-1} with molar absorptivity values $7.20x10^3$, $7.67x10^3$ and $5.93\ x10^3$ L mol^{-1} cm^{-1} for the above mentioned isomers respectively. The mean percent recoveries are ranged between 97.3 % and 101.07 % with relative standard deviation (RSD) ≤ 4.7 % for all the isomers. In addition, the stability constant has been determined and the mechanism is proposed for the 9-CA-aminophenol products.

* Corresponding Authors
E-Mail: dr_theiaa@yahoo.co.uk
[a] Chemistry department, College of Education, Mosul University, Mosul, Iraq
[b] Chemistry department, College of Sciences, Zakho University, Zakho, Iraq

Introduction

Aminophenol isomers are primarily used as intermediates in the manufacture of dyes and pigments. Also used as a vulcanization accelerator and as an antioxidant in rubber compounds. These are crystalline solids of low volatility and cause contact dermatitis, which appears to be the greatest hazard arising from their use in industry.[1] These compounds are also the main metabolites of aniline both in vivo and in vitro.[2]

Several spectrophotometric methods using various reagents such as 4-aminoantipyrine,[3] 2-methyl-5-vinylpyridine[4] and salicylaldehyde[5] are used for determination of *o*-aminophenol. Potassium iodate,[6,7] crowned 2,4-dinitrophenolazophenol-barium (II) complex[8] and 2,4-dinitrofluorobenzene[9] are used for determination of *m*-aminophenol. Resorcinol,[10] sodium sulphide,[11] 4-nitro- or 2,4-dinitrobenzaldehyde[12] and 5,7-dichloro-4,6-dinitrobenzofuroxan[13] have been described for the determination of *p*-aminophenol. Charge transfer complex formation reactions have been widely used for determination of aminophenol isomers as n-donors with different π-acceptors such as chloranil,[14] bromanil,[15] fluoranil[16] and DDQ.[17] Also, 1,2-naphthoquinone-4-sulphonate (NQS) reagent has been used for determination of aminophenol isomers.[18] However; most of these methods are either insufficiently sensitive or tedious and required an extraction step. Various analytical techniques have been reported for determination of aminophenol isomers such as thin layer chromatography.[19] adsorptive stripping voltammetry.[20,21] liquid chromatography.[22-25] potentiometry[26] and fluorimetry.[27] These methods needed of highly sophisticated instruments. The present work describes a simple and sensitive spectrophotometric method for analyses of aminophenol isomers. The method is based on the formation of coloured products from the reaction of these isomers with 9-chloroacridine reagent in ethanolic medium.

Experimental

Apparatus

Spectra and absorbance measurements were made with UV-Visible double beam spectrophotometers (Perkin-Elmer, lambda 25). with 1-cm matched silica cells. The pH measurements were made by using both Cyber Scan 510 pc. pH meter with a combined glass electrode. Heating of solutions is carried out on a water bath of frost instruments, LTD). Weighing is carried out on a sensitive balance type of Mettler H 54AR. All calculations in the computing process were done in Microsoft Excel for Windows.

Reagents

All chemicals used are of the highest purity available which are provided by BDH, Fluka and Molekula companies. 9-Chloroacridine (Eastman chemical Co.) was used as the chromogenic reagent. Absolute ethanol is used (ROTH Co.). Sodium hydroxide (1×10^{-2} M) and hydrochloric acid (1×10^{-2} M) solution are prepared by appropriate dilution of the concentrated NaOH (1 M) or HCl (1 M) solutions with distilled water.

*9-chloroacridine reagent (1×10^{-3} M) (*9-CA*).* The 25 ml solution is prepared by dissolving 0.0053 g of 9-chloroacridine in ethanol absolute and then the volume is completed to 25 ml in a volumetric flask. The solution is prepared daily and used immediately[28].

Aminophenol isomers. Ethanolic solution of 25 µg mL^{-1} prepared for each of *o*-aminophenol (*oA*), *m*-aminophenol (*mA*) and *p*-aminophenol (*pA*).

Recommended procedure

Appropriate volumes containing 0.25-12, 0.20-10 and 0.00-10 µg mL^{-1} of *oA*, *mA* and *pA* standard solutions followed by addition of 2.0, 2.5 and 2.0 ml of 9-CA reagent solution into separated 5-ml volumetric flasks; respectively. The solutions were diluted to the mark with absolute ethanol, and were left for 30 min at 50 °C for *oA* and for 30 and 15 min at 40 °C for each of *mA* and *pA* respectively. A portion of the solution was transferred into a 1cm silica cell to measure the absorbance at 436 nm against their respective reagent blank.

Results and Discussion

The reagent 9-CA was reacted quantitatively with aminophenol isomers in alcoholic medium and produce yellowish-green colored solutions immediately. The intensity of this colour increased when the reaction mixtures were heated in contrast to the reagent blank and show a maximum absorption at 436 nm, which was used in all subsequent experiments, where as blank reagent shows no absorption at this wavelength (Figure 1).

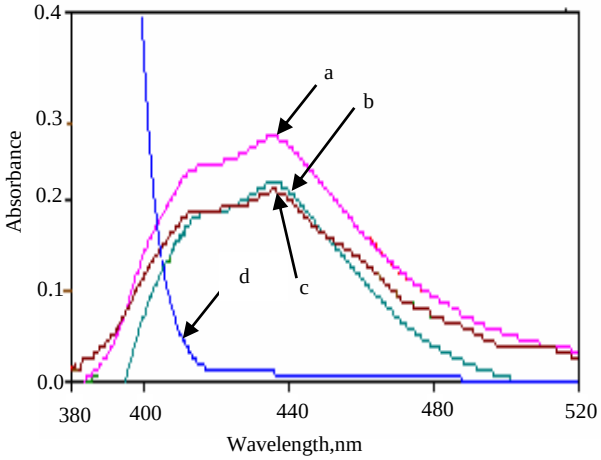

Figure 1. Absorption spectra of 2.5 µg ml^{-1} of a) *pA*, b) *oA*, c) *mA* and d) Reagent blank against ethanol at optimum conditions

Selecting optimum reaction conditions

Preliminary experiments were carried out to choose the best solvent from water, methanol, ethanol, acetone and acetonitrile, optimum pH of the reaction mixtures, concentration of 9-CA, temperature of the reaction mixture and time allowed to the reaction mixture to develop highest colour intensity of the final product at 436 nm.

It was observed that a reaction mixture prepared from mixing 1 ml solution containing 2.5 µg mL^{-1} of *pA* , as typical sample, with 1 ml of 1×10^{-3} M 9-CA in 5 ml of the reaction mixture prepared in ethanol absolute as solvent gave maximum absorbance compared to reaction mixtures prepared with other solvents (Table 1).

Table 1. Effect of solvent on colour intensity of *pA*-9-CA product.

***pA*, 5 µg mL^{-1} dissolved in**	**9-CA 1 ml of 1×10^{-3} M dissolved in**	**Final dilution with**	**Absorbance**
Water	Water	Water	------
Water	Ethanol	Water	------
Water	Ethanol	Ethanol	0.189
Ethanol	Ethanol	Ethanol	0.349
Water	Methanol	Water	-----
Water	Methanol	Methanol	0.326
Methanol	Methanol	Methanol	0.143
Water	Acetone	Water	0.274
Water	Acetone	Acetone	0.025
Acetone	Acetone	Acetone	-----
Water	Acetonitrile	Water	0.027
Water	Acetonitrile	Acetonitrile	0.276
Acetonitrile	Acetonitrile	Acetonitrile	-----

The pH of the reaction mixture was varied between pH 2.5 and 11.5 by adding 0.01 M of HCl or NaOH. It was found that the sensitivity of products were decreased. However; the pH of final solutions were measured in the absence of HCl and NaOH and found 9.50, 9.48 and 9.60 for *oA*, *mA* and *pA* respectively. Different buffer solutions (bicarbonate, borate and phosphate of pH 9.6) were also examined. These showed a negative effect on the absorbance of the products.

It was found that 2.0, 2.5 and 2.0 ml of 1×10^{-3} M solution of 9-CA in 5 ml of the reaction mixtures, containing 2.5 µg mL^{-1} of each isomer in ethanol medium separately, showed maximum absorbance at 436 nm after 10 min at room temperature for *oA*, *mA*, and *pA* respectively.

The effect of temperature on the maximum absorbance of the reaction products for aminophenol isomers was studied at temperatures 24 °C, 40 °C and 50 °C at the above stated optimum conditions. It was found that the maximum absorbance was obtained at 50 °C after 30 min for *oA*, 40 °C after 30 min for *mA* and 40 °C after 15 min for *pA*. The absorbance remained constant over an appreciable time period ranging from 40-55 mins but decreased thereafter indicating dissociation of the product.

Quantitation

Under the experimental conditions described above, standard calibration graphs of products for aminophenol isomers with 9-CA reagent were constructed by plotting absorbance versus concentration as shown in Figure 2. The linear regression coefficient of the plot were 0.999, 0.999 and 0.999 with molar absorptivity values 7.202×10^{3}, 7.671×10^{3} and 5.936×10^{3} for *oA*, *mA* and *pA* respectively indicating the high sensitivity of the method

Limit of detection (*LOD*), which is the smallest concentration that can be measured, and limit of quantitation (*LOQ*), which is the level above which quantitative results may be obtained with a specified degree of confidence, are determined by taking the ratio of standard deviation of the blank with respect to water and the slope of calibration curve by applying the following equations:

$$LOD = \frac{3.3\,\sigma B}{S}$$

$$LOQ = \frac{10\sigma B}{S}$$

whereas:

σB= standard deviation for six determinations of blank

S= slope of calibration graph for each isomer

LOQ is approximately 3.3 times *LOD*. Naturally, the *LOQ* slightly crosses the lower limit of Beer's law range, (Table 2). Sandell's sensitivity was determined by 0.001/slope.

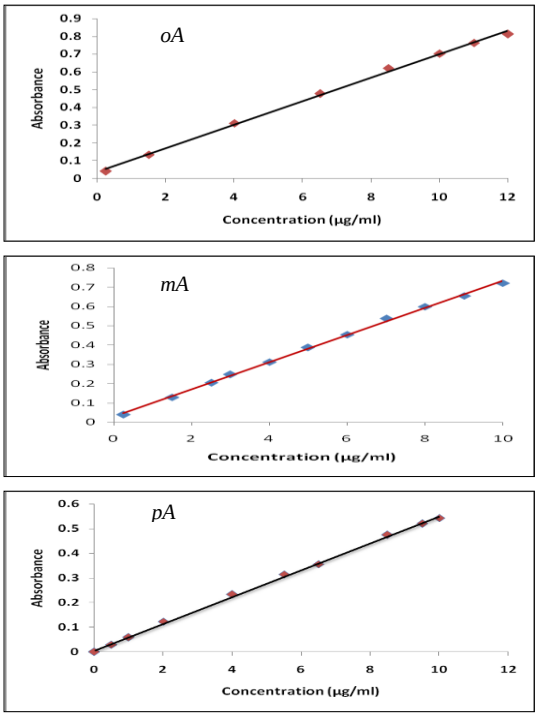

Figure 2. Calibration graphs of 9-CA-aminophenol isomers products

Table 2. Summary of optical characteristics and statistic data for the proposed method

Parameter	***oA***	***mA***	***pA***
Beer's law limits, µg mL^{-1}	0.25 -12	0.20 -10	0.00 -10
Molar absorptivity L mol^{-1} cm^{-1}	7.20x10^3	7.67x10^3	5.93x10^3
LOD, µg mL^{-1}	0.233	0.133	0.177
LOQ, µg mL^{-1}	0.706	0.404	0.539
Sandell's sensitivity µg cm^{-2}	0.0151	0.0142	0.0183
Average recovery, %*	98.83	97.33	101.07
Correlation coefficient	0.998	0.998	0.999
Regression equation, *Y***			
Slope, *a*	0.066	0.070	0.054
Intercept, *b*	0.037	0.030	0.007
RSD**	≤4.6	≤4.7	≤1.36

*Average of six determinations.
**Y = aX + b, where X is the concentration of isomer in µg mL-1.

Interferences

The interference from various organic nitrogenous compounds including primary, secondary, tertiary aliphatic amines, amides, phenols and n-hexane on the determination of 5 µg mL^{-1} of *pA* (as example for aminophenol isomers) was examined by using recommended procedure. It was found that these compounds did not affect the accuracy of the determination of the above compound indicating the method is selective for the determination of aminophenol isomers which are containing primary aromatic amino group. An error of ± 5.0 % in the absorbance readings was considered tolerable. The results are summarized in Table 3.

Table 3. Effect of foreign compounds on the determination of 5 µg mL^{-1} *pA*

Foreign compound	**Amount added , µg mL^{-1}**	**Recovery, %**
Hexylamine	40	98.90
	100	98.18
	300	93.80
Di-n-propylamine	40	97.82
	100	96.73
	300	93.09
Tri-butylamine	40	97.46
	100	97.09
	300	93.46
Phenol	250	100.00
	500	96.36
	800	94.91
Acrylamide	250	101.46
	500	103.64
	1000	105.09
Benzamide	250	98.91
	500	95.30
	1000	94.20
Toluene	250	102.50
	500	96.40
	1100	94.50
n-Hexane	250	103.63
	500	97.10
	1100	94.57

Stoichiometry and Stability constant

The stoichiometry of the reaction of aminophenol isomers with 9-CA reagent was studied by the molar ratio and Job methods,[29] using solutions of 1x10^{-4} M for each isomer and 9-CA reagent. As shown in Figure 3, the results indicate that 1:1 aminophenol to reagent was formed using both above methods. This indicates that amino group present in the isomer is responsible for the formation of the products.

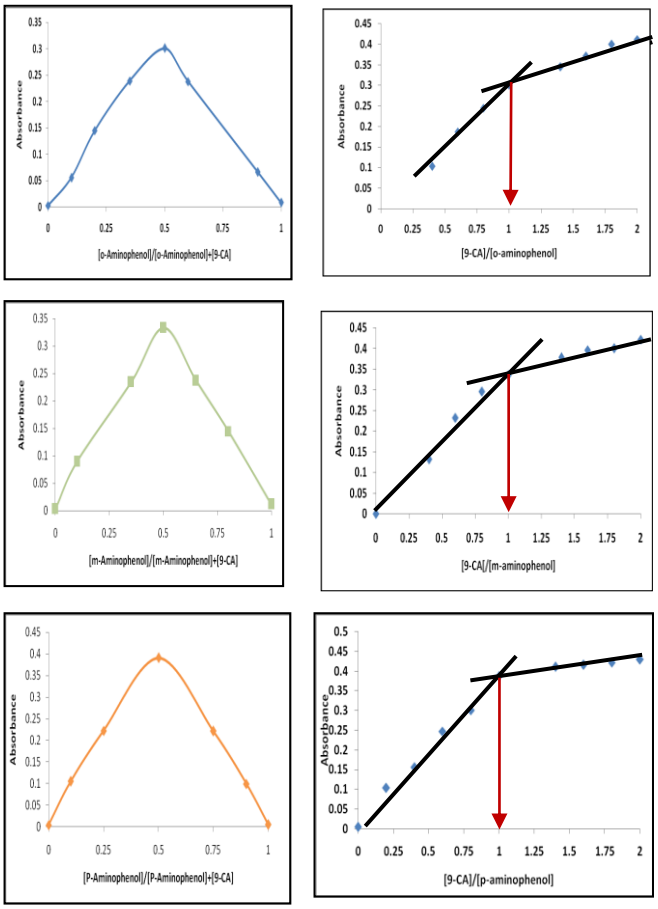

Figure 3. Job and mole ratio plots for aminophenol isomer–9-CA products.

According to the results obtained from above stoichiometry**,** the apparent stability constant was estimated by comparing the absorbance of a solution containing stoichiometric amounts of the each isomer and 9-CA (A_s) to one containing an excessive amount of 9-CA reagent (A_m). The average conditional stability constants of the complexes are calculated by the following equation :

$$K_C = \frac{1-\alpha}{\alpha^2 C}$$

where

K_c is the association constant (L mol^{-1})

α is the dissociation degree and

C is the concentration of the product which is equal to the concentration of aminophenol and

$$\alpha = \frac{A_m - A_s}{A_m}$$

The results shown in Table 4 indicate that the products are relatively stable.

Table 4. Association constants of the 9-CA-aminophenol isomer products.

Iso-mer	Volume of 1x10^{-4} M, ml	Absorbance		α	Average K_{st}, L mol^{-1}
		A_s	A_m		
oA	0.5	0.213	0.409	0.4792	3.06×10^4
	1.0	0.307	0.557	0.4488	
	1.5	0.335	0.601	0.4426	
mA	0.5	0.283	0.305	0.07213	1.61×10^5
	1.0	0.358	0.430	0.1674	
	1.5	0.448	0.533	0.1595	
pA	0.5	0.260	0.400	0.3500	3.7 × 10^4
	1.0	0.380	0.511	0.2564	
	1.5	0.422	0.535	0.2112	

Mechanism

The colored products produced from the reaction of aminophenol isomers with 9-chloroacridine suggested that the amino functional group present in the molecule is necessary for the reaction. Aromatic nucleophihc substitution is enhanced in structures which contain an electronegative heteroatom.[30] This ease of nucleophihc substitution can be harnessed for the purposes of analytical chemistry when the 9-position of the acridine ring bears a facile leaving group and substituted by amino group in this reaction to form 9-aminoacridinium derivatives. However; the chemical reaction mechanism is proposed in Scheme 1.

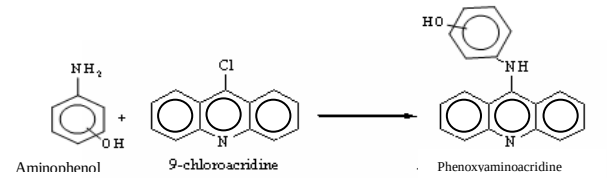

Scheme 1. Proposed chemical reaction mechanism

Comparison of the proposed method with reported methods

The proposed method compared favourably with other reported spectrophotometric methods as shown in Table (5). However, the present method is simpler than other methods as no pH adjustment or use of buffer solutions and no need of surfactants, moreover the proposed method is more sensitive than other methods.

Conclusion

The proposed method is simple, rapid, selective, sensitive and economical compared to previously reported methods as it does not require any pretreatment or extraction procedure and has good accuracy and precision. The method, in terms of simplicity and expense, is considered superior to the previously reported methods.

 DOI: 10.17628/ecb.2014.3.195-199

Table 5. Comparison of spectrophotometric methods with the proposed method

Reagent	Amine	λ_{max}, nm	T, °C	Developing time, min	Linearity range ($\mu g.ml^{-1}$)	Molar absorptivity, L mol^{-1} cm^{-1}	Remark	Ref.
p-BA	*oA*	430	25	40	0.2 - 5.0	9.43 x10^3	Need surfactant	21
	mA	420	55	40	0.4 - 6.0	6.45 x10^3	and buffer	
	pA	355	40	40	0.2 - 6.4	3.36 x10^3	solution	
NQS	*oA*	488	25	5	0.20-10.0	5.16 x10^3	Need surfactant	18
	mA	480			0.08-7.2	6.61 x10^3	and buffer	
	pA	535			0.08-18.0	7.64 x10^3	solution	
9-CA	*oA*	436	50	30	0.25 -12.0	7.20x10^3	Need heating	Present
	mA		40	30	0.20 -10.0	7.67x10^3		method
	pA		40	15	0.00 -10.0	5.93x10^3		

References

[1]Stellman, J. M., *Encyclopedia of Occupational Health and Safety*, **1998**, *104*, 96.

[2]Parke, D. V., *Biochem. J*., **1960**, *77*, 493.

[3]Mohammed, H. J. and Hassen, H. S., *Islam. Univ. J., (Ser. Natural Stud. Engg.)*, **2009**, *17*, 25.

[4]Nelson, K. H. and Grimes, M. D., *Anal. Chem*., 1**958**, *30*, 1928.

[5]Izao, A., Yasao, Y. and Kuuihiro, W., *Japan Analyst.*, **1989**, *38*, 674.

[6]Deodher, R. D. and Metha, R. C., *Indian J. Pharm*., **1976**, *38*, 131.

[7]Hashmi, M. H., Adil, A. S. and Ajmal, A. I., *Mikrochim. Acta*, **1969**, *92*, 1.

[8]Nakashima, K., Maraki, K., Nakatsuji, S. and Akiyama, S., *Analyst*, **1989**, *114*, 501.

[9]Al-Sabha, T. N. and Hamody, I. A., *Arab. J. Chem*., Article in press.

[10]Van, B. J. F., Clauwart, K. M., Lambert, W. E. and Deleenheer, A. P., *Clin. Chem*., **1997**, *43*, 627.

[11]Mohamed, F. A., AbdAllah, M. A. and Shammat, S. M., *Talanta*, **1997**, *44*, 61.

[12]Kalatzis, E. and Zarbi, I., *J. Pharm. Sci.*, **1976**, *65*, 71.

[13]Bakeeva, R. F., Gorbunova, T. S., Vakhitova, O. E., Gaisina, A. I. and Yusupova, L. M., *Pharm. Chem. J*., **2010,** *44*, 282.

[14]Al-Sabha, T. N., *Spectrophotometric microdetermination of some organic nitrogen compounds (amines and aldoximes) and their binary mixtures with chloranil*, M.Sc. Thesis, Mosul University, **1984**.

[15]Al-Sabha, T. N., *The use of charge-transfer complex in selective spectrophotometric determination of amines and application to pharmaceutical preparations*, Ph.D. Thesis, Mosul University, **1997**, 6, 25.

[16]Al-Mtaiwti, S. M., *The use of charge transfer complex formation in selective spectrophotometric determination of some amines and drugs compounds*, Ph. D. Thesis, Mosul University, **2004**, 30.

[17]Hanna, G. K., *Application of charge transfer technique in the trace analysis*, M. Sc., Thesis, Mosul University, **1986,** 21,77.

[18]Kouimtzisa, Th. A., Papadoyannisa, I. N. and Sofoniou, M. C., *Microchem. J*., **1981**, *26*, 51.

[19]Huang, W., Hu, W. and Song, J., *Talanta*, **2003**, *61*, 411.

[20]Zhang, X., Wang, Sh. and Shen, Q., *Microchim. Acta*, **2004**, *149*, 37.

[21]Sakurai, H. and Shunjiro, O., *J. Chromatogr. Sci.*, **1976**, *14*, 499.

[22]Penner, N. A. and Nesterenko, P. N., *Analyst*, **2000,** *125*, 1249.

[23]Narita, M., Murakami, K. and Michel, J., *Anal. Chim. Acta*, **2007**, *588*, 316.

[24]Wany, S. P. and Huany, T. H., *Anal. Chim. Acta*, **2005**, *534*, 207.

[25]Zayed, M. A., El-Dien, H. K. and Nour, F. A., *Microchem. J*., **1986**, *34*, 204.

[26]Rafael, J. A., Jabor, J. R., Casagrande, R., Georgetti, S. R., Vieira B. M. F and Fonseca, M. J. V., *Braz. J. Pharm. Sci.*, **2007**, *43*, 97-103.

[27]Street, K. J., Schenk, G., *J. Pharm. Sci.*, **1979**, *68*, 1306.

[28]Albert, A., *The Acridines*, 2nd ed., St. Martin·s press, New York, N. Y., **1966**, 254.

[29]Willard, H. H., Merrit, L. M. and Dean, J. A., *Instrumental Methods of Analysis*, 5th ed., D. van Nostr and company New York, **1974**,121.

[30]Scriven, E. F. V Katritzky, M. A. R. and Rees, C. W., *Comprehensive Heterocylic Chemistry*, Vol. 2, Pergamon Press, Oxford, 1984, 166.

Received: 15.11.2013.
Accepted: 05.01.2014.

PRODUCTION OF DICALCIUM PHOSPHATE

Fathi Habashi[a] and Ali Atbir[b]

Keywords: Dicalcium phosphate; phosphate ores; uranium and fluoride removal from phosphate ores.

We became aware of the article, "*Production of Calcium Monohydrogenphosphate from Sebaiya Phosphate Ore Leaching by Nitric Acid*" published in Eur. Chem. Bull. 2013, 2(10), 752-757. We do not recommend using dicalcium phosphate prepared by this method as animal feed unless uranium and fluorine are first removed from solution before forming the product.

* Corresponding Authors
E-Mail: Fathi.Habashi@arul.ulaval.ca
[a] Department of Mining. Metallurgical, and Materials Engineering, Laval University, Quebec City, Canada,
[b] Department of Chemistry, Ibn Zohr University, Agadir, Morocco, aliatbir@gmail.com

Comment

We became aware of the article, "*Production of Calcium Monohydrogenphosphate from Sebaiya Phosphate Ore Leaching by Nitric Acid*" published in Eur. Chem. Bull., 2013, 2(10), 752-757. We were glad that the authors used a method that did not pollute the environment with phosphogypsum. However, we have the following remarks.

The authors are apparently unaware of the production of $CaHPO_4$ using hydrometallurgical methods which are far more superior than the agitation method they used.[1-3]

We do not recommend using dicalcium phosphate prepared by this method as animal feed unless uranium and fluorine are first removed from solution before forming the product.[4,5]

If calcium carbonate is added to the phosphoric acid then uranium will be co-precipitated as calcium uranate and fluorine will be co-precipitated as calcium fluoride, thus both will contaminate the product. Uranium can be extracted by organic solvents[6] while fluorine can be precipitated as Na_2SiF_6 by a sodium salt.[7]

References

[1]Habashi F. and Awadalla, F. T., *Ind. Eng. Chem. Res.*, **1988**, *27*, 2165–2169.

[2]Habashi, F. *Fertilizer Res.*, **1989**, *18*, 275–279.

[3]Habashi, F., *Ind. Miner.*, **1994**, *318*, 65–69.

[4]Habashi, F., *Econ. Geol.*, **1966,** *61*, 402–405.

[5]Habashi, F. *J. Ass. Offic. Anal. Chemists*, **1966,** *49*, 944–945.

[6]Awadalla, F. T. and Habashi, F., *Ind. Eng. Chem. Res.*, **1989**, *28*, 1101–1103.

[7]Habashi F. and Awadalla, F. T., *Sep. Sci. Techn.*, **1983**, *18(5)*, 485–491.

Received: 01.01.2014.

REPLY FOR COMMENT[1] ON "PRODUCTION OF DICALCIUM PHOSPHATE"

Ahmed El-Asmy[a]

Keywords: Production of dicalcium phosphate; uranium contamination; fluoride precipitation

We have been concerned with a method which is applicable in commercial scale. $CaHPO_4$ was produced by precipitating a fraction of P_2O_5 using calcium carbonate (not any other calcium salt) in order to achieve the precipitation reaction in a pH below the pH of uranium and fluoride precipitation range. Finally we adjusted the pH of the final product and the ratio between Ca and P. Therefore, the final product is not contaminated with uranium.

Corresponding Authors
E-Mail: aelasmy@yahoo.com
[a] Chemistry Department, Faculty of Science, Mansoura University, Mansura, Egypt

Reply

In the paper "*Eur. Chem. Bull., 2013, 2(10), 752-757*" we published our method[2] for manufacturing of $CaHPO_4$ in industrial scale.

$CaHPO_4$ is produced in commercial scale generally in two possible ways. The first method based on production of phosphoric acid and precipitating $CaHPO_4$ using calcium salts.

The second method based on phosphate ore leaching with nitric acid (without producing phosphor gypsum) followed by direct precipitation of $CaHPO_4$.

The other, e.g. hydrometallurgical methods are just being at laboratory or pilot plant scale testing (we have no knowledge about commercial scale production by these methods).

In our previous paper[2] we have been concerned with the methods which are applicable at commercial scales.

According to our method $CaHPO_4$ was produced by precipitating a fraction of P_2O_5 formed in a nitric acid digestion of sphosphate ore using calcium carbonate (and not with other calcium salts) in order to achieve the precipitation reaction in a pH range below the pH of uranium and fluoride compounds precipitation range. In this way we could reach lower fluoride content than that is permitted by the standards (see in Table 5 in the original paper).[2]

Finally we adjust the pH of the final product and the ratio between Ca and P outside the reaction vessel contained the uranium or fluoride content occurred in the starting ore. Therefore, the final product is not contaminated with uranium or fluoride.

References

[1] Habashi, F. and Atbir, A., *Eur. Chem.Bull.*, **2014**, *3(2)*, 200

[2] El-Zahhar, A. A., Aly, M. M., Ahmad, A. M., Khalifa, M. I., El-Asmy, A., *Eur. Chem. Bull.*, **2013**, *2(10)*, 752-757.

Received: 04.01.2014.